SYNTHESIS AND BIOPHYSICAL EVALUATION OF MODIFIED AND FLUORESCENT PNAs: APPLICATIONS IN ANTISENSE THERAPEUTICS AND DIAGNOSTICS

A THESIS SUBMITTED TO THE

UNIVERSITY OF PUNE

FOR THE DEGREE OF

DOCTOR OF PHILOSOPHY

IN

BIOTECHNOLOGY

BY

PRAVIN S. SHIRUDE

DIVISION OF ORGANIC CHEMISTRY (SYNTHESIS)

NATIONAL CHEMICAL LABORATORY

PUNE 411 008, INDIA

APRIL 2005

National Chemical Laboratory

Division of Organic Chemistry (Synthesis)
Pune - 411 008, INDIA

Dr. K. N. Ganesh,
FNA, F.A.Sc.
Head

TeleFax: +91 20 589 3153
Residence: +91 20 589 8320
E-mail: kng@ems.ncl.res.in

CERTIFICATE

This is to certify that the work presented in the thesis entitled "**SYNTHESIS AND BIOPHYSICAL EVALUATION OF MODIFIED AND FLUORESCENT PNAs: APPLICATIONS IN ANTISENSE THERAPEUTICS AND DIAGNOSTICS"** submitted by **Pravin S. Shirude** was carried out by the candidate at the National Chemical Laboratory, Pune, under my supervision. Such materials as obtained from other sources have been duly acknowledged in the thesis.

K. N. Ganesh **April 2005**
(Research Guide)

CANDIDATE'S DECLARATION

I hereby declare that the thesis entitled "**SYNTHESIS AND BIOPHYSICAL EVALUATION OF MODIFIED AND FLUORESCENT PNAs: APPLICATIONS IN ANTISENSE THERAPEUTICS AND DIAGNOSTICS"** submitted for the degree of Doctor of Philosophy in Biotechnology to the University of Pune has not been submitted by me to any other University or Institution. This work was carried out at the National Chemical Laboratory, Pune, India.

Pravin S. Shirude **April 2005**
Senior Research Fellow (CSIR)
Division of Organic Chemistry (Synthesis)
National Chemical Laboratory
Pune 411 008, INDIA

DEDICATED

TO MY

PARENTS

ACKNOWLEDGEMENTS

It gives me great pleasure to place on record my deep sense of gratitude to my research supervisor Dr. K. N. Ganesh for his encouragement and scientific temperament, which furthered my interest in bioorganic chemistry. I wish to thank him for the confidence he had in me which allowed me near total freedom in pursuing avenues which I thought were interesting. His undying enthusiasm for science and unwavering support is always a source of inspiration.

I owe much to Dr. V. A. Kumar who never failed to stop by and discuss interesting results. She truly helped shape and improve my thinking. Without her boundless love and support, I would not have been able to complete this work.

My special thanks goes to Dr. Murali Sastry (Nanoscience group, Physical Chemistry Division) for his encouragement, understanding and suggestions. Without his support, I would not have been able to complete this work.

I am equally indebted to Dr. S. D. Prasad for his help during the course of this work.

My sincere thanks go to Mrs. Anita Gunjal and Dr. A. A. Natu for their help during the course of this work.

I take this opportunity to thank my respectable teachers Prof. H. P. S. Chawla, Prof. A. K. Chakraborti (NIPER, Chandigarh) and Prof. V. Balasubramaniam, Prof. Tambe, Prof. Amrutkar (MGV's Pharmacy college, Nasik) who continuously provided me the encouragement and motivation.

I wish to thank Dr. Vairamani, IICT, Hyderabad and Dr. Mahaesh, NCL for their help in recording the MALDI-TOF spectra.

I wish to acknowledge Mrs. Phalgune and Mr. Sathe for their assistance in recording the NMR; Mrs. Mane and Mrs. Kunte for the HPLC analysis and Mrs. Shantakumari for the mass spectra.

I also wish to thank Dr. Deshpande, Dr. Likhite, and Dr. Maybhate for their support during the course of this work.

The KNG group has been my family for past few years. During this time, all members past and present have helped me, inspired me and entertained me. I was glad to be a member of such a diverse and lively

group. Thanks to Moneesha, Pradeep, Nagamani, Meena, Ramesh, Pallavi, Dinesh, Nagendra, Govind, Gourishankar, Raman, Umashankar, Smita, Madhuri, Khirud, Sushmita, Amit, Ashwani, Sridhar, Geetali, Satish, Rupa and Nasarin for always willing to help and for making the lab a pleasant and productive place. I also thank Pawar and Bhumkar for their assistance.

I wish to thank many friends and colleagues who have helped in one way or other, especially Hrushikesh, Kannan, Ambrish, Tanushri, Vinod, Ujwal, Nilesh, Shailesh, Deepak, Dnyaneshawar, Yogesh, Sandeep, Madhuri, Sachin and many in NCL who are not named in person, for their valuable friendship and helping hand.

I acknowledge The Council of Scientific and Industrial Research, New Delhi and DST, New Delhi for providing me financial support. I am grateful to the Director, NCL, for giving me the opportunity to work in this institute.

Finally I would like to thank in a special way to my Parents, Sisters and Brother-in-law who extended support, encouragement, love and appreciation throughout my research work to excel in whatever I did.

Pravin

CONTENTS

CHAPTER 2:
SYNTHESIS OF (2*R/S*,5*S/R*)-1-(*N*-BOC-AMINOETHYL)-5-(THYMIN-1-YL)PIPECOLIC ACID: SYNTHESIS AND DNA BINDING STUDIES

CHAPTER 3:
APPLICATIONS OF BIS-PNA FOR TARGETTING COMPLEMENTARY DNA: EFFECT OF N7G IN *aeg*/*aep* PNA BACKBONE

CHAPTER 4:

SECTION A: SYNTHESIS AND BIOPHYSICAL EVALUATION OF FLUORESCENT PNAs

SECTION B: INDUCTION OF CHIRALITY IN ACHIRAL *aeg*PNA

CHAPTER 5:

APPLICATIONS OF ISOTHERMAL TITRATION CALORIMETRY TO STUDY BIOMOLECULAR INTERACTIONS: *aeg/aep/aepip* PNA:DNA HYBRIDS, ENZYME/NUCLEOSIDES BINDING TO NANOPARTICLES, AND CHIRAL RECOGNITION OF DNA BY AMINO ACID-MODIFIED GOLD NANOPARTICLES

ABBREVIATIONS

β-ala	β-alanine
A	Adenine
aeg	Aminothylglycine
aep	Aminoethylprolyl
ala	Alanine
ap	Antiparallel
AuNP	Gold nanoparticles
Boc	Tert. butyloxycarbonyl
C	Cytosine
Cbz	benzyloxy carbonyl
CD	Circular Dichroism
dA	Deoxy adenine
DCC	Dicyclohexylcarbodiimide
DCM	Dichloromethane
DCU	Dicyclohexyl urea
dG	2'-deoxyguanine
DIAD	Diisopropylazodicarboxylate
DIPCDI	Diisopropylcarbodiimide
DIPEA	Diisopropylethylamine
DMF	N,N-Dimethylformamide
DNA	2'-deoxyribonucleic acid
DP	D-Proline
ds	Double stranded
EDTA	Ethylenediaminetetraacetic acid

Fmoc	9-Fluorenylmethoxycarbonyl
FPLC	Fast Protein Liquid Chromatography
g	Gram
G	Guanine
gly	Glycine
h	Hours
HBTU	*O*-(1H-Benzotriazol-1-yl) *N*,*N*,*N*^{1},*N*^{1}-tetramethyl uronium hexafluorophosphate
HOBt	1-Hydroxybenztriazole
HPLC	High Performance Liquid Chromatography
Hz	Hertz
IR	Infra red
ITC	Isothermal Titration Calorimetry
LP	L-Proline
MALDI-TOF	Matrix Assisted Laser Desorption Ionisation-Time Of Flight
MF	Merrifield Resin
mg	Milligram
MHz	Megahertz
M	Molar
µM	Micromolar
ml	Milliliter
mM	Millimolar
mmol	Millimoles
N	Normal
nm	Nanometer
NMP	N-methyl pyrrolidine
NMR	Nuclear Magnetic Resonance

ONs	Oligonucleotides
p	Parallel
PCR	Polymerase Chain Reaction
PPh_3	Triphenyl phosphine
PNA	Peptide Nucleic Acid
Pro	Proline
Pyr	pyrrolidinone
RNA	Ribonucleic acid
r.t.	Room temperature
ss	Single strand/ Single stranded
s	Seconds
T	Thymine
TBTU	*O*-(1H-Benzotriazol-1-yl) *N*,*N*,N^{l},N^{l}-tetramethyl uronium tetrafluoroborate
TEA	Triethylamine
TFA	Trifluroacetic unhydride
TFMSA	Trifluromethanesulphonic acid
THF	Tetrahydrofuran
UV-Vis	Ultraviolet- Visible

ABSTRACT

The Thesis entitled "**Synthesis and Biophysical Evaluation of Modified and Fluorescent PNAs: Applications in Antisense Therapeutics and Diagnostics**" is divided into five chapters.

Chapter 1 introduces background literature for undertaking the research work and defines the objectives.

Chapter 2 details the synthesis and DNA hybridization studies of diastereomeric *aepip*PNA.

Chapter 3 describes design of bis-*aep*PNAs for orientation discrimination of binding to complementary DNA and effect of N7G in *aeg*/*aep*PNA backbone.

Chapter 4 Section A describes the synthesis and biophysical evaluation of fluorescent PNAs and Section B describes the effect of chiral ligands on *aeg*PNA backbone.

Chapter 5 introduces applications of isothermal titration calorimetry to study biomolecular interactions: the hybridization of *aeg/aep/aepip*PNAs with DNA, enzyme/nucleosides binding to nanoparticles and chiral recognition of DNA by amino acid-modified gold nanoparticles.

Chapter 1: Introduction.

The potential of oligodeoxynucleotides to act as antisense agents that inhibit viral replication in cell culture was discovered by Zamecnik and Stephenson in 1978. Since then antisense technology has been developed as a powerful tool for target validation and therapeutic purposes. To be effective as medicinal agents, the therapeutic oligonucleotides should be made to cross the membrane and be stable to cellular nucleases. Among the several chemical modifications, PNAs are emerging as one of the potential candidates.

Peptide nucleic acids (PNAs) are a new class of DNA analogues invented 12 years ago, in which the charged sugar-phosphate backbone of DNA is replaced by a neutral and achiral polyamide backbone. The monomeric unit consists of N- (2-

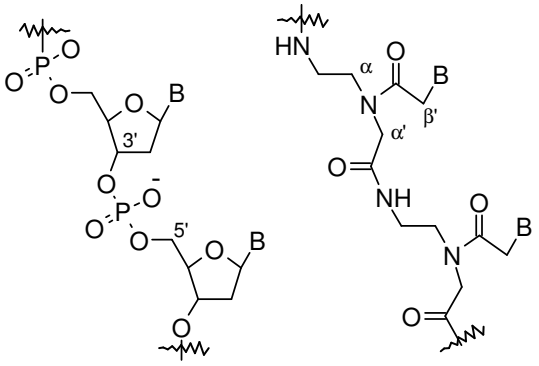

DNA: *Deoxyribo Nucleic Acid*

PNA: *Peptide Nucleic Acid*

aminoethyl) glycine units to which the nucleobases are attached through a conformationally rigid, tertiary acetamide linker group. The binding of PNA to the target DNA/RNA sequences occurs with high sequence specificity and affinity. Despite having several advantages like resistance to cellular enzymes such as nucleases and proteases, the major limitations confounding its application are ambiguity in orientational selectivity of binding (parallel/antiparallel), poor solubility in aqueous media and inefficient cellular uptake.

The deficiencies of PNA are addressed by rational structural modifications of PNA based on conformational preorganization of backbone using cyclic monomeric units. Among the five membered ring PNAs, pyrrolidyl PNA (*aep*PNA, I) has emerged as a result of previous efforts to achieve optimum fine-tuning of aminoethyl glycyl PNA structure to bind to complementary nucleic acids, thus imposing entropic advantages. These analogues to some extent improved the solubility, affinity and orientational selectivity in DNA: PNA binding.

Chapter 2: Synthesis of (2*R/S*,5*S/R*)-1-(*N*-Boc-aminoethyl)-5-(thymin-1-yl)pipecolic acid: Synthesis and DNA binding studies. This chapter presents synthesis and evaluation of six membered ring analogues of pyrrolidines – the aminoethyl pipecolic acid PNAs (*aepip*PNA, II). These are conceptually derived by

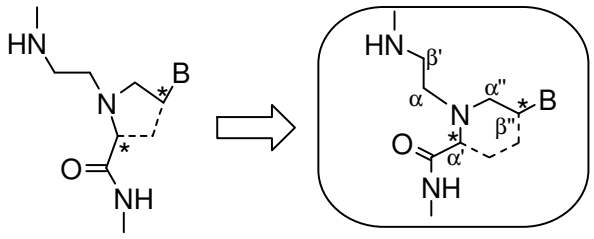

aep **PNA (I)** ***aepip*** **PNA (II)**

linking the α'-carbon of glycyl unit with β"-carbon of side chain via an ethylene linker instead of methylene linker as in *aep*PNA. These have two chiral centers leading to the possibility of existence of four diasteromers.

2.1. Chemical Synthesis of *aepip*PNA monomers. The synthesis of the protected monomers (2*R*,5*S*) and (2*S*,5*R*) 1-(*N*-Boc-aminoethyl)-5-(*N*3-benzoylthymin-1-yl)pipecolic acid methyl ester (**9**) was achieved in ten steps starting from the D-glutamic acid **1** and the naturally occurring L-glutamic acid respectively (Scheme 1).

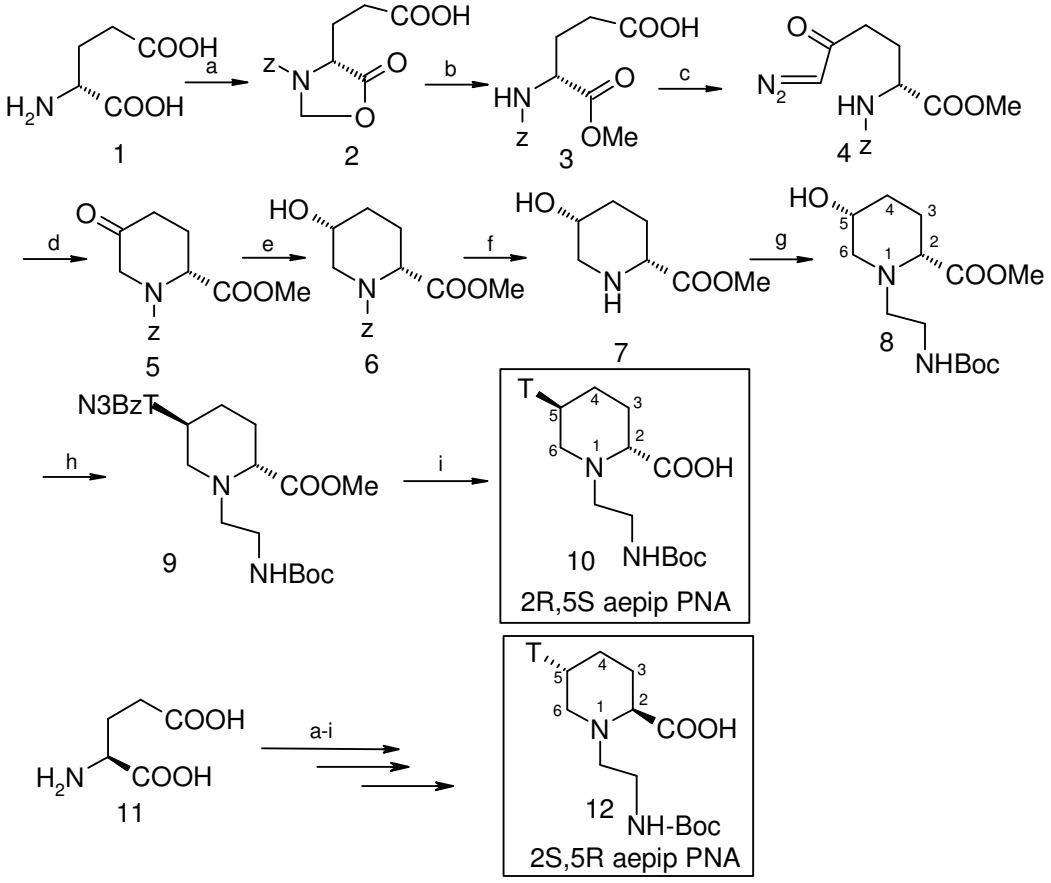

Scheme 1: Synthesis of *aepip*PNA monomers. a.(i) Benzyloxy carbonyl chloride, $NaHCO_3$ (94%) (ii) $(CH_2O)_n$, TsOH, benzene, reflux (82%); b. NaOMe, MeOH (93%); c. (i) EtOCOCl, Et_3N, THF (ii) CH_2N_2, Et_2O (65%); d. $[Rh(OAc)_2]_2$, benzene, reflux (52%); e. $NaBH_4$, MeOH (93%); f. H_2/Pd-C, 60psi (92%); g. BOC-NH-$(CH_2)_2$OMs, DIPEA, ACN:DMF (37%); h. *N*3-BzT, DIAD, PPh_3, THF (32%); i. 1M NaOH, MeOH:water (95%).

2.2. Solid Phase Synthesis of *aeg-aepip*PNA Oligomers. The *aepip*PNA monomers **10** and **12** were incorporated into the PNA oligomer sequences at predefined positions to yield the modified *aeg*PNAs **13**-**15** and **16**-**19**. For control studies, the unmodified

*aeg*PNA sequences **20** and **21** were used. PNAs (**13**-**21** and **25-26**) after cleavage from the resin were purified by HPLC on RPC-18 column and characterized by MALDI-TOF mass spectrometry. The complementary DNA oligomers **22-24, 27-28** were synthesized on an automated DNA synthesizer.

2.3. UV-T_m studies on PNA_2-DNA triplexes. The polypyrimidine PNA oligomers (**13**-**21**) (Table 1) are homopyrimidine sequences that are well known to form DNA:PNA_2 triplexes. The thermal stabilities of PNA_2:DNA complexes were studied by temperature dependent UV absorbance measurements. The mixed purine-pyrimidine *aeg*-*aepip*PNA (**25**) and control *aeg*PNA (**26**) oligomers were synthesized to examine the orientational selectivity in binding to DNA (Table 2). The T_m values indicate that the *aepip*PNA oligomers **13** and **14** having single modification of either stereomer at N or C terminus exhibited stabilization compared to the unmodified PNA T_8 homooligomer (**20**).

Table 1: UV-T_m(°C) of DNA:PNA_2 complexes*

	PNA	PNA_2:DNA	UV-T_m °C	
			2*S*,5*R*	2*R*,5*S*
1	**13**, H-**t** T T T T T T T T –(β-Ala)-OH	**13:22**	43	36
2	**14**, H-T T T T T T T **t** –(β-Ala)-OH	**14:22**	48	76
		14:24	24	23
3	**15,** H-**t** T C T C T T T –(β-Ala)-OH	**15:23**	60	56
4	**16**, H-T TT T **t** T T T –(β-Ala)-OH	**16:22**	44	ND
5	**17**, H-T T T T T **t** T **t** –(β-Ala)-OH	**17:22**	52	ND
6	**18**, H-T T T **t** T T T **t** –(β-Ala)-OH	**18:22**	51	ND
7	**19**, H-T **t** T T T T T **t** –(β-Ala)-OH	**19:22**	49	ND
8	**20,** H-T T T T T T T T–(β-Ala)-OH	**20:22**	43	
9	**21,** H-T T C T C T T T–(β-Ala)-OH	**21:23**	51	

*DNA: **22**, 5'-GCAAAAAAAACG–3'; **23**, 5'-AAAGAGAA–3'; **24**, 5'-GCAAAATAAACG –3'; T=*aeg*-PNA; **t**=*aepip*PNA; Buffer: 10 mM sodium phosphate, pH 7.30.

Table 2: UV-T_m(°C) of DNA:PNA (2*S*,5*R*) duplexes*

PNA		PNA:DNA	UV-T_m °C
25, H-AT G **t** T C T C T T T –(β-Ala)-OH	(*ap*)	**25:27**	57.8
	(*p*)	**25:28**	40.8
26, H-AT G T T C T C T T T –(β-Ala)-OH	(*ap*)	**26:27**	51.2
	(*p*)	**26:28**	43.0

DNA: **27**, 5'-AAAGAGAACAT –3'; **28**, 3'-TACAAGAGAAA– 5'

The T_m values from Table 1 and Table 2 indicates-

- (2*S*,5*R*) compared to (2*R*,5*S*) *aepip* unit at the N-terminus has better stability with the complementary DNA **22**.
- The (2*R*,5*S*) *aepip* unit at C-terminus forms much more stable hybrid compared to that of the (2*S*,5*R*).
- The stability of *aeg-aepip*PNA oligomers with mixed pyrimidine base sequence and N-terminus modifications (**15:23**) was higher to that of the control complex **21**:**23**.
- A synergistic stabilizing effect was observed with a second modified *aepip* unit in all the cases (entry 5-7).
- The modified *aeg-aepip*PNA (2*S*,5*R*) stabilized the antiparallel duplex (**25:27**) more effectively over the parallel duplex (**25:28**) as compared to control complexes.

Thus overall, the substitution of the six-membered *aepip*PNA monomer in both (2*S*,5*R*) and (2*R*,5*S*) enantiomeric forms fit into the *aeg*PNA backbone with increased Tm of the derived complexes with DNA.

Chapter 3: Applications of bisPNA for Targetting Complementary DNA: Effect of N7G in *aeg*/*aep*PNA Backbone.

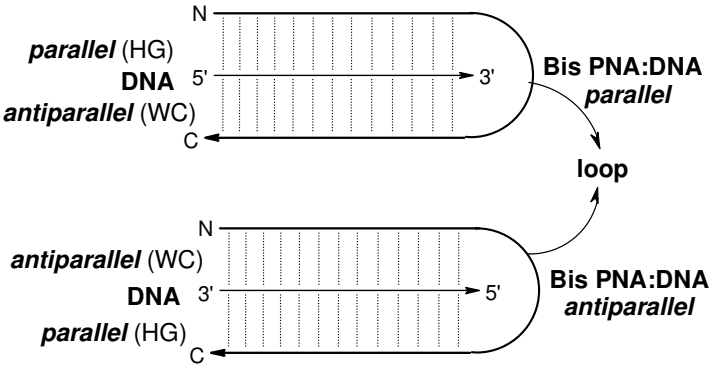

Figure 1. Triplex formation with bisPNAs

BisPNAs are obtained where two strands of homopyrimidine PNAs are connected by a flexible linker molecule. BisPNAs bind to double-stranded (ds) DNA by strand invasion leading to so-called P-loop complexes. Such PNAs can in principle be used to distinguish parallel and antiparallel binding of complementary DNA.

The work presented in this chapter involves synthesis of bisPNAs containing N7-substituted guanine (N7G), having the two arms of PNA joined by neutral

tetraethylene glycol linker (TEG) (Figure 1). The introduction of chiral, cationic aminoethylprolyl units with the C+ mimic N7G was introduced into the backbone of bisPNAs to examine its influence on the recognition of complementary DNA in an orientation-selective manner. The process of strand invasion of target DNA duplex by these modified bisPNAs is followed by a fluorescence assay, to compare the kinetics of invasion by different polypyrimidine (C/T) and purine-pyrimidine (N7G/T) mixmer-bisPNAs.

3.1. Synthesis of tetraethylene glycol linker and N7G *aeg/aep*PNA monomers. The TEG linker (**2**) was synthesized from tetraethylene glycol **1** using usual protection/deprotection chemistry. The PNA-N7G monomers (**4** & **6**) and the appropriately protected PNA-C (**7**) monomers were prepared as shown in Scheme 3.

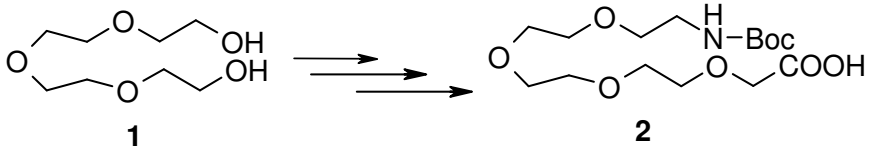

Scheme 2. Synthesis of Tetraethylene glycol linker

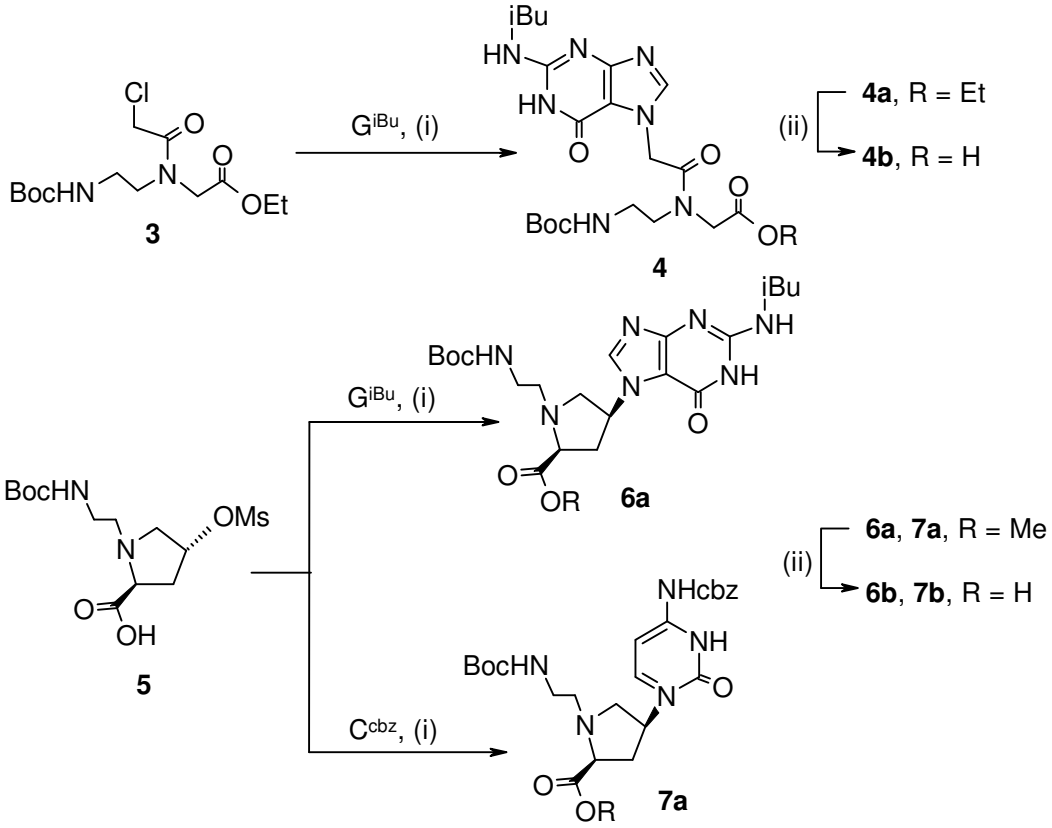

Scheme 3. Synthesis of *aeg*N^{7}G, *aep*N^{7}G, *aep*C monomers (i) K_2CO_3, 18-crown-6, DMF, (ii) NaOH, H_2O: MeOH (1:1)

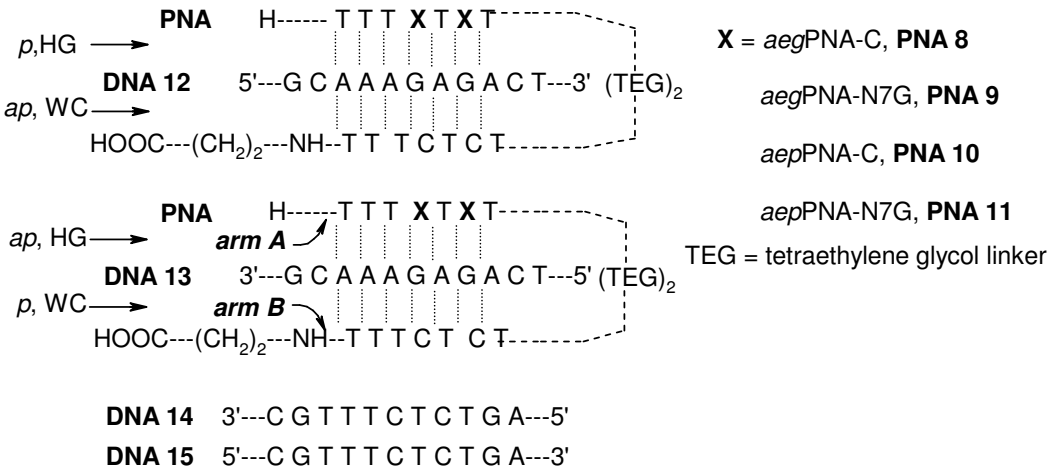

Figure 2. Design of hairpin bisPNAs.

The monomers were incorporated at appropriate positions in the PNA sequences **8-11** (Figure 2) along with the monomer **2** to introduce tetraethylene glycol linker between the two polypyrimidine arms A and B. After the assembly, the PNA oligomers were deprotected-cleaved from the resin by TFMSA-TFA, purified by HPLC and characterized by MALDI-TOF mass spectrometry.

3.2. UV-T_m studies on hairpin PNA-DNA triplexes. The oligodeoxynucleotides **12** and **13**, identical in sequence but reversed in 5'-3' direction, were used to probe the parallel/antiparallel binding preferences by UV melting experiments at pH 5.8 and 7.4. The control bisPNA **8** having *aeg*PNA-C units as X in arm A binds to either DNA **12** or DNA **13** with little different affinities at pH 7. At acidic pH 5.8, a higher Tm was seen with DNA **13** as expected from N3 protonation of cytosine.

Table 3. UV -T_m of bisPNA-DNA complexes[a]

Entry	PNA	DNA **12**		DNA**13**	
		pH 7.3	pH 5.8	pH 7.3	pH 5.8
1	**8**	21	29	27	42
2	**9**	32	29	44	41
3	**10**	23	49	42	52
4	**11**	38	30	41	44

[a]UV T_m data (^oC) for PNA:DNA complexes with DNA **12** and **13**. Experiments were performed in 10 mM sodium phosphate buffer, pH 7.3 and 5.8.

The replacement of *aeg*PNA-C at X in arm A by the C+ mimic *aeg*PNA-N7G (PNA **9**) gave complexes of different stabilities with the target DNA strands **12** and **13** with the preference for antiparallel orientation over the parallel orientation of arm A as in complex **9**:**13**. In contrast to the achiral *aeg*PNA units, introduction of a chiral *aep*PNA-C unit as X in arm A in **10** leads to a stronger binding with DNA **13** at pH 7.3. At acidic pH (5.8), the stability was further enhanced in case of both DNA **12** and **13**, as expected from the protonation of N3 in cytosine. PNA **11** containing the chiral *aep*PNA-N7G unit as X in arm A also exhibited a slightly antiparallel preference to bind DNA **13** over parallel DNA **12** at neutral pH conditions with more relative stability at acidic pH 5.8. The overall results suggest that hairpin bisPNAs having chiral units bind to DNA **13** (*parallel* HG, *antiparallel* WC) better than DNA **12** (*antiparallel* WC, *parallel* HG).

3.3. Fluorescence assay for strand invasion. The effects of nucleobase and backbone modifications of bisPNAs on the kinetics of strand invasion of a complementary DNA duplex **12:14** and **13:15** were studied by ethidium bromide displacement assay (Figure 4). The DNA duplex **12**:**14/13:15** was saturated with ethidium bromide and the kinetics of the strand invasion process was examined by monitoring the fluorescence emission decay at 590nm (λ_{ex} 490nm) as a function of time after individually adding the four PNAs **8-11** for over 60 hours.

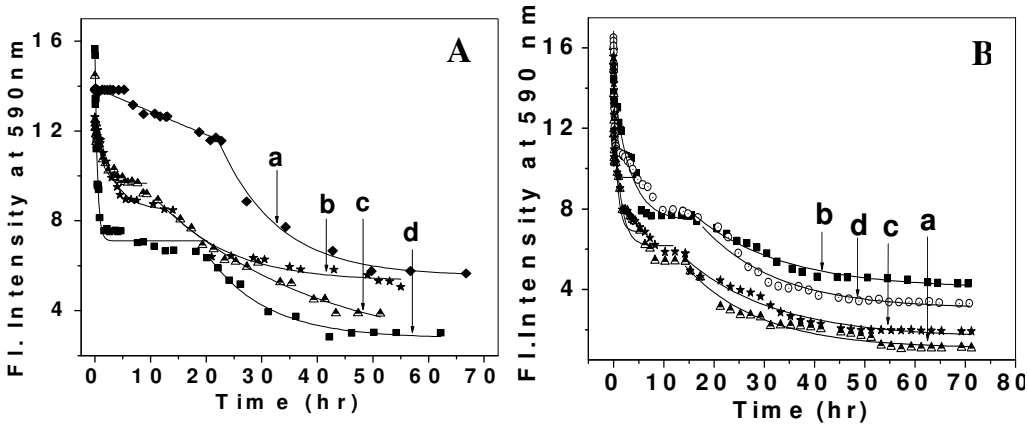

Figure 4. Ethidium bromide fluorescence as a function of time studied for the (**A**) DNA duplex **12**:**14** after the addition of PNA **8** (d); PNA **9** (b); PNA **10** (c) and PNA **11** (a) and DNA duplex **13**:**15** after the addition of PNA **8** (a); PNA **9** (b); PNA **10** (c) and PNA **11** (d) at pH 7.3.

The emission intensity monitored in each case over 60 hours showed exponential decrease at different rates followed by reaching a plateau (Figure 4). Interestingly as compared to the cationic peptide linker, the decay profile of polyoxyethylene bisPNAs was not monophasic, but could be fitted into biexponential decay, suggesting that strand invasion is a two-step process. This is in agreement with earlier conclusions based on electrophoretic studies: first step, DNA **12/13** forming HG pairing with arm A of bisPNAs **8**-**11** in a parallel binding motif and the second step leading to formation of WC pairing in antiparallel fashion.

Chapter 4A: Synthesis and biophysical evaluation of Fluorescent PNAs.

2-Aminopurine is a fluorescent isomer of adenine (6-aminopurine). The incorporation of 2-aminopurine into PNA would lead to fluorescent PNA with useful

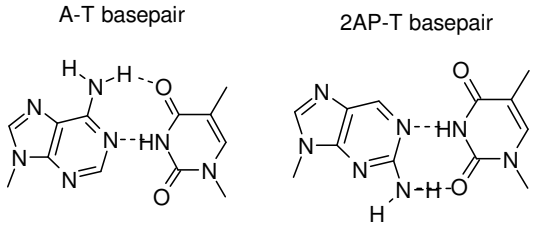

attributes. Selective excitation of 2-aminopurine in presence of standard bases (A, C, T or G) makes it ideal for use as a label, to study local environment changes resulting from PNA binding with DNA and other ligands. This chapter describes PNA-DNA hybrid formation by monitoring changes in 2-aminopurine fluorescence. The desired PNA monomer **3** carrying a 2-aminopurine moiety was synthesized in two steps

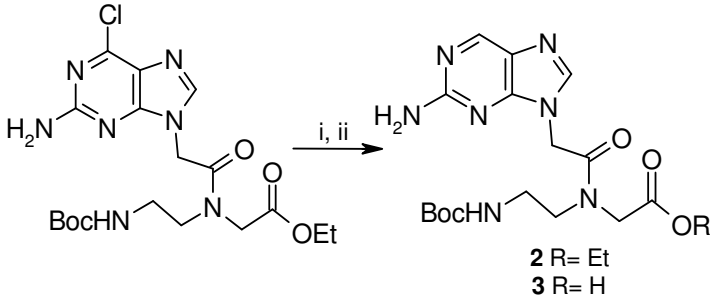

Scheme 4. Reagents I) H_2/Pd-C, ii) aq. NaOH

(Scheme 4) starting from the previously known compound ethyl N-(2-amino-6-chloropurin-9-ylacetyl)-N-(2-butoxycarbonyl-aminoeth-yl)-glycinate **1**. This monomer was directly incorporated into PNA oligomers **4** to **11**. The complementary oligonucleotides **12** and **13** designed for parallel and antiparallel PNA·DNA duplexes were synthesized on an automated DNA synthesizer.

4 H_2N–T A T T A T T A T T **A*** T T–$CONHCH_2CH_2CO_2H$
5 H_2N–T A T T A T T **A*** T T A T T– $CONHCH_2CH_2CO_2H$
6 H_2N–T A T T **A*** T T A T T A T T– $CONHCH_2CH_2CO_2H$
7 H_2N–T **A*** T T A T T A T T A T T– $CONHCH_2CH_2CO_2H$
8 H_2N–T A T T A T T A T T **A*** T T–CONH-Spermine
9 H_2N–T A T T A T T **A*** T T A T T–CONH-Spermine
10 H_2N–T A T T **A*** T T A T T A T T–CONH-Spermine
11 H_2N–T **A*** T T A T T A T T A T T–CONH-Spermine
12 DNA **5'** A T A A T A A T A A T A A **3'**
13 DNA **3'** A T A A T A A T A A T A A **5'**
A* = 2-aminopurine

PNA:DNA duplex formation: Fluorescence studies: The 2-aminopurine PNA monomer (**3**) and the PNA oligomers (**4-11**) exhibited fluorescence emission with maxima at 371nm upon excitation at 308nm. The fluorescent PNAs **4-7** upon binding to its cDNA **13** affected a decrease in fluorescence intensity indicating a successful hybridization. Similar behavior was obtained with *sp*-PNA conjugate **8-11** incorporating 2-aminopurine upon addition of cDNA **13**.

The strength of PNA self-organisation and PNA-DNA binding was also studied by temperature dependent fluorescence experiments. Upon heating, both fluorescent intensity of PNA alone and PNA:DNA duplex showed a gradual decrease.

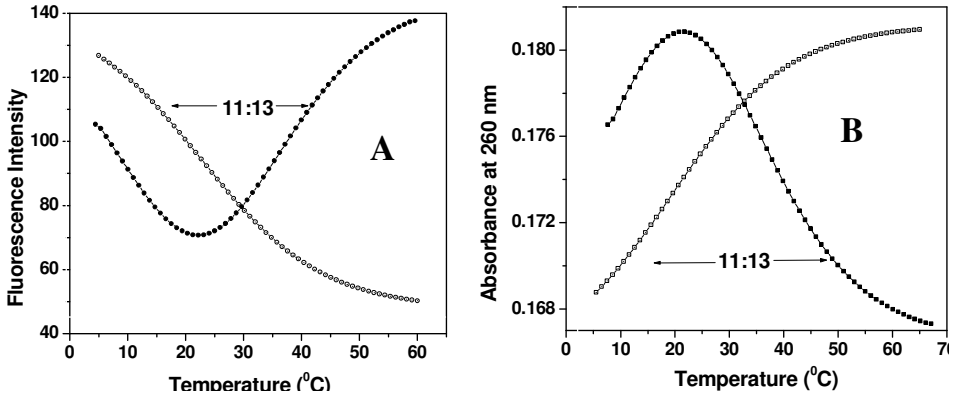

Figure 5. (**A**) Fluorescence melting isotherm and (**B**) UV melting isotherm of PNA:DNA duplex (**11:13**) shown with the first derivative plots.

The kinetics of PNA:DNA hybridization process was examined by monitoring the fluorescence emission decay at 371nm as a function of time after mixing 2-aminopurine PNA (**4-11**) with the complementary, antiparallel DNA (**13**).

Fluorescence Anisotropy: A higher fluorescence anisotropy and polarization value implies that the fluorophore is more rigid. The polarization and anisotropy values of 2-aminopurine fluorescence was measured as a function of temperature for both PNA **4-11** and PNA:DNA duplex (**4-11**:**13**). The observed overall changes in anisotropy of 2-aminopurine PNA upon mixing with DNA and/or heating, suggests its utility for monitoring such dynamic events.

This section demonstrates the incorporation of intrinsically fluorescent 2-aminopurine to monitor the binding property of PNAs with the cDNA and to follow the accompanying structural changes.

Chapter 4B: Induction of chirality in achiral *aeg* PNA.

In order to examine the influence of imparting chirality to intrinsically non-chiral PNA and its effect on the induction of PNA helical structures and stability of the PNA-DNA hybrids. Chiral ligand conjugated PNAs were synthesized and the complexes were studied by UV-T_m and CD specroscopy.

Table 4. UV-T_m(°C) of DNA:PNA_2 complexes*

	PNA
1	**14**, H- T T T T T T T T –L-Pro-(β-Ala)-OH
2	**15**, H- T T T T T T T T –D-Pro-(β-Ala)-OH
3	**16**, H-L-Pro-T T C T C T T T –(β-Ala)-OH
4	**17**, H-D-Pro- T T T T T T T T –(β-Ala)-OH
5	**18**, H- T T T T T T T T –(β-Ala)-OH

The chiral amino acids D and L-Proline were introduced at N and C-terminus of PNA octamers **14-17** (Table 5 entry 1-4) and the effect on derived PNA:DNA hybrids were examined by UV-T_m and CD spectral analyses. This section describes observed results in terms of preferred helicity induction in PNA by terminal stereogenic amino acids.

Chapter 5: Applications of isothermal titration calorimetry to study biomolecular interactions: *aeg/aep/aepip*PNAs:DNA hybrids, enzyme/nucleosides binding to nanoparticles, and chiral recognition of DNA by amino acid-modified gold nanoparticles.

Molecular recognition is a complex, fundamental process; essential for existence of life and hence understanding the thermodynamics governing such processes is of enormous interest. The isothermal titration calorimetry (ITC) has now become a valuable tool for measurement of thermodynamic data relating to molecular associations. In a single experiment, ITC gives information on the association constant (K_a), stoichiometry (n), free energy (ΔG°), enthalpy (ΔH°) and entropy (ΔS°) of binding.

(I) Thermodynamic study of PNA/DNA interactions.

Despite much research in characterizing PNA/DNA interactions, the thermodynamic data on PNA/DNA hybridization interactions have been largely determined so for indirectly from UV-melting studies. In this section the aim is to evaluate the different thermodynamic parameters [enthalpy (ΔH), binding entropy (ΔS), binding constant (k), and Gibb's free energy (ΔG)] for interactions of modified PNA with DNA by ITC. The isothermal titration calorimetry experiments were done with *aep* and *aepip*PNAs synthesized in chapter 2 with their complementary DNAs (Table 5). The results are discussed in relation to structural modifications.

Table 5. Thermodynamic quantities for PNA/DNA hybridization reactions from ITC measurements.

PNA	*aepip*PNA (2S,5R)	Uv-T_m (^{0}C)	ITC (kcal/mole)		
			-ΔH	-ΔG	TΔS
1	H-tTTTTTTT–(β-Ala)-OH	43.0	108	44.9	-63
2	H-TTTTTTTt–(β-Ala)-OH	48.0	89	45.6	-43
3	H-tTCTCTTT–(β-Ala)-OH	60.0	61	47.4	-14
4	H-ATGtTCTCTTT–(β-Ala)-OH	57.8	89	47.0	-42
5	H-TTTTTTTT–(β-Ala)-OH	43.0	134	44.9	-89
6	H-TTCTCTTT–(β-Ala)-OH	51.0	89	46.0	-43
7	H-ATGTTCTCTTT–(β-Ala)-OH	51.2	90	46.1	-43
	***aep*PNA (2S,4S)**				
8	H-t t t t t –(β-Ala)-OH	37.5	50	44.1	-6
9	H-t t t t t t t –(β-Ala)-OH	>85	60	50.9	-9

10	H-tTTTTT–(β-Ala)-OH	42.5	13	44.9	32
11	H-TTTt TT–(β-Ala)-OH	45.2	28	45.2	17
12	H-TTTTTt –(β-Ala)-OH	42.4	13	44.8	32
13	H-TTTTT–(β-Ala)-OH	21.0	35	41.8	7
14	H-TTTTTTT–(β-Ala)-OH	32.6	72	43.4	-28
15	H-TTTTTT–(β-Ala)-OH	26.2	64	42.5	-21

The ITC results are rationalised in relation to thermal stabilities seen by UV-T_m.

(II) Nucleosides binding on keggin nanoparticle.

DNA-based nanotechnology has generated considerable interest in a number of applications due to the specificity, programmability and reproducibility of DNA interaction with nanoparticles. Keggin ions are polyoxometalates, which are well, defined metal-oxygen cluster anions. They participate in catalytic redox processes as electron relays. Similar applications can be envisaged for the keggin ions and DNA nucleosides. We show here that ITC may be used to directly observe the energetics of interaction of the DNA nucleosides with keggin ions. The ITC data (Figure 6) shows that strength of interaction of the nucleosides decreases in the order dA > dG > dC > dT indicating that exocyclic amine groups may be responsible for binding as in case of aqueous Au-NPs. The observed differential binding strengths of the four nucleosides may be useful to develop suitable strategies of designing oligonucleotides for interaction with ligands.

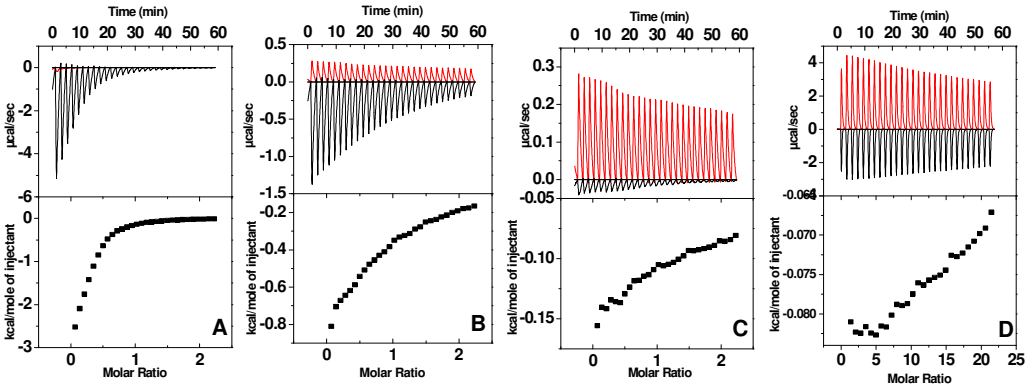

Figure 6. ITC data recorded for Keggin- DNA nucleosides interactions A – D correspond to keggin interaction with nucleosides C, A, G and T respectively.

(III) Chiral recognition of DNA by amino acid-modified gold nanoparticles.

As part of ongoing investigation into the use of ITC in nanobioconjugate chemistry, we address the following question: can ITC differentiate between recognition interactions occuring on the surface of nanoparticles based on the chirality of the nanoparticle surface? A preferred handedness (chirality) on the surface of gold nanoparticles may be induced by modifying the surface of the nanoparticles through chiral capping ligands such as L- or D-lysine.

We studied the interaction of chiral DNA templates with the L- and D-lysine modified gold nanoparticles by ITC. D-lysine modified gold nanoparticles that are positively charged were found to bind more strongly to negatively charged DNA than the L-lysine modified nanoparticles. This suggests a chirality-based recognition of the modified gold nanoparticle surface by DNA. In addition to ITC, the differential interaction of L- and D-lysine-modified gold nanoparticles before and after complexation with DNA have also been studied by circular dichroism CD spectroscopy and results are presented.

(IV) Study of Fungal protease binding on gold nanoparticles.

Immobilization of biomolecules on different surfaces provides novel biomaterials that have useful applications in the areas such as immunosensors and biomedical devices. Such encapsulation protects the biomolecules e.g. enzymes against degradation, aggregation and deamidation while rendering the enzymes accessible to substrates and co-factors for biosensing and biocatalytic applications. Gold nanoparticles are biocompatible, bind readily to a range of biomolecules such as amino acids, proteins/enzymes, and DNA and expose large surface areas for immobilization of biomolecules.

In this section ITC is used to measure interactions between the fungal protease (F-prot) in solution and gold nanoparticle bioconjugates with the substrate haemoglobin (Hb). It was observed that the interactions between the free enzyme and haemoglobin in solution are strong as compared to the enzyme-gold nanoparticle conjugates (Figure 7, 8). CD spectroscopy was used to monitor the changes in secondary structures of the F-prot in the bioconjugates as compared with the free enzyme in solution. These studies indicate that the altered secondary structure of the

enzyme in the bioconjugates may cause weak interactions with the substrate compared with the free enzyme in solution and related to decrease in its biocatalytic activity.

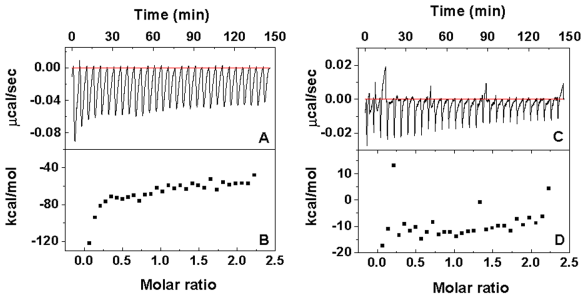

Figure 7. ITC titration data describing the interaction of substrate Hb with free enzyme F-prot in solution and in immobilized form at pH 3.

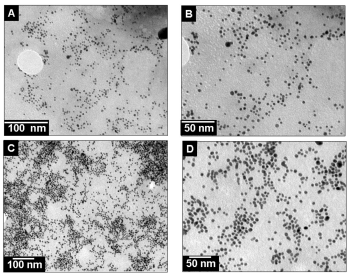

Figure 8. (A), (B) and (C), (D) Representative TEM images of gold and F-prot gold nanoparticle bioconjugate.

PUBLICATIONS/ CONFERENCES/SYMPOSIA PARTICIPATED

PUBLICATIONS

1) Chimeric peptide nucleic acids incorporating (2*S*,5*R*)-aminoethyl pipecolyl units: synthesis and DNA binding studies. **Shirude, P. S.**; Kumar, V. A.; Ganesh, K. N. *Tetrahedron Lett.* **2004**, *45,* 3085- 3088.

2) (2*S*,5*R*/2*R*,5*S*)-Aminoethylpipecolyl *aepip-aeg*PNA chimera: synthesis and duplex/triplex stability. **Shirude, P. S.**; Kumar, V. A.; Ganesh, K. N. *Tetrahedron,* **2004**, *60*, 9485-9491.

3) Isothermal titration calorimetry studies on the binding of amino acids to gold nanoparticles. Joshi, H.; **Shirude, P. S.**; Bansal, V.; Ganesh, K. N.; Sastry, M. *J. Phys. Chem. B* **2004**, 108, 11535-11540.

4) Synthesis of aqueous Au core-Ag shell nanoparticles using tyrosine as a pH-dependent reducing agent and assembling phase-transferred silver nanoparticles at the air-water interface. Selvakannan, PR.; Swami, A.; Srisathiyanarayanan, D.; **Shirude, P. S.**; Pasricha, R.; Mandale, A. B.; Sastry, M. *Langmuir.* **2004**, 20, 7825-7836.

5) Studies on the structure and the interactions of the fungal protease immobilized on gold nanoparticles during the biocatalytic reactions. **Shirude, P. S.**; Phadtare, S.; Joshi, H.; Vinod, V. P.; Ganesh, K. N.; Sastry, M. *Biotech. Progress* **2005** (communicated).

6) Isothermal titration calorimetry studies on the binding of DNA nucleosides to keggin ions. **Shirude, P. S.**; Prasad, S. D.; Ganesh, K. N.; Sastry, M. *Chem. Commun.* **2005** (communicated).

7) Chiral recognition of DNA by amino acid-modified gold nanoparticles: an isothermal titration calorimetry study. **Shirude, P. S.**; Joshi, H. P.; Ganesh, K. N.; Sastry, M. *J. Am. Chem. Soc.* **2005** (communicated).

8) Isothermal titration calorimetry study of the binding of different metal ions with sodium dodecyl sulfate (SDS). Bala, T.; Joshi, H.; **Shirude, P. S.**; Prasad, B. L. V.; Sastry, M. *J. Colloid. Interf. Sci.* **2005** (communicated).

9) Isothermal titration calorimetric investigation of the binding of keggin ions to amino acids. Sanyal, A.; **Shirude, P. S.**; Sastry, M. *J. Phys. Chem. B* **2005** (communicated).

SYMPOSIA/CONFERENCES ATTENDED

- Fourth National Symposium of the Chemical Research Society of India, National Chemical Laboratory, Pune, India, 2002.
- Shirude, P. S.; Kumar, V. A.; Ganesh, K. N. Title: **Conformationally Restricted Cationic Aminoethyl Pipecolyl Peptide Nucleic Acids (*aepip*PNA): Design, Synthesis and DNA Binding Studies**. RSC-student symposium, West India section, held at IIT-Bombay from 24th-25th Sept 2004. **(Poster)**
- Shirude, P. S.; Joshi, H. S.; Phadtare, S; Vinod, V. P.; Rao, M.; Sastry, M.; Ganesh, K. N. Title: **Studies on the Structure and Interactions of Fungal Protease Immobilized on Gold Nanoparticles during Biocatalytic Reactions** . Raman Memorial Conference, held at Pune University from 24th-25th Feb 2005. **(Oral presentation)**
- Shirude, P. S.; Rao, M.; Sastry, M.; Ganesh, K. N. Title: **Studies on the Structure and Interactions of Fungal Protease Immobilized on Gold Nanoparticles during Biocatalytic Reactions**. Nanoscience & Technology Conference, held at NCL, Pune from 7th-8th March 2005. **(Poster)**

CHAPTER 1:

INTRODUCTION

1.1. INTRODUCTION

DNA is the basic hereditary material in cells and contains all the information necessary to make proteins. DNA is a linear polymer that is made up of nucleotide units. The nucleotide unit consists of a base, a deoxyribose sugar, and a phosphate. There are four types of bases: adenine (A), thymine (T), guanine (G), and cytosine

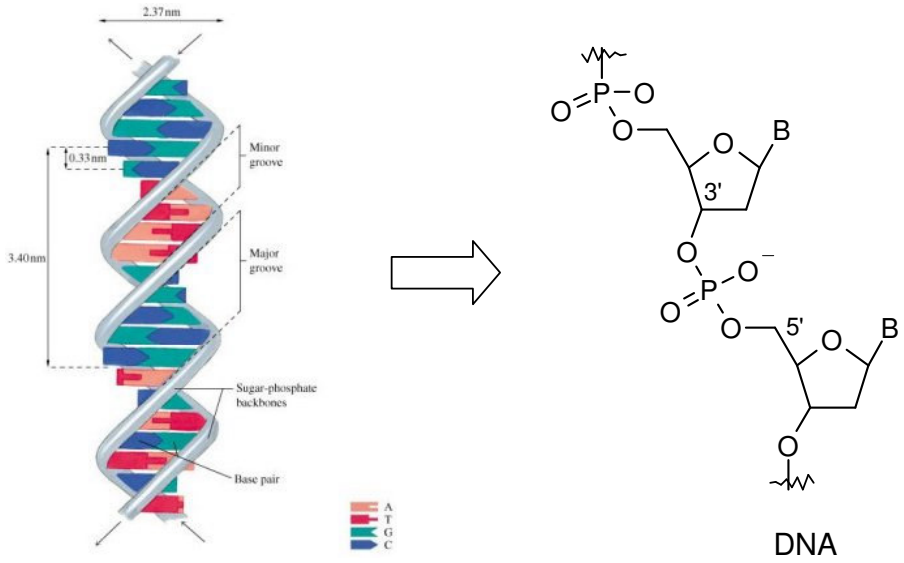

(C). Each base is connected to a sugar via a β̃glycosyl linkage. The nucleotide units are connected via the O3' and O5' atoms forming phosphodiester linkages. In normal DNA, the bases form pairs: A to T and G to C, which is “complementarity” principle. Two complementary chains that are arranged in an antiparallel manner form a duplex of DNA. The results of fiber and single crystal x-ray crystallographic studies have shown that DNA can have several conformations. The most common one is called B-DNA, which is a right-handed double helix with a wide major groove and narrow minor groove. The bases are perpendicular to the helix axis. DNA can also exist in the A form, in which the major groove is very deep and the minor groove is quite shallow. A very unusual form of DNA is the left-handed Z DNA. In this DNA, the

basic building block consists of two nucleotides, each with different conformations.[1] The recognition of DNA or RNA sequences by complementary oligonucleotides is a central feature of molecular biology and biotechnology and is important for hybridization-based biological applications.

1.2. GENE BASED THERAPEUTIC DRUG DESIGN

Zamecnik and Stephenson[2] were the first to propose, in 1978, the use of synthetic antisense oligonucleotides for therapeutic purposes. They used a 13-mer oligonucleotide that was complementary to the RNA of Rous sarcoma virus to inhibit the growth of this virus in cell culture. The principle mode of action of these modified oligonucleotides (ODNs) is through binding *via* Watson-Crick base pairing[3] to a specific mRNA sequence associated with a diseased state. The subsequent inhibition of the translational event leads to inhibition of synthesis of corresponding disease causing protein (antisense strategy).[4] The process of binding of the oligonucleotides to a complementary nucleic acid is called hybridization. In addition, the binding of an ODN can also inhibit transcription to a duplex DNA *via* formation of triple helix (antigene strategy)[5] (Figure 1).

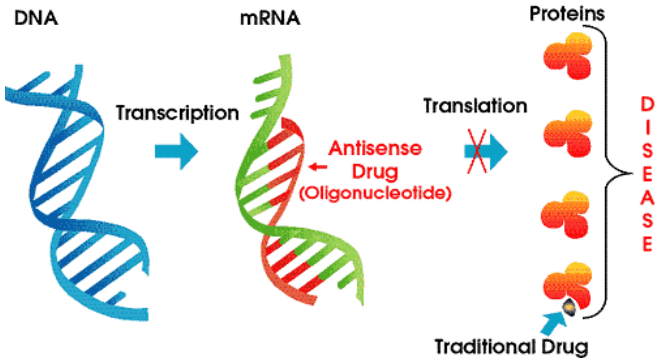

Figure 1: Antisense and antigene technology.

In the 'antigene' concept, similar to antisense approach, the therapeutic oligonucleotide is targeted to the complementary duplex DNA principally through Hoogsteen base pairing[6] (Figure 2). This leads to inhibition of DNA transcription and replication.

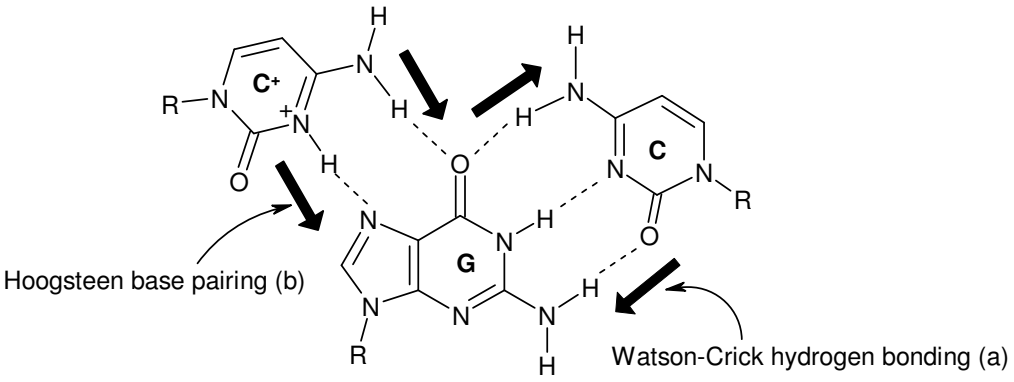

Figure 2. a) Watson-Crick hydrogen-bonding scheme for G:C base pairs and b) Hoogsteen base pairing scheme for C:G base pairs.

Antisense oligonucleotides (AS-ONs) usually consist of 15–20 nucleotides, which are complementary to their target mRNA. As illustrated in Figure 3, two major mechanisms contribute to their antisense activity. The first mechanism is inhibition of translation by steric blockade of the translation machinery[7] by the bound AS-ONs. The second mechanism is activation of RNase H, which specifically cleaves the RNA moiety of a DNA/RNA heteroduplex and thereby leading to degradation of the target mRNA.

A) Blocking of Translation:

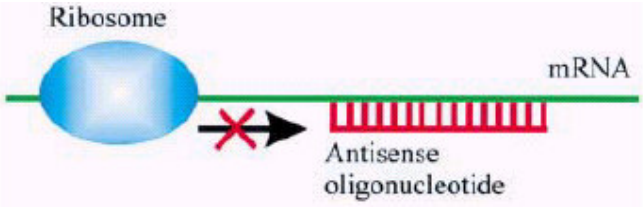

B) RNase H Clevage:

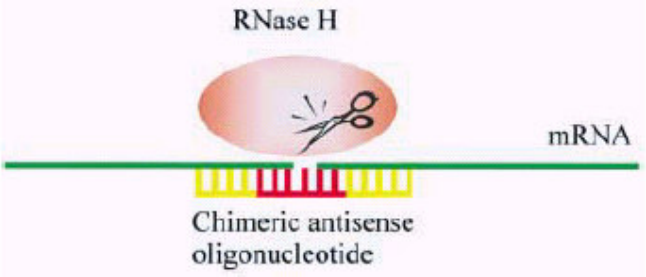

Figure 3. Mechanisms of antisense activity. (A) Translational arrest by blocking the ribosome. (B) RNase H cleavage induced by (chimeric) antisense-oligonucleotides.

1.2.1 Advantages of Oligonucleotides for Chemical Genetics

Nucleic acids possess significant advantages as chemical genetic tools for manipulating cellular processes.[8,9] The most obvious advantage is use of a target gene sequence to design the complementary oligonucleotide as a high-affinity ligand. Among the several possible sequences, particular sequences are chosen based on some empirical rules or by "mRNA walking" protocols of various sequences for activity. The automated synthesis of ONs makes it possible to obtain hundreds of oligonucleotides for large-scale investigations of genome function, whereby potent inhibitory oligonucleotides are identified and tested. Oligonucleotides that contain mismatched bases can serve as controls to establish the mechanism and specificity of the observed phenotype. A practical hope for therapeutic development is that one oligonucleotide, Fomivirsen, is FDA approved antisense drug, demonstrating the "proof of concept" of this class of molecules to advance through the stringent regulatory process, while several others are in clinical trials.[8,9] Clinical experience demonstrates that oligonucleotides can be efficacious and can be synthesized on large scale for systemic administration. Oligonucleotides have become a realistic option for

therapy, and their favorable properties will reduce the time needed to translate a lead compound into a drug that can be tested in the clinic. In antisense therapeutic strategy a different "drug" means a different "sequence" of oligonuleotide.

1.3. ANTISENSE-OLIGONUCLEOTIDE MODIFICATIONS

One of the major challenges for antisense approaches is the stabilization of ONs, as unmodified oligodeoxynucleotides are rapidly degraded in biological fluids by nucleases, lack the ability to penetrate through the cell membrane and possess relatively poor water solubility. In order to overcome all these limitations it is necessary to chemically modify the oligonucleotides in a suitable manner. One-modification strategies include appending with polyamines and cationic peptides to increase the aqueous solubility and improve binding to the target DNA. Several other types of chemically modified nucleotides[10] have been used in antisense experiments. In general, three types of modifications of oligonucleotides can be distinguished (Figure 3): analogs with unnatural bases modified sugars (especially at the 2' position of the ribose) or altered phosphate backbones.[11]

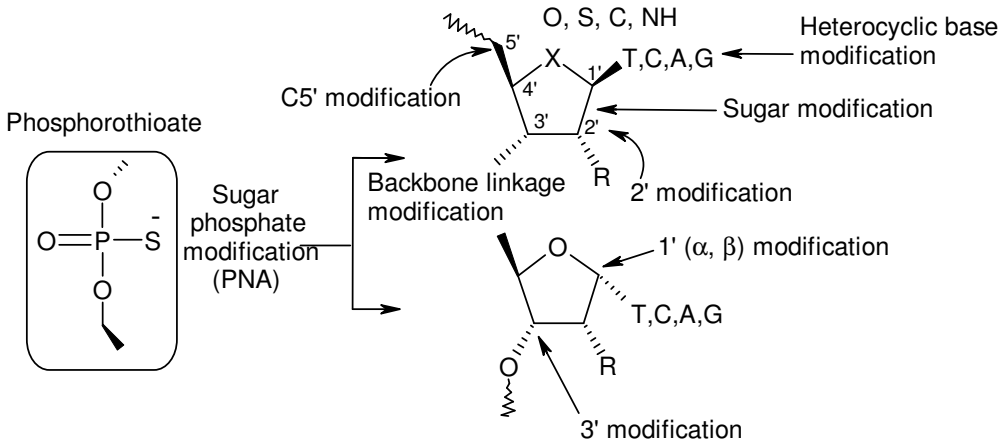

Figure 4. Structurally possible DNA modification sites.

1) 'First generation' antisense-oligonucleotides

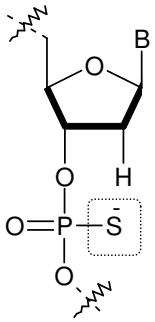

Phosphorothioate (PS) oligodeoxynucleotides are the major representatives of first generation DNA analogs that are the best-known and most widely used AS-ONs to date.[12] In this class of ONs, one of the nonbridging oxygen atoms in the phophodiester bond is replaced by sulfur. PS DNA ONs were first synthesized in the 1960s by Eckstein and colleagues[13] and were first used as AS-ONs for the inhibition of HIV. In addition to nuclease resistance, PS DNAs form regular Watson–Crick base pairs, activate RNase H, carry negative charges for cell delivery and display attractive pharmacokinetic properties. But the major disadvantage of PS oligodeoxynucleotides is their non-specific binding to certain proteins, particularly those that interact with polyanions such as heparin-binding proteins. Phosphorothioates are chiral at P and this leads to problems in stereospecific synthesis.

2) 'Second generation' antisense-oligonucleotides

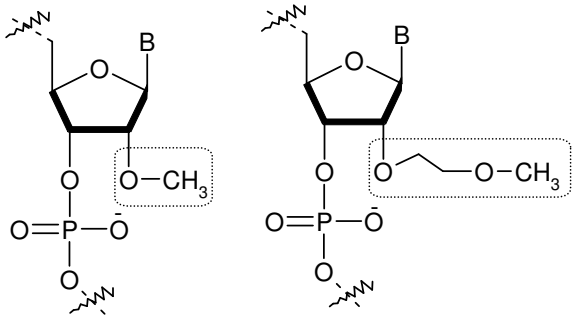

The problems associated with phosphorothioate oligodeoxynucleotides are to some degree solved in second generation ONs containing sugars with *O*-alkyl modifications at the 2' position of the ribose. 2'-*O*-methyl and 2'-*O*-methoxy-ethyl RNA are the most important members of this class of ONs. AS-ONs made of these building blocks are less toxic than phosphorothioate DNAs and have a slightly enhanced affinity towards their complementary RNAs.[14,15]

These desirable properties are, however, counterbalanced by the fact that 2'-*O*-alkyl RNA cannot induce RNase H cleavage of the target RNA. Mechanistic studies of the RNase H reaction has revealed that a correct geometry of the minor groove of the AS-ON:RNA duplex (closer to A-type rather than B-type), flexibility of the AS-ON and availability of the 2'-OH group of the RNA are essential for efficient RNase H cleavage.[16] Hence modifications that affect these parameters are poor activators of RNase H.

3) 'Third generation' antisense-oligonucleotides

In recent years a variety of modified nucleotides have been developed to improve properties such as target affinity, nuclease resistance and pharmacokinetics. The concept of conformational restriction has been used widely to enhance the

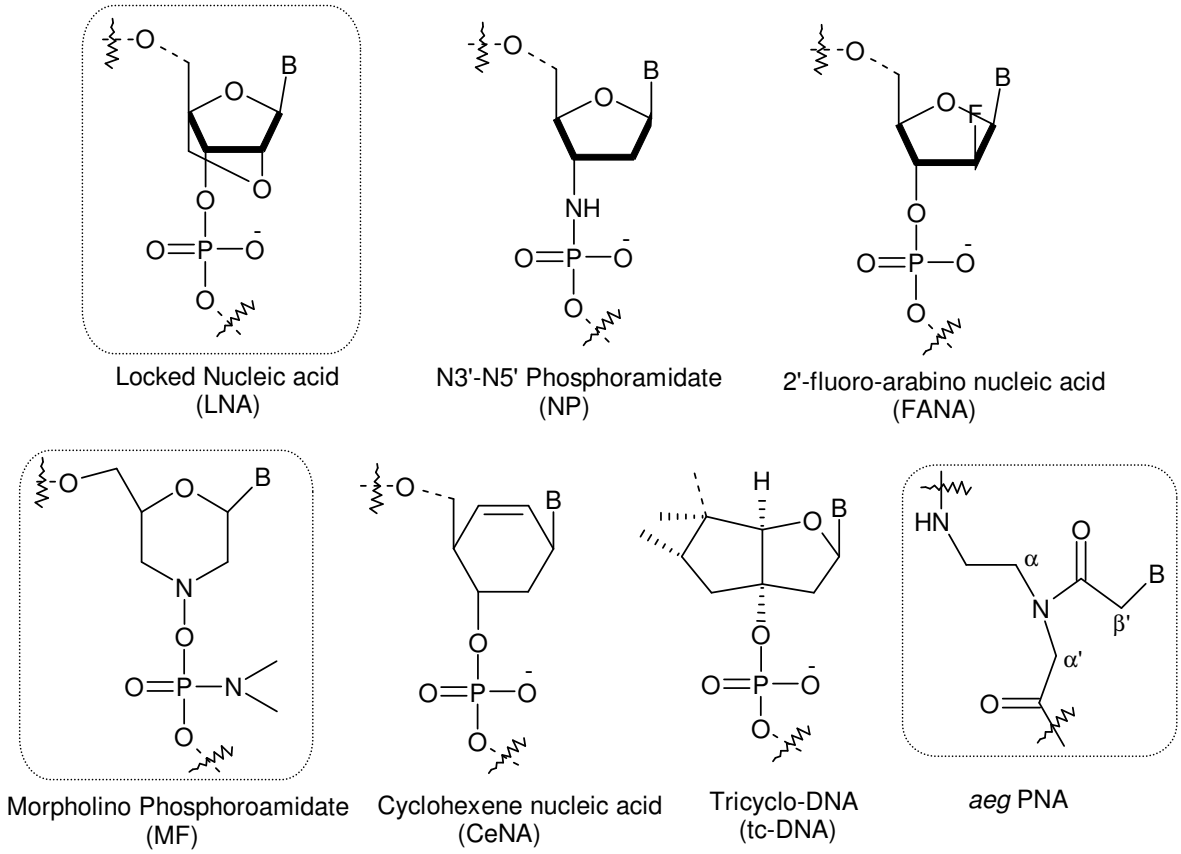

Figure 5. Third generation antisense oligonucleotides.

binding affinity and biostability. In comparison to the previous strategies of first generation phosphorothioate DNA and second-generation 2'-*O*-alkyl-RNA, the 'third generation' antisense agents comprise of modifications that are directed to conformationally preorganize the monomer structure towards that found in oligomers (Figure 5). DNA and RNA analogs with modified phosphate linkages or riboses as well as nucleotide analogs/mimics with a completely different chemical backbone substituting the furanose ring have been developed. Some examples are shown in Figure 5. In LNA, the conformations of the flexible deoxyribose rings determine the overall structure of a (deoxy)ribo nucleic acid duplex. Duplexes in A-type conformation contain nucleotides with an N-type (C3'-*endo*) sugar conformation while B-type duplexes contain nucleotides with an S-type (C2'-*endo*) sugar conformation.[17] Due to the low energy barrier between these two conformations [~2 kcal/mol] nucleotides are not trapped completely in either conformation, but rather exist in a fast equilibrium.

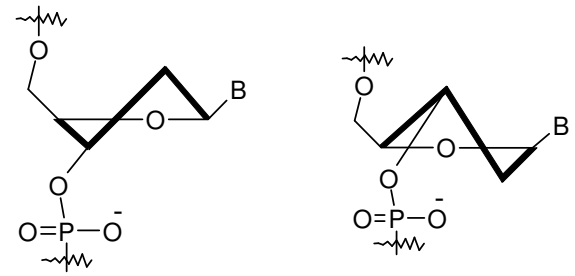

LNA

Some of third generation antisense oligonucleotides like LNA, MF and PNA have shown new promising biological activity with high potential for development as antisense drugs.

1.4. PEPTIDE NUCLEIC ACIDS

Peptide nucleic acids (PNA) have been known for almost fifteen years and during this time, some but not all of the promises expected from this molecule have materialized. Most important property of PNA is the high affinity binding of complementary DNA and RNA sequences with Watson-Crick base pairing mechanism and without compromising the sequence specificity. Most success has been achieved with diagnostic use of PNA oligomers in hybridization (in particular in situ hybridization) and PCR (polymerase chain reaction) based technologies.[18,19,20] The development of PNA oligomers into gene therapeutic drugs is still in its infancy. However, major progress - in particular concerning cellular delivery - has been made within the past couple of years.[21,22] The stability of PNA to nucleases and proteases is expected to increase its bioavailability within the cell to favour target binding.

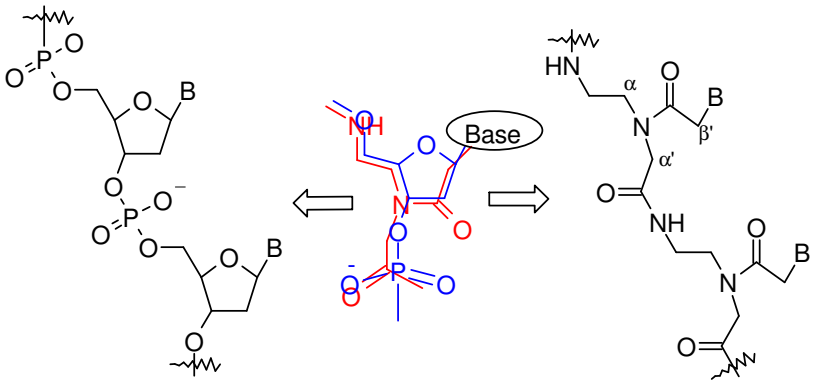

DNA (I) **_aeg_ PNA (II)**

Not surprisingly, the very simple structure of PNA in combination with its impressive DNA (I) mimicking properties was an immediate inspiration and open invitation for synthetic organic chemists to make derivatives and analogues of aminoethyl glycinyl PNA (II). The aim was towards a better understanding of the physico-chemical properties of this molecule as well as efforts to improve its

"biological" properties.[18] PNAs recognize complementary DNA/RNA by Watson-Crick hydrogen bonding and are true DNA mimics in terms of base-pair recognition. PNAs being peptides possess amine and carboxy termini instead of 3' to 5' polarity of DNA and can bind DNA/RNA in either parallel or antiparallel modes. [Although PNA does not show predominant preferences for binding DNA/RNA in either direction, in general the antiparallel mode is slightly preferred over the parallel one.[23]] In the antiparallel mode the PNA 'N' terminus is towards the 3'- end and the 'C' terminus, towards the 5'- end of the complementary DNA/RNA oligonucleotide. The parallel mode of binding consists of PNA 'N' terminus being towards the 5'- end with the 'C' terminus towards the 3'- end of the complementary DNA/ RNA oligonucleotide (Figure 6).

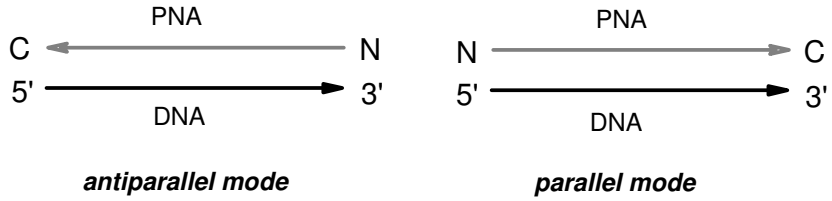

Figure 6. Parallel and antiparallel modes of PNA-DNA binding.

1.4.1. Peptide nucleic acid (PNA): Targeting Double Stranded DNA

PNA was originally conceived as a mimic of a triplex forming oligonucleotide.[17] However, despite being an extremely efficient structural mimic of DNA (or RNA), homopyrimidine PNAs do not bind very efficiently to double stranded DNA targets by triplex formation, but through a very interesting alternating mechanism: duplex invasion (Figure 7).[24]

During this process, the complementary PNA binds to duplex and displaces the existing complementary DNA strand followed by binding of a second PNA strand to form PNA_2:DNA triplexes.[25]

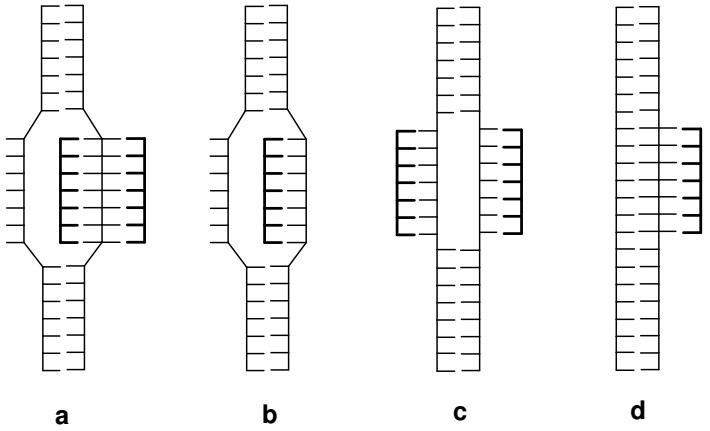

Figure 7. Strand invasion complexes **a.** Triplex invasion **b.** Duplex invasion **c.** Double duplex invasion **d.** Third strand binding forming a PNA:DNA$_2$ complex.

1.4.2. PNA complex stability

Duplexes between PNA and DNA or RNA are in general thermally more stable than the corresponding DNA-DNA or DNA-RNA duplexes.[22,26] The sequence dependence of the stability is more complex than that found for DNA-DNA complexes because of the inherent asymmetry of the duplex. In fact PNA-DNA duplexes show significantly increased stability when purines are in the PNA strand. In addition to the G-C content, the stability of PNA:DNA duplexes also depends on the purine fraction of the PNA strand as expressed in the empirical formula derived for the thermal stability of PNA-DNA duplexes.[27]

In general it is observed that the thermal stability of PNA-PNA duplexes exceeds that of PNA-RNA duplexes, which are more stable than PNA-DNA duplexes. Importantly the stability of PNA-DNA duplexes are almost unaffected by the ionic strength of the medium (actually the stability decreases slightly with increasing Na^+ concentration due to counterion release upon duplex formation). This is in sharp contrast, of course, to the behavior of DNA-DNA (or RNA) duplexes, the stability of

which decreases dramatically at low ionic strength because of the requirement of counterion shielding of the phosphate backbone.[28]

PNA hybridization kinetics have been studied by BIAcore technology and the results indicate no major difference in PNA and DNA hybridization duplex formation.[26] Though PNA_2:DNA triplexes exhibit extraordinary high stability, the rate of formation of such ternary triplexes is slow giving rise to significant hysteresis in the thermal transition.

1.4.3. Structure of PNA complexes

So far the three-dimensional structures of four PNA complexes have been determined. The PNA-RNA[29] and PNA-DNA[30] duplex structures were determined by NMR methods, while the structures of a PNA_2DNA triplex[31], PNA-PNA duplex[32] and PNA-RNA duplex were solved by X-ray crystallography. Several general conclusions can be drawn from these structural studies (Figure 8).

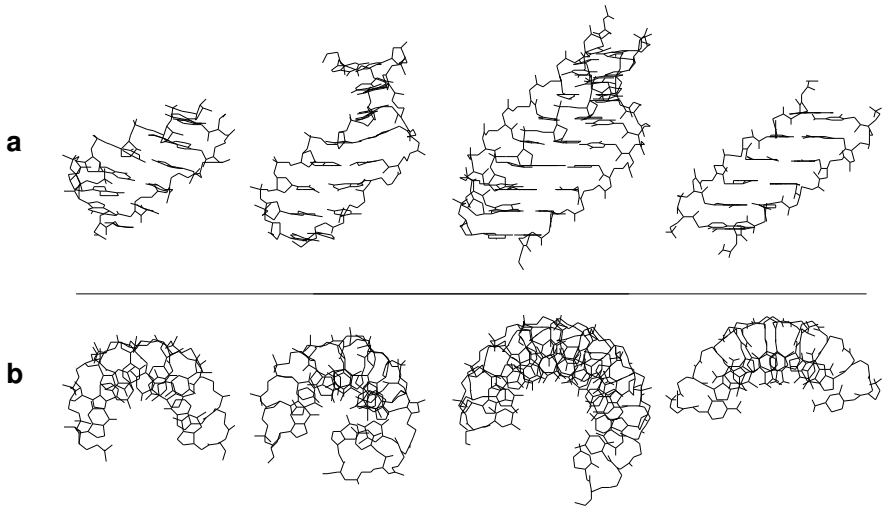

Figure 8: Structures of PNA complexes shown in side view (**a**) and top view (**b**). The complexes from left to right are PNA:RNA, PNA:DNA, PNA:DNA:PNA and PNA:PNA.

PNA is able to a great extent to adapt to its partner's conformation in the complexes. In the PNA-RNA and PNA-DNA duplexes the oligonucleotide adopts close to its natural A and B-conformations respectively in terms of sugar puckering, while the helix parameters have both A and B-form characteristics. The PNA however, prefers a unique, different helix form, the P-form, which is adapted to some extent in the PNA_2:DNA triplex and completely in the PNA-PNA duplex. This P-helix is very wide (28Å diameter) and has a very large pitch (18 base pairs). In terms of base pair conformations it is a very regular helix, and the base pairs are virtually perpendicular to the helix axis.

1.5. CHEMICAL MODIFICATIONS OF PNA

The structure of the classical PNA monomer has been subjected to a variety of rational modifications with the aim of understanding the structure-activity relationship in this class of DNA mimics as well as obtaining PNA oligomers with specifically improved properties for various applications in medicine, diagnostics and molecular biology. The limitations of PNA for such applications include low aqueous solubility, ambiguity in DNA binding orientation and poor membrane permeability. Structurally, the analogues can be derived from modifications in the ethylenediamine or glycine part of the monomer, linker to the nucleobase, the nucleobase itself or a combination of the above. The strategic rationale behind the modifications are (i) introduction of chirality into the achiral PNA backbone to influence the orientational selectivity in complementary DNA binding, (ii) rigidification of PNA backbone *via* conformational constraint to pre-organize the PNA structure and entropically drive the duplex formation, (iii) introduction of cationic functional groups directly in the PNA

backbone, in a side chain substitution or at the N or C terminus of the PNA to improve water solubility (iv) modulate nucleobase pairing either by modification of the linker or the nucleobase itself for effective binding at physiological conditions and (v) conjugation with 'transfer' molecules for effective penetration into cells. In addition to improving the PNA structure as above for therapeutics, several modifications are directed towards their applications in diagnostics. Some of the modifications are discussed below.

The earliest and the simplest of the modifications involved extension of the PNA structure with a methylene group individually in each of the structural sub-units (aminoethyl,[33] glycine[34] and base linker[34]) of the PNA monomer. These resulted in PNAs with N-(2-aminoethyl)-β-alanine (Figure 9**a**) and N-(3-aminopropyl)glycine **b** backbone and ethylene carbonyl linked nucleobase **c**. However, these modifications resulted in a significant lowering of T_m of the derived PNA:DNA hybrids. The deleterious consequences of such subtle changes to the PNA structure suggested the high structural organization to which the original PNA structure is inherently tuned for interaction with DNA.

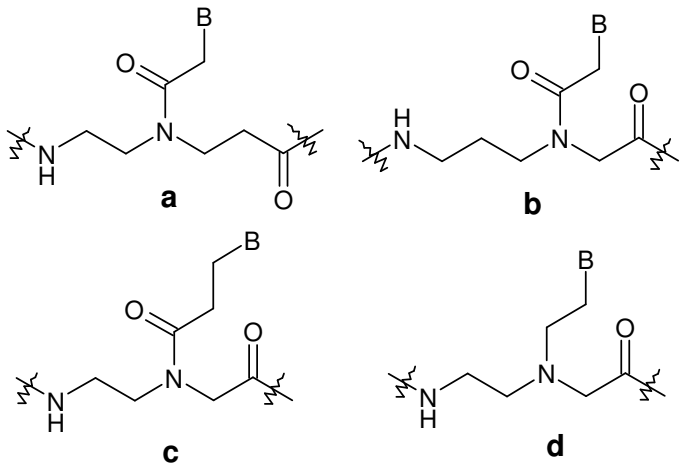

Figure 9. PNA modifications.

The replacement of the tertiary amide carbonyl by a methylene group leading to a flexible, cationic tertiary amine monomer **d** resulted in a large destabilization of the PNA:DNA hybrids.[35] The necessity of such a pseudo rigid amide group pointed to the importance of constrained flexibility in the backbone.

Improvement of aqueous solubility of PNAs has been achieved by the introduction of charges within the molecule or by the introduction of ether linkages in the backbone (Figure 10).

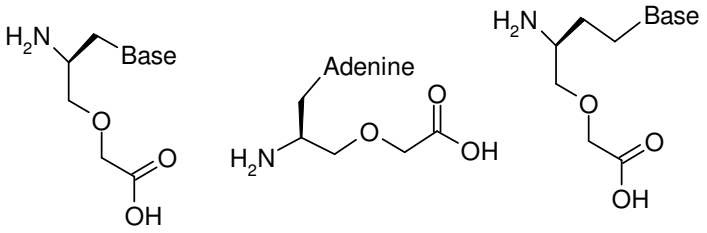

Figure 10. Ether-linked PNA (OPNA).

Making PNA anionic also aided in increasing the water solubility as in the case of the phosphonate analogs, but was accompanied by a decrease in the binding affinity to complementary nucleic acid sequence[36,37,38,39,40] (Figure 11).

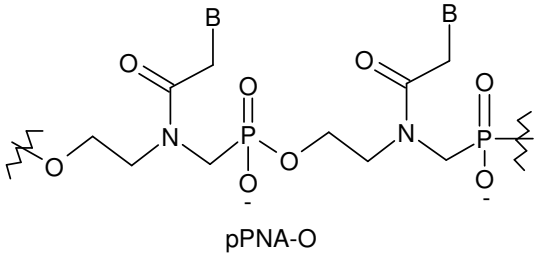

Figure 11. Phosphonate PNA.

The chiral versions of these analogs similar to original PNAs led to excellent aqueous solubility properties. PNAs composed of monomers derived from serine and

homoserine coupled by ether linker with glycine or alanine, were able to bind sequence specifically to RNA, though with much weaker affinity.[41, 42]

Novel class of cationic PNA (DNG/PNA), which binds to DNA/RNA targets with high affinity, has been also reported[43] (Figure 12a). In another report, guanidium functional group was introduced into the PNA backbone, which exhibited remarkable cellular uptake properties while maintaining Watson-Crick recognition with complementray DNA strand[44] (Figure12b).

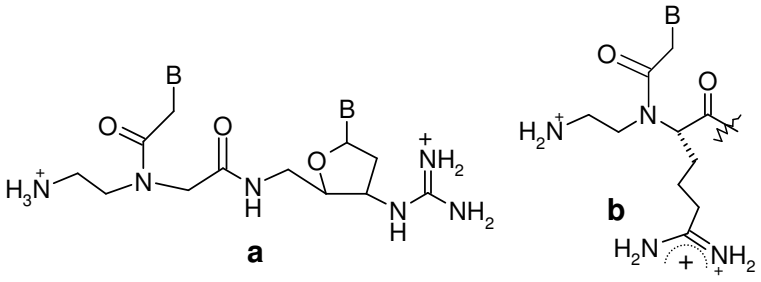

Figure 12. a) PNA-DNG chimera b) GPNA.

Another type of modification involved interchanges of various CO and NH groups on the peptide linkages leading to retero inverse,[45-46] peptoid[46] and heterodimeric analogs[47] (Figure 13). Except for the heterodimer analogue (Figure 13c), these exhibited a lower potency for duplex formation with complementary DNA/RNA suggesting that in addition to geometric factors, other subtle requirements such as hydration and dipole-dipole interactions influencing the environment of backbone, may be involved in effecting efficient PNA:DNA hybridization.

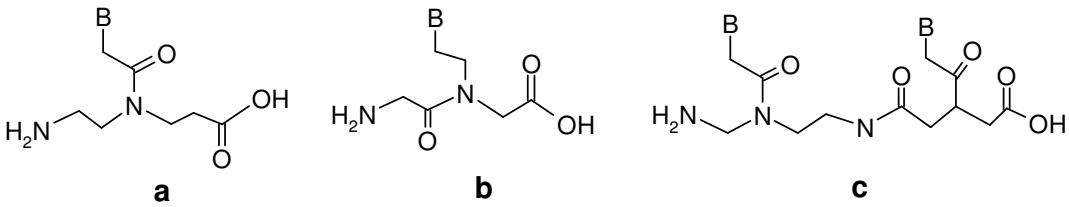

Figure 13. (a) Retero-inverso, **(b)** Peptoid and **(c)** Heterodimeric PNA.

1.5.1. Construction of bridged PNA structures

Any favourable structural preorganization of PNA may trigger the shift in the equilibrium towards the desired complex form because of the reduced entropy loss upon complex formation, provided that the enthalpic contributions suitably compensate. This may be achieved if the conformational freedom in *aeg*PNA is curtailed by bridging the aminoethyl or glycyl acetyl linker arms (Figure 14) to give rise to cyclic analogues with preorganized structures without affecting the nucleobase recognition ability through hydrogen bonding.

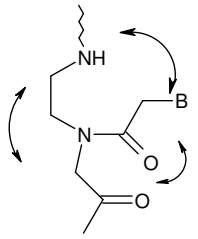

Figure 14. Possible positions for introduction of methylene or ethylene bridges.

Additionally, the introduction of chemical bridges into *aeg*PNA to provide cyclic structures may help in controlling the rotameric populations by fixing the nucleobase orientation and also in directional selective binding by virtue of the chirality in the backbone. Such a structural preorganization approach using additional conformational constraint has been extremely successful in the case of DNA analogues. Prominent examples are conformationally locked nucleic acids[48] or conformationally frozen hexitol[49] and altritol nucleic acids[50] (Figure 15), which have preorganized 3'-*endo* sugar conformations as prevalent in highly stable DNA-RNA duplexes.

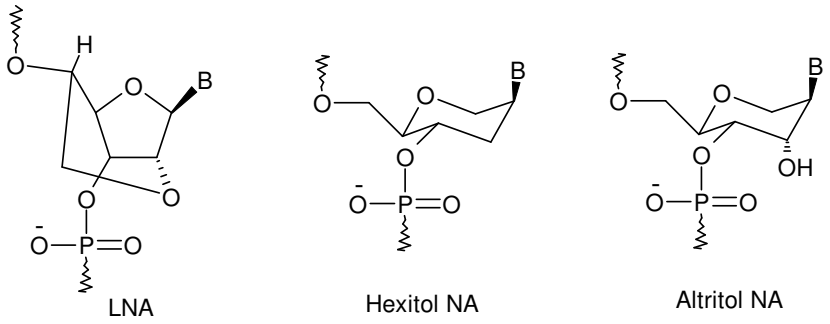

Figure 15. a) Locked 3'-*endo* conformation in LNA; b) frozen 3'-*endo* conformation in hexitol and altritol NA.

1.5.2. PNA with five-membered nitrogen heterocycles

The naturally occurring amino acid *trans*-4-hydroxy-proline, a five-membered nitrogen heterocycle with useful substitutions and well known and easily manipulated stereochemistry,[51,52] is a versatile, commercially available starting material amenable for creating structural diversity to mimic the DNA/PNA structures. Many researchers have exploited *trans*-4-hydroxy-L-proline for the synthesis of a wide variety of chiral, constrained and structurally preorganized PNAs.

1.5.2.1. Aminoprolyl PNA

The introduction of a methylene bridge between the β- carbon atom of the aminoethyl segment and the α' -carbon atom of the glycine segment of the *aeg*PNA resulted in 4- aminoprolyl PNA, with the introduction of two chiral centres (Figure 16).[53] The incorporation of single chiral D-*trans*- and L-*trans*-prolyl PNA monomeric units in the PNA oligomers at the N-terminus resulted in discrimination of parallel/antiparallel binding orientation preferences towards the target DNA

sequences. A backbone combining *aeg*PNA alternating with L-*trans*-4-aminoprolyl

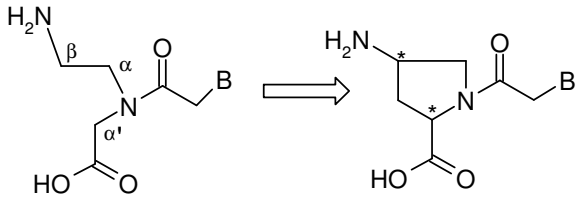

Figure 16. Aminoprolyl PNA.

PNA was later shown to bind to the target sequences with higher affinity than the pure *aeg*PNA oligomers.[54] Efforts directed towards releasing the structural strain in aminoprolyl PNA resulted in the synthesis of prolyl carbamate nucleic acids. Here the backbone amide bond was replaced by a carbamate linkage, extended by two additional atoms[55] in comparison to the unmodified *aeg*PNA oligomers.

1.5.2.2. Gly-Pro-Peptide PNA

Lowe *et al*.[55] used 4-Hydroxyproline for the synthesis of a novel chiral prolylglycyl PNA. The methylene bridge was inserted between the α'-carbon atom of the glycine unit and the β'-carbon atom of the nucleobase linker of *aeg*PNA (Figure 17).[56,57]

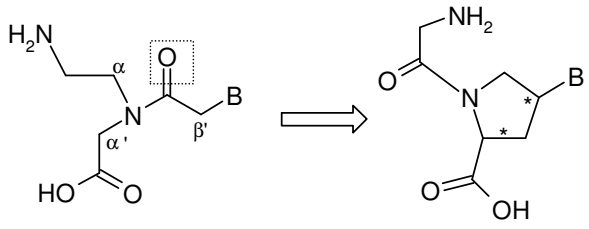

Figure 17. Gly-pro peptide PNA.

The tertiary amide bond in the backbone between proline and glycine units replaced the aminoethylglycyl backbone. The oligomers with such a backbone did not

bind to the target sequences, the geometry imposed by the rigidity of the system probably being inappropriate for correct recognition. The sequences with *aeg*PNA alternating with the proline-glycine PNA unit showed reduced binding to the target sequences, unlike the 4-aminoproline PNA.

1.5.2.3. Aminoethylprolyl PNA, aepPNA

A proline-based PNA in which a pyrrolidine ring would replace the tertiary amide linker to the nucleobase might balance the flexibility and rigidity in the PNA backbone. The α'-carbon atom of the glycine unit and the β'-carbon atom of the nucleobase linker were joined through a methylene bridge (Figure 18).[58]

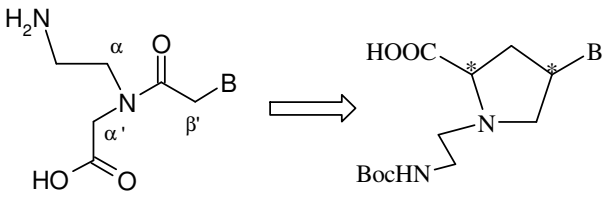

Figure 18. *aep*PNA.

The flexibility in the aminoethyl segment of *aeg*PNA was retained, unlike that in the proline-glycine PNA. The oligomers comprising 4-(*S*)-2-(*S*/*R*) *aep*PNA thymine units showed very favourable binding properties towards the target sequences without compromising the specificity. The stereochemistry at the C-2 centre did not exert any significant effect on the binding ability of the homooligomeric sequences.

1.5.2.4. Pyrrolidinone PNA

Another conformationally restricted cyclic PNA analogue was derived from a pyrrolidinone ring system. A methylene bridge was inserted between the α-carbon atom of the aminoethyl segment and the β'-carbon atom of the acetyl linker to the

nucleobase of *aeg*PNA[59] (Figure 19). The carbonyl group of the nucleobase linker was retained and was forced to point towards the carboxy terminus of the backbone. The hybridization properties of PNA decamers containing this analogue with complementary DNA, RNA and PNA strands were investigated. The oligomers

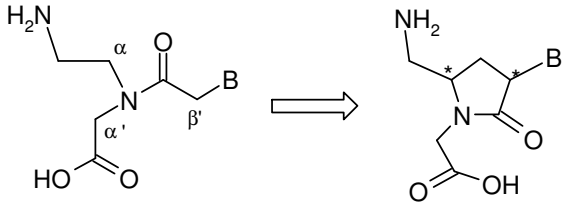

Figure 19. Pyrrolidinone PNA.

incorporating the (3*S*,5*R*) isomer were shown to have the highest affinity towards RNA in comparison with DNA.[60]

1.5.2.5. aeponePNA

In order to get the best characteristics from both the *aeg*PNA and the *aep*-PNA, monomer was synthesized restoring the amide character to the pyrrolidine ring nitrogen *via* selective C5 oxidation of *aep*-proline derivatized intermediate[61] (Figure 20). *aepone*PNA oligomer stabilizes the derived triplexes with DNA but destabilizes the complexes formed with poly (rA).

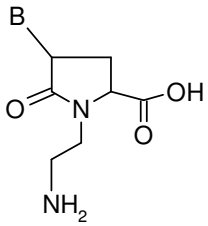

Figure 20. *aepone*PNA.

1.5.2.6. Prolyl-(β-amino acid) peptide PNA

The conformational strain in the alternating proline-glycine backbone was released by replacement of the α amino acid residue by different β amino acid spacers with appropriate rigidity.[62] Novel pyrrolidinyl PNAs comprising alternate units of

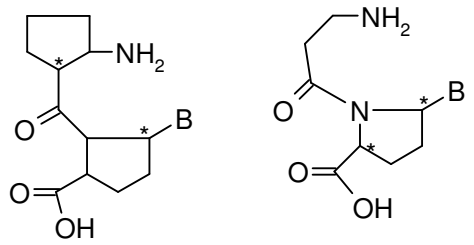

Figure 21. a) Prolyl-2-amino-cyclopentanecarboxylic acid, b) Prolyl-β-alanine.

nucleobases modified with D-proline, either D/L aminopyrrolidine 2 carboxylic acid, (1*R*,2*S*) –2-aminocyclopentanecarboxylic acid or β alanine were synthesized (Figure 21).[63]

1.5.2.7. Pyrrolidine PNA and pyrrolidine PNA-DNA chimera

Insertion of a methylene bridge in *aeg*PNA, linking the α-carbon atom of the aminoethyl segment and the β'-carbon atom of the tertiary amide linker, afforded the pyrrolidine PNA.[64] A fully modified (2*R*,4*S*) pyrrolidine PNA decamer formed very stable complexes with both DNA and RNA targets. The incorporation of the (2*S*,4*S*) thymine monomer into oligomers and mixed pyrimidine oligomers resulted in a decreased binding efficiency with the target DNA/RNA sequences. The (2*R*,4*R*) isomer was incorporated into a PNA:DNA dimer amenable to the synthesis of PNA:DNA chimeras. The chimeric PNA:DNA bound to the target DNA with decreased efficiency relative to the native DNA.

Comparative complexation of PNA oligomers incorporating diastereomeric pyrrolidine monomers[65] having nucleobases T, A, G and C with complementary DNA and RNA sequences, It is found that (i) (2*R*,4*S*)-PNA oligomers that stabilize PNA_2:DNA homopyrimidine:homopurine triplexes destabilize the mixed pyrimidine:homopurine duplexes, (ii) the presence of (2*S*,4*R*) and (2*R*,4*R*) stereoisomers affects enhanced DNA duplex stability, (iii) *cis*-(2*S*,4*S*) and -(2*R*,4*R*) remarkably enhance PNA:RNA duplex stability.

1.5.2.8. A cyclopentane conformational restraint for a peptide nucleic acid

Based on molecular modelling studies (*S*,*S*) cyclopentadiamine ring was used for conformational restraint of the C2-C3 dihedral angle of the PNA backbone. The *trans* cyclopentane modification improves the stability of PNA-DNA triplexes and PNA-RNA duplexes for a poly-T PNA.[66] Recently cyclopentyl PNAs[67,68] having *cis* and *trans* isomers have been reported (Figure 22). The results suggest that these have a stereochemistry dependent stabilization effect on binding both DNA and RNA. The *cp*PNAs have a better selectivity for mismatch DNA sequence and a higher binding to complementary DNA sequence than the unmodified PNA.

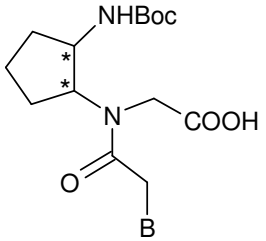

Figure 22. Cyclopentyl PNA.

1.5.2.9. bepPNA

One-carbon extended conformationally constrained pyrrolidine PNA monomer (*bep*PNA) has been synthesized, incorporated into PNA sequences at predefined

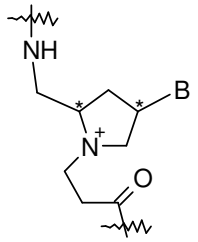

Figure 23. *bep*PNA.

positions, and showed selective RNA binding properties (Figure 23).[69]

1.5.3. PNA with six membered ring structures

Six-membered ring structures exhibit unique conformational preferences, and the binding abilities of hexose sugar phosphate containing oligonucleotide have been extensively studied by Eschenmoser *et al*.[70] The ability of morpholino,[71] hexitol,[72] and cyclohexene oligonucleotides[73] to bind to DNA/RNA are well established and are dictated by the conformational preferences of the six membered ring structures. Conformations in the six membered ring structures are rigid, in contrast to the relatively flexible five membered ring, and hence their influence on the stability of the resulting PNA-DNA/RNA complexes may be expected to make important contributions to the stabilities of the DNA/RNA complexes.

1.5.3.1.Glucosamine nucleic acids, GNAs

The six membered glucosamine ring appeared to fulfill the requirement of optically pure and constrained conformational scaffolding for the attachment of nucleobases (Figure 24). The homopyrimidine and mixed base sequences using GNA monomer were constructed. The binding affinities and selectivities of these oligomers to DNA and RNA targets indicated selective recognition of RNA by Watson–Crick

hydrogen bonding.[74] The entropy changes were found to be smaller for GNA-DNA/RNA than for DNA-DNA/RNA, consistent with idea that the GNA oligomer was preorganized for binding to the target sequences.

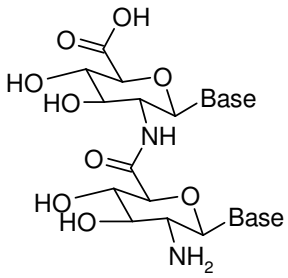

Figure 24. GNA.

1.5.3.2. Piperidinone PNA

Introduction of an ethylene bridge between the α carbon atom in the ethylene diamine and β' carbon atom and acetyl linker resulted in a six-membered ring structure – piperidinone PNA[75] (Figure 25). (3*R*,6*R*) and (3*S*,6*R*) adenine monomers were synthesized and incorporated into *aeg*PNA which resulted in a large decrease in the duplex stability.

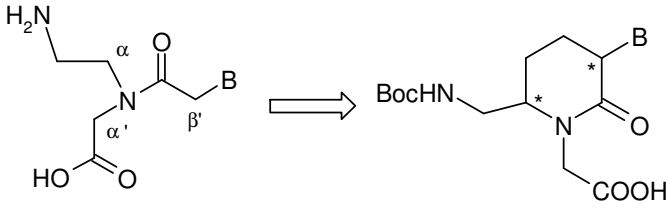

Figure 25. Piperidinone PNA.

1.5.3.3. Cyclohexyl PNA

Introduction of conformational constraint in the *aeg*PNA resulted in the chiral cyclohexyl-derived backbone[76] (Figure 26). The aminoethyl segment of the *aeg*PNA was replaced with a 1,2 diaminocyclohexyl moiety, either in the (*S*,*S*) or (*R*,*R*) configuration. The oligomers with (*S*,*S*)-cyclohexyl residues were able to hybridize

with DNA or RNA, with little effect on thermal stability. Molecular modeling studies reveled that (*S*,*S*) isomer can be accommodated more easily in duplex than (*R*,*R*) isomer. In contrast, incorporation of the (*R*,*R*) isomer resulted in a drastic decrease in the stability of PNA-DNA/RNA complexes. The complexes formed by the two isomers were of the opposite handedness, as evident from CD spectroscopy.

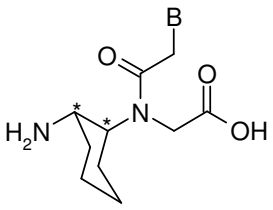

Figure 26 Cyclohexyl PNA.

Recently, synthesis of ethyl *cis*–(1*S*,4*R*/1*R*,2*S*)-2-aminocyclohex-1-yl-*N*-(thymin-1-yl-acetyl)glycinate *via* enzymatic resolution of the *trans*-2 azido cyclohexanols has been reported.[77] The crystal structure of intermediate showed equatorial disposition of the tertiary amide group, with the torsion angle β in the range 60°-70°. UV-Tm experiments showed that (1*S*,2*R*) isomer preferred to bind RNA and (1*R*,2*S*) isomer showed higher affinity towards DNA in homothymine sequences leading to stereodiscrimination in recognition of DNA and RNA.[66]

1.5.3.4. Chiral piperidine PNA

This PNA analog takes advantage of the conformationally frozen six-membered ring (Figure 27) having substituents in definite preferred orientations with respect to each other.[78] DNA complementation studies of the modified PNAs by UV-Tm measurements indicate that these PNAs form stable PNA_2:DNA complexes. The tertiary ring nitrogen is protonatable at physiological pH and may add favorable

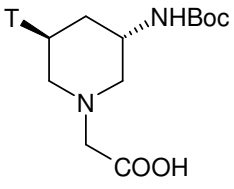

Figure 27. Chiral piperdine PNA.

therapeutic features to the oligomers, as the positive charges in the backbone are known to aid cellular uptake.

1.5.3.5. [(Aminoethyl) amino] cyclohexanoic acid

Rigidity was introduced into the *aeg*PNA by replacing the glycyl segment in the backbone by α amino cyclohexanoic acid[79] (Figure 28). Incorporation of these monomers into oligomers and their DNA/RNA binding properties has not yet been reported.

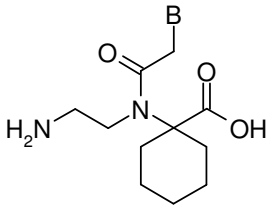

Figure 28. [(Aminoethyl) amino]cyclohexanoic acid.

1.5.3.6. Morpholino PNA

The set of morpholino analogues with phosphonate esters, amide or ester linkages between the morpholino nucleoside residues was synthesized. Preliminary results indicated that amide-linked morpholino PNAs were better accommodated in the complexes than the ester or the phosphonate linked oligomers**.**

1.6. MODIFIED NUCLEOBASES

Non-natural nucleobases could aid in understanding of the recognition process between the natural nucleobase-pairs in terms of factors such as hydrogen bonding and internucleobase stacking. They could also generate new recognition motifs with potential applications in diagnostics. Only a few nucleobase modifications have been reported in the PNA context (Figure 29). Pseudoisocytosine mimics the C^+

recognition pattern[80] for triplex formation and 2,6-diaminopurine offers increased affinity and selectivity for thymine.[81] 2-Aminopurine[82] can hydrogen bond with uracil and thymine in the reverse Watson-Crick mode and being inherently fluorescent, can be used to study the kinetics of the hybridization process with complementary nucleic acids. Replacement of *aeg*PNA with thiazole orange afforded a PNA probe that

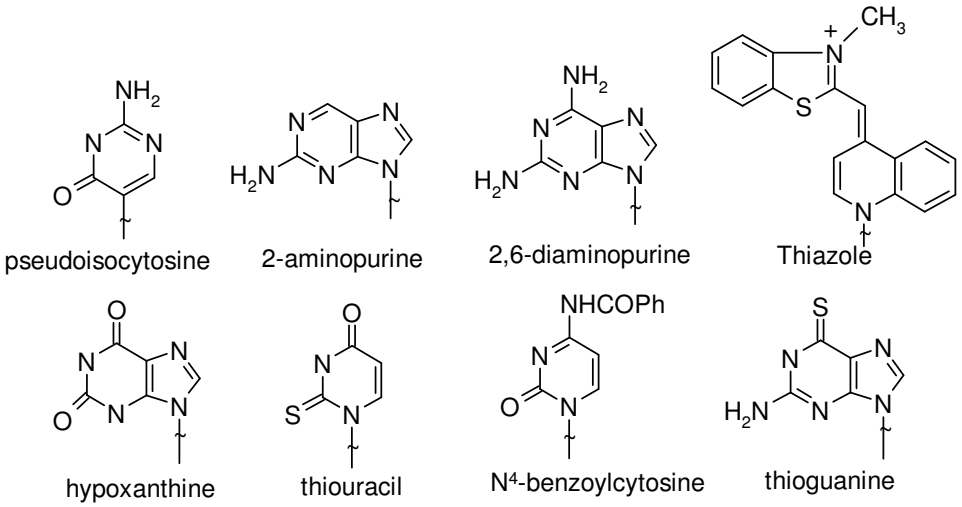

Figure 29. Modified nucleobases.

fluoresced upon hybridization. [83]

The E-base,[84] hypoxanthine,[85] N^4-benzoylcytosine[86] and 6-thioguanine[87] represent some more examples of modified nucleobases. Thiouracil along with 2,6-diaminopurine has been utilized as a non-natural base pair in PNA-DNA recognition and was shown for the first time to lead to a phenomenon termed as 'double duplex invasion'.

1.7. BIOLOGICAL APPLICATIONS OF PNA

Antigene and antisense applications of PNA

Peptide nucleic acids have promise as candidates for gene therapeutic drugs design. They require well-identified targets and a well-characterized mechanism for their cellular delivery. In principle, two general strategies can be adapted to design gene therapeutic drugs. Oligonucleotides or their potential analogs are designed to recognize and hybridize to complementary sequences in a particular gene whereby they should interfere with the transcription of that particular gene (antigene strategy). Alternatively, nucleic acid analogs can be designed to recognize and hybridize to complementary sequences in mRNA and thereby inhibit its translation (antisense strategy). PNAs are chemically and biologically stable molecules and have significant effects on replication, transcription, and translation processes, as revealed from *in vitro* experiments. Moreover, no sign of any general toxicity of PNA has so far been observed.[88,89,90]

1.7.1. Inhibition of transcription

Peptide nucleic acids should be capable of arresting transcriptional processes by virtue of their ability to form a stable triplex structure or a strand-invaded or strand displacement complex with DNA (Figure 30). Such complexes can create a structural hindrance to block the stable function of RNA polymerase and thus are capable of working as antigene agents. Evidence from *in vitro* studies supports the idea that such complexes are indeed capable of affecting the process of transcription involving both prokaryotic and eukaryotic RNA polymerases. Nielsen *et al*.[91] have demonstrated that even an 8-mer PNA (T_8) is capable of blocking phage T3 polymerase activity. The presence of a PNA target within the promoter region of IL-2Ra gene has been used to understand the effect of PNA binding to its target on this gene expression.[92,93] The

PNA_2:DNA triplex arrests transcription *in vitro* and is capable of acting as an antigene agent. But one of the major obstacles to applying PNA as an antigene agent is that the

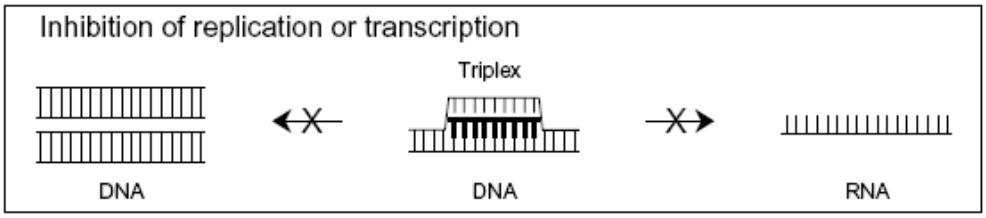

Figure 30. Mechanism of inhibition of replication or transcription.

strand invasion or the formation of strand displacement complex is rather slow at physiological salt concentrations.[94,95]

Several modifications of PNA have shown improvement in terms of binding. Modifications of PNA by chemically linking the ends of the Watson-Crick and Hoogsteen PNA strands to each other, introducing pH-independent pseudoisocytosines into the Hoogsteen strand,[96] incorporating intercalators, or positively charged lysine residues[97] in PNA strand can drastically increase the association rates with dsDNA. Lee *et al*.[98] have demonstrated that PNA as well as the PNA–DNA chimera complementary to the primary site of the HIV-I genome can completely block priming by $tRNA_3Lys$. Consequently, *in vitro* initiation of the reverse transcription by HIV-1 RT is blocked. Thus, oligomeric PNAs targeted to various critical regions of the viral genome are likely to have a strong therapeutic potential for interrupting multiple steps involved in the replication of HIV-1.

1.7.2. Inhibition of translation

The basic mechanism of the antisense effects by oligodeoxynucleotides is considered to be either a ribonuclease H (RNase H) -mediated cleavage of the RNA strand in oligonucleotide-RNA heteroduplex or a steric blockage in the

oligonucleotide–RNA complex of the translation machinery (Figure 31).[99] Oligodeoxynucleotide analogs such as phosphorothioates activate RNase H and thus hold promise of working as antisense agents. However, they also exhibit some nonspecificity in their action. PNA/RNA duplexes, on the other hand, cannot act as substrates for RNase H. Normally, the peptide nucleic acid antisense effect is based on the steric blocking of either RNA processing, transport into cytoplasm, or translation. It has been concluded from the results of *in vitro* translation experiments involving rabbit reticulocyte lysates that both duplex- (mixed sequence) and triplex-

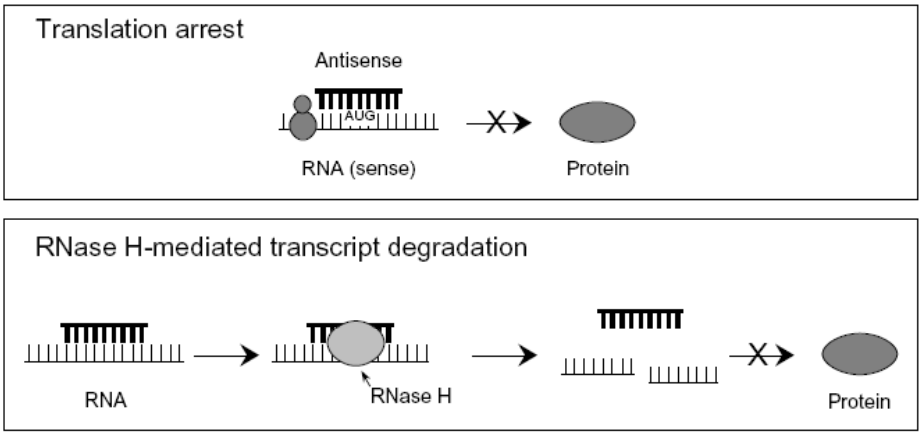

Figure 31. **Mechanisms of inhibition of translation. (A) Translational arrest by blocking the ribosome. (B) RNase H cleavage induced by antisense-oligonucleotides**

forming (pyrimidine-rich) PNAs are capable of inhibiting translation at targets overlapping the AUG start codon.

Triplex-forming PNAs are able to hinder the translation machinery at targets in the coding region of mRNA. However, translation elongation arrest requires a PNA_2:RNA triplex and thus needs a homopurine target of 10–15 bases. In contrast, duplex-forming PNAs are incapable of this. Triplex-forming PNAs can inhibit translation at initiation codon targets and ribosome elongation at codon region targets. Triple helix-forming PNAs can also hinder the translation process. Bis-PNA or

clamp-PNA structures are capable of forming internal triple helical constructs. In principle, if targeted against the coding region of mRNA, PNA_2:RNA triple helix-forming derivatives can also cause a stop in translation, which can be easily verified by the detection of a truncated protein. However, this methodology requires a sequence optimization for each new target. Recent studies show that *E. coli* cells are somewhat permeable for PNA molecules. Good and Nielsen[100,101] have shown that it is possible to achieve PNA antisense effects in the 'leaky' mutant strains of *E. coli*. PNAs targeted against the AUG region of the mRNA corresponding to b-galactosidase and b-lactamase genes were indeed capable of down-regulating the expression of these two genes.

1.7.3. Inhibition of replication

It is also possible to use PNA for inhibiting the elongation of DNA primers by DNA polymerase. Further, the inhibition of DNA replication should be possible if the DNA duplex is subjected to strand invasion by PNA under physiological conditions or if the DNA is single stranded during the replication process. Efficient inhibition of extrachromosomal mitochondrial DNA, which is largely single-stranded during replication, has been demonstrated by Taylor *et al.*[102] The PNA-mediated inhibition of the replication of mutant human mitochondrial DNA is a novel (and also potential) approach toward the treatment of patients suffering from ailments related to the heteroplasmy of mitochondrial DNA. Here wild type and mutated DNA are both present in the same cell. Experiments have shown that PNA is capable of inhibiting the replication of mutated DNA under physiological conditions without affecting the wild-type DNA in mitochondria.

1.7.4. Interaction of PNA with enzymes

RNase H

The activation of the intracellular enzyme RNase H by oligonucleotides to cleave RNA bound to deoxyribonucleic acid oligomers depends on the chemical structure of RNase H-stimulating oligonucleotides. The antisense oligonucleotide with an RNase H activity (e.g., phosphorothioate oligos) is considered a better antisense molecule (inhibitor) than one without the activity (methylphosphonates and hexitol nucleic acids).[103] Despite their remarkable nucleic acid binding properties, PNAs generally are not capable of stimulating RNase H activity on duplex formation with RNA. However, recent studies have shown that DNA/PNA chimeras are capable of stimulating RNase H activity. On formation of a chimeric RNA double strand, PNA/DNA can activate the RNA cleavage activity of RNase H (Figure 32). Cleavage occurs at the ribonucleotide parts base paired to the DNA part of the chimera. Moreover, this cleavage is sequence specific in such a way that certain sequences of

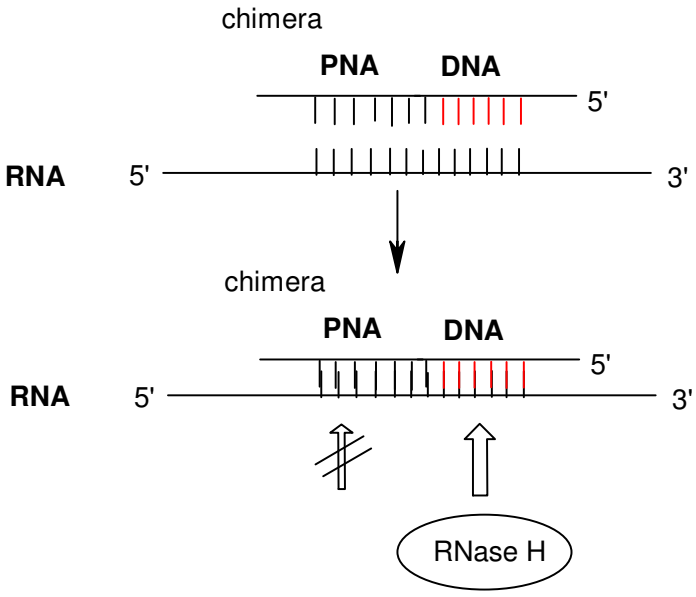

Figure 32. Schematic representation of Rnase H- mediated cleavage activity after the binding of PNA-DNA chimera to target RNA.

DNA/PNA chimeras are preferred over others. They are also reported to be taken up by cells to a similar extent as corresponding oligonucleotides. Thus, PNA/DNA chimeras appear by far the best potential candidates for antisense PNA constructs.

Polymerase and reverse transcriptase

In general, there is no direct interaction of PNA with either DNA polymerase or reverse transcriptase. However, different groups have shown indirect involvement of PNA in inhibiting these enzyme functions (activity) under *in vitro* conditions. For example, PNA oligomers are capable of terminating the elongation of oligonucleotide primers by either binding to the template strand or directly competing with the primer for binding to the template. Primer extension by MMLV reverse transcriptase has been shown to be inhibited by introducing a PNA oligomer. In another experiment, Nielsen *et al*.[104] demonstrated that the primer extension catalyzed by *Taq*-polymerase can be terminated by incorporating a PNA oligomer (PNA-H$(t)_{10}$) into the system. The latter can bind to a $(dA)_{10}$ sequence in the template and thereby terminate the primer extension. Moreover, the reverse transcription of *gag* gene of HIV I is also inhibited *in vitro* by PNAs.[105] The inhibition has been achieved by using a bis-PNA construct, which is more efficient than the corresponding mono PNA construct.[106] Also, the reverse transcription can be completely inhibited by a pentadecameric antisense PNA, using a molar ratio of 10:1 (PNA/RNA), without any noticeable RNase H cleavage of the RNA. PNA oligomers that are complementary to the RNA primer-binding site can inhibit the telomerase activity. Studies have shown that the telomerase inhibition activity of PNA is better than that of corresponding activity of phosphorothioate oligonucleotides. This is mainly due to a higher binding affinity of PNA compared to phosphorothioates.[107] Corey and co-workers[108] have demonstrated

an efficient inhibition of telomerase after lipid-mediated delivery of template- and nontemplate- directed PNA into the cell.

1.7.5. PNA as a molecular-biological tool

Peptide nucleic acids also exhibit potential for use as a tool in biotechnology and molecular biology. Here we will mainly present indications of PNA becoming an important molecular biology tool.

Enhanced PCR amplification

The polymerase chain reaction (PCR) has been widely used for various molecular genetic applications including the amplification of variable number of tandem repeat (VNTR) loci for the purpose of genetic typing.[109,110] PNA has been used to achieve an enhanced amplification of VNTR locus D1S80.[111] Small PNA oligomers are used to block the template, and the latter becomes unavailable for intra- and interstrand interaction during reassociation. On the other hand, the primer extension is not blocked; during this extension, the polymerase displaces the PNA molecules from the template and the primer is extended toward completion of reaction (Figure 33). This approach shows the potential of PNA application for PCR

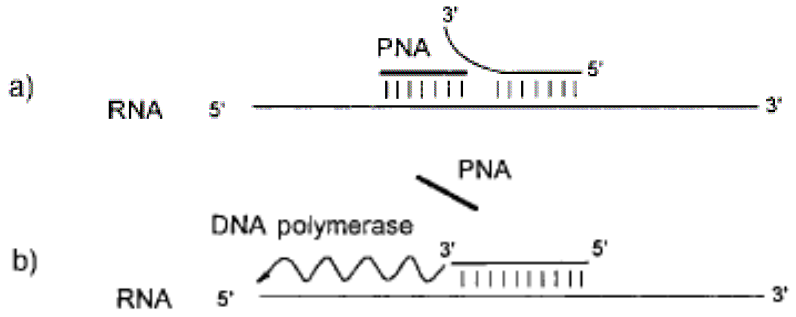

Figure 33. Schematic representation of "PCR clamping" technique.

amplification where fragments of different sizes are more accurately and evenly amplified.

1.7.6. PNA hybridization as alternative to Southern hybridization

Southern hybridization is perhaps one of the most widely used techniques in molecular biology. Despite its great potential to predict both size and sequence information and information regarding the genetic context, there are certain disadvantages of this process. It requires a laborious multistep washing procedure and there could sometimes be poor sequence discrimination between closely related species. PNA pre-gel hybridization simplifies the process of Southern hybridization by reducing the required time, as the cumbersome post separation, probing, and washing steps are eliminated. Labeled (fluoresceinated) PNA oligomers are used as probes and allowed to hybridize to a denatured DNA sample at low ionic strength. The mixture is thereafter subjected directly to electrophoresis for size separation and singlestranded DNA fragments separated on the basis of length. The charge-neutral PNA allows hybridization at low ionic strength and renders higher mobility to the complex compared to the excess unbound PNA. The DNA-PNA hybrids are blotted (transferred) onto a nylon membrane, dried, UV cross-linked, and detected using standard chemiluminescent techniques.[112] Alternatively, the bound PNA can be detected by using capillary electrophoresis (*vide infra*), which can make use of the direct fluorescence detection method. Under the same conditions, a normal DNA–DNA duplex will tend to disrupt whereas the PNA–DNA duplex will remain intact due to the strong binding of PNA to DNA. This allows specific sequence detection with simultaneous size separation of the target DNA following a simple and

straightforward protocol. Consequently, the analysis is much faster than the conventional Southern hybridization technique.

1.7.7. PNA-assisted rare cleavage

Peptide nucleic acids, in combination with methylases and other restriction endonucleases, can act as rare genome cutters.[113] The method is called PNA-assisted rare cleavage (PARC) technique. It uses the strong sequence-selective binding of PNAs, preferably bis-PNAs, to short homopyrimidine sites on large DNA molecules, e.g., yeast or λ DNA. The PNA target site is experimentally designed to overlap with the methylation/ restriction enzyme site on the DNA, so a bound PNA molecule will efficiently shield the host site from enzymatic methylation whereas the other, unprotected methylation/restriction sites will be methylated. After the removal of bis-PNA, followed by restriction digestions, it is possible to cleave the whole DNA by enzymes into limited number of pieces. DNA is efficiently protected from enzymatic digestion due to methylation in most of the sites except for those previously bound to PNA. Thus, short PNA sequences, particularly positively charged bis-PNAs in combination with various methylation/restriction enzyme pairs or recently reported pseudocomplementary PNA[114] (pcPNAs, which completely cover the desired

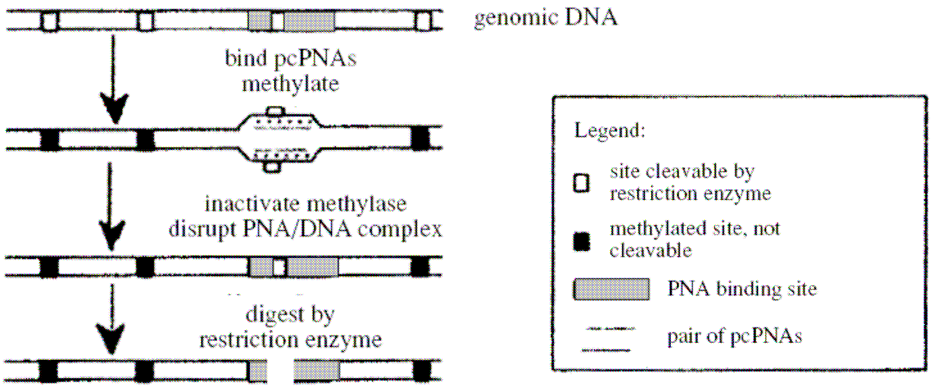

Figure 34. Schematics of the PARC method involving pcPNAs.

methylation/restriction site) (Figure 34), can constitute an extraordinary new class of genome rare cutters.

1.7.8. Artificial restriction enzyme system

S1 nuclease cleaves single-stranded nucleic acids releasing 5'-phosphoryl mono- or oligonucleotides. It removes the single-stranded overhangs of DNA fragments and can be used in RNA transcript mapping and construction of unidirectional deletions. PNA in combination with S1 nuclease can work as an 'artificial restriction enzyme' system. Homopyrimidine PNA oligomers hybridize to the complementary targets on dsDNA via a strand invasion mechanism, leading to the formation of looped-out noncomplementary DNA strands. The enzyme nuclease S1 can degrade this single-stranded DNA part into well-defined fragments. If two PNAs are used for this purpose and allowed to bind to two adjacent targets on either the same or opposite DNA strands, it will essentially open up the entire region, making

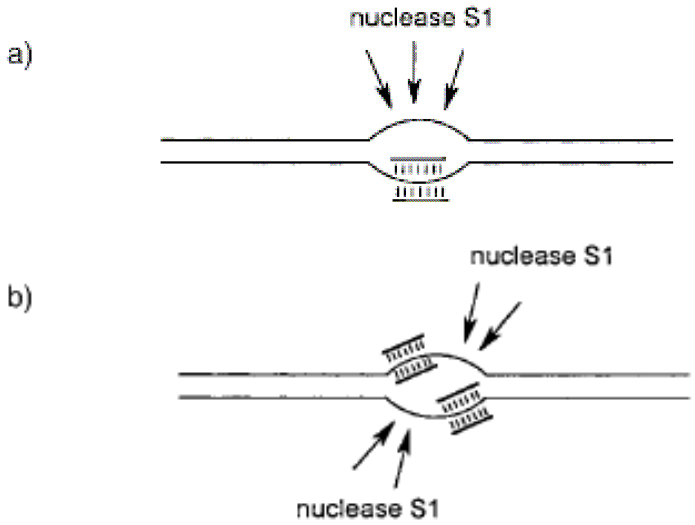

Figure 35. Artificial restriction enzymes: a) Single strand cleavage by PNA; b) double strand cleavage by double PNA clamping.

the substrate accessible for the nuclease digestion and thereby increasing the cleavage efficiency (Figure 35).[115]

1.7.9. Determination of telomere size

The conventional method for the determination of telomere length involves Southern blot analysis of genomic DNA and provides a range for the telomere length of all chromosomes present. The modern approach uses fluorescein-labeled oligonucleotides and monitor *in situ* hybridization to telomeric repeats. However, a more delicate approach resulting in better quantitative results is possible by using fluorescein-labeled PNAs, as shown by Lansdorp *et al.*[116] This PNA-mediated approach permits accurate estimates of telomeric length. *In situ* hybridization of fluorescein-labeled PNA probes to telomeres is faster and requires a lower concentration of the probe compared to its DNA counterpart. Low photobleaching and an excellent signal-to-noise ratio make it possible to quantitate telomeric repeats on individual chromosomes in this way. Experiments suggest that variations of this approach can possibly be applied to other repetitive sequences.

1.7.10. Nucleic acid purification

Based on its unique hybridization properties, PNAs can also be used to purify target nucleic acids. PNAs carrying six histidine residues have been used to purify target nucleic acids using nickel affinity chromatography (Figure 36).[117] Also, biotinylated PNAs in combination with streptavidin-coated magnetic beads may be used to purify *Chlamydia trachomatis* genomic DNA directly from urine samples. However, it appears that this simple, fast, and straightforward 'purification by hybridization' approach has certain drawbacks. It requires the knowledge of a target sequence and depends on a capture oligomer to be synthesized for each different

target nucleic acid. Such target sequences for the short pyrimidine PNA, i.e., the most efficient probe for strand invasion, are prevalent in large nucleic acids. Thus, short PNAs can also be used as generic capture probes for purification of large nucleic acids. It has been shown that a biotin tagged PNA-thymine heptamer could be used to efficiently purify human genomic DNA from whole blood by a simple and rapid procedure.

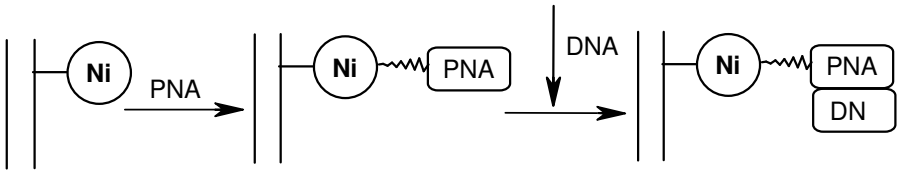

Figure 36. Nucleic acid purification by Ni affinity chromatography.

1.7.11. PNA as a diagnostic tool

The high-affinity binding of PNA oligomers has led to the development of new applications of PNA, especially as a diagnostic probe for detecting genetic mutations: applications are possible for the detection of genetic mutation and mismatch analysis that can use its unique hybridization properties. The ensuing sections will highlight some of the recent developments related to the use of PNA as a probe to detect genetic mutations and corresponding mismatch analysis confirming its potential as a diagnostic tool for clinical applications.

Single base pair mutation analysis using PNA directed PCR clamping

Amplification of the target nucleic acid by the PCR technique is considered an important step for detection of genetic diseases. The higher specificity of PNA binding to DNA, higher stability of a PNA–DNA duplex compared to the corresponding DNA–DNA duplex, and its inefficiency to act as a primer for DNA polymerases are the basis for this novel technique. This strategy includes a distinct

annealing step involving the PNA targeted against one of the PCR primer sites. This step is carried out at a temperature higher than that for conventional PCR primer annealing where the PNA is selectively bound to the DNA molecule. The PNA/DNA complex formed at one of the primer sites effectively blocks the formation of a PCR product. PNA is also able to discriminate between fully complementary and single mismatch targets in a mixed target PCR. Sequence-selective blockage by PNA allows suppression of target sequences that differ by only one base pair. Also, this PNA clamping was able to discriminate three different point mutations at a single position.[118,119] One major advantage of this PNA-mediated PCR clamping is that it allows detection of mutations stretched over 4–6 bp regions in a single reaction, and this could also be used to detect other hot-spot mutations.

Molecular Beacons

Molecular beacons are single-stranded oligonucleotide hybridization probes that form a stem-and-loop structure. The loop contains a probe sequence that is complementary to a target sequence, and the stem is formed by the annealing of complementary arm sequences that are located on either side of the probe sequence. A

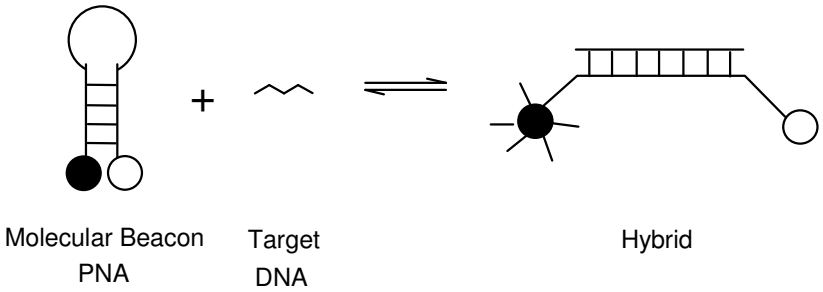

fluorophore is covalently linked to the end of one arm and a quencher is covalently linked to the end of the other arm. Molecular beacons do not fluoresce when they are free in solution. However, when they hybridize to a nucleic acid strand containing a

target sequence they undergo a conformational change that enables them to fluoresce brightly.[120]

Molecular beacons can be used as amplicon detector probes in diagnostic assays. Because nonhybridized molecular beacons are dark, it is not necessary to isolate the probe-target hybrids to determine the number of amplicons synthesized during an assay. Molecular beacons have three key properties that enable the design of new and powerful diagnostic assays: 1) they only fluoresce when bound to their targets, 2) they can be labeled with a fluorophore of any desired color, and 3) they are so specific that they easily discriminate single-nucleotide polymorphisms.[121] PNA offers an opportunity of advancing biosensor technology, especially with regard to sensitivity, automation and system integration.[122]

1.8. CELLULAR UPTAKE OF PNA

It is essential for any therapeutic agent to have good bioavailability. The activity of the antisense oligonucleotides is crucially affected by how well they reach their site of action unmetabolized. The protein biosynthesis apparatus of the cell is located in the cytoplasm where thousands of enzymes carry out the biosynthesis of sugars, fatty acids, nucleotides, amino acids, and proteins. The mRNA produced in the nucleus by transcription of the DNA is translated into the corresponding protein on the ribosomes in the cytoplasm. In order for the antisense oligonucleotides to be able to stop translation by hybridization, they must pass through the plasma membrane to enter interior of the cell. The plasma membrane is a natural barrier to many large or negatively charged molecules. It might therefore be supposed that this

membrane barrier would form a bottleneck in the antisense oligonucleotide concept.[123,124]

It is important to understand the effect of peptide nucleic acids on intact cells and problems related to its delivery into the cell. The cellular uptake of this unique nucleic acid analog is very slow, which is still the major challenge that needs to be overcome before it can be used as a therapeutic drug. So far, there is hardly any report of the antisense activity of PNA in cell culture without the use of brute techniques to help bypass the membrane barrier. Effects of PNA on intact cells have been demonstrated by cellular microinjection; antisense activity against a transfected gene has also been established in this way.[125] Serious efforts are being made to increase the cellular uptake of PNA, particularly by modifying the molecule itself or conjugating to it suitable potential ligand molecules that could enhance a physical or receptor-mediated cellular uptake.[126,127,128] Incorporation of a 'guide' sequence or some 'vector' peptides is one potential approach whereby PNA is attracted to the cell membrane and helped in docking into it (Figure 37). Several methods have been proposed to facilitate the uptake of PNAs in eukaryotic cells. These include transient

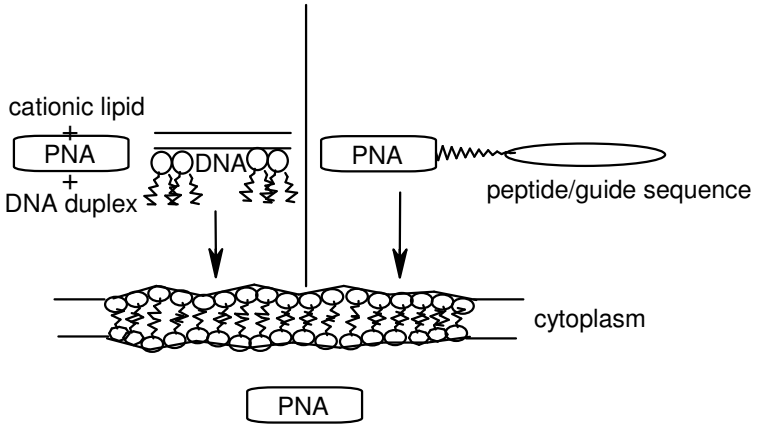

Figure 37. Methods for cellular uptake of PNA.

permeabilization with streptolysin O, cell membrane permeabilization by lysolectin or detergents like Tween, or conjugation with peptides capable of being internalized easily.[129] Aldrian-Herrada *et al.*[130] showed that peptide nucleic acids are rapidly internalized in cultured neurons when coupled to a delivery peptide (retro p-Antp peptide). This result is promising and demonstrates that PNAs guided by suitable vector peptides could work as antisense agents. Corey and co-workers[131] have reported a novel method for *in vitro* cellular delivery of peptide nucleic acids using a cationic lipid. The cationic lipid is capable of associating with the negatively charged phosphodiester backbone of DNA and RNA and fusing with the cell membrane to allow the oligonucleotide to enter into the cell through an endocytotic pathway. This technique has been improvised for the delivery of PNA molecules into the cells. Desired PNA oligomers are hybridized to overlapping oligonucleotides and the complex is mixed with cationic lipid. The cationic lipid–DNA–PNA complex thus formed can be internalized, and the partially hybridized PNA is imported into the cell as a passive cargo. On passive delivery into the cell, peptide nucleic acid is expected to dissociate itself from the complex.[132] Another strategy that has been adapted to improvise the delivery of PNA *in vitro* is to incorporate it into delivery vehicles (vesicles), e.g., liposomes. There are also some reports of direct PNA uptake.

G-PNA

In the past few years fusion of the human HIV-1 Tat transduction domain (GRKKRRQRRR) to a number of different moieties including proteins[31] and synthetic molecules[133] has led to their efficient uptake by cells. Subsequently, replacement of this Tat domain by a homoarginine peptide as well as various unnatural peptoid constructs containing guanidinium groups retained the ability to

promote efficient uptake.[134] Based on these findings, Ly *et al* synthesized PNA oligomers based on the previously reported 2-aminoethylarginine backbone.[135] Incorporation of the arginine side chain (*i.e.* the guanidinium functional group) into the PNA backbone at the α-position caused efficient uptake of the PNA by human colon and osteosarcoma cell lines. The disadvantage to G-PNA is currently the need to synthesize the monomers, which are not commercially available.

1.9. RECENT ADVANCES IN GENE THERAPEUTICS

1.9.1. RNAi

Introduction of double-stranded RNA (dsRNA) into cells activates a process known as RNA interference (RNAi) that ultimately promotes the degradation of messenger RNAs that are homologous to the dsRNA trigger. Using genetically altered strains of the roundworm *C. elegans* (round worms) Fire *et al*[133] in fall of 2000, discovered genes responsible for a process called RNA interference (RNAi)—in which double-stranded RNA triggers the natural degradation of a homologous mRNA. RNA interference (RNAi) is a process in which double-stranded RNA triggers the degradation of a homologous messenger RNA (sharing sequence-specific homology to particular "target" mRNAs).[136]

Today RNA interference (RNAi), is a technique in which exogenous, double-stranded RNAs (dsRNAs) that are complementary to known mRNA's, are introduced into a cell to specifically destroy that particular mRNA, thereby diminishing or abolishing gene expression. The technique has proven effective in *Drosophila*, *Caenorhabditis elegans*, plants, and recently, in mammalian cell cultures. To make the technique work in cultured mammalian cells for research purpose, scientists must

deliver small interfering RNAs (siRNAs), which are dsRNAs and of some 21-25 nucleotides into the cell (Figure 38). This is done with transfection reagents, optimized for allowing DNA and RNA to be absorbed by cultured cells.

Artificial siRNAs can be made in the lab by a phage enzyme referred to as

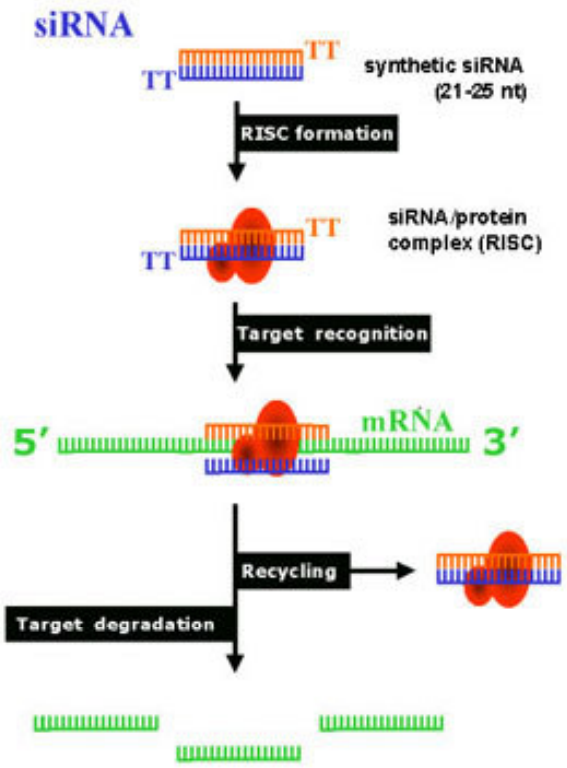

Figure 38. Mechanism of RNA interference.

DICER. The mechanism involves complexing siRNA into a multi-protein siRNA complex termed RISC (RNA Induced Silencing Complex). Typically, 3-5 double-stranded siRNA molecules are designed per gene in order to find siRNA that has a strong effect. This involves synthesis and purification of 6-10 RNA oligonucleotides of 20+ nucleotide pairs, costing around $1500 per gene.[137]

1.9.2. miRNA

A group of small RNA molecules, distinct from but related to siRNAs, have been identified in a variety of organisms. These small RNAs, called microRNAs (miRNAs), are transcribed as parts of longer RNA molecules that can be as long as 1000 nt. The RNAs are processed in the nucleus into hairpin RNAs of 70-100 nt by the dsRNA-specific ribonuclease Drosha. The hairpin RNAs are transported to the cytoplasm via a transportin-5 dependent mechanism where they are digested by a second, double-strand specific ribonuclease called Dicer. The resulting 19-23 mer miRNA is bound by a complex that is similar to the RNA-Induced Silencing Complex (RISC) that participates in RNA interference (RNAi). In animals, the complex-bound, single-stranded miRNA binds specific mRNAs through sequences that are significantly, though not completely, complementary to the mRNA. By a mechanism that is not fully characterized— but which apparently does not involve mRNA degradation as in RNAi— the bound mRNA remains untranslated, resulting in reduced expression of the corresponding gene.[138,139,140]

1.9.3. Ribozymes

Ribozymes are molecular scissors that cut RNA, the molecular messages given by genes in order to produce proteins. These molecular scissors provide a very useful means of studying gene function since by cutting the RNA with a ribozyme, a gene can be effectively turned off. The earliest reports of these ribozymes or catalytic RNAs (Figure 39) were first discovered by Cech in 1987. This was seen as a major discovery, since until then proteins were thought to be the only entity capable of behaving as enzymes. Ribozymes can be used to study gene function most notably in the study of HIV, the AIDS virus, and in Cancer research.[141,142]

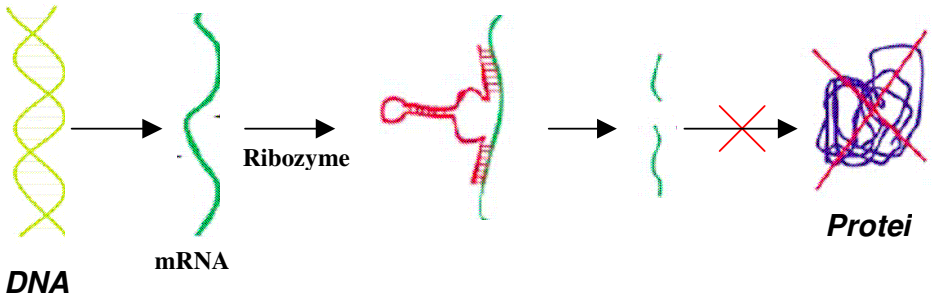

Figure 39. Catalytic ribozymes target RNA.

1.10. PRESENT WORK

The preceding sections give an overview of the peptide nucleic acids (PNAs), the synthetic imitator of natural nucleic acids that is DNA analogues with a homomorphous but chemically different backbone consisting of *N*-(2-aminoethyl)-glycine units in contrast to the sugar-phosphate backbone of DNA. In spite of this, PNAs bind to complementary nucleic acid oligomers obeying the Watson-Crick hydrogen bonding rules for PNA:DNA duplexes and Hoogsteen hydrogen bonding mode for third strand binding in a triplex. The attractive binding properties of PNAs, both in terms of affinity and specificity, coupled with their strand invasion potential have promoted PNA as a useful tool in molecular biology, diagnostics, and as a possible candidate for antisense/ antigene drug therapy.

The major drawbacks like poor water solubility, inefficient cell uptake, self-aggregation and ambiguity in directionality of binding restrict its applications. In order to overcome these limitations, several modifications of PNA have been carried out. PNAs have also been linked to helper molecules in various chimerae in an endeavour to improve its favourable properties.

The work presented in this thesis in the next 4 chapters involves the design, synthesis and biophysical evaluation of these backbone modified, chiral, charged

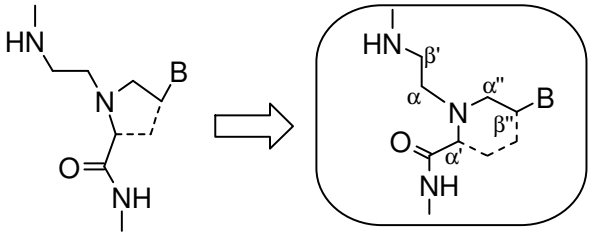

***aep*PNA** ***aepip*PNA**

PNA analogues- *aepip*PNA, bisPNA, fluorescent 2-aminopurine PNA and chiral PNA and some biophysical applications of ITC to study PNA:DNA hybridization, DNA:Au nanoparticle interactions and enzyme nanoparticle interactions.

Chapter 2 addresses the deficiencies of PNAs by rational structural modifications of PNA, based on conformational preorganization of backbone using cyclic monomeric units. These analogues to some extent improved the solubility, affinity and orientational selectivity in DNA: PNA binding. The synthesis and evaluation of six membered ring analogues of pyrrolidines (*aep*PNA) – the aminoethyl pipecolic acid PNAs (*aepip*PNA) have been described. These are conceptually derived by linking the α'-carbon of glycyl unit with β"-carbon of side chain via an ethylene linker instead of methylene linker as in *aep* PNA. These have two chiral centers leading to the possibility of existence of four diasteromers.

The syntheses of the protected monomers (2*R*,5*S*) and (2*S*,5*R*) 1-(*N*-Boc-aminoethyl)-5-(*N*3-benzoylthymin-1-yl)pipecolic acid is described. The *aepip*PNA monomers have been incorporated into the PNA oligomer sequences by solid phase peptide synthesis. Cleavage of the synthesized oligomers from the solid support, their

subsequent purification procedures, followed by suitable characterization is also detailed.

These oligomers have been subjected to biophysical studies like UV-melting, CD spectroscopy, Isothermal titration calorimetry and gel electrophoresis to examine complementary DNA binding affinity.

Chapter 3 describes the synthesis of bis-PNAs containing N7-substituted guanine (N7G) in which the two arms of PNA are joined by neutral tetraethylene glycol linker (TEG). The introduction of chiral, cationic aminoethylprolyl units with C+ mimic N7G in the backbone of bisPNAs have been described to examine influence on the recognition of complementary DNA in an orientation-selective manner. The process of strand invasion of target DNA duplex by these modified bisPNAs is followed by a fluorescence assay, to compare the kinetics of invasion by different polypyrimidine (C/T) and purine-pyrimidine (N7G/T) mixmer-bisPNAs.

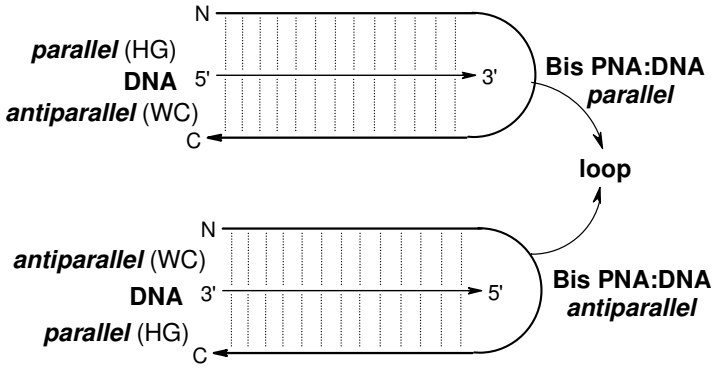

Figure 40. Triplex formation with bisPNAs

Chapter 4 is divided into two sections. Section A is devoted to the synthesis of 2-aminopurine, which is a fluorescent isomer of adenine (6-aminopurine). The

incorporation of 2-aminopurine into PNA oligomers, which would lead to fluorescent PNAs with useful attributes, has been described.

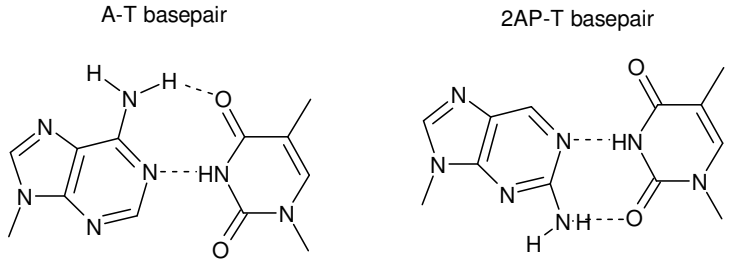

This section demonstrates the incorporation of intrinsically fluorescent 2-aminopurine to monitor the binding property of PNAs with the cDNA and to follow the accompanying structural changes.

Section B deals with the influence of imparting chirality to intrinsically non-chiral PNA and its effect on the induction of PNA helical structures and handedness of the PNA-DNA hybrids have been demonstrated. The chiral ligands D and L-Proline have been introduced at N and C-terminus of PNAs to study the effect of these stereogenic centers on chiral preorganization of the PNA backbone and its DNA binding properties. These complexes have been studied by UV-Tm and CD spectroscopy.

Chapter 5 presents the applications of isothermal titration calorimetry (ITC) and is divided into four sections.

Section I describes the thermodynamic parameters like enthalpy (ΔH), binding entropy (ΔS), binding constant (k), and Gibb's free energy (ΔG)) of interactions of modified PNA (*aepip*PNA & *aep*PNA) with cDNA as determined by ITC. The results are discussed in relation to structural modifications.

Section II is devoted to determine the energetics of interaction of the DNA nucleosides with keggin ions by ITC. The differential binding strengths of the four nucleosides have been described and can be exploited to develop suitable strategies of designing oligonucleotides for interaction with ligands.

Section III demonstrates the interaction of chiral DNA templates with the L- and D-lysine modified gold nanoparticles by ITC have been demonstrtaed. The chirality-dependent recognition of the modified gold nanoparticle surface by DNA is also described.

Section IV is a study of the interactions between the fungal protease (F-prot) in solution and gold nanoparticle bioconjugates with the substrate hemoglobin (Hb) as determined by ITC. The altered secondary structure of the enzyme in the bioconjugates and its interactions with the substrate compared with the free enzyme in solution are described and related to decrease in its biocatalytic activity.

1.11. REFERENCES

[1] Dickerson, R. E.; Drew, H. R.; Conner, B. N.; Wing, R. M.; Fratini, A. V.; Kopka, M. L. The anatomy of A-, B-, and Z-DNA. *Science,* **1982**, *216,* 475-485.

[2] Zamecnik, P. C.; Stephenson, M. L. Inhibition of Rous sarcoma virus replication and cell transformation by a specific oligodeoxynucleotide. *Proc. Natl. Acad. Sci. USA.* **1978**, *75*, 280-284.

[3] Watson, J. D.; Crick, F. H. C. Molecular structure of nucleic acid. A structure for deoxyribose nucleic acid. *Nature,* **1953**, *171*, 737-738.

[4] Crooke, S. T. *Therapeutic Applications of oligonucleotides*, 1995**,** Springer-Verlag:Heidolbery.

[5] Soyfer, V. N.; Potman, V. N. *Triple- Helical Nucleic Acids*, 1996**,** Springer-Verlag: NewYork.

[6] Hoogsteen, K. The crystal and molecular structure of a hydrogen-bonded complex between 1-methyl thymine and 9-methyl adenine. *Acta. Crystal.* **1963**, *16*, 907.

[7] Kurreck, J. Antisense technologies oligonucleotides Improvement through novel chemical modifications. *Eur. J. Biochem.* **2003**, *270*, 1628-1644.

[8] Opalinska, J. B.; Gewirtz, A. M. Nucleic-acid therapeutics: basic principles and recent applications. *Nat. Rev. Drug Discov.* **2002**, *1*, 503–514.

[9] Braasch, D. A.; Corey, D. R. Novel antisense and peptide nucleic acid strategies for controlling gene expression. *Biochemistry,* **2002**, *41*, 4503–4510.

[10] Herdewijn, P. Heterocyclic modifications of oligonucleotides and antisense technology. *Antisense Nucleic Acid Drug Dev.* **2000**, *10*, 297-310.

[11] Mickelfield, J. Backbone modification of nucleic acids: Synthesis, structure and therapeutic applications. *Current Med. Chem.* **2001**, *8*, 1157-1179.

[12] Eckstein, F. Phosphorothioate oligonucleotides: What is their origin and what is unique about them? *Antisense Nucleic Acids Drug Dev.* **2000**, *10*, 117–121.

[13] De Clercq, E.; Eckstein, F.; Merigan, T. C. Interferon induction increased through chemical modification of a synthetic polyribonucleotide. *Science,* **1969**, *165*, 1137 – 1139.

[14] Kurreck, J.; Wyszko, E.; Gillen, C.; Erdmann, V. A. Design of antisense oligonucleotides stabilized by locked nucleic acids. *Nucleic Acids Res.* **2002**, *30*, 1911–1918.

[15] Crooke, S. T.; Lemonidis, K. M.; Neilson, L.; Griffey, R.; Lesnik, E. A.; Monia, B. P. Kinetic characteristics of *Escherichia coli* RNase H1: cleavage of various antisense oligonucleotide- RNA duplexes. *Biochem. J.* **1995**, *312*, 599–608.

[16] Zamaratski, E.; Pradeepkumar, P. I.; Chattopadhyaya, J. A critical survey of the structure-function of the antisense oligo/RNA heteroduplex as substrate for RNase H. *J. Biochem. Biophys. Methods,* **2001**, *48*, 189–208.

[17] Petersen, M.; Nielsen, C. B.; Nielsen, K. E.; Jensen, G. A.; Bondensgaard, K.; Singh, S. K.; Rajwanshi, V. K.; Koshkin, A. A.; Dahl, B. M.; Wengel, J.; Jacobsen, J. P. The conformations of locked nucleic acids (LNA). *J. Mol. Recognit.* **2000,** *13*, 44–53.

[18] Nielsen, P.E.; Egholm, M.; Berg, R. H.; Buchardt, O. Sequence selective recognition of DNA by strand displacement with a thymine substituted ployamide. *Science,* **1991,** *254*, 1497-1500

[19] Nielsen, P.E.; Egholm, M. *Peptide Nucleic Acid (PNA). Protocols and Applicat*ions. Horizon Scientific Press. Norfolk, 1999.

[20] Nielsen, P.E. Applications of peptide nucleic acids. *Current Opinion in Biotechnology*, **1999**, *10*, 71-75.

[21] Nielsen, P.E. Peptide nucleic acids as therapeutic agents. *Current Opinion in Struct. Biology*, **1999**, *9*, 353-357.

[22] Nielsen, P.E. Antisense peptide nucleic acids. *Current Opinion in Molecular Therapeutics*, **2000**, *2*, 282-287.

[23] Egholm, M.; Buchardt, O.; Christensen, L.; Behrens, C.; Freier, S. M.; Driver, D. A.; Berg, R. H.; Kim, S. K.; Nordén, B.; Nielsen, P. E. PNA hybridizes to complementary oligonucleotides obeying the Watson-Crick hydrogen bonding rules. *Nature,* **1993**, *365*, 566-568.

[24] Bentin, T.; Nielsen, P. E. In *Triple Helix Forming Oligonucleotides* (Malvy, C., Barel-Bellan, A., Pritchard, L., eds.) Kluwer Academic Publishers, pp. 245-255.

[25] Lohse, J.; Dahl, O.; Nielsen, P.E. Double duplex invasion by peptide nucleic acid: A general principle for sequence-specific targeting of double stranded-DNA. *Proc. Natl. Acad. Sci. USA*. **1999,** *96,* 11804-11808.

[26] Jensen, K. K.; Orum, H.; Nielsen, P. E.; Norden, B. Kinetics for hybridisation of Peptide Nucleic Acids (PNA) with DNA and RNA studied with the BIAcore technique. *Biochemistry,* **1997,** *36*, 5072-5076.

[27] Giesen, U.; Kleider, W.; Berding, C.; Geiger, A.; Orum, H.; Nielsen, P. E. A formula for thermal stability (T_m) prediction of PNA/DNA duplexes. *Nucleic Acids Res*. **1998**, *26*, 5004-5009.

[28] Tomac, S.; Sarkar, M.; Ratilainen, T.; Wittung, P.; Nielsen, P. E.; Nordén, B.; Gräslund, A. Ionic effects on the stability and conformation of PNA complexes. *J. Amer. Chem. Soc.* **1996**, *118*, 5544-5552.

[29] Brown, S. C.; Thomson, S. A.; Veal, J. M.; Davis. D. G. NMR Solution structure of a Peptide nucleic acid complexed with RNA. *Science,* **1994,** *265*, 777-780.

[30] Eriksson, M.; Nielsen, P. E. Solution structure of a peptide Nucleic Acid-DNA duplex. *Nature Struct. Biol.* **1996**, *3*, 410-413.

[31] Betts, L.; Josey, J. A.; Veal, J. M.; Jordan, S. R. A nucleic acid triple helix formed by a Peptide Nucleic Acid-DNA complex. *Science*, **1995,** *270*, 1838-1841.

[32] Rasmussen, H.; Kastrup, J. S.; Nielsen, J. N.; Nielsen, J. M.; Nielsen, P.E. Crystal structure of a Peptide Nucleic acid (PNA) duplex at 1.7 A Resolution. *Nature Struct. Biol.* **1997,** *4*, 98-101.

[33] Hyrup, B.; Egholm, M.; Rolland, M.; Nielsen, P. E.; Berg, R. H.; Buchardt, O. Modification of the binding affinity of peptide nucleic acids (PNA). PNA with extended backbones consisting of 2-aminoethyl-β-alanine or 3-aminopropylglycine units. *J. Chem. Soc. Chem. Commun.* 1993, 518-519.

[34] Hyrup, B.; Egholm, M.; Nielsen, P.E.; Wittung, P.; Nordén, B.; Buchardt, O. Structure-activity studies of the binding of modified peptide nucleic acids (PNAs) to DNA. *J. Amer. Chem. Soc*. **1994,** *116*, 7964-7968.

[35] Hyrup, B.; Egholm, M.; Buchardt, O.; Nielsen, P. E. A flexible and positively charged PNA analogue with an ethylene-linker to the nucleobase: Synthesis and hybridization properties. *Bioorg. Med. Chem. Lett*. **1996**, *6*, 1083-1087.

[36] Efimov, V. A.; Choob, M. V.; Buryakova, A. A.; Chakhmakhcheva, O. G. Synthesis and binding study of phosphonate analogues of PNAs and their hybrids with PNA. *Nucleosides Nucleotides,* **1998**, *17*, 1671-1679.

[37] Efimov, V. A.; Buryakova, A. A.; Choob, M. V.; Chakhmakhcheva, O. G. Phosphonate analogues of peptide nucleic Acids and related compounds: synthesis and hybridazation properties. *Nucleosides Nucleotides,* **1999**, *18*, 1393-1396.

[38] Van der Laan, A. C.; Strömberg, R.; Van Boom, J. H.; Kuyl-Yeheskiely, E.; Chakhmakhcheva, O. G. An approach towards the synthesis of oligomers containing a N-2 hydroxyethyl-aminomethyl phosphonate backbone: A novel PNA analogue. *Tet. Lett.* **1996**, *37*, 7857-7860.

[39] Peyman, A.; Uhlmann, E.; Wagner, K.; Augustin, S.; Breipohl, G.; Will, D. W.; Schäffer, A.; Wallmeier, H. Phosphonic ester nucleic acids (PHONAs): oligonucleotide analogues with an achiral phosphonic acid ester backbone. *Angew. Chem. Int. Ed. Engl.* **1996**, *35*, 2636-2638.

[40] Kehler, J.; Henriksen, U.; Vekbjerg, H.; Dahl, O. Synthesis and hybridization properties of an acyclic phosphonate PNA analogues. *Bioorg. Med. Chem.* **1998**, *6*, 315-322.

[41] Altmann,K. H.; Chiesi, S.; Echevevria, C. Polyamide based nucleic acid analogues and 2013, 2013: Synthesis of δ amino acids with nucleic acid bases bearing side chains. *Bioorg. Med. Chem. Lett.* **1997**, *7*, 1119-1122.

[42] Kuwahara, A. M.; Sisido, M. Novel PNA that shows high sequence specificity and all-or none type hybridization with the complementary DNA. *J. Am, Chem. Soc*. **1999**, *121*, 256-257.

[43] Barawkar, D.; Bruice, T. Deoxynucleic guanidines/PNA(DNG/PNA) chimeras: Oligonucleoside analogues containing cationic guanidium and neutral amide linkages. *J. Am. Chem. Soc*. **1999**, *121*, 10418-10419.

[44] Zhou, P.; Wang, M.; Du, L.; Fisher, G. W.; Waggoner A.; Ly, W. H. Novel binding and efficient cellular uptake of guanidine-based peptide nucleic acids (GPNA). *J. Am. Chem. Soc*. **2003,** *125*, 6878-6879.

[45] Krotz, A. H.; Buchardt, O.; Nielsen P. E. Synthesis of retro-inverso peptide nucleic acids: 1chracterisation of the monomer. *Tetrahedron Lett.* **1995**, *36*, 6937-6940.

[46] Almarison, O.; Bruice, T. C. Peptide Nucleic Acids (PNA) conformation and polymorphism in PNA-DNA and PNA-RNA hybrids. *Proc. Natl. Acad. Sci*. USA **1993**, *90*, 9542-9546.

[47] Lagriffoule, P. H.; Egholm, M.; Nielsen, P. E.; Berg, R. H.; Buchardt, O. The synthesis, co-oligomerisation and hybridization of thymine-thymine heterodimer containing peptide Nucleic Acid. *Bioorg. Med. Chem. Lett*. **1994**, *4*, 1081-1082.

[48] Wengel, J. Synthesis of 3'-*C*- and 4'-*C*-Branched Oligodeoxynucleotides and the Development of Locked Nucleic Acid (LNA). *Acc. Chem. Res.* **1999**, *32*, 301-310.

[49] Lescrinier, E.; Esnouf, R.; Schraml, J.; Busson, R.; Heus, H. A.; Hilbers, C. W.; Herdewijn, P. Solution structure of a HNA–RNA hybrid. *Chem. Biol.* **2000**, *7*, 719-731.

[50] Allart, B.; Khan, K.; Rosemeyer, H.; Schepers, G.; Hendrix, C.; Rothenbacher, K.; Seela, F.; Van Aerschot, A.; Herdewijn, P. D-altritol nucleic acids (ANA): hybridisation properties, stability, and initial structural analysis. *Chem. Eur. J.* **1999**, *5*, 2424-2431.

[51] Robinson, D. S.; Greenstein, J. P. Stereoisomers of hydroxyproline. *J. Biol. Chem.* **1952**, *195*, 383-388.

[52] Webb, T. R.; Eigenbrot, C. Conformationally restricted arginine analogs. *J. Org. Chem.* **1991**, *56*, 3009-3016.

[53] Gangamani. B. P.; Kumar, V. A.; Ganesh, K. N. Synthesis of N-(purinyl/pyrimidinyl acetyl)-4-aminoproline diastereomers with potential use in PNA synthesis. *Tetrahedron,* **1996**, *52*, 15017-15030.

[54] Jordan, S.; Schwemler, C.; Kosch, W.; Kretschmer, A.; Schwenner, E.; Milke, B. New hetero-oligomeric peptide nucleic acids with improved binding properties to complementary DNA. *Bioorg. Med. Chem. Lett.* **1997**, *7*, 687-692.

[55] Meena; Kumar, V. A.; Ganesh, K. N. Synthesis and evaluation of prolyl carbamate nucleic acids (PrCNA). *Nucleosides, Nucleotides, Nucleic Acids,* **2001**, *20*, 1193-1196.

[56] Lowe, G.; Vilaivan, T. Amino acids bearing nucleobases for the synthesis of novel peptide nucleic acids. *J. Chem. Soc. Perkin Trans 1,* **1997**, 539-546.

[57] Lowe, G.; Vilaivan, T. Solid phase synthesis of novel peptide nucleic acids. *J. Chem. Soc. Perkin Trans I* **1997**, 555-560.

[58] D'Costa, M.; Kumar, V. A.; Ganesh, K. N. Aminoethylprolyl peptide nucleic acids(*aep*PNA) : chiral PNA analogues that forms highly stable DNA:*aep*PNA_2 triplexes. *Org. Lett*. **1999**, *1*, 1513-1516.

[59] Puschl, A.; Boesn, G.; Zuccarello, G.; Dahl, O.; Pitsch, S.; Nielsen, P. E. Synthesis of pyrrolidinone PNA: A novel conformationally restricted peptide nucleic acid analogues. *J. Org. Chem.* **2001**, *66*, 707-712.

[60] Samuel, T. H.; David, T.; Hickman, T.; Morral, J.; Beadham, I. G.; Micklefield, J. Nucleic acid binding properties of thyminyl and adeninyl pyrrolidine-amide oligonucleotide mimics (POM). *Chem. Comm*. **2004**, 516-517.

[61] Sharma, N. K.; Ganesh, K. N. Expanding the repertoire of pyrrolidyl PNA analogues for DNA/RNA hybridization selectivity: aminoethylpyrrolidinone PNA (*aepone*-PNA) *Chem. Commun.* **2003**, 2484-2485.

[62] Vilaivan, T.; Khongdeesameor, C.; Harnyuttanokam, P.; Lowe, G. Synthesis and properties of novel pyrrolidinyl PNA carrying β amino acid spacers. *Tetrahedron Lett.* **2001**, *42*, 5533-5536.

[63] Vilaivan, T.; Khongdeesameor, C.; Harnyuttanokam, P.; Lowe, G. J. A novel pyrrolidinyl PNA showing high sequence specificity and preferential binding to DNA over RNA. *J. Am. Chem. Soc.* **2002,** *124,* 9326-9327.

[64] Puschl, A.; Tedeschi, T.; Nielsen, P. E. Pyrrolidine PNA: A novel conformationally restricted PNA analogues. *Org. Lett.* **2000**, *2*, 4161-4163.

[65] Lonkar, P. S.; Ganesh, K. N.; Kumar, V. A. Chimeric (*aeg*-pyrrolidine)PNAs: synthesis and stereodiscriminative duplex binding with DNA/RNA. *Org. Biomol. Chem.* **2004**, *2*, 2604-2611.

[66] Michael, C. Mark, M.; Witschi, A.; Larionova, N.; John, M.; Russell; Haynes, D.; Toshiaki, H.; Grajkowski, A.; Appella, D. H. A cyclopentane conformational restraint for a Peptide Nucleic Acid: Design, asymmetric synthesis and improved binding affinity to DNA & RNA. *Org. Lett.* **2003**, *5*, 2695-2698.

[67] Govindaraju, T.; Kumar, V. A.; Ganesh, K. N. *cis*-Cyclopentyl PNA (*cp*PNA) as constrained chiral PNA analogues: stereochemical dependence of DNA/RNA hybridization. *Chem. Commun*. **2004**, *7*, 860-861.

[68] Pokorski, J. K.; Witschi, M. A.; Purnell, B. L.; Appella, D. H. *(S,S)-trans-c*yclopentane constrained peptide nucleic acids. A general backbone

modification that improves binding affinity and sequence specificity. *J. Am. Chem. Soc.* **2004**, *126*, 15067-15073.

[69] Govindaraju, T.; Kumar, V. A. Backbone-extended pyrrolidine peptide nucleic acids (*bep*PNA): design, synthesis and DNA/RNA binding studies. *Chem. Commun.* **2005**, 4, 495-497.

[70] Schoning, K.; Scholz, P.; Guntha, S.; Wu, X.; Krishnamurthy, R.; Eschenmoser, A. Chemical etiology of nucleic acid structure: The–threofuranosyl (3'-2) oligonucleotide system. *Science,* **2000**, *290*, 1347-1351.

[71] Summerton, J. D.; Weller. Morpholino antisense oligomers: design, preparation and properties. *Antisense Nucleic Acid Druug Dev.* **1997,** *7*, 187-195.

[72] Lescrinier, E.; Esnouf, R.; Schraml, J.; Busson, R.; Heus, H. A.; Hilbers, C. W.; Herdewijn, P. Solution structure of HNA-RNA hybrid. *Chem. Biol*. **2000**, *7,* 719-731.

[73] Wang, B.; Verbeure, I.; Luyten, E.; Lescrinier, M.; Froeyen, C.; Hendrix, H.; Rosemeyer, F.; Seela, A.; Van-Aerschot.; Herdwijn, P. Cyclohexene nucleic acids(CeNA): Serum stable oligonucleotides that activate RNase H and increase duplex stability with complementary RNA. *J. Am. Chem. Soc*. **2000,** *122*, 8595-8602.

[74] Goodnow, R. A.; Tam, S.; Pruess, D. L.; McComas, W. Oligomer synthesis and DNA/RNA recognition properties of a novel oligonucleotide backbone analog: Glucopyranosyl nucleic amide (GNA). *Tetrahedron Lett.* **1997,** *38*, 3199-3202.

[75]Puschl, A.; Boesen, T.; Tedeschr, T.; Dahl, O.; Nielsen, P. E. Synthesis of (3*R*,6*R*)- and (3*S*,6*R*)-piperidinone PNA. *J. Chem.Soc. Perkin 1* **2001,** 2757-2763.

[76] Lagriffoule, P.; Wittung, P.; Eriksson, M.; Jensen, K. K.; Norden, P.; Buchardt, O.; Nielsen, P. E. Peptide nucleic acids with a conformationally constrained chiral cyclohexyl-derived backbone. *Chem. Eur. J.* **1997**, *3*, 912-919.

[77] Govindaraju, T. G.; Ganesh, K. N.; Kumar, V. A. Synthesis and evaluation of (1*S*,2*R*/1*R*,2*S*)-aminocyclohexylglycyl PNAs as conformationally preorganised PNA analogues for DNA/RNA recognition. *J. Org. Chem.* **2003**, *69*, 1858-1865.

[78] Lonkar, P. S.; Kumar, V. A. Design and synthesis of conformationally frozen peptide nucleic acid backbone: chiral piperidine PNA as a hexitol nucleic acid surrogate. *Bioorg. Med. Chem. Lett.* **2004**, *14*, 2147–2149.

[79] Maison, W.; Schlemminger, I.; Westterhoff, O.; Martens. J. Modified PNAs : A simple method for the synthesis of monomeric building blocks. *Bioorg. Med. Chem. Lett*. **1999**, *9*, 581-584.

[80] Egholm, M.; Christensen, L.; Dueholm, K.; Buchardt, O.; Coull, J.; Nielsen, P. E. Efficient pH-independent sequence-specific DNA binding by pseudoisocytosine containing bis-PNA. *Nucleic Acids Res.* **1995**, *23*, 217-222.

[81] Haaima, G.; Hansen, H. F.; Christensen, L.; Dahl, O.; Nielsen, P. E. Increased DNA binding and sequence discrimination of PNA oligomers containing 2,6-diaminopurine. *Nucleic Acids Res.* **1997**, *25*, 4639.

[82] Gangamani, B. P.; Kumar, V. A.; Ganesh, K. N. 2-Aminopurine peptide nucleic acids (2-*ap*PNA): intrinsic fluorescent PNA analogues for probing PNA–DNA interaction dynamics. *J. Chem. Soc. Chem. Commun.* **1997**, 1913-1914.

[83] Kohler, O; Seitz, O. Thiazole orange as fluorescent universal base in PNA. *Chem. Commun.* **2003**, 2938-2939.

[84] Eldrup, A. B.; Dahl, O.; Nielsen, P. E. A novel Peptide Nucleic Acid monomer for recognition of thymine in triple helix structure. *J. Am. Chem. Soc.* **1997**, *119*, 11116.

[85] Timar, Z.; Bottka, S.; Kovacs, L.; Penke, B. Synthesis and preliminary thermodynamic investigation of hypoxanthine-containing peptide nucleic acids. *Nucleosides Nucleotides* **1999**, *18*, 1131-1133.

[86] Bergmann, F.; Bannwarth, W.; Tam, S. Solid phase synthesis of directly linked PNA-DNA hybrids. *Tetrahedron Lett.* **1995**, *36*, 6823-6826.

[87] Nielsen, P. E.; Egholm, M.; Berg, R. H.; Buchardt, O. Sequence specific inhibition of DNA restriction enzyme cleavage by PNA. *Nucleic Acids Res*. **1993**, *21*, 197-200.

[88] Pooga, M..; Soomets, U.; Hällbrink, M.; Valkna, A.; Saar, K.; Rezaei, K.; Kahl, U.; Hao, Jing-Xia; Xu, Xiao-Jun; Weisenfeld-Hallin, Z.; Hökfelt, T.; Bartfai, T.; Langel, Ü. Cell penetrating PNA constructs regulate galanin receptor levels and modify pain transmission *in vivo*. *Nat. Biotech.* **1998**, *16*, 857-861.

[89] Hamilton, S. E.; Simmons, C. G.; Kathiriya, I. S.; Corey, D. R. Cellular delivery of peptide nucleic acids and inhibition of human telomerase. *Chem. Biol.* **1999,** *6,* 343-347.

[90] Fraser, G. L.; Holmgren, J.; Clarke, P. B.; Wahlestedt, C. Antisense inhibition of δ-opioid receptor gene function in vivo by peptide nucleic acids. *Mol. Pharmacol.* **2000,** *57*, 725-731.

[91] Nielsen, P. E.; Egholm, M.; Buchardt, O. Sequence specific transcription arrest by peptide nucleic acid bound to the DNA template strand. *Gene,* **1994**, *149*, 139–145.

[92] Hanvey, J. C.; Peffer, N. C.; Bisi, J. E.; Thomson, S. A.; Cadilla, R.; Josey, J. A.; Ricca, D. J.; Hassman, C. F.; Bonham, M. A.; Au, K. G.; Carter, S. G.; Bruckenstein, D. A.; Boyd, A. L.; Noble, S. A.; Babiss, L. E. Antisense and antigene properties of peptide nucleic acids. *Science,* **1992**, *258*, 1481–1485.

[93] Praseuth, D.; Grigoriev, M.; Guieysse, A. L.; Pritchard, L. L.; Harel-Bellan, A.; Nielsen, P. E.; Helene, C. Peptide nucleic acids directed to the promoter of the alpha-chain of the interleukin-2 receptor. *Biochim. Biophys. Acta,* **1996**, *1309***,** 226–238.

[94] Tomac, S.; Sarkar, M.; Ratilainen, T.; Wittung, P.; Nielsen, P. E.; Norden, B.; Graslund, A. Ionic effects on the stability and conformation of peptide nucleic acid complexes. *J. Am. Chem. Soc.* **1996**, *118*, 5544–5552.

[95] Bentin, T.; Nielsen, P. E. Enhanced peptide nucleic acid binding to supercoiled DNA: possible implications for DNA 'breathing' dynamics. *Biochemistry,* **1996**, *35*, 8863–8869.

[96] Egholm, M.; Christensen, L.; Dueholm, K. L.; Buchardt, O.; Coull, J.; Nielsen, P. E. Efficient pH-independent sequence-specific DNA-binding by pseudoisocytosine-containing bis-PNA. *Nucleic Acids Res.* **1995**, *23*, 217–222.

[97] Kuhn, H.; Demidov, V. V.; Frank-Kamenetskii, M. D.; Nielsen, P. E. Kinetic sequence discrimination of cationic bis-PNAs upon targeting of double-stranded DNA. *Nucleic Acids Res.* **1998**, *26*, 582–587.

[98] Lee, R.; Kaushik, N.; Modak, M. J.; Vinayak, R.; Pandey, V. N. Polyamide nucleic acid targeted to the primer binding site of the HIV-1 RNA genome blocks *in vitro* HIV-1 reverse transcription. *Biochemistry,* **1998**, *37*, 900–910.

[99] Knudsen, H.; Nielsen, P. E. Antisense properties of duplex- and triplex-forming PNAs. *Nucleic Acids Res.* **1996**, ***24,*** 494–500.

[100] Good, L.; Nielsen, P. E. Inhibition of translation and bacterial growth by peptide nucleic acid targeted to ribosomal RNA. *Proc. Natl. Acad. Sci. USA.* **1998**, *95*, 2073–2076.

[101] Good, L.; Nielsen, P. E. Antisense inhibition of gene expression in bacteria by PNA targeted to mRNA. *Nat. Biotech.* **1998**, *16*, 355–358.

[102] Taylor, R. W.; Chinnery, P. F.; Turnbull, D. M.; Lightowlers, R. N. Selective inhibition of mutant human mitochondrial DNA replication *in vitro* by peptide nucleic acids. *Nature Genet.* **1997**, *15*, 212–215.

[103] Uhlmann, E.; Peyman, A.; Breipohl, G.; Will, D. W. PNA: synthetic polyamide nucleic acids with unusual binding properties. *Angew. Chem. Int. Ed.* **1998***, 37*, 2796–2823.

[104] Nielsen, P. E.; Egholm, M.; Berg, R. H.; Buchardt, O. Peptide nucleic acids (PNAs): potential antisense and antigene agents. *Anti-Cancer Drug Design,* **1993**, *8,* 53–63.

[105] Koppelhus, U.; Zachar, V.; Nielsen, P. E.; Liu, X.; Eugen-Olsen, J.; Ebbesen, P. Efficient in vitro inhibition of HIV-1gag reverse transcription by peptide nucleic acid (PNA) at minimal ratios of PNA/RNA. *Nucleic Acids Res.* **1997**, *25*, 2167–2173.

[106] Mologni, L.; leCoutre, P.; Nielsen, P. E.; Gambacorti-Passerini, C. Additive antisense effects of different PNAs on the *in vitro* translation of the PML/RARa gene. *Nucleic Acids Res.* **1998**, *26*, 1934–1938.

[107] Norton, J. C.; Piatyszek, M. A.; Wright, W. E.; Shay, J. W.; Corey, D. R. Inhibition of human telomerase activity by peptide nucleic acids. *Nat. Biotech.* **1996**, *14*, 615–620.

[108] Hamilton, S. E.; Simmons, C. G.; Kathiriya, I. S.; Corey, D. R. Cellular delivery of peptide nucleic acids and inhibition of human telomerase. *Chem. Biol.* **1999**, *6*, 343–351.

[109] Petersen, M. B.; Economou, E. P.; Slaugenhaupt, S. A.; Chakravarti, A.; Antonarakis, S. E. Linkage analysis of the human HMG14 gene on chromosome 21 using a GT dinucleotide repeat as polymorphic marker. *Genomics,* **1990**, *7*, 136–138.

[110] Pena, S. D.; Chakraborty, R. Paternity testing in the DNA era. *Trends Genet.* **1994**, *10*, 204–209.

[111] Demers, D. B.; Curry, E. T.; Egholm, M.; Sozer, A. C. Enhanced PCR amplification of VNTR locus D1S80 using peptide nucleic acid (PNA). *Nucleic Acids Res.* **1995**, *23,* 3050–3055.

[112] Perry-O'Keefe, H.; Yao, X. W.; Coull, J. M.; Fuchs, M.; Egholm, M. Peptide nucleic acid pre-gel hybridization: an alternative to Southern hybridization. *Proc. Natl. Acad. Sci. USA*. **1996**, *93*, 14670–14675.

[113] Veselkov, A. G.; Demidov, V.; Nielsen, P. E.; Frank-Kamenetskii, M. D. A new class of genome rare cutters. *Nucleic Acids Res.* **1996**, *24*, 2483–2487.

[114] Frank-Kamenetskii, M. D.; Demidov, V. V. PNA directed genome rare cutting: new developments. *http://www.bu.edu/cab*

[115] Demidov, V.; Frank-Kamenetskii, M. D.; Egholm, M.; Buchardt, O.; Nielsen, P. E. Sequence specific double strand DNA cleavage by peptide nucleic acid (PNA) targeting using nuclease S1. *Nucleic Acids Res.* **1993**, *21*, 2103–2107.

[116] Lansdorp, P. M.; Verwoerd, N. P.; van de Rijke, F. M.; Dragowska, V.; Little, M. T.; Dirks, R. W.; Raap, A. K.; Tanke**,** H. J. Heterogeneity in telomere length of human chromosomes. *Hum. Mol. Genet.* **1996**, *5*, 685–691.

[117] Orum, H.; Nielsen, P. E.; Jorgensen, M.; Larsson, C.; Stanley, C.; Koch, T. Sequence-specific purification of nucleic acids by PNA-controlled hybrid selection. *BioTechniques,* **1995**, *19*, 472–480.

[118] Orum, H.; Nielsen, P. E.; Egholm, M.; Berg, R. H.; Buchardt, O.; Stanley, C. Single base pair mutation analysis by PNA directed PCR clamping. *Nucleic Acids Res.* **1993**, *21*, 5332–5336.

[119] Thiede, C.; Bayerdorffer, E.; Blasczyk, R.; Wittig, B.; Neubauer, A. Simple and sensitive detection of mutations in the ras proto-oncogenes using PNA-mediated PCR clamping. *Nucleic Acids Res.* **1996**, *24*, 983–984.

[120] Bonnet, G.; Tyagi, S.; Libchaber, A.; Kramer, F. R. Thermodynamic basis of the enhanced specificity of structured DNA probes. *Proc. Natl. Acad. Sci.* USA, **1999**, *96*, 6171-6176.

[121] Marras, SAE.; Kramer, F. R.; Tyagi, S. Efficiencies of fluorescence resonance energy transfer and contact-mediated quenching in oligonucleotide probes. *Nucleic Acids Res.* **2002**, *30*, 122-127.

[122] Brandt, O.; Hoheisel, J. D. Peptide nucleic acids on microarrays and other biosensors. *Trends Biotech.* **2004**, *22*, 617-622.

[123] Miller, P. S.; McParland, K. B.; Jayaraman, K.; Ts'O, P. O. P. Biochemical and biological effects of nonionic nucleic acid methylphosphonates. *Biochemistry,* **1981,** *20*, 1874.

[124] Marcus-Secura, C. J.; Woerner, A. M.; Shinozuka, K.; Zon, G.; Quinnan, G. V. Jr. Comparative inhibition of chloramphenicol acetyltransferase gene expression by antisense oligonucleotide analogues having alkyl phosphotriester, methylphosphonate and phosphorothioate linkages. *Nucleic Acids Res.* **1987**, *15*, 5749.

[125] Nielsen, P. E. Sequence-specific recognition of double stranded DNA by peptide nucleic acids. *Adv. DNA Sequence-Specific Agents,* **1998**, *3*, 267–278.

[126] Faruqi, A. F.; Egolm, M.; Glazer, P. M. Peptide nucleic acid-targeted mutagenesis of a chromosomal gene in mouse cells. *Proc. Natl. Acad. Sci. USA.***1997**, *95*, 1398–1403.

[127] Pooga, M.; Soomets, U.; Hallbrink, M.; Valkna, A.; Saar, K.; Rezaei, K.; Kahl, U.; Hao, J. X.; Xu, X. J.; Wiesenfeld-Hallin, Z. Cell penetrating PNA constructs regulate galanin receptor levels and modify pain transmission *in vivo. Nat. Biotech.* **1998**, *16*, 857–861.

[128] Basu, S.; Wickstrom, E. Synthesis and characterization of a peptide nucleic acid conjugated to a D-peptide analog of insulin-like growth factor 1 for increased cellular uptake. *Bioconj. Chem.* **1997**, *8*, 481–488.

[129] Simmons, C. G.; Pitts, A. E.; Mayfield, L. D.; Shay, J. W.; Corey, D. R. Synthesis and permeability of PNA-peptide conjugates. *Bioorg. Med. Chem. Lett.* **1997**, *7*, 3001–3007.

[130] Aldrian-Herrada, G.; Desarmenien, M. G.; Orcel, H.; Boissin-Agasse, L.; Mery, J.; Brugidou, J.; Rabie, A. A peptide nucleic acid (PNA) is more rapidly internalized in culture neurons when coupled to a retro-inverso delivery peptide. The antisense activity depresses the target mRNA and protein in magnocellular oxytocin neurons. *Nucleic Acids Res.***1998**, *26*, 4910–4916.

[131] Hamilton, S. E.; Simmons, C. G.; Kathiriya, I. S.; Corey, D. R. Cellular delivery of peptide nucleic acids and inhibition of human telomerase. *Chem. Biol.* **1999**, *6*, 343–351.

[132] Kaihatsu, K.; Huffman, K. E.; Corey D. R. Intracellular Uptake and Inhibition of Gene Expression by PNAs and PNA-Peptide Conjugates. *Biochemistry,* **2004**, *43,* 14340-14347.

[133] Ratilainen, T.; Holmen, A.; Tuite, E.; Haaima, G.; Christensen, L.; Nielsen, P. E.; Norden, B. Hybridization of peptide nucleic acid. *Biochemistry,* **1998**, *37*, 12331–12342.

[134] Holmen. A.; Norden, B. Thermodynamics of PNA-nucleic acid interactions. In *Peptide Nucleic Acids: Protocols and Applications* (Nielsen, P. E., and Egholm, M., eds) 1999, pp. 87–97, Horizon Press, Wymondham, U.K.

[135] Marky, L. A.; Breslauer, K. J. Calculating thermodynamic data for transitions of any molecularity from equilibrium melting curves. *Biopolymers,* **1987**, *26*, 1601–1620.

[136] Fire, A. *et al*. Potent and specific genetic interference by double-stranded RNA in *Caenorhabditis elegans*. *Nature,* **1998**, *391*, 806–811.

[137] Mello, C. C.; Conte Jr, D. Revealing the world of RNA interference. *Nature,* **2004**, *431*, 338-341

[138] Carrington, J. C.; Ambros, V. Role of microRNAs in plant and animal development. *Science* **2003**, *301*, 336-338.

[139] Ambros, V. MicroRNA pathways in flies and worms: growth, death, fat, stress, and timing. *Cell,* **2003**, *113*, 673-676.

[140] Xu, P.; Vernooy, S. Y.; Guo, M.; Hay, B. A. The Drosophila microRNA mir-14 suppresses cell death and is required for normal fat metabolism. *Curr. Biol*. **2003**, *13*, 790-795.

[141] Tang, J.; Breaker, R. R. Structural diversity of self-cleaving ribozymes. *Proc. Natl. Acad. Sci.* USA, **2000**, *97*, 5784-5789.

[142] Winkler, W. C.; Nahvi, A.; Roth, A.; Collins, J. A.; Breaker, R. R. Control of gene expression by a natural metabolite-responsive ribozyme. *Nature,* **2004,** *428,* 281-286.

CHAPTER 2:

SYNTHESIS OF (2*R/S*,5*S/R*)-1-(*N*-BOC-AMINOETHYL)-5-(THYMIN-1-YL)PIPECOLIC ACID: SYNTHESIS AND DNA BINDING STUDIES

2.1. INTRODUCTION

Chapter 1 described how the search for effective antigene/antisense agents has led to the development of novel DNA/RNA analogues in the past decade.[1-8] The most prominent outcome of this search is the Peptide Nucleic Acids (PNA).[9-14] In this class

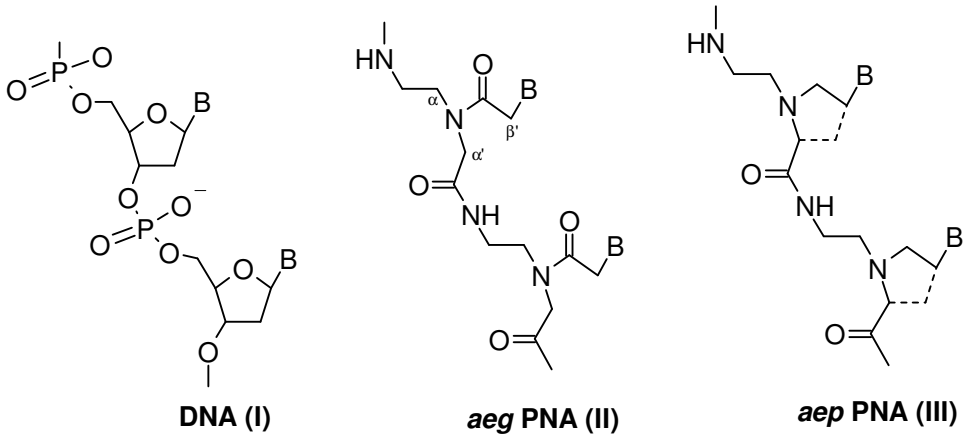

Figure 1. The basic structures of DNA, PNA and *aep*PNA.

of compounds, the entire negatively charged sugar-phosphate backbone of DNA is replaced by a neutral and achiral polyamide backbone consisting of N-(2-aminoethyl)glycine units. The nucleobases are attached to the backbone through a conformationally rigid tertiary acetamide linker (Figure 1). PNA binding to the target DNA/RNA sequences occurs with high sequence specificity and affinity.[15] Despite having several advantages like resistance to cellular enzymes like nucleases and proteases, the major limitations confounding its application are ambiguity in orientational selectivity of binding, poor solubility in aqueous media and inefficient cellular uptake.[16] To overcome these problems, attempts have been made to introduce asymmetry into PNA backbone in a novel fashion that not only makes it chiral but also introduces certain conformational constraint to induce unambiguous binding to

complementary DNA/RNA. These have resulted in novel class of PNA analogues as shown in Figure 2.

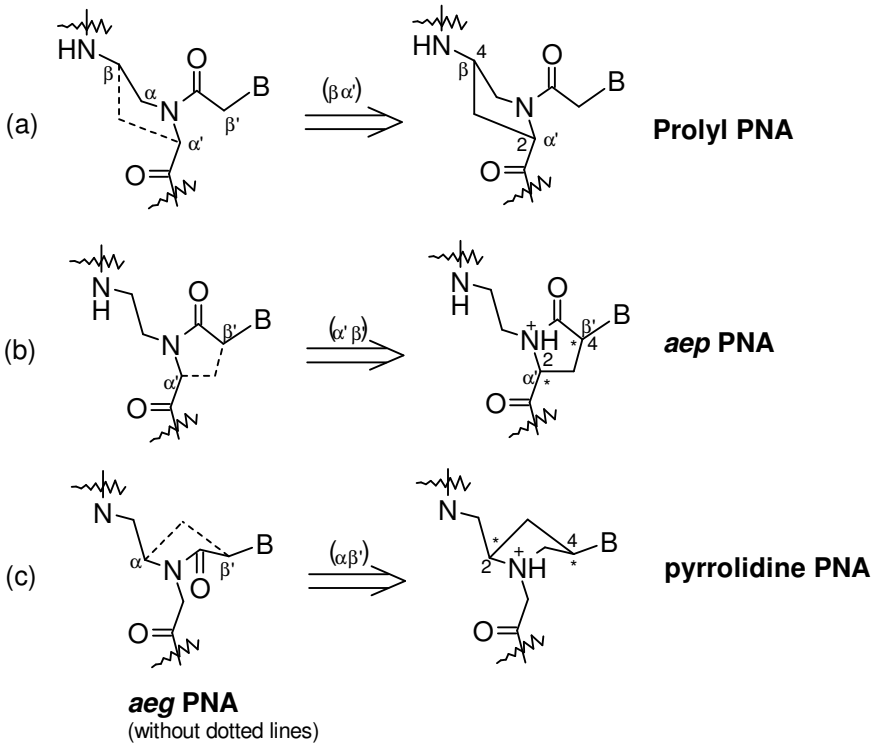

Figure 2. Strategies for the design of conformationally constrained PNA analogues.

Previous efforts[17,18,19] from this laboratory and that of others[20] to improve the properties of *aeg*PNA to achieve optimal fine-tuning of aminoethylglycyl, *aeg*PNA backbone has resulted in a number of five-membered pyrrolidyl PNA analogues. The *aeg*PNA backbone is highly flexible due to the presence of 2-aminoethyl and glycyl segments that slowly reorganize to the preferred conformations during complex formation with DNA/RNA. Preorganizing the *aeg*PNA backbone into "hybridization competent conformations" should be associated with entropic advantages for binding DNA/RNA. We reported previously from our laboratory, chiral aminoethylprolyl *aep*PNA (**III**), designed by linking the glycyl α'-carbon in the *aeg*PNA to the acetamido β'-carbon via a methylene bridge.[18] In *aep*PNA, the nucleobase is directly

attached to a pyrrolidine ring that is a part of the backbone along with a flexible ethylene amino linker. In *aeg*PNA the nucleobase is linked to the backbone via acetamido moiety. This PNA analogue with positively charged tertiary amine in the backbone, along with conformational constraint due to the five-membered pyrrolidine ring significantly improved the solubility, affinity and selectivity in DNA:PNA binding. The high affinity was achieved without compromising the base-pairing specificity.[17] The stability of the duplexes was found to be dependent upon the stereochemistry of the pyrrolidine ring and also the nucleobase.

2.1.1. Present work: A Rationale

The present work is directed towards further studying the performance of *aep*PNA molecules, by aiming to synthesize and evaluate their six membered ring analogues - aminoethyl pipecolic acid PNAs (*aepip*PNA, **IV**). These have two chiral centers leading to the possibility of synthesizing four diasteromers. This is designed by bridging the α'-C atom of the glycyl unit and the β'-C atom of linker to nucleobase in PNA with an ethylene bridge to generate a six-membered piperidine ring **IV**, with simultaneous introduction of two chiral centers. The nucleobase in **IV** is directly

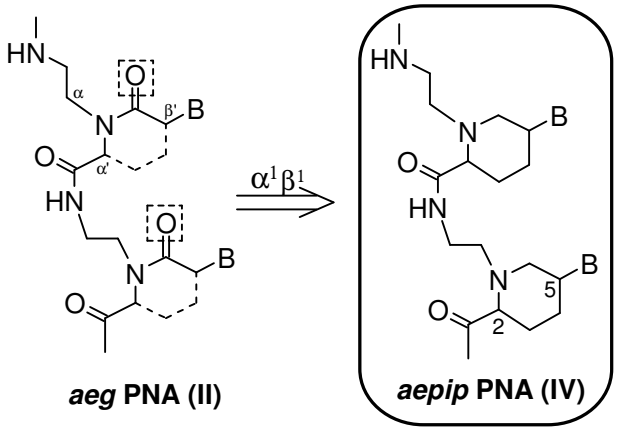

Figure 3. Design of *aepip*PNA.

attached to the piperidine ring at the C5 position, without changing the net number of atoms connecting two successive nucleobases. Further, the two chiral centers at C2 and C5 offer an opportunity to study the stereochemical implications on the interactions of chiral PNA with ss/ds DNA/RNA.

The objectives of this chapter are:

(i) Synthesis of 1-(*N*-Boc-aminoethyl)-5(*R*)-(thymin-1-yl)-2(*S*)-pipecolic acid monomer (**13**).

(ii) Synthesis of 1-(*N*-Boc-aminoethyl)-5(*S*)-(thymin-1-yl)-2(*R*)-pipecolic acid (**26**).

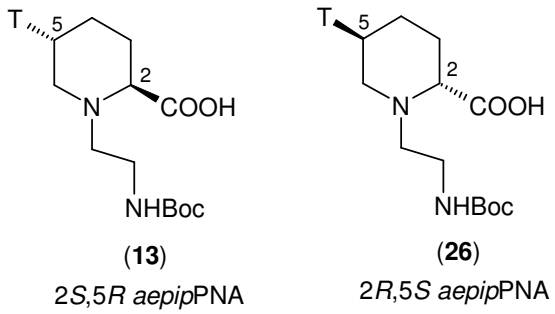

Figure 4. *aepip*PNA monomers.

(iii) Solid phase synthesis of PNA oligomers incorporating aminoethylglycyl and/or aminoethylpipecolyl PNA units followed by purification and characterization.

(iv) Biophysical studies of *aepip*PNA:DNA hybrids using UV-T_m, CD and gel electrophoresis.

2.2. RESULTS AND DISCUSSION

The Synthetic Strategy

The conformations in the six-membered ring structures are rigidly locked into chair/boat forms in contrast to the relatively flexible five-membered ring structures and hence their influence on the stability of the resulting PNA-DNA/RNA complexes may be expected to make important contributions to the stabilities of the DNA/RNA complexes. All the four stereoisomers of *aepip*PNA monomers were subjected to energy minimization by silicon graphics using IRIX 6.2, it was found that upon energy minimization, 2*S*,5*R* *aepip*PNA has a lower energy structure compared to 2*R*,5*S* *aepip*PNA (2*S*,5*R* *aepip*PNA = 15.248 kcal, 2*R*,5*S* *aepip*PNA = 16.097 kcal). Upon energy minimization, it was observed that C5-base and C2-carboxyl groups are axial in 2*S*,5*R* *aepip*PNA and equatorial in 2*R*,5*S* *aepip*PNA (Figure 5).

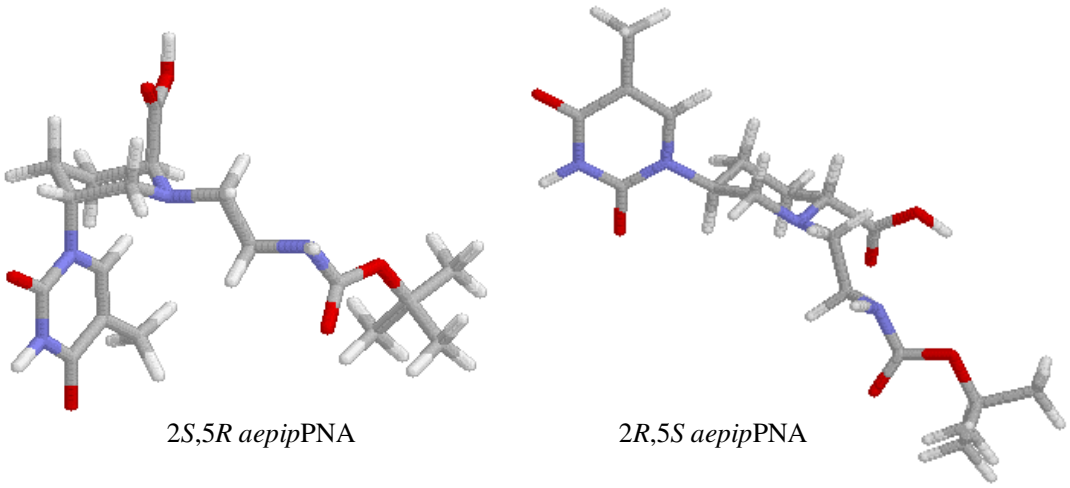

2*S*,5*R* *aepip*PNA 2*R*,5*S* *aepip*PNA

Figure 5. Energy minimised structures of *aepip*PNA monomers using IRIX 6.2.

The synthesis of the (2*S*,5*R*) 1-(*N*-Boc-aminoethyl)-5-(*N*3-benzoylthymin-1-yl)pipecolic acid (**13**) can be achieved via the intermediates (**7**) and (**10**) in ten steps starting from the naturally occurring L-glutamic acid. The retro-synthetic analysis (Figure 6) is via the putative intermediates (**8**) and (**10**) synthesized from L-glutamic

acid through the diazoketone (**7**) where cyclisation proceeds with retention of configuration at C2. The key step is the direct conversion of diazoketone to the protected 5-oxopipecolic acid which can be achieved by ring closure carbene insertion

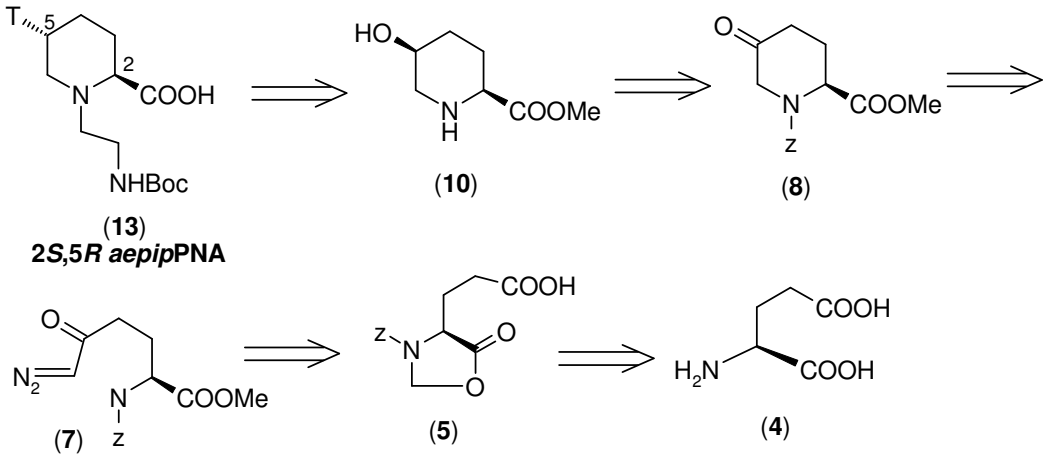

Figure 6. Retro-synthetic analysis of *aepip*PNA monomer.

into the N-H bond using rhodium (II) acetate as catalyst. Finally, stereospecific reduction to *cis*-5-hydroxy-pipecolic acid ester.[21,22] *N*1-deprotection and further alkylation with N-Boc-aminoethyl mesylate should afford the (1-*N*-Boc-aminoethyl)pipecolic acid ester (**11**) in which the replacement of the 5*S*-hydroxyl function with *N*3-benzoylthymine under Mitsunobu reaction conditions would yield

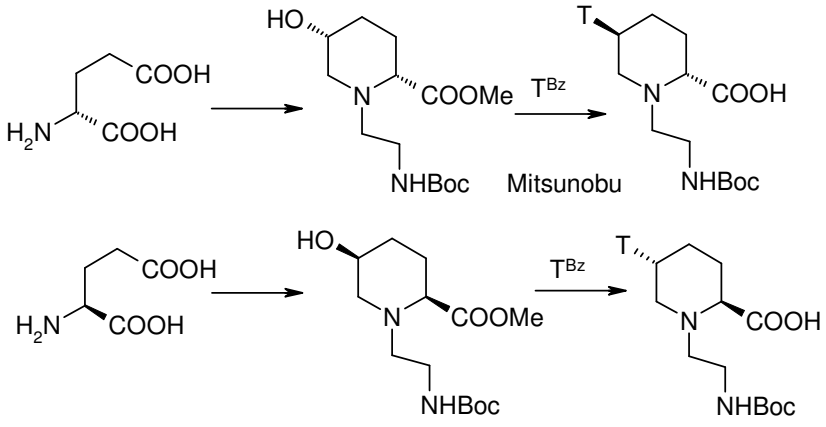

Figure 7. Schematic synthesis of *aepip*PNA monomer.

the desired (2*S*,5*R*)-5-(*N*3-benzoylthymin-1-yl) pipecolate ester, accompanied by inversion of stereochemistry at C5. This can be converted to (2*S*,5*R*)-1-(*N*-Boc-aminoethyl)-5-(thymin-1-yl)pipecolic acid as the desired monomer (Figure 7).

Similarly starting from the D-Glutamic acid and an identical set of reaction should lead to (2*R*,5*S*)-1-(*N*-Boc-aminoethyl)-5-(thymin-1-yl)pipecolic acid as the desired monomer (Figure 7).

2.2.1. Synthesis of Protected Nucleobases

The nucleobases (A/T/G/C) possess groups like the imide NH and exocyclic amines that are reactive in Mitsunobu conditions and hence need to be protected. Thymine was protected at N3 by a benzoyl group and exocyclic amino group of cytosine was protected with benzyloxycarbonyl group.

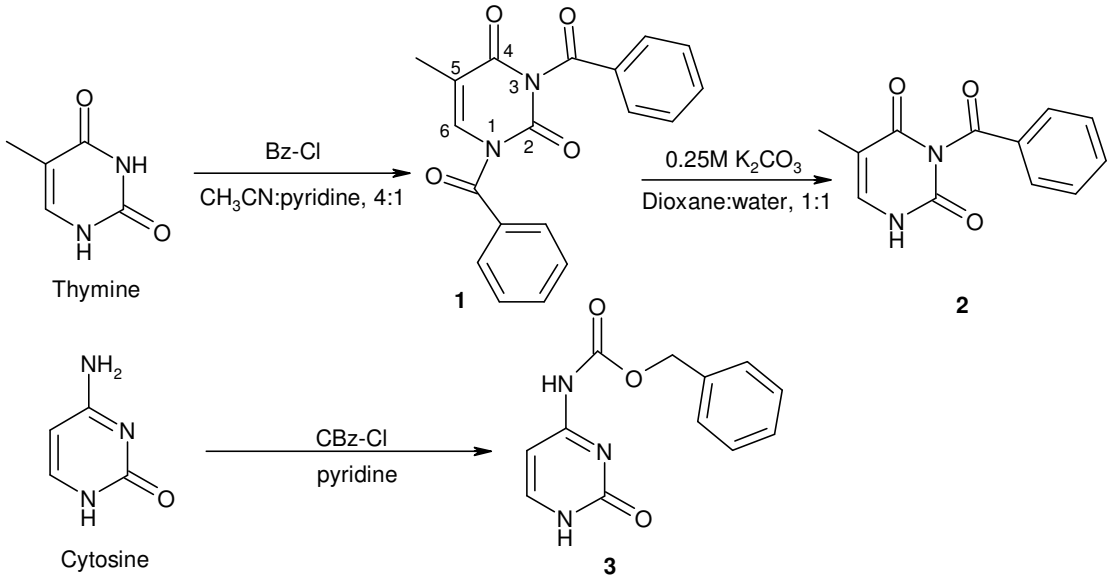

Scheme 1. Protection of the exocyclic amino groups of the nucleobases.

2.2.1a N3-benzoylthymine[23] (2). Thymine was treated with benzoyl chloride in acetonitrile:pyridine to obtain the N1, N3-dibenzoyl thymine derivative **1**. The N1-benzoyl group, being more labile than the imide N3-benzoyl group, was preferentially

hydrolyzed using K_2CO_3 in dioxane:water, to yield the N3-benzoyl thymine **2** (Scheme 1).

2.2.1b N^4-benzyloxycarbonylcytosine[24] (3). Cytosine was treated with benzyloxycarbonyl chloride in dry pyridine to get the desired product, N^4-benzyloxycarbonylcytosine (**3**) (Scheme 1).

2.2.2. Synthesis of Aminoethylpipecolyl PNA Monomers

2.2.2a 1-(N-Boc-aminoethyl)-5(R)-(thymin-1-yl)-2(S)-pipecolic acid. The synthesis of the (2*S*,5*R*) 1-(*N*-Boc-aminoethyl)-5-(*N*3-benzoylthymin-1-yl)pipecolic acid methyl ester was achieved in ten steps starting from the naturally occurring L-glutamic acid **4** (Scheme 2). The key step in this scheme is conversion of L-glutamic acid to the intermediates (**7**) and (**8**) has been reported in literature.[21,22] The selective protection of the α-amino group in L-glutamic acid **4** was achieved *via* formation of the oxazolidinone **5** by refluxing with paraformaldehyde and catalytic amount of *p*-toluene sulphonic acid in benzene, this was followed by ring opening with sodium methoxide to yield the α-ester **6** in 82% yield which was confirmed by characteristic singlet at δ 3.73 of the CH_3 protons of methyl ester. This, upon treatment with ethyl chloroformate, gave the corresponding mixed anhydride that on reaction with diazomethane generated the diazoketone **7** in 65% overall yield from **6**. Characteristic peaks appearing at 2140cm^{-1} in the IR spectrum confirmed the formation of diazo adduct. The direct conversion of diazoketone **7** to the protected 5-oxopipecolic acid **8** was achieved by ring closure carbene insertion into the N-H bond using rhodium (II) acetate as catalyst. Lack of characteristic diazo peak at 2140cm^{-1} in the IR spectrum confirmed the ring closure. Finally, regio and stereospecific reduction with sodium borohydride in methanol gave the *cis*-5-hydroxy-L-pipecolic acid methyl ester **9**,

which was confirmed by characteristic multiple peaks at δ 4.32-4.17 of the H5 proton. Further the *cis* stereochemistry of compound **9** was confirmed by lactonization, which achieved readily by brief treatment of **9** with *p*-TsOH in benzene with $[\alpha]_D^{25}$ - 9.2^0 (c=0.1 in MeOH) (Lit.[21] $[\alpha]_D^{25}$ -8.9^0 for c=0.76 in MeOH). The ester **9** was *N*1-deprotected to give the amine **10**. *N*1-Alkylation of the piperdine ring in the pipecolic acid methyl ester **10** with N-Boc-aminoethyl mesylate **16** afforded the (1-*N*-Boc-aminoethyl)pipecolic acid ester **11**. The replacement of the 5*S*-hydroxyl function in **11** with *N*3-benzoylthymine under Mitsunobu reaction conditions[25] yielded the (2*S*,5*R*)-

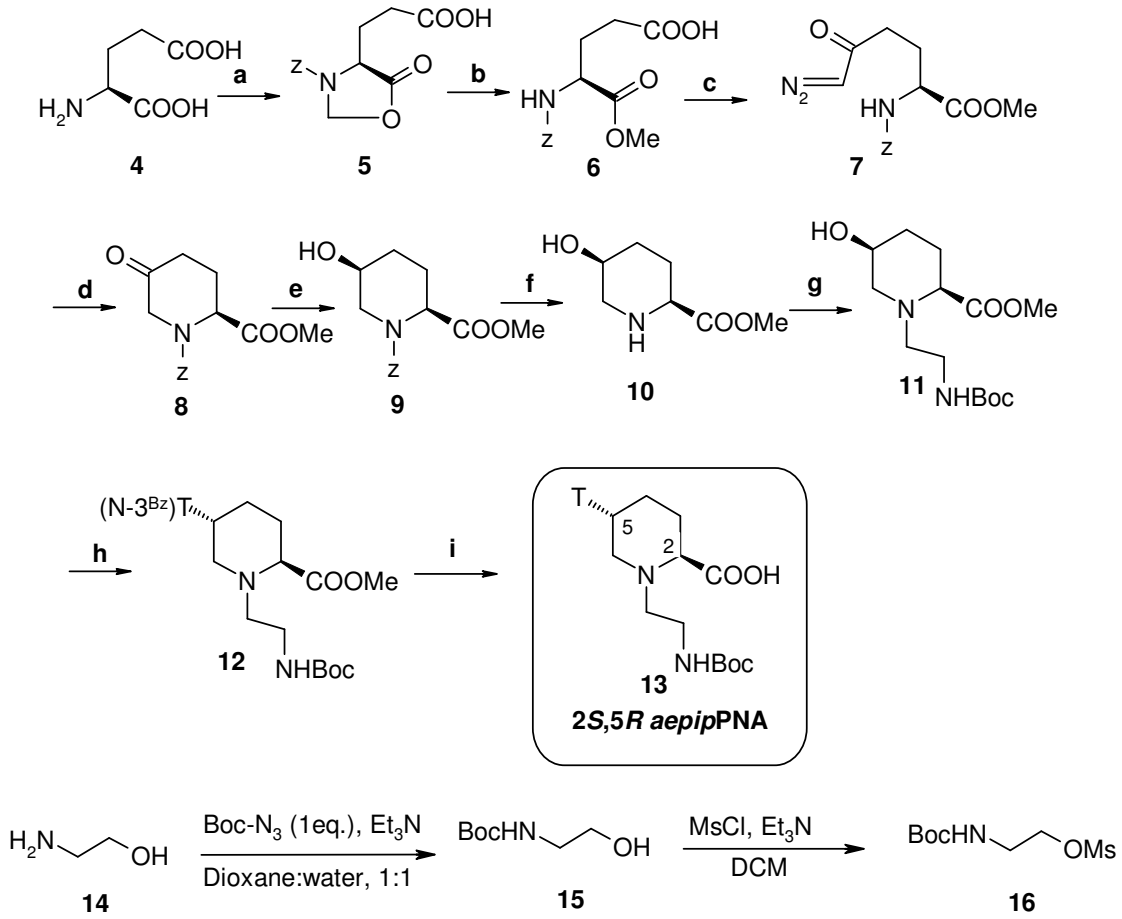

Scheme 2. Synthesis of *aepip*PNA monomers. a.(i) Benzyloxy carbonyl chloride, $NaHCO_3$ (94%) (ii) $(CH_2O)_n$, TsOH, benzene, reflux (82%); b. NaOMe, MeOH (93%); c. (i) EtOCOCl, Et_3N, THF (ii) CH_2N_2, Et_2O (65%); d. $[Rh(OAc)_2]_2$, benzene, reflux (52%); e. $NaBH_4$, MeOH (93%); f. H_2/Pd-C, 60psi (92%); g. BOC-NH-$(CH_2)_2$OMs, DIPEA, ACN:DMF (37%); h. *N*3-BzT, DIAD, PPh_3, THF (32%); i. 1M NaOH, MeOH:water (95%).

5-(*N*3-benzoylthymin-1-yl) pipecolate ester **12** in 32% yield, accompanied by inversion of stereochemistry at C5.

The appearance of a characteristic peak at δ 7.92 of the H6 proton of thymine confirmed the identity of the Mitsunobu product (**12**). Thus, this scheme involving a single inversion step results in the overall transformation of 5(*S*)-hydroxy-2(*S*)-pipecolic acid methyl ester to 1-(*N*-Boc-aminoethyl)-5(*R*)-(N3-benzoylthymin-1-yl)-2(*S*)- pipecolic acid methyl ester **12**. The simultaneous hydrolysis of the methyl ester and removal of N3-benzoyl protecting group of thymine was achieved by treatment with 1 M sodium hydroxide in aqueous methanol to obtain 1-(*N*-Boc-aminoethyl)-5(*R)* -(thymin-1-yl) 2(*S)*-pipecolic acid **13** as the desired monomer.

2.2.2b 1-(N-Boc-aminoethyl)-5(S)-(thymin-1-yl)-2(R)-pipecolic acid.

The synthesis of the (2*R*,5*S*) 1-(*N*-Boc-aminoethyl)-5-(*N*3-benzoylthymin-1-yl)pipecolic acid methyl ester (**25**) was achieved in ten steps by an identical set of reactions starting from the D-glutamic acid **17**. The key step in the Scheme 3 is the direct conversion of diazoketone **20** to the protected 5-oxopipecolic acid **21** which was achieved by ring closure carbene insertion into the N-H bond using rhodium (II) acetate as catalyst. Lack of characteristic diazo peak at 2140cm^{-1} in the IR spectrum confirmed the ring closure. Finally, stereospecific reduction to *cis*-5-hydroxy-D-pipecolic acid ester **22** was achieved which was confirmed by characteristic multiple peaks at δ 4.25-4.15 of the H5 proton. *N*1-deprotection and further alkylation with N-Boc-aminoethyl mesylate **16** afforded the (1-*N*-Boc-aminoethyl)pipecolic acid ester **24**. The replacement of the 5*R*-hydroxyl function in with *N*3-benzoylthymine under Mitsunobu reaction conditions yielded the (2*R*,5*S*)-5-(*N*3-benzoylthymin-1-yl) pipecolate ester **25**, accompanied by inversion of stereochemistry at C5. The

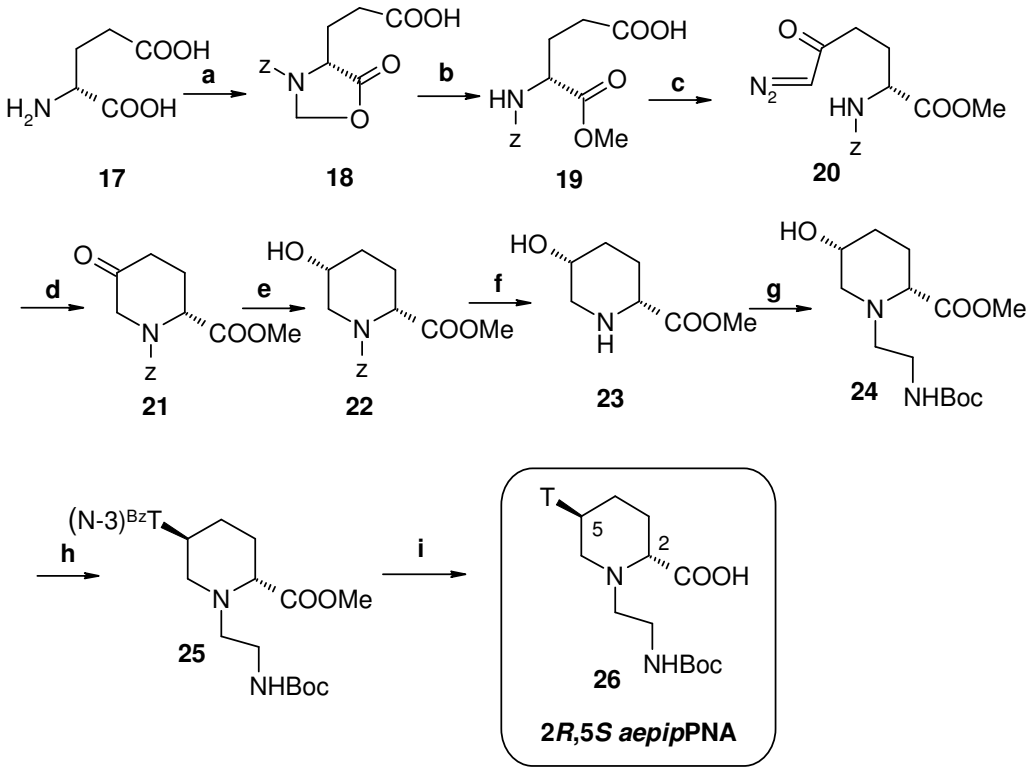

Scheme 3. Synthesis of *aepip*PNA monomers. a.(i) Benzyloxy carbonyl chloride, $NaHCO_3$ (94%) (ii) $(CH_2O)_n$, TsOH, benzene, reflux (82%); b. NaOMe, MeOH (93%); c. (i) EtOCOCl, Et_3N, THF (ii) CH_2N_2, Et_2O (65%); d. $[Rh(OAc)_2]_2$, benzene, reflux (52%); e. $NaBH_4$, MeOH (93%); f. H_2/Pd-C, 60psi (92%); g. BOC-NH-$(CH_2)_2$OMs, DIPEA, ACN:DMF (37%); h. *N*3-BzT, DIAD, PPh_3, THF (32%); i. 1M NaOH, MeOH:water (95%).

appearance of a characteristic peak at δ 7.92 of the H6 proton of thymine confirmed the identity of the Mitsunobu product (**25**). This was converted to (2*R*,5*S*)-1-(*N*-Boc-aminoethyl)-5-(thymin-1-yl)pipecolic acid **26** as the desired monomer. All the compounds were characterized by spectroscopic techniques and optical rotation. The optical rotation signs of monomer units (2*R*,5*S*) were found to be opposite as compared to 2*S*,5*R* *aepip*PNA monomer units.

2.2.3. Hydrolysis of Esters

Solid phase synthesis of *aepip*PNA requires N-protected free carboxylic acids. The methyl ester groups of the *aepip*PNA monomers were subjected to saponification

by sodium hydroxide in water-methanol mixture to yield the corresponding carboxylic acids (Scheme 4).

2.2.3a Synthesis of 1-(N-Boc-aminoethyl)-5(R/S)-(thymin-1-yl)-2(S/R)-pipecolic acid (13, 26). The hydrolysis of the methyl ester and the N3-benzoyl group of thymine in 1-(*N*-Boc-aminoethyl)-5(*R*/*S*)-(thymin-1-yl)-2(*S*/*R*)-pipecolic acid methyl ester (**12** & **25**) were achieved in a single step, upon treatment with 1M NaOH in methanol: water. As followed by TLC the ester function was found to be hydrolyzed within 10 min. However, the cleavage of the benzoyl group was complete only after 9h. Neutralization of the excess alkali with Dowex 50 H^+ and work-up gave 1-(*N*-Boc-aminoethyl)-5(*R*/*S*)-(thymin-1-yl)-2(*S*/*R*)-pipecolic acid (**13/26**) in quantitative yield.

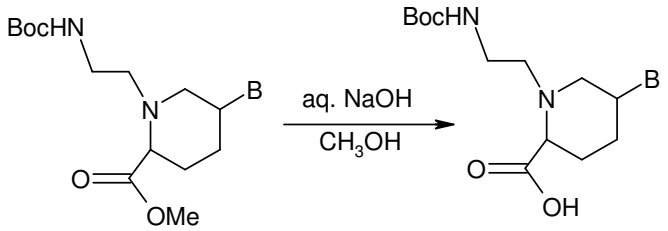

Scheme 4. Hydrolysis of the methyl esters of the *aepip*PNA monomers.

2.2.4. Synthesis of Aminoethylglycyl PNA Monomers

The synthesis of unmodified *aeg*PNA monomers is necessary for synthesis of control *aeg*PNA and was carried out according to the literature procedures.[26] The synthesis was carried out starting from the easily available 1,2-diaminoethane (**27**) (Scheme 5). This was treated with Boc-azide to give the mono-protected derivative **28**, obtained by using a large excess of 1,2-diaminoethane over the Boc-azide in high dilution. The di-Boc derivative was also obtained in very small amounts (< 5%), but

being insoluble in water, could be removed by filtration. The *N1*-Boc-1,2-diaminoethane was then subjected to *N*-alkylation using ethylbromoacetate and KF-Celite in dry acetonitrile. The use of KF-Celite[27] was found to be advantageous over K_2CO_3 both, in terms of the yield of the product, as well as the ease of work-up. The aminoethylglycine **29** was further treated with chloroacetyl chloride to yield the corresponding chloro derivative **30** in good yield. The use of triethylamine as the base in this reaction gave poor yields. However, when Na_2CO_3 was used as the base in aqueous dioxane, the desired product was obtained in good yield.

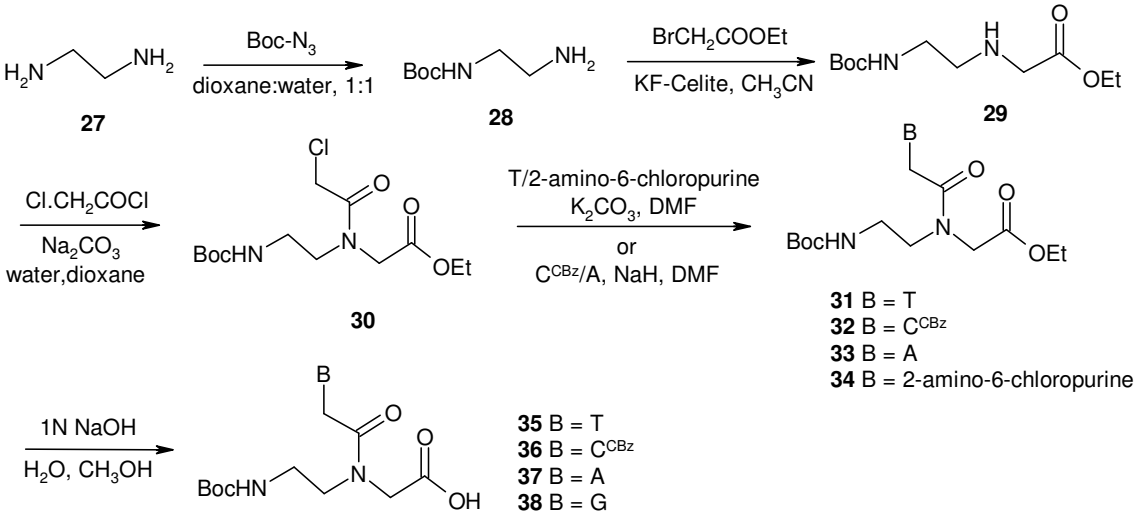

Scheme 5. Synthesis of the *aeg*PNA monomers.

The ethyl *N*-(Boc-aminoethyl)-*N*-(chloroacetyl)-glycinate (**30**) was used as a common intermediate in the preparation of all the PNA monomers. The N- alkylation of thymine and cytosine with ethyl *N*-(Boc-aminoethyl)-*N*-(chloroacetyl)-glycinate is regiospecific. Thymine was reacted with ethyl *N*-(Boc-aminoethyl)-*N*-(chloroacetyl)-glycinate using K_2CO_3 as a base to obtain the *N*-(Boc-aminoethylglycyl)-thymine ethyl ester **31** in high yield. In the case of cytosine, the N^4-amino group was protected as its benzyloxycarbonyl derivative, and used for alkylation employing NaH as the

base to provide the N1-substituted product (**32**). Although adenine is known to undergo both N7- and N9-substitution, N7-alkylation was not observed when NaH was used as the base. It reacted with adenine forming sodium adenylide, which was then reacted with ethyl *N*-(Boc-aminoethyl)-*N*-(chloroacetyl)-glycinate to obtain *N*-(Boc-aminoethylglycyl)-adenine ethyl ester (**33**) in moderate yield. The alkylation of 2-amino-6-chloropurine with ethyl *N*-(Boc-aminoethyl)-*N*-(chloroacetyl)-glycinate was facile with K_2CO_3 as the base and yielded the corresponding *N*-(Boc-aminoethylglycyl)-(2-amino-6-chloropurine)-ethyl ester (**34**) in excellent yield. All the compounds exhibited ^{1}H and ^{13}C NMR spectra consistent with the reported data. The ethyl esters were hydrolyzed in the presence of NaOH to give the corresponding acids (**35**-**38**), which were used for solid phase synthesis. The need for the exocyclic amino groups of adenine and guanine to be protected was eliminated, as these have been found to be unreactive under the conditions used for peptide coupling.

2.2.5. pK_a Determination

Since the *aepip*PNA monomers carry tertiary nitrogen in the piperdine ring that has the potential to get protonated, it is important to determine the pK_a of this group. Therefore, a pH titration experiment was carried out to determine the exact pK_a of the piperidine ring nitrogen atom.

The titration of the *aepip*PNA-T monomer **13** after Boc-deprotection, with NaOH was performed in order to determine the pKa of the piperidine ring nitrogen. The pH titration curve exhibited three pK_a values, the first one at 2.95 pH corresponding to the carboxylic acid, the second at 6.76 pH corresponding to the piperdine ring nitrogen and the third at 10.90 pH corresponding to the primary amine (Figure 8).

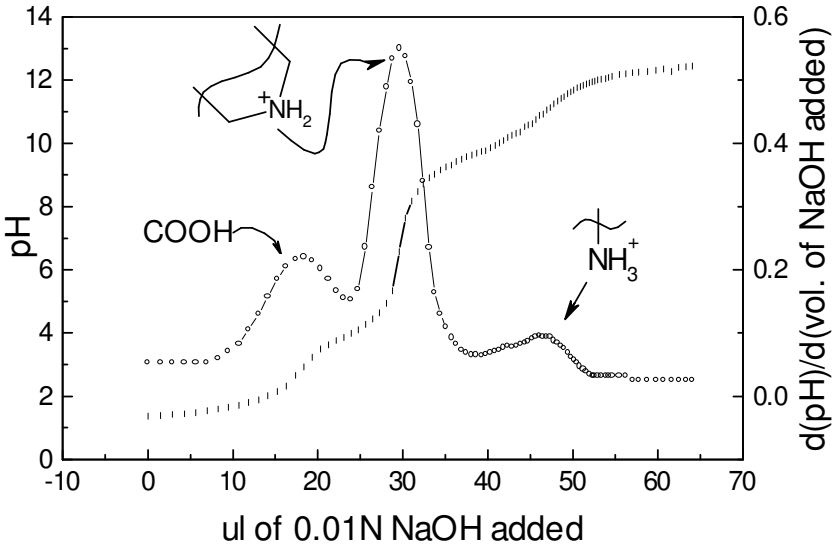

Figure 8. pH titration curve of (2*S*,5*R*) *aepip*PNA-T monomer **13** with 0.01N NaOH.

2.2.6. Solid Phase Peptide Synthesis

2.2.7a General Protocols for PNA Synthesis. Solid phase peptide synthesis protocols can be easily applied to the synthesis of PNAs. The experimental ease of solid phase protocol have made possible the synthesis of PNAs incorporating a large number of modified monomers to obtain PNA analogues in attempts to improve its DNA/RNA binding and biological properties.

As with solid phase peptide synthesis, PNA synthesis is also done conveniently from the 'C' terminus to the 'N' terminus. For this, the monomeric units must have their amino functions suitably protected, and their carboxylic acid functions free. The most commonly used N-protecting groups for solid phase peptide syntheses are the *t*-butyloxycarbonyl (Boc) and the 9-flurorenylmethoxycarbonyl (Fmoc) groups. The Fmoc protection strategy has a drawback in PNA synthesis since a small amount of acyl migration has been observed under basic conditions from the tertiary amide to the free amine formed during piperidine deprotection.[28] Hence, the

Boc-protection strategy was selected for the present work. The amino function of the monomers was protected as the corresponding Boc-derivative and the carboxylic acid function was free to enable coupling with the resin-linked monomer. The *O*-(Benzotriazol-1-yl)-*N*,*N*,*N*′,*N*′ tetramethyl-uronium hexafluorophosphate (HBTU)/1-hydroxybenzotriazole (HOBt) activation strategy was employed for the coupling reaction.[29] Merrifield resin was selected as the solid polymeric matrix on which the oligomers were built. The first amino acid is linked to this matrix *via* a benzyl ester linkage. This can be cleaved either with a strong acid to yield the C-terminal free carboxylic acid, or with an amine to afford the C-terminal amide.

All the oligomers of the present work were synthesized manually on Merrifield resin. β-Alanine was selected as the linker amino acid. Being achiral, it would not interfere with the chirality-induced structural and spectral properties of the final PNA that bear two chiral centers each in monomeric units. Its contribution to the hydrophobicity of PNA is also negligible since it has only a short alkyl chain. *N*-Boc-β-alanine was linked to the resin by a benzyl ester linkage *via* the formation of its cesium salt.[30] The loading value of β-alanine derivatized Merrifield resin was determined by picrate assay[31,32] and found to be ~0.500meq/gm. The loading value of resin was suitably lowered by partial capping of the free amino groups obtained after Boc-deprotection with acetic anhydride. The free uncapped amino groups on the resin were estimated once again by the picrate assay prior to commencing solid phase synthesis.

The PNA oligomers were synthesized using repetitive cycles, each comprising the following steps:

(i) Deprotection of the N-protecting Boc- group using 50% TFA in CH_2Cl_2.

(ii) Neutralization of the TFA salt formed with diisopropylethyl amine (DIPEA) (5% DIPEA in CH_2Cl_2) to liberate the free amine.

(iii) Coupling of the free amine with the free carboxylic acid group of the incoming monomer (3 to 4 equivalents). The coupling reaction was carried out in the presence of *O*-(Benzotriazol-1-yl)-*N*,*N*,*N*′,*N*′-tetramethyl-uronium hexafluorophosphate (HBTU) and 1-hydroxybenzotriazole (HOBt), used as a suppressing agent of racemization, in DMF or NMP as the solvent. The deprotection of the *N*-Boc protecting group and the coupling reaction were monitored by Kaiser's test.[33] The Boc-deprotection step generates free amine on resin, which gives a positive Kaiser's test, wherein the resin beads as well as the solution are blue in colour. On the other hand, upon completion of the coupling reaction, the Kaiser's test is negative, the resin beads remaining colourless.

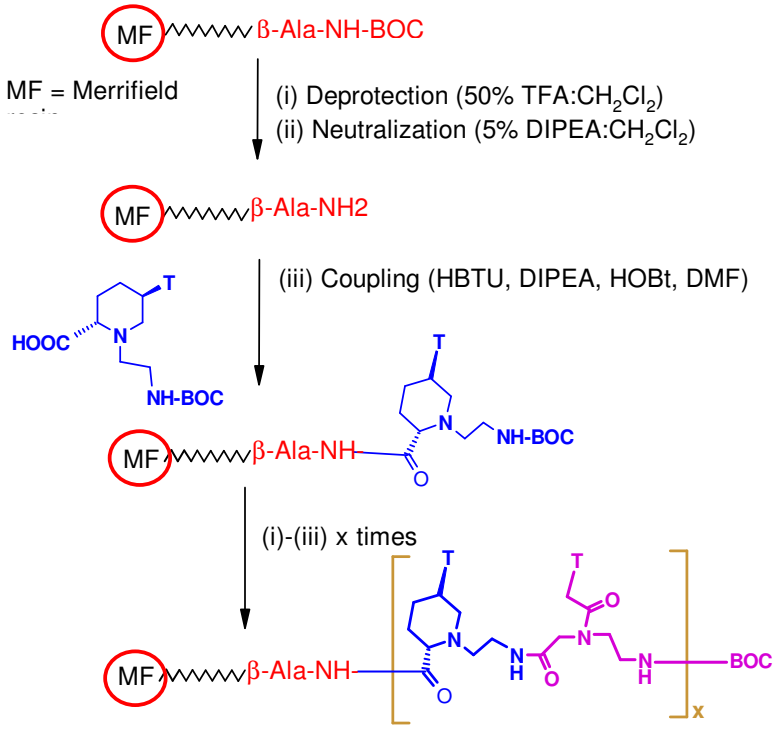

Scheme 6. Schematic representation of solid phase peptide synthesis using the Boc-protection strategy.

(iv) Capping of the unreacted amino groups using acetic anhydride in pyridine:CH_2Cl_2. A typical synthesis cycle is depicted in Scheme 6.

2.2.7b Synthesis of Cationic Aminoethylpipecolyl Peptide Nucleic Acids

The control aminoethylglycyl (*aeg*) PNA T_8 oligomer (entry 1, Table 1) was first synthesized following the Boc- protection strategy outlined above. Chiral, positively charged aminoethylpipecolyl (*aepip*) PNA-T monomer- containing sequences were subsequently made incorporating the *aepip*PNA-T unit at one or more pre-determined positions within the octamer. The series of octamer sequences comprising aminoethylglycyl PNA-T and/or aminoethylpipecolyl PNA-T units is detailed in Table 1.

Table 1. Resin-linked PNA Sequences Synthesized by Solid Phase Synthesis.

Entry	Resin-linked PNA Oligomer
1	MF--β-ala- TTTTTTTT -Boc
2	MF--β-ala- TTTTTTT **t** -Boc
3	MF--β-ala- TTTTTTT **<u>t</u>** -Boc
4	MF--β-ala- **t** TTTTTTT -Boc
5	MF--β-ala- **<u>t</u>** TTTTTTT -Boc
6	MF--β-ala- TTTT **t** TTT -Boc
7	MF--β-ala- **t** T **t** TTTTT -Boc
8	MF--β-ala- **t** TTT **t** TTT -Boc
9	MF--β-ala- **t** TTTTT **t** T -Boc
10	MF--β-ala- TTTCTCTT -Boc
11	MF--β-ala- TTTCTCT **t** -Boc
12	MF--β-ala- TTTCTCT **<u>t</u>** -Boc
13	MF--β-ala- TTTCTCTTGTA -Boc
14	MF--β-ala- TTTCTCT **t** GTA -Boc

MF = Merrifield resin; Uppercase letters denote *aeg*PNA units. Lowercase letters denote *aepip*PNA units. **t** = (2*S*,5*R*) *aepip*PNA T; **<u>t</u>** = (2*R*,5*S*) *aepip*PNA T.

The capping step at the end of each coupling cycle was not deemed necessary, as the coupling reaction was monitored manually went to completion with a high coupling efficiency (greater than 90%). With a view to systematically explore the

effects of the *aepip*PNA units, single *aepip* unit was introduced either at the 'N' or 'C' terminus (Table 1, entry 2-5) or in the middle of sequence (Table 1, entry 6). The study of the effect of introduction of increasing number of *aepip* units on the stability and selectivity of DNA complexation made it necessary to design sequences with more than one *aepip* unit. Therefore, octamers bearing two *aepip* units were synthesized (Table 1, entry 7–9). In order to examine the base effects on modifications homopyrimidine sequences bearing both thymine and cytosine, were synthesized but with only *aepip*-T (Table 1, entry 11,12).

The effect of the *aepip* unit on triplex-forming ability was tested by synthesizing polypyrimidine (poly-T) octamers. These are known to complex with the complementary DNA A_8 oligomer in a 2:1 PNA:DNA stoichiometry. In order to study the duplex formation potential of the *aepip*PNA backbone, it was imperative to synthesize mixed sequences incorporating both, purines and pyrimidines. The *aepip*PNA-T monomer was therefore incorporated into 11-mer (Table 1, entry 14).

2.2.7. Cleavage of the PNA Oligomers from the Solid Support

2.2.8a Cleavage from the Resin by Strong Acid. The cleavage of peptides from the Merrifield resin by strong acids like trifluoromethane sulphonic acid (TFMSA)-trifluoroacetic acid (TFA) yields peptides with free carboxylic acids at their 'C' termini.[34] The synthesized PNA oligomers were cleaved from the resin using this procedure to obtain sequences bearing β-alanine free carboxylic acids at their 'C' termini (Entry 1-14). After commencing the cleavage reaction, aliquots were removed after 30min, 1h, 2h and 24h, the peptides isolated and analyzed by HPLC. A cleavage time of ~2h at room temperature was found to be optimum. The peptides from aliquots removed prior to 2h indicated incomplete deprotection. This was evident

from the greater number of peaks with a higher retention time as observed by analytical HPLC. These peaks were absent in the aliquots removed after 2h. The exocyclic amino groups of cytosine, adenine and guanine, if protected as benzyloxycarbonyl, are also cleaved during this process. If the N6-exocyclic amino group of adenine is, however, protected as a benzoyl group, then its deprotection must be carried out under alkaline conditions employing ammonia or ethylenediamine.

2.2.8. Purification of the PNA Oligomers

All the cleaved oligomers were subjected to initial gel filtration for desalting. These were subsequently purified by reverse phase FPLC on a semi-preparative C8 RP column by gradient elution using an ascending gradient of 5-50% acetonitrile in water containing 0.1% TFA, or by isocratic elution in 10% acetonitrile- water containing 0.1% TFA on a semi- preparative HPLC RP C4 column. In some cases, FPLC did not produce a clean single peak profile. Hence, the sample was heated at ~80^{o}C for 4-5 min and then injected to destroy any secondary structure that might exist. Samples containing-multiple *aep*PNA units, and therefore, multiple positive charges were suspended in buffer containing 0.1% TFA and allowed to stand for 2-3h prior to injection and chromatography. The purity of the oligomers was then checked by reverse phase HPLC on a C18 RP column and confirmed by MALDI-TOF mass spectroscopic analysis. Some representative HPLC profiles and mass spectra are shown in figures 9 and 10.

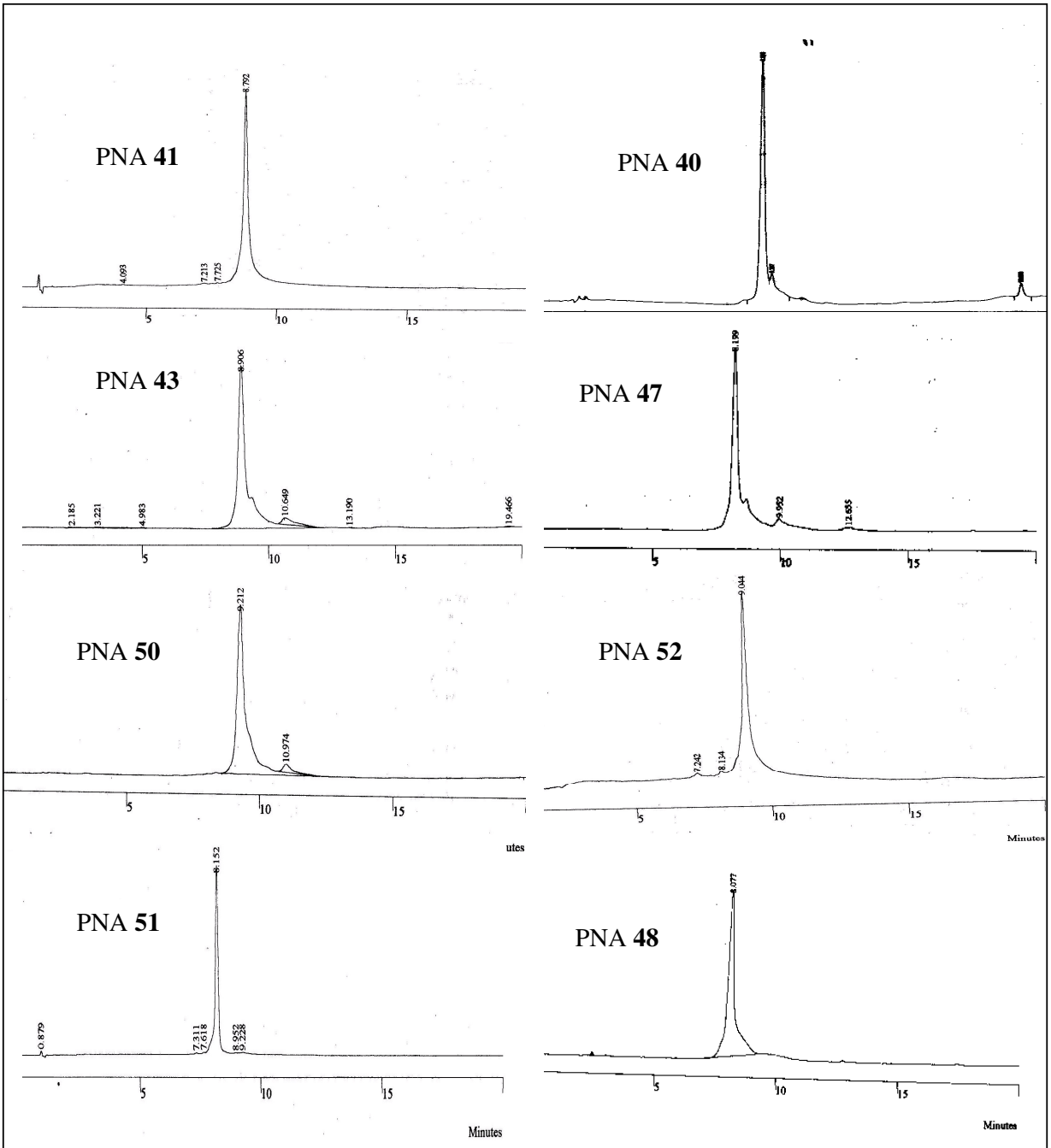

Figure 9. Representative HPLC profiles of *aepip*PNA oligomers.

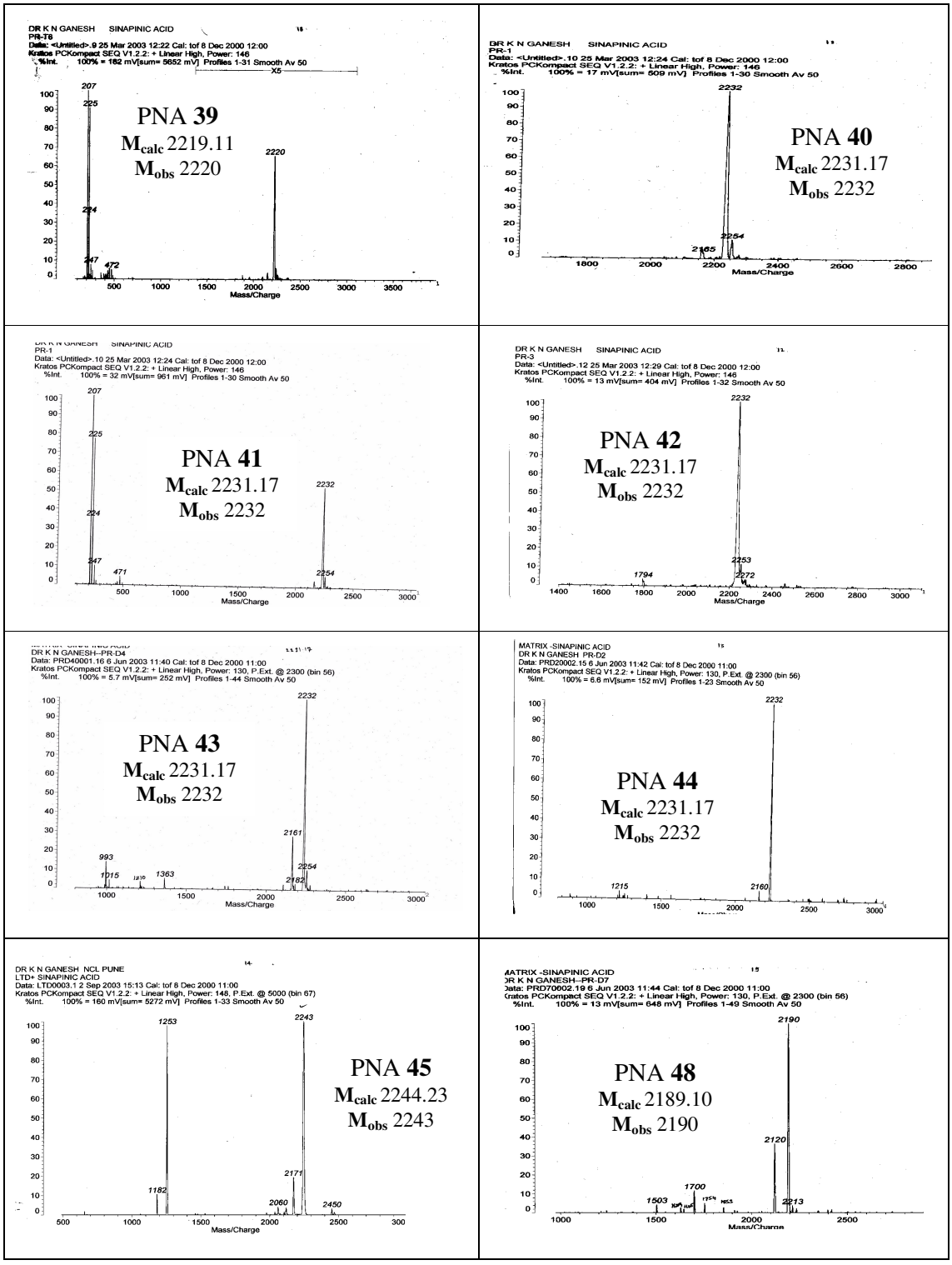

Figure 10. MALDI-TOF spectra of representative *aeg*PNA & *aepip*PNA oligomers.

The PNA sequences obtained are listed in Table 2.

Table 2. PNA Sequences.

PNA	Sequence Composition	
39	H- TTTTTTTT -NH-$(CH_2)_2$-COOH	*aeg*PNA control
40	H- **t** TTTTTTT -NH-$(CH_2)_2$-COOH	one (2*S*,5*R*) *aepip*PNA unit at N. T.
41	H- **t** TTTTTTT -NH-$(CH_2)_2$-COOH	one (2*R*,5*S*) *aepip*PNA unit at N. T.
42	H- TTTTTTT **t** -NH-$(CH_2)_2$-COOH	one (2*S*,5*R*) *aepip*PNA unit at C. T.
43	H- TTTTTTT **t** -NH-$(CH_2)_2$-COOH	one (2*R*,5*S*) *aepip*PNA unit at C. T.
44	H- TTTT **t** TTT -NH-$(CH_2)_2$-COOH	one (2*S*,5*R*) *aepip*PNA unit at middle
45	H- TTT TT **t** T**t** -NH-$(CH_2)_2$-COOH	two (2*S*,5*R*) *aepip*PNA units
46	H- TTT **t** TTT **t** -NH-$(CH_2)_2$-COOH	two (2*S*,5*R*) *aepip*PNA units
47	H- T **t** TTTTT **t** -NH-$(CH_2)_2$-COOH	two (2*S*,5*R*) *aepip*PNA units
48	H- TTCTCTTT -NH-$(CH_2)_2$-COOH	*aeg*PNA control
49	H- **t** TCTCTTT -NH-$(CH_2)_2$-COOH	one (2*S*,5*R*) *aepip*PNA unit at N. T.
50	H- **t** TCTCTTT -NH-$(CH_2)_2$-COOH	one (2*R*,5*S*) *aepip*PNA unit at N. T.
51	H- ATGTTCTCTTT -NH-$(CH_2)_2$-COOH	*aeg*PNA control
52	H-ATG **t** TCTCTTT -NH-$(CH_2)_2$-COOH	one (2*S*,5*R*) *aepip*PNA unit

Uppercase letters denote *aeg*PNA units. Lowercase letters denote *aepip*PNA units. **t** = (2*S*,5*R*) *aepip*PNA T; **t** = (2*R*,5*S*) *aepip*PNA T.

2.2.9. Synthesis of Complementary Oligonucleotides

The oligodeoxynucleotides (**53-57**, Table 3) were synthesized on a Pharmacia Gene Assembler Plus DNA synthesizer using the standard β-cyanoethyl phosphoramidite chemistry. The oligomers were synthesized in the 3' - 5' direction on a CPG solid support, followed by ammonia treatment.[35] The oligonucleotides were de-salted by gel filtration, their purity ascertained by RP HPLC on a C18 column to be more than 98% and were used without further purification in the biophysical studies of PNA.

Table 3. DNA Oligomer Sequences.

DNA	Oligomer Sequences 5' → 3'	
For the Homopyrimidine PNA Sequences		
53	G C A A A A A A A A C G	Complementary to PNA-T_8 **39-47** with CG clamps
54	G C A A A A T A A A C G	Mismatch DNA for PNAs **39-47**
55	A A A G A G A A	Complementary to PNAs **48-50**
For Mixed Base PNA Sequences Comprising A, T, G & C Bases		
56	A A A G A G A A C A T	Antiparallel DNA to PNAs **51**-**52**
57	T A C A A G A G A A A	Parallel DNA to PNAs **51**-**52**

2.3. BIOPHYSICAL SPECTROSCOPIC TECHNIQUES FOR STUDYING PNA-DNA INTERACTIONS

2.3.1. UV-Studies

Monitoring the UV absorption at 260nm as a function of temperature has been extensively used to study the thermal stability of nucleic acid systems and consequently, PNA:DNA hybrids as well. Increasing the temperature perturbs PNA/DNA hybrids, inducing a structural transition by causing disruption of hydrogen bonds between the base-pairs, leading to a loss of secondary and tertiary structure. This is evidenced by an increase in the UV absorption at 260nm, termed as 'hyperchromicity'. The magnitude of hyperchromicity is a measure of the extent of the secondary structure present in nucleic acids. The process is co-operative and the plot of the absorbance at 260nm Vs the temperature is sigmoidal (Figure 11a). This also represents a two-state "all or none" model for nucleic acid melting, i.e., the nucleic acids exist in only two states, either as duplexes or as single strands and at varying temperatures, the relative proportions change. A non-sigmoidal (e.g., linear)

transition with low hyperchromicity is a consequence of non-duplexation (non-complementation). In many cases, the transitions are broad and the exact T_ms are obtained from the peak in the first derivative plots. This technique has provided valuable information regarding complementary interactions in nucleic acid hybrids involving DNA, RNA and PNA.[36]

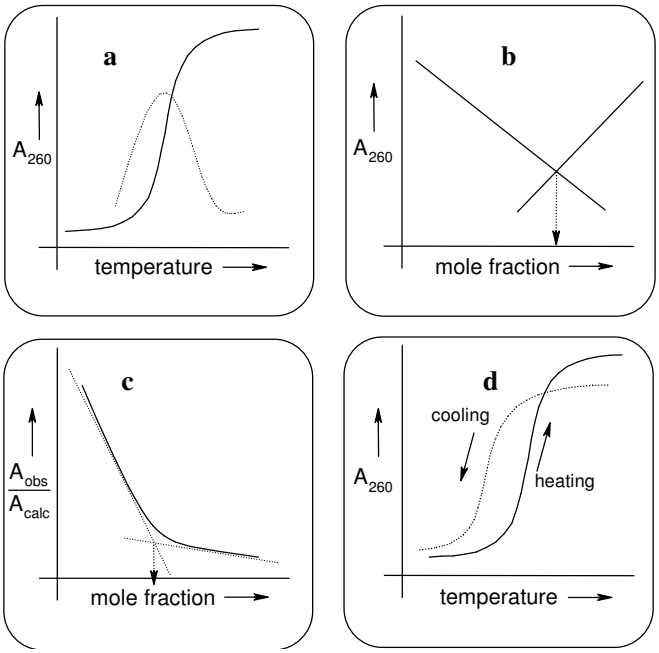

Figure 11. Schematic representation of **a**. UV-melting (thermal stability), **b**. UV-mixing, **c**. UV-titration (stoichiometry) and **d**. Hysteresis (rate of hybridization).

The binding stoichiometry of nucleic acids can be determined from UV-mixing or UV-titration experiments. The UV-mixing experiments are carried out by mixing the appropriate oligomers in different mole ratios, keeping the total concentration constant. The UV-absorbance of these samples is plotted as a function of the mole fraction of one of the components, in what is termed as a Job's plot[37] (Figure 11b). The absorbance steadily decreases until all the strands present are involved in complex formation as a result of the hypochromic effect, and then rises

afterwards when one strand is present in excess. The stoichiometry of the complexation is derived from the minimum in such a plot.

The stoichiometry of complexation can also be determined by UV-titration (Figure 11c). In this method, one of the strand involved in complexation is sequentially added in aliquots to a fixed amount of the complementary component and the UV-absorbance is recorded at each addition. Upon successive addition of the complementary strand, complex formation results in hypochromicity, which leads to a progressive decrease in the ratio of the observed to the calculated absorbance. After the first strand present in the buffer is completely bound as duplex, the absorbance reaches a plateau and the stoichiometric point at which the plateau is reached indicates the stoichiometry of complexation.

PNA/DNA strands bearing charged groups could be tested for hysteresis by thermal dissociation vs re-association plots. The experiment consists of recording the UV absorbance by first heating the duplexes/triplexes (UV-melting) followed by cooling the sample while recording the absorbance (re-association, cooling curve). In DNA:DNA complexes, the cooling curve does not reversibly follow the melting curve and exhibits a hysteresis (Figure 11d). This is due to the fact that the re-association of duplexes or triplexes is much slower than melting due to the interstrand repulsion on account of the negative phosphate groups. When one of the strands bears cationic charges, the net repulsion between the two strands is reduced, leading to a lower hysteresis in the heating-cooling plots.

The fidelity of base-pairing in the PNA:DNA complexes can be examined by challenging the PNA oligomer with a DNA strand bearing a mismatch at a desired site, preferably opposite the site of modification. The base mismatch leads to the

absence of or incorrect hydrogen bonding between the bases and causes a drop in the measured melting temperature. A modification of the PNA structure is considered good if it gives a significantly lower Tm with DNA sequences containing mismatches as compared to that with unmodified PNA. It is to be pointed out that in all biophysical experiments described herein, the modified PNAs are always evaluated against the unmodified control PNA.

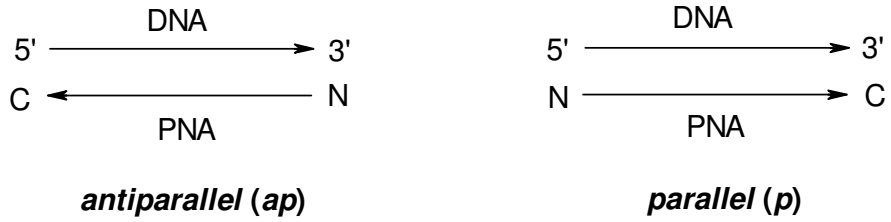

Figure 12. Schematic representation of the antiparallel and parallel modes of complexation of PNA with complementary DNA.

Homopyrimidine thymine PNA sequences bind to the complementary homopurine DNA sequence forming PNA_2:DNA triplexes in which it is difficult to distinguish the PNA strand that binds to the central DNA strand by WC hydrogen bonding from that which binds by HG hydrogen bonding. Mixed base sequences form duplexes of antiparallel or parallel orientations that can be selected by proper design of the complementary DNA sequences. By convention, antiparallel PNA:DNA complexes are defined as those in which the 'N' terminal of the PNA faces the 3'-end of the DNA with the 'C' terminal facing the 5'-end and parallel PNA:DNA complexes are those in which the 'C' terminal of PNA faces the 3'-end of DNA with the 'N' terminal towards the 5'-end of the DNA[38] (Figure 12).

2.3.2. Circular Dichroism

Circular Dichroism (CD) is a well-established tool used to study the conformational aspects of nucleic acids.[39,40] Upon comparison with reference samples, CD spectra can provide reliable and useful data concerning the conformational states of the system under study. However, CD does not give detailed structural data as obtained from X-ray crystallography or NMR, but it can be used as a complementary tool to UV spectroscopy to evaluate the overall base-stacking patterns. The differences in secondary structure and handedness of helices can be differentiated conformationally as changes in CD profiles.

CD of nucleic acids arises predominantly as an effect of coupling between the transition moments of adjacent nucleobases due to continuous stacking. The PNA backbone is inherently achiral. However, PNA, a polyamide, can be expected to form helices *via* intramolecular hydrogen bonding leading to a racemic mixture of right- and left-handed helices and no net CD is observed.[41] Upon complexation with DNA/RNA, which are chiral molecules, PNA:DNA/RNA duplexes/triplexes exhibit strong CD signals.

Thus, the complex formed as a consequence of the binding of achiral PNA and chiral DNA leads to the formation of a chiral complex. CD thus, assumes importance in the characterization of such complexes.

2.3.3. Gel Electrophoresis

Electrophoretic gel shift assay is used to establish the binding of different PNAs to the complementary DNA. The modified PNAs and the control PNA are individually treated with oligonucleotide and the complexation is monitored by nondenaturing gel electrophoresis at 10°C. The spots can be visualized on a TLC with

fluorescent background. The formation of PNA_2:DNA complexes is accompanied by the disappearance of the single strand DNA and appearance of a lower migrating band due to PNA:DNA complexes. The migration of modified PNA_2:DNA complexes can be compared with that of the unmodified PNA:DNA complex. Under the electrophoretic conditions employed, the single stranded PNAs that carry net positive charge do not move out of the well. The PNA_2:DNA triplexes show more retardation as compared to PNA:DNA duplexes. This can be attributed to the increased molecular weight upon formation of triplex.

2.4. RESULTS

In the present Chapter, studies on PNA-DNA interactions as investigated by UV, CD and gel electrophoresis techniques are presented with discussion on the effect of PNA modifications on duplex/triplex formation.

2.4.1. Homopyrimidine PNA Sequences: UV Studies

2.4.1a PNA:DNA Binding Stoichiometry.

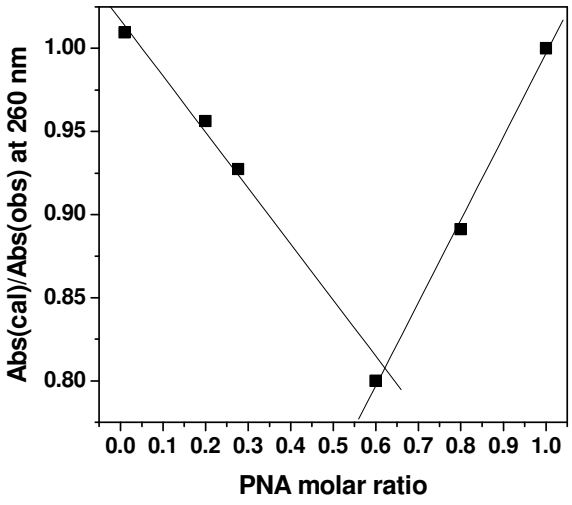

Figure 13. UV-titration of PNA_2:DNA complexes **40: 53**.

The UV-titration (Figure 13) experiments involving the stoichiometric addition of *aepip*PNA **40** to DNA **53** led to a decrease in UV absorbance with *aepip* PNAs. The absorbance showed a similar saturation minima around 2:1 stoichiometry suggesting the formation of a PNA_2:DNA triplex.

2.4.1b PNA_2:DNA Triplexes: UV-Tm Studies. The thermal stabilities of PNA_2:DNA complexes were studied by temperature dependent UV absorbance measurements (Figure 14). Table 4 shows the Tm values for PNA_2:DNA complexes derived from various *aeg*PNA and *aepip*PNA sequences of different stereochemistry and degree of modification. The temperature - percent hyperchromicity first derivative plots for DNA:PNA_2 triplexes indicated a single transition (Figure 15B), characteristic of both PNA strands dissociating simultaneously from DNA in a single step. The T_m values (entry 1,2, Table 4) indicate that the *aepip*PNA oligomers **40-43** having single modification of either stereomer at N or C terminus exhibited stabilization compared to the unmodified PNA T_8 homooligomer (**39**).

Table 4. UV-T_m (^oC) of PNA_2:DNA complexes.*

NO	**PNA Sequence**	**(2*S*,5*R*)**		**(2*R*,5*S*)**	
		PNA_2:DNA	**T_m (^0C)**	**PNA_2:DNA**	**T_m (^0C)**
1	H-**t/<u>t</u>**TTTTTTT -NH-$(CH_2)_2$-COOH	**40:53**	43 (23.4)	**41:53**	36 (8.0)
2	H- TTTTTTT**t/<u>t</u>** -NH-$(CH_2)_2$-COOH	**42:53**	48 (19.2)	**43:53**	76 (2.3)
3	H- **t/<u>t</u>** TCTCTTT -NH-$(CH_2)_2$-COOH	**49:55**	60 (26.7)	**50:55**	56 (26.6)
4	H- TTTTTTTT -NH-$(CH_2)_2$-COOH	**39:53**	43 (18.3)		
5	H- TTCTCTTT -NH-$(CH_2)_2$-COOH	**48:55**	51 (18.5)		

*Buffer: 10mM sodium phosphate, pH 7.4. Values in parentheses represent % hyperchromicity. T_m values are accurate to (±) 0.5°C. Experiments were repeated at least thrice and the T_m values were obtained from the peaks in the first derivative plots.

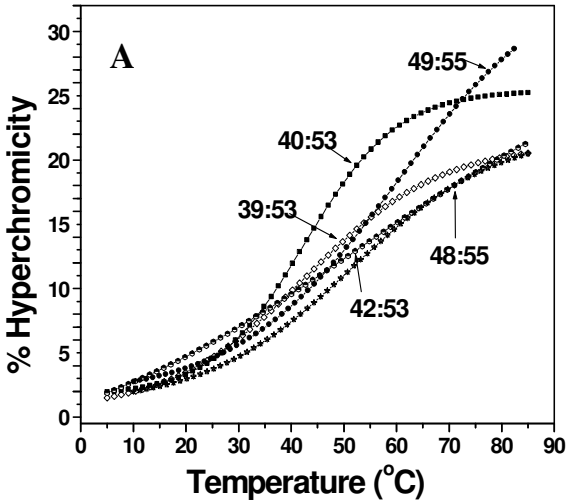

Figure 14A. UV-Melting profiles of PNA_2:DNA (2*S*,5*R*) complexes.

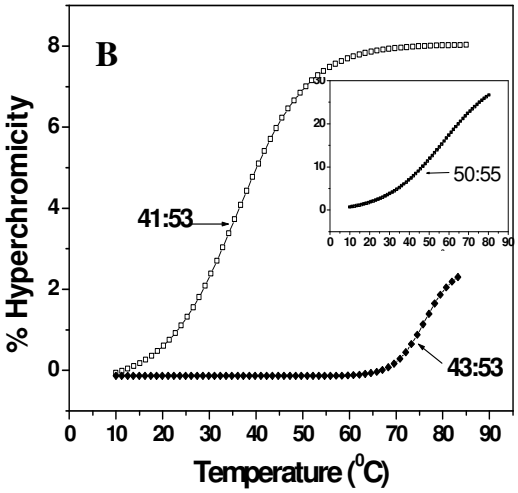

Figure 14B. UV-Melting profiles of PNA_2:DNA (2*R*,5*S*) complexes.

While a (2*S*,5*R*) *aepip* unit at the N-terminus has better stability of its complex with the complementary DNA **53** compared to (2*R*,5*S*), the situation was reversed for corresponding modification at C-terminus; the (2*R*,5*S*) oligomer forming the much more stable hybrid compared to that of the (2*S*,5*R*) oligomers (entry 2).

The stability of the DNA complexes of *aeg-aepip*-PNA oligomers with mixed pyrimidine base sequence and N-terminus modifications (**49:55** and **50:55**) was higher by 5°C for (2*R*,5*S*) and 9°C for (2*S*,5*R*) as compared to that of the control complex **48**:**55** (entry 3,4 Table 4). The percent hyperchromicity was enhanced compared to the control complex in these transitions when chiral unit is at the N-terminus. Only in the case of the complex **41**:**53** (2*R*,5*S*) and **44:43** (2*S*,5*R*), (Table 5) where the *aepip* unit is in the center of the sequence, percent hyperchromicity accompanying the melting was found to be low. A single (2*S*,5*R*) *aepip* modification in the middle of the sequence did not affect the stability of the DNA hybrid (Table 5, entry 2). Increasing the number of *aepip*PNA modifications further enhanced the T_m (Table 5, entry 3-5).

Table 5. UV-T_m (^oC) of PNA_2:DNA complexes.*

No	PNA Sequence	(2*S*,5*R*)	
		PNA_2:DNA	**T_m (^0C)**
1	H- TTTTTTTT -NH-$(CH_2)_2$-COOH	**39:53**	43 (18.3)
2	H- TTTT **t** TTT -NH-$(CH_2)_2$-COOH	**44:53**	44 (10.9)
3	H- TTT TT **t** T**t** -NH-$(CH_2)_2$-COOH	**45:53**	52 (26.7)
4	H- TTT **t** TTT **t** -NH-$(CH_2)_2$-COOH	**46:53**	51 (25.2)
5	H- T **t** TTTTT **t** -NH-$(CH_2)_2$-COOH	**47:53**	49 (14.3)

*Buffer: 10mM sodium phosphate, pH 7.4. Values in parentheses represent % hyperchromicity. T_m values are accurate to (±) 0.5°C. Experiments were repeated at least thrice and the T_m values were obtained from the peaks in the first derivative plots.

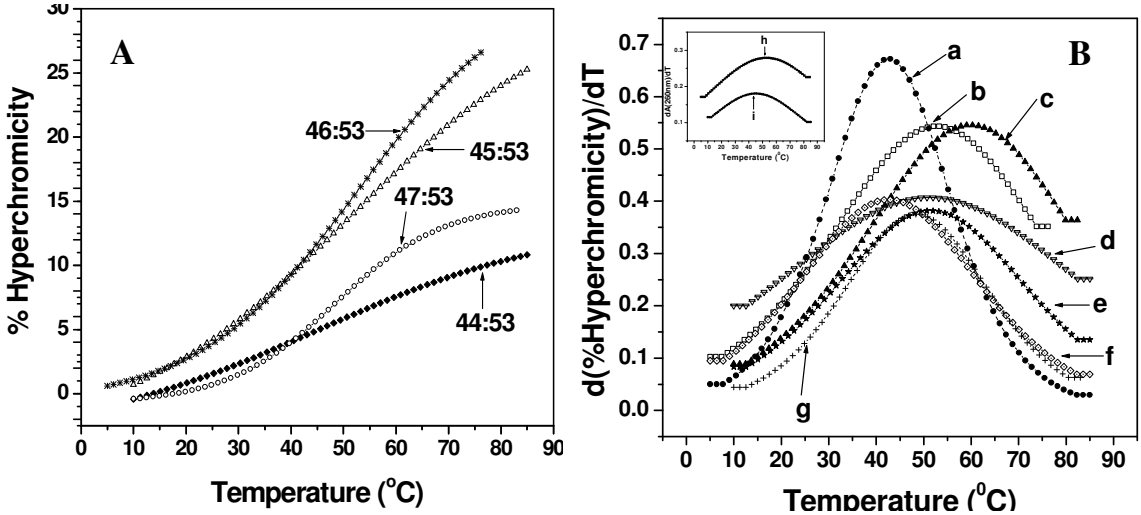

Figure 15. A) UV-Melting profiles of PNA_2:DNA (2*S*,5*R*) complexes. **B) UV**-Melting first derivative curves of PNA_2:DNA (2*S*,5*R*) complexes. a**. 40:53**; b. **45:53**, c. **49:55**, d. **46:53**, e. **48:55**, f. **39:53**, g. **47:53**. **Inset:** h. **42:53**, i. **44:53**.

PNA oligomers with one *aepip* modification at C-terminus and a second *aepip* unit at the third (**45**), fifth (**46**) or seventh (**47**) base positions respectively were used to study the relative positional effects of the modifications. A synergistic stabilizing effect was observed with a second modified *aepip* unit in all the cases (**45:53, 46:53** and **47:53**). The maximum benefit per additional unit observed was (ΔT_m +4°C) when the second *aepip*PNA unit was separated by one base (**45:53)** (Table 5).

2.4.1c Mismatch studies. The complexes of PNAs were constituted with DNA containing a mismatch base (Figure 16). The PNA_2:DNA complexes comprising the *aepip*PNAs (**39**-**43**) and DNA **54** having a single mismatch were subjected for UV-melting. The mismatched complex **43:54** was destabilized by a larger extent (ΔT_m – 53°C) for (2*R*,5*S*) *aepip* stereochemistry and by ΔT_m ~ -24°C for (2*S*,5*R*) *aepip* stereochemistry (Table 6 & Figure 17).

T T T	T	T T T T	**PNA**
G C A A A	**T**	A A A A C G	**DNA**
T T T	T	T T T T	**PNA**

Figure 16. Mismatched PNA_2:DNA complex.

Table 6. UV-T_m (°C) of PNA_2:DNA mismatched complexes.*

No	PNA Sequence	(2*S*,5*R*)		(2*R*,5*S*)	
		PNA_2:DNA	**T_m (^{0}C)**	**PNA_2:DNA**	**T_m (^{0}C)**
1	H- **t/t** TTTTTTT -NH-$(CH_2)_2$-COOH	**40:54**	19 (8.9)	**41:54**	ND
2	H- TTTTTTT **t/t** -NH-$(CH_2)_2$-COOH	**42:54**	24 (3.8)	**43:54**	23 (3.3)
4	H- TTTTTTTT -NH-$(CH_2)_2$-COOH	**39:54**	ND		

*ND: Not detected.

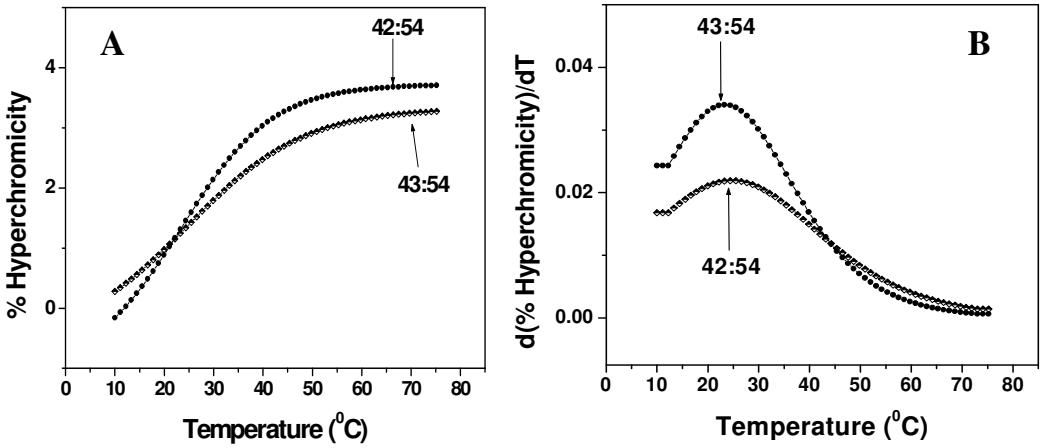

Figure 17. A) UV-Melting profiles and **B) UV**-Melting first derivative curves of mismatched PNA_2:DNA (**42:54**) (2*S*,5*R*) & (**43:54**) (2*R*,5*S*) mismatched complexes.

The PNA:DNA complexes comprising the control *aeg*PNA (**39**) and modified *aepip*PNA (**41**) and DNA **54** having a single mismatch gave linear, non-sigmoidal plots and failed to show any peak in the first derivative plots. As a consequence, no melting temperature was detected for these complexes.

2.4.1d Salt effects. The presence of salt (50mM NaCl) in the medium is known to destabilize the PNA_2:DNA complexes.[42] The DNA **53** complexes with control PNA **39** and PNA with one *aepip*PNA unit, **40** exhibited ΔT_m = ~ -5^oC upon salt addition.

2.4.2. UV-T_m Studies in Duplexes

The oligothymine sequences described above were found to form triplexes in which the binding orientation (parallel-antiparallel) of the two PNA strands involved in complex formation remains inconsequential. In order to study the orientational preferences (parallel/antiparallel, Figure 12) of PNA:DNA binding, mixed purine-pyrimidine sequences were synthesized.

The mixed PNA sequences such as **51**-**52** have been demonstrated to form duplexes with the complementary DNAs **56** (antiparallel, *ap*) and **57** (parallel, *p*) and are useful to examine the orientational selectivity in binding to DNA. Hence, T_m studies of PNA:DNA duplexes of these oligomers containing *aepip*PNA units were carried out. The duplexes were constituted by individually mixing equimolar amounts of complementary achiral *aeg*PNA **51** and chiral *aepip*PNA **52** with DNA oligomers **56/57** in phosphate buffer. The UV-T_m profiles of complexes of PNAs **51** and **52** with DNA sequences **56** and **57** designed to bind in antiparallel and parallel orientations respectively, is shown in Figure 18 and the values given in Table 7. In both PNAs, the antiparallel duplex was more stable than the parallel duplex. However, the modified

*aeg-aepip*PNA **52** (2*S*,5*R*) stabilized the antiparallel duplex (DNA **56**) by 17°C compared to the 8.2°C by *aeg*PNA over the parallel duplex.

Table 7. UV-T_m (°C) of PNA:DNA duplexes containing the nucleobases A, G, C & T.

		(2*S*,5*R*)	
Entry	**PNA:DNA**	**T_m (°C)**	**$\Delta T_m ap$-$\Delta T_m p$**
1	**52:56** (*ap*)	57.8 (20.2)	17°C
2	**52:57** (*p*)	40.8 (15.0)	
	Control *aeg*PNA:DNA complex		
3	**51:56** (*ap*)	51.2 (16.2)	8.2°C
4	**51:57** (*p*)	43.0 (11.3)	

*Buffer: 10mM sodium phosphate, pH 7.4. Values in parentheses represent % hyperchromicity. T_m values are accurate to (±)0.5°C. Experiments were repeated at least thrice and the T_m values were obtained from the peaks in the first derivative plots.

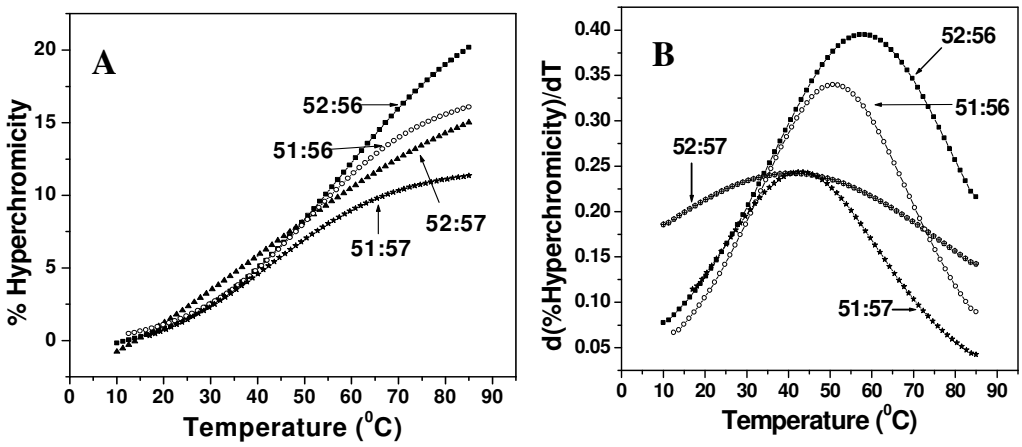

Figure 18. A) UV-Melting profiles and **B) UV**-Melting first derivative curves of PNA:DNA duplexes.

2.4.2b Dissociation Vs Re-association Kinetics

The UV-melting and re-association (by cooling) curves for hybrids of DNA with *aeg*PNA **39** and *aepip*PNA **42** as a typical representative example are shown in Figure 19. It is seen that while the *aeg*PNA cooling curve is displaced significantly indicating a hysteresis, that of *aep*PNA exhibited overlapping curves. This suggests a

faster re-association of *aep*PNA:DNA duplexes compared to the *aeg*PNA:DNA duplexes.

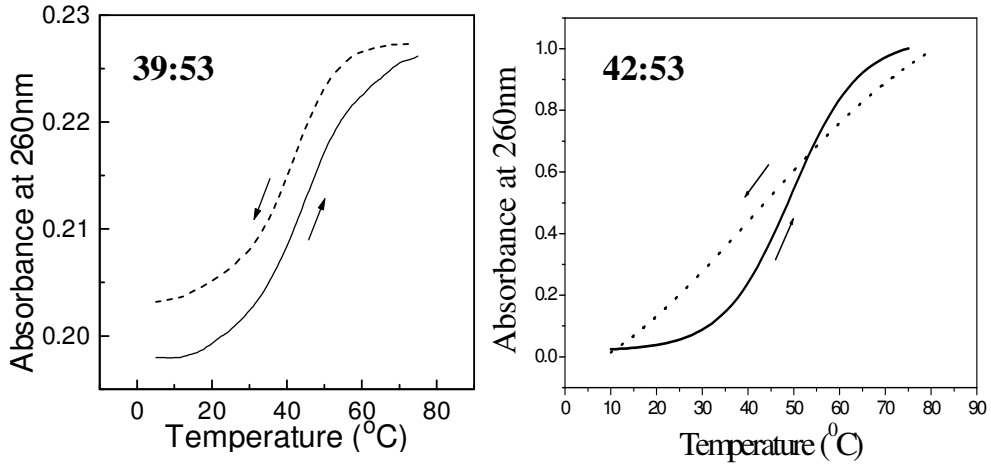

Figure 19. Hysteresis between the dissociation and re-association phenomena in *aeg*PNA (**39**) and *aepip*PNA (**42**).

2.4.3. CD Studies: Effect of Chiral PNAs

The achiral PNA backbone does not show any significant CD spectrum. However, single-stranded (*ss*) PNAs with modified chiral backbone when complexed with complementary DNA sequences are capable of exhibiting characteristic CD signals. A preferred handedness in the complex may be induced by introducing chiral centers within the PNA strand. The process was described as a "seeding of chirality, beginning from the terminal base pair and migrating through the stack of the bases".[43] The presence of chiral monomers reorganizes the single stranded PNAs and also enhance the helical preferences of the PNA:DNA complexes. The CD profiles of the single strand *aepip*PNAs show "somewhat" mirror image relationship (Figure 20) of CD bands at 270nm- 300nm and the sign of CD bands is significantly influenced by the stereochemistry of monomeric units. In single strand *aepip*PNA CD signals must arise due to asymmetry induced in base stacking by the chiral *aepip* unit.

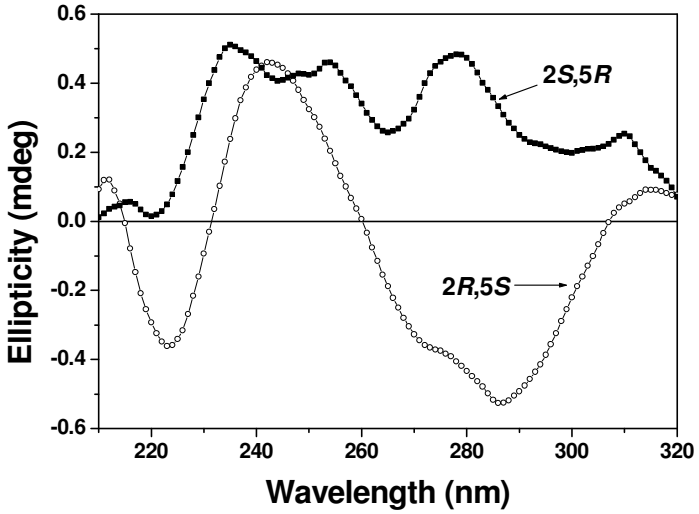

Figure 20. CD spectra of *aepip*PNA T_8 single strands **40** (2*S*,5*R*) & **41** (2*R*,5*S*).

2.4.3a. CD of Triplexes

As part of the chimeric backbone in *aepip-aeg*PNA oligomers, the chirality of *aepip*PNA oligomers was thought to direct the preferred structure of *ss* PNAs. These monomers were therefore incorporated into triplex forming homopyrimidine PNA T_8 sequences at N-terminus (PNA **40-41**), C-terminus (PNA **42-43**), center of the sequence (**44**) and at two positions i.e. at C terminus and second *aepip* unit at the third (**45**), fifth (**46**) or seventh (**47**) base positions respectively to study the additivity of any structural pre-organization due to preferential base stacking. Although the CD spectra of the *aepip*PNA-T_8 single strands differed depending on the stereochemistry and the number of *aepip*PNA units (Figure 21), upon complex formation with the complementary DNA oligomer, the CD exhibited by the complex was similar to that of the control *aeg*PNA_2:DNA triplex (Figure 21B).

Thus, the CD spectra of the complexes formed by (2*S*,5*R*) *aepip*PNA-T (e.g., **40:53**, **42:53**) and (2*R*,5*S*) *aepip*PNA-T (e.g., **41:53**, **43:53**) (Figure 22) were similar to that of the control *aeg*PNA **39:53**. The PNA_2:DNA triplexes exhibited two maxima

at 265nm and 280nm while minima at 246nm and crossover points at ~250- ~260nm. (Figure 21B, 22B). The double hump profile is characteristic of poly T-poly A-poly T triplexes.

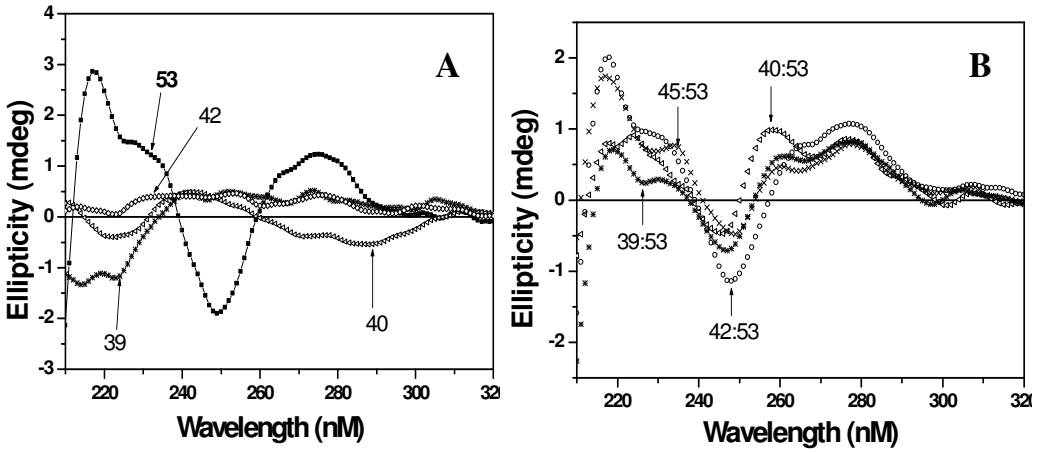

Figure 21. A) CD profiles of *aepip*PNA-T_8 (2*S*,5*R*) single strands **39**, **40**, **42** and DNA single strand **53**. B) CD profiles of PNA_2:DNA triplexes **39:53**, **40:53, 42:53** & **45:53**.

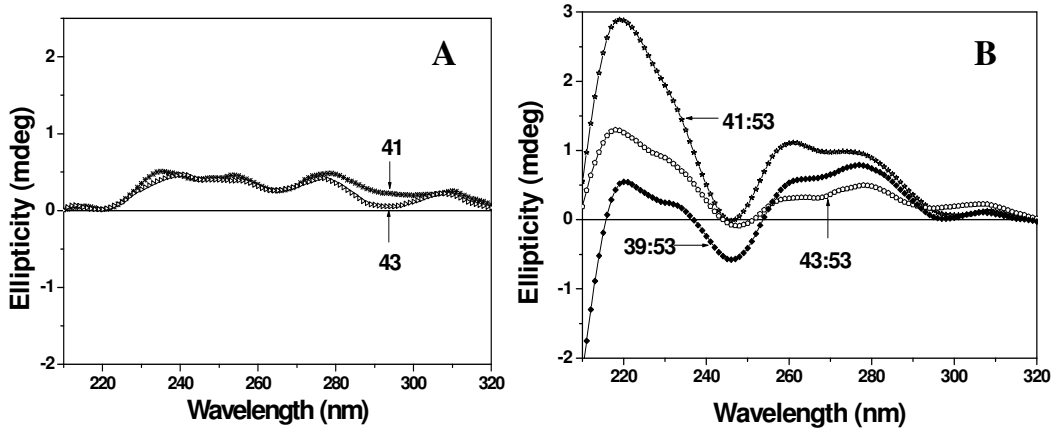

Figure 22. A) CD profiles of *aepip*PNA-T_8 (2*R*,5*S*) single strands **41** & **43** B) CD profiles of PNA_2:DNA triplexes **39:53**, **41:53** & **43:53**.

2.4.3b. CD of Duplexes

The mixed base *aepip*PNAs that were found to form duplexes with DNA by UV-melting were also analyzed by CD. The antiparallel complexes of PNAs **51**-**52** with DNA **56** exhibited different patterns with maxima at ~270nm and ~220nm and a

minimum at ~250nm (Figure 23B) unlike PNA_2:DNA triplexes (Figure 23A) which exhibit positive double hump profile seen in 260-280 nm region. [The chimeric *aepip-aeg*PNA single strand sequence **52** (2*S*,5*R*) which contains one *aepip* unit, was used to study the changes in CD signals upon complexation with DNA.]

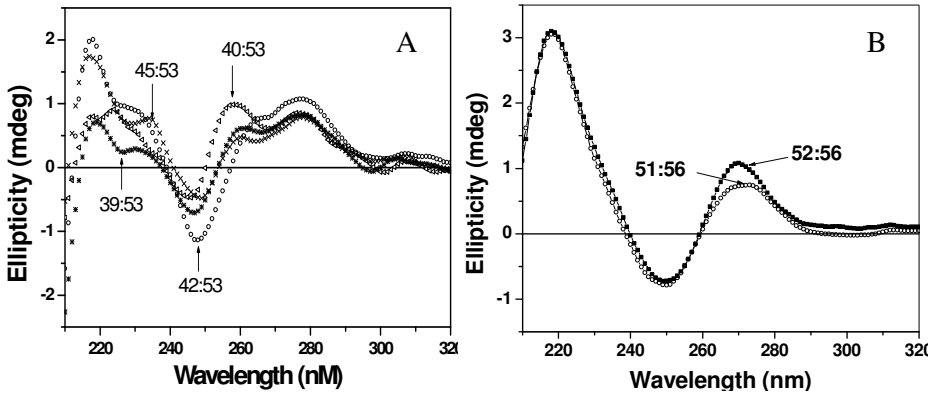

Figure 23. CD profiles of (A) PNA_2:DNA triplexes **39:53**, **40:53, 42:53** & **45:53** in comparison with the (B) PNA:DNA duplex **51:56 & 52:56**.

2.4.3c. Stoichiometry Determination

The circular dichroism spectroscopy can also be used to study the binding stoichiometry of PNA:DNA complexes and change in ellipticity is used to find out the binding stoichiometry of PNA:DNA complexes.[44] The chimeric *aepip-aeg*PNA single strand sequence **40** (2*S*,5*R*) and **43** (2*R*,5*S*) which contains one *aepip* unit, was used to study the changes in CD signals upon complexation with DNA. *aepip-aeg*PNA **40** and **43** and DNA **53** were mixed in various proportions separately and figure 23A and 24A shows the CD spectra for these mixtures of *aepip* PNA and DNA respectively.

The ellipticity at 260nm when plotted against mole fraction of PNA gave an inflection point at ~0.62 to ~0.64 mol fraction of PNA indicating PNA_2:DNA binding stoichiometry (Figure 24B and 25 B). Further, the positive maxima at 220, 260-

280nm and two isobastic points at 238nm and 258nm which are characteristics of PNA_2:DNA triplex confirms the 2:1 binding stoichiometry.

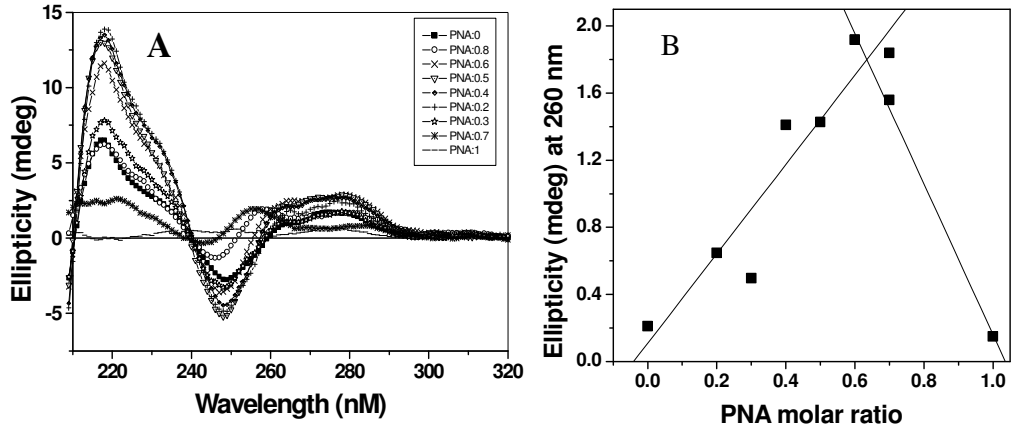

Figure 24. A) CD spectra of molar mixtures of *aepip*PNA **40** and DNA **53** showing isodichroic points. B) CD mixing curve for PNA **40** and DNA **53** mixtures in the various molar proportions indicating 2:1 binding stoichiometry of PNA:DNA.

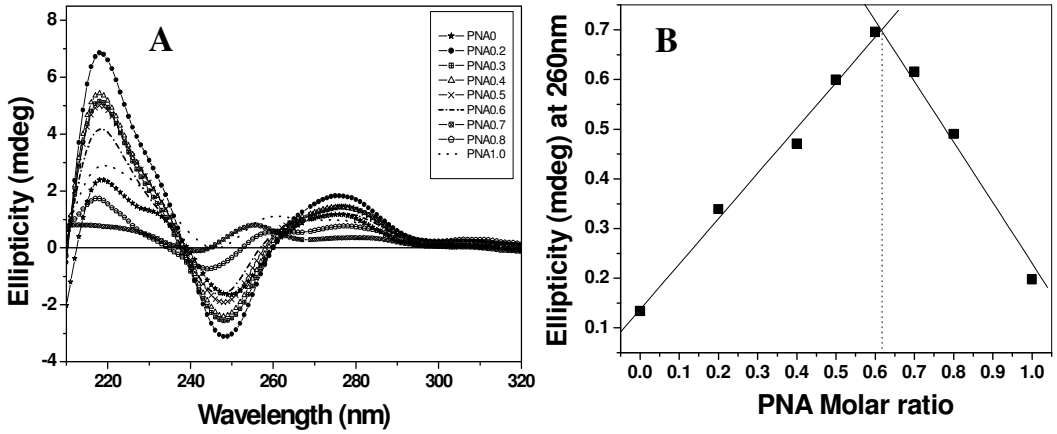

Figure 25. A) CD spectra of molar mixtures of *aepip*PNA **43** and DNA **53** showing isodichroic points. B) CD mixing curve for PNA **43** and DNA **53** mixtures in the various molar proportions indicating 1:1 binding stoichiometry of PNA:DNA.

*aepip-aeg*PNA **52** and DNA **56** were mixed in various proportions and Figure 26A shows the CD spectra for these mixtures of *aepip*PNA and DNA. The ellipticity at 263nm when plotted against mole fraction of PNA gave an inflection point at ~0.52 mol fraction of PNA indicating PNA:DNA binding stoichiometry (Figure 26B). Further, the positive maxima at 270nm, minima at 250nm and two isobastic points at

235nm and 265nm which are characteristics of PNA: DNA duplex confirms the 1:1 binding stoichiometry (Figure 26).

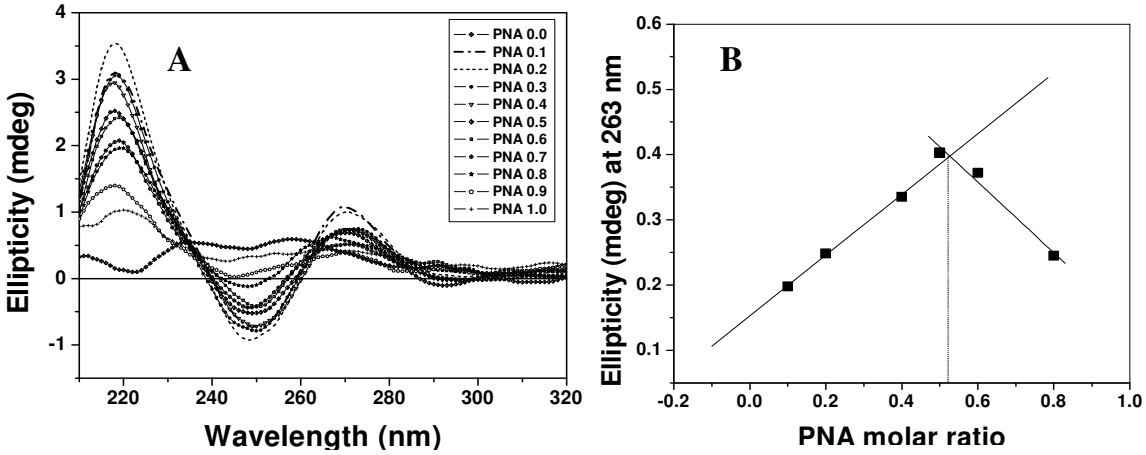

Figure 26. A) CD spectra of molar mixtures of *aepip*PNA **52** and DNA **56** showing isodichroic points. B) CD mixing curve for PNA **52** and DNA **56** mixtures in the various molar proportions indicating 1:1 binding stoichiometry of PNA:DNA.

2.4.4. Gel shift assays

The binding of *aepip*PNAs to complementary DNA was also examined by gel retardation as shown in Figure 27. The modified PNA's and the control PNA were individually treated with complementary DNA and complexation was monitored by non-denaturing gel electrophoresis at 10°C. The single stranded DNA, PNA and PNA:DNA complexes were visualized on a fluorescent TLC background. The PNA:DNA complexes derived from *aepip*PNAs with even a single *aepip*PNA unit

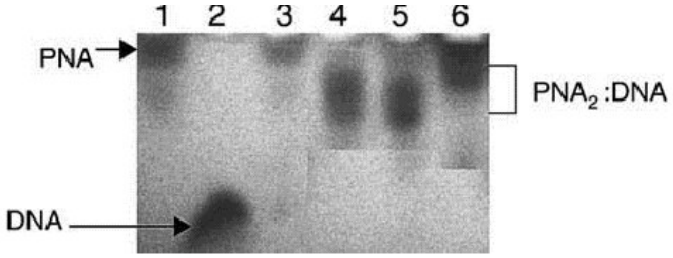

Figure 27. 15% Polyacrylamide Gel Electrophoresis of *aepip*PNA:DNA complexes. Lanes **1** through **6**: PNA **39**, single strand; DNA **53** single strand; PNA **42** single strand; PNA **42**:DNA **53**; PNA **39**:DNA **53**; PNA **45**:DNA **53**.

e.g. **42:53** were significantly retarded in the gel (lane 4). The complexes involving PNAs with two *aepip*PNA units e.g. **45:53** were retarded even more (lane 6) and remained close to the well in which they were loaded. The single strand PNAs alone (lane 1,3) moved much more slowly compared to the complexes.

2.5. DISCUSSION

The effect of PNA backbone modification in the form of *aepip*PNA is expected to significantly affect the PNA:DNA thermal stability. The UV-T_m, CD and gel shift assay data presented in the last section suggests that the *aepip*PNA:DNA interaction is significantly diversified.

2.5.1. UV-Spectroscopy

*aeg*PNA homopyrimidine sequences comprising thymine units are known to form PNA_2:DNA triplexes.[45] Both UV-mixing and UV-titration experiments indicated a 2:1 binding stoichiometry (PNA_2:DNA) for PNA oligomers of (2*S*,5*R*) *aepip-aeg* units **40** as well as (2*R*,5*S*) *aepip-aeg* units **43**. The percent hyperchromicity Vs temperature plots derived from the UV-melting data indicated a single transition, characteristic of PNA_2:DNA triplex melting, wherein both the PNA strands dissociate from the DNA strand simultaneously, in a single step. The stabilizing effect of the *aepip*PNA units on the derived PNA_2:DNA complex progressively increased with an increase in the number of *aepip*PNA units.

PNA oligomers with one *aepip* modification at C-terminus and a second *aepip* unit at the third (**45**), fifth (**46**) or seventh (**47**) base positions respectively were used to study the relative positional effects of the modifications. A synergistic stabilizing

effect was observed with a second modified *aepip* unit in all the cases (**45:53, 46:53** and **47:53**). The maximum benefit per additional unit was observed (ΔT_m +4^{o}C) when the second *aepip*PNA unit was separated by one base (**45:53)** (Table 6). More importantly, the specificity is retained in these cases. This was evident from the mismatch studies, where the presence of a single T-T mismatch in the center of the sequence made the PNA_2:DNA complexes very unstable. The PNA/DNA single strands, when subjected to the same temperature program as the PNA_2:DNA complexes, exhibited <3% change in absorbance, thus ruling out any significant contribution from single stranded ordering to the sigmoidal transition observed for the PNA_2:DNA triplexes. The tight binding of the T_8 *aep*PNAs with DNA was also seen in diagnostic gel mobility shift experiments, where even a single modification effected significant retardation.

PNA_2:DNA complexes are known to be destabilized by the presence of salts and the stability of complexes of DNA with positively charged ligands is strongly salt-dependent. The presence of salt in the medium caused a destabilization of both *aepip*PNA_2:DNA complex, **40:53** and *aeg*PNA_2:DNA complex **39:53** (ΔTm ≥5^{o}C). The pH-titration plot of *aepip*PNA-T monomeric unit exhibited three distinct transitions, wherein the pK_as of the three functional groups that can be deprotonated *viz*., the carboxylic acid, the piperidine ring nitrogen and the primary amine, were clearly resolved. The plot indicated a pK_a ≈6.76 for the piperidine nitrogen, substantiating its protonation status even at neutral pH. The homopyrimidine-*aeg*PNA backbone comprising both the isomers of *aepip* units effect stabilization of the resulting triplexes with complementary DNA strands depending upon stereochemistry and position of the modified unit.

The effect of backbone chirality of *aepip*PNA while binding to complementary DNA sequences seems to be unimportant in such homopyrimidine (T_8) sequences since these bind to complementary DNA in both parallel (HG) and antiparallel (WC) orientations. The mixed purine-pyrimidine sequences (**51-52**) were constructed to explore the effect of the *aepip* backbone chirality on the directionality of binding in duplexes.

The presence of a single 2*S,*5*R aepip*PNA unit in the center of a mixed purine-pyrimidine duplex forming oligomer discriminates the parallel versus antiparallel DNA sequence much better than the unmodified *aeg*PNA. The fairly rigid 6-membered ring structures as in hexose[46] and hexitol[47] nucleic acids have shown excellent selection of parallel/antiparallel modes of binding to DNA. This has triggered interest in six-membered PNA analogs,[48] although with some initial misgivings.[49]

2.5.2. CD Spectroscopy

*aeg*PNA is inherently achiral. However, upon complexation with complementary nucleic acids, it is rendered chiral and exhibits an induced CD signal. Chirality can be induced in the achiral PNA strand by linking chiral moieties like amino acids,[50] peptides,[51] or oligonucleotides[52-57] to the PNA termini. PNA has also been rendered chiral by the incorporation of chiral amino acids in its backbone.[58-67] The CD is predominantly an effect of coupling between the transition moments of the nucleobases as a result of their helical stacking.

The introduction of chiral monomers in the backbone allows the investigation of specifically positioned stereogenic centers within the achiral PNA oligomer. Thus, it is of general interest to investigate how many stereogenic centers inserted at which

positions of a PNA oligomer can coherently induce a preferred handedness of the single or double stranded PNA, and if eventual stereochemical preorganization of PNAs can favour the DNA/RNA recognition process.[68] It has been suggested[69,70] that effective mechanisms of inducing chirality would involve some immobilization of the rotation around the bonds of the α-carbon of the amino acid.[71]

A comparison of the structures of the complexes formed by PNA with complementary DNA/RNA and the corresponding DNA:DNA and DNA:RNA complexes suggested that PNA hybrids are right handed helices with a base-pair geometry not very much different from 'A' or 'B' form DNA. The preferred handedness of the PNA:DNA duplexes seems to be dictated by the DNA.

PNA-T_8 oligomers were demonstrated to form PNA_2:DNA triplexes with the DNA polypurine strand as the central strand. In such cases, CD supported the fact that a triplex is formed as the only PNA_2:DNA complex, and that it is a right-handed helix. The conformation of bases in the PNA_2:DNA triplex was found to be very similar to that of the conventional DNA_2:DNA T*A:T triplex.

Of the two stereocenters present in each chiral *aepip*PNA unit presented here, the C2-stereocenter is present directly in the backbone (Figure 28) and hence, this is expected to exert a greater effect in inducing chirality in the oligomer backbone. The

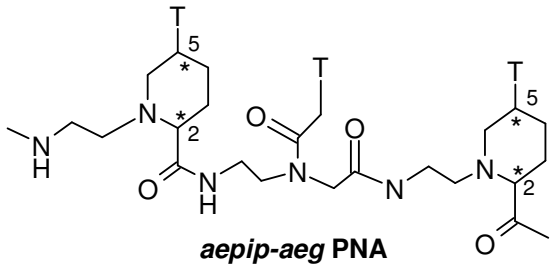

Figure 28. The *aepip*PNA backbone showing the two chiral centers of each *aepip*PNA unit.

C5 stereocenter carrying the nucleobase may mostly affect the base stacking. However, since both are part of the piperdine ring, the two roles may be correlated.

The CD induced by the *aepip*PNA units in the PNA single strands seemed to be inconsequential, since the *aepip*PNA oligomers formed complexes (duplexes/triplexes) (e.g. **40:53**, **42:53**, **52:56**) that gave very similar CD signals upon complexation with DNA. Significantly, these CD profiles were similar to those of the control achiral *aeg*PNA complexes (**39:53**, **51:56**). Thus, in a PNA:DNA complex, it is the CD of the DNA that dominates over any inherent CD of the PNA involved in the structure.

2.5.3. Gel Retardation Assays

The gel mobility shift assays described in section 2.4.4. are confirmative proof for the formation of PNA:DNA complexes. The formation of such a complex with DNA **53** resulted in significant retardation in the polyacrylamide gel electrophoresis. These results were in concordance with the data obtained from the UV-thermal melting studies with these oligomers. This underlined the specificity of the hydrogen bonding between the complementary base pairs even in modified PNAs, which is of utmost importance for the application of oligonucleotide/PNA analogues in antisense/antigene therapy.

The PNAs containing *aepip*PNA units remained in solution for a much longer time duration even at lower temperature as compared to the uncharged *aeg*PNA oligomers, which precipitated out of solution as a result of self-aggregation. The *aepip*PNAs enhanced solubility in aqueous media is probably a resultant of the positive charge present in the monomeric units (pK_a of the piperdine ring nitrogen is ~6.76, which suggests that it should be at least partly protonated at pH 7.4).

2.6. COMPARISION OF *aepip*PNA AND pip-PNA

Nielsen *et al*[49] has reported two conformationally restricted piperidinone PNA adenine monomers (Figure 29). They have been synthesised and incorporated into a PNA dodecamer (once in a central position). Modifying PNA with either monomer resulted in a large decrease in duplex stability with RNA (ΔT_m 10–11.5^{0}C) as well as with DNA, and a smaller decrease with complemetary PNA. Thus, any expected preorganisation of the PNA single strand induced by these cyclic six-membered pip-PNA analogues seems to be inferior to the preorganisation by the cyclic five membered PNA analogues studied earlier in terms of producing a hybridisation-competent conformation.

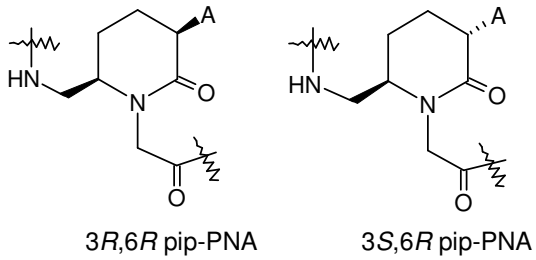

Figure 29. pip-PNA monomers.[49]

But in contrast, the *aepip*PNAs presented in this chapter-effected stabilization of the resulting triplexes with complementary DNA strands depending upon stereochemistry and position of the modified unit. A single modified 2*S,*5*R* *aepip*PNA unit in the center of a mixed purine-pyrimidine duplex forming oligomer discriminates the parallel versus antiparallel DNA sequence much better than the unmodified *aeg*PNA. The results reported here further expand the repertoire of cyclic PNA analogues to six-membered series.

2.7. SUMMARY

In summary, this chapter promulgates the design and synthesis of novel six-membered pipecolic acid derived PNA analogues (2*S,*5*R* and 2*R*,5*/S*)-1-(*N*-Boc-aminoethyl)-5-(thymin-1-yl)pipecolic acid. *aeg*PNA homopyrimidine sequences are known to form triplexes. UV-mixing and CD-mixing experiments indicated a 2:1 binding stoichiometry (PNA_2:DNA) for homopyrimidine *aepip*PNA:DNA complex, while 1:1 stoichiometry was observed for purine-pyrimidine mixed sequences. The % hyperchromocity *vs* temperature plots derived from the UV-melting data indicated a single transition characteristic of PNA_2:DNA melting, wherein both PNA strands dissociate from the DNA strand simultaneously, in a single step. The binding of these modified oligomers with DNA was also seen in diagnostic gel mobility shift experiments, where a single modification effected significant retardation.

The homopyrimidine-*aeg*PNA backbone comprising these units effect stabilization of the resulting triplexes with complementary DNA strands depending upon stereochemistry and position of the modified unit. A single modified 2*S,*5*R* *aepip*PNA unit in the center of a mixed purine-pyrimidine duplex forming oligomer discriminates the parallel versus antiparallel DNA sequence much better than the unmodified *aeg*PNA. The results reported here further expand the repertoire of cyclic PNA analogues to six-membered series. The positive charge on the piperidine nitrogen is at least partly responsible for the high binding affinity. The main contributing factor to the enhanced affinity however, remains the specific hydrogen bonding between the A-T and G-C nucleobases. An added and important asset of this positively charged chiral backbone is its enhanced solubility in aqueous media.

In order to explain all the observed results, more work needs to be carried out, including studying the properties of other nucleobases and to investigate the undiluted effect of the aminoethylpipecolyl backbone, in homooligomeric *aepip*PNA sequences and in mixed base duplexes.

2.8. EXPERIMENTAL

The chemicals used were of laboratory or analytical grade. All the solvents used were purified according to the literature procedures.[72] All the reactions were monitored for completion by TLC. Usual work-up implies sequential washing of the organic extract with water and brine followed by drying over anhydrous sodium sulphate and evaporation under vacuum.

Column chromatography was performed for purification of compounds on Spectrochem silica gel (100-200 mesh). TLCs were carried out on pre-coated silica gel GF_{254} aluminium sheets (Merck 5554). TLCs were run in either dichloromethane with an appropriate quantity of methanol or in petroleum ether with an appropriate quantity of added ethyl acetate for most compounds. Free acids were chromatographed on TLC using a solvent system of *iso*-propanol: acetic acid: water in the proportion 9:1:1. The compounds were visualized with UV light and/ or by spraying with ninhydrin reagent subsequent to Boc-deprotection (exposing to HCl vapors) and heating.

^{1}H (200MHz/300MHz/500MHz) and ^{13}C (500MHz) NMR spectra were recorded on a Bruker ACF 200 spectrometer fitted with an Aspect 3000 computer and all the chemical shifts are referred to internal TMS for ^{1}H and chloroform-d for ^{13}C. The chemical shifts are quoted in δ (ppm) scale. In compounds that bear a tertiary

amide group, splitting of NMR signals was observed due to the presence of rotamers. In such cases, the major isomer is designated as 'maj' and the minor isomer, 'min'.

Optical rotation values were measured on Bellingham-Stanley Ltd, ADP220 polarimeter and CD spectra were recorded on a JASCO J715 spectropolarimeter.

Mass spectra were recorded on a Finnigan-Matt (LCMS) mass spectrometer, while MALDI- TOF spectra were obtained from a KRATOS PCKompact and Applied Biosystems instrument.

***N-benzyloxycarbonyl-L-glutamic acid*[21,22]**

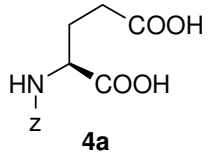

4a

To a solution of L-glutamic acid **4** (68mmol, 10g) in 1,4-dioxan was added a 2M sodium hydroxide solution and cooled to 0^0C. After stirring for 5min at 0^0C a 50% solution of benzylchloroformate in toluene (81.6mmol, 23.3ml) was added dropwise to the above solution. After complete addition, reaction mixture was stirred overnight at rt. The reaction mixture was concentrated to remove 1,4-dioxan and then washed with diethyl ether to remove unreacted benzylchloroformate. Then reaction mixture was acidified with conc. HCl to pH 2.0 and extracted with ethyl acetate. The organic layer was dried with sodium sulfate and concentrated in *vacuum*, resulting in white solid **4a** (18g, 94% yield).

^{1}H NMR ($CDCl_3$) δ: 7.34 (s, 5H, Ar-*H*), 5.67-5.63 (d, 1H, N*H*), 5.11 (s, 2H, Ph-CH_2), 4.51-4.39 (m, 1H, *H1*), 2.50-2.19 (m, 4H, *Hα*, *Hα'*, *Hβ*, *Hβ'*).

(S)-3-benzyloxycarbonyl-5-oxo-4-oxazolidine propanoic acid [21,22] ***(5)***

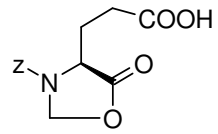

5

A mixture containing *N*-benzyloxycarbonyl-L-glutamic acid **4a** (64.06mmol, 16g), paraformaldehyde (160.15mmol, 4.80g) and *p*-toluenesulphonic acid monohydrate (3.84mmol, 0.731g) in benzene was heated at reflux for 3-4h, with removal of water with a dean stark setup. The solution was allowed to cool to room temperature and to it ethyl acetate was (100ml) added, the solution was washed with 0.3M aqueous potassium carbonate (10ml), water (10ml x 2) and dried with sodium sulfate. The solvent was evaporated to give colourless syrup **5** (13.63g, 82% yield). $[\alpha]_D^{25}$ = +67.27 (c=2.2, MeOH).

^{1}H NMR ($CDCl_3$) δ: 7.40 (s, 5H, Ar-*H*), 5.60 (br s, 1H, *H2*), 5.30-5.25 (d, 1H, *H2'*), 5.20 (s, 2H, Ph-CH_2), 4.45-4.35 (m, 1H, *H4*), 2.55-2.05 (m, 4H, *Hα*, *Hα'*, *Hβ*, *Hβ'*).

N-benzyloxy-L-glutamic acid α-methyl ester[21,22] ***(6)***

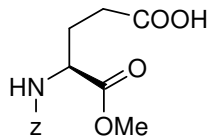

6

Oxazolidinone **5** (40.96mmol, 12g) was added to a solution of sodium methoxide (49.15mmol, 2.65g) in methanol at 0 to -10^0C with stirring under an atmosphere of nitrogen. After stirring for 60min, the solution is warmed to room temp and partitioned between ethyl acetate (200ml) and saturated solution of potassium hydrogen sulphate (50ml) and organic layer worked up to give ester as clear oil **6** (11.2g, 93% yield). $[\alpha]_D^{25}$ = -7.5 (c=2.0, MeOH).

^{1}H NMR ($CDCl_3$) δ: 7.35 (s, 5H, Ar-*H*), 5.56-5.52 (d, 1H, N*H*), 5.12 (s, 2H, Ph-CH_2), 4.50-4.40 (m, 1H, *H1*), 3.75 (s, 3H, OCH_3), 2.46-1.95 (m, 4H, *Hα*, *Hα'*, *Hβ*, *Hβ'*).

N-benzyloxycarbonylamino-6-diazo-5-oxo-L-glutamic acid-2-methyl ester[21,22] (7)

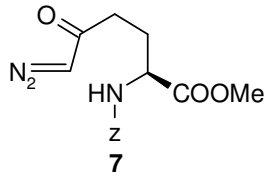

7

To a cooled solution of N-benzyloxy-L-glutamic acid α-methyl ester **6** (33.90mmol, 10g) in THF (40ml) was added triethylamine (37.29mmol, 5.2ml) and stirred for 5-10min. After that ethylchloroformate (37.29mmol, 3.6ml) was added slowly and stirred for 15-20min at 0 to -10^0C, resulting in white thick suspension. To this mixed anhydride was added previously generated diazomethane (339.0mmol) in ether and reaction kept at -20^0C, for overnight. Evaporation of the solvent followed by column chromatography gave thick yellow oil **7** (7.0g, 65% yield).

^{1}H NMR ($CDCl_3$) δ: 7.35 (s, 5H, Ar-*H*), 5.59-5.55 (d, 1H, N*H*), 5.24 (s, 1H, *H1*), 5.11 (s, 2H, Ph-CH_2), 4.39-4.31 (m, 1H, N=N-C*H*), 3.74 (s, 3H, OCH_3), 2.40-1.94 (m, 4H, *Hα*, *Hα'*, *Hβ*, *Hβ'*).

IR (neat) cm^{-1}: 2140, 1728 and others.

5-oxo-N-benzyloxycarbonyl-2-(S)-pipecolic acid methyl ester[21,22] (8)

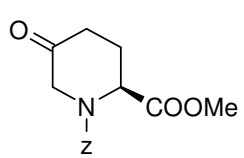

8

A concentrated solution of the diazoketone **7** (21.22mmol, 6.77g) in benzene was added dropwise to a solution of rhodium (II) acetate (89.50mg, 1mol %) at reflux in benzene (360ml, final concentration 0.02mol/ml). The solution was heated for a further 30min. Evaporation of the solvent followed by column chromatography gave as a colourless oil **8** (3.2g, 52% yield). $[\alpha]^{25}_D$ +11.7 (c=0.5, $CHCl_3$).

^{1}H NMR ($CDCl_3$) δ: 7.33 (s, 5H, Ar-*H*), 5.4-5.0 (m, 2H, CH_2-Ar), 4.7 (m, 1H, *H2*), 4.3-4.0 (m, 3H, *H6*, *H5*), 3.74 (s, 3H, OCH_3), 2.6-2.3 (m, 2H, *H4*).

^{13}C NMR ($CDCl_3$) (major rotamer) δ: 198.3 (*C*5), 170.4 (*C*OOCH$_3$), 155.8, 135.6, 128.3, 128.0 (Ar) 68.0 (*C*H$_2$-Ar), 62.4 (*C*6), 54.9(*C*3), 33.2 (*C*4), 21.8 (OC*H*$_3$).

IR (neat) cm^{-1}: 1728 and others.

5-(S)-hydroxy-N-benzyloxycarbonyl-2-(S)-pipecolic acid methyl ester[21,22] (9)

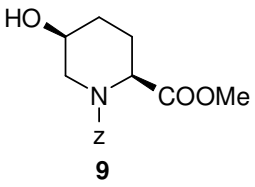

9

A cooled (0^{0}C) solution of 5-oxo-N-benzyloxycarbonyl-2-(*S*)-pipecolic acid methyl ester **8** (10.85mmol, 3.2g) in methanol (50ml) was treated with sodium borohydride (16.28 mmol, 0.615g). After being stirred for 2h, the reaction mixture was concentrated *in vacuuo* and the residue was dissolved in ethyl acetate (100ml). The organic solution was washed with 10% ammonium chloride solution, brine, and dried over sodium sulfate and concentrated. The resulting residue was chromatographed to give colourless oil **9** (3.0g, 93% yield). $[\alpha]_D^{25}$ = -17.78 (c=0.9, MeOH).

^{1}H NMR ($CDCl_3$) δ: 7.35 (s, 5H, Ar-*H*), 5.14 (s, 2H, Ph-C*H*$_2$), 4.90-4.78 (dd, 1H, *H5*), 4.30-4.10 (m, 1H, *H6*), 3.73-3.55 (m, 4H, OC*H*$_3$, *H6'*), 2.89-2.72 (m, 1H, *H2*), 2.55 (br s, 1H, O*H*), 2.00-1.93 (m, 4H, *Hα*, *Hα'*, *Hβ*, *Hβ'*).

5-(S)-hydroxy-2-(S)-pipecolic acid methyl ester (10)

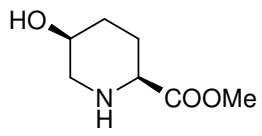

10

Deprotection of 5-(*S*)-hydroxy-N-benzyloxycarbonyl-2-(*S*)-pipecolic acid methyl ester **9** (7.80mmol, 2.20g,) using hydrogenation (Pd/C, 10%) gave 5-(*S*)-hydroxy-2-(*S*)-pipecolic acid methyl ester **10** (1.10g, 92% yield).

^{1}H NMR ($CDCl_3$) δ: 3.83-3.81 (m, 1H, *H5*), 3.74 (s, 3H, OC*H*$_3$), 3.40-3.33 (t, 1H, *H6*), 3.08-3.00 (dd, 1H, *H6'*) 2.88-2.80 (dd, 1H, *H2*), 1.90-1.83 (m, 3H, *H4*, *H4'*, *H3*), 1.74-1.61 (m, 1H, *H3'*).

1-(N-Boc-aminoethyl)-5-(S)-hydroxy-2-(S)-pipecolic acid methyl ester (11)

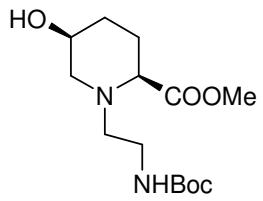

11

To a cooled solution of 5-(*S*)-hydroxy-2-(*S*)-pipecolic acid methyl ester **10** (6.29mmol, 1.0g), DMAP (1.26mmol, 0.15g) in dry DMF:Acetonitrile (1:1) (10ml) was added *N,N*-diispropyl ethylamine (15.73mmol, 2.7ml). Stirring was continued for 15min and then to this N-Boc amino mesylate (6.29mmol, 1.50g) in DMF (3ml) was added. Reaction mixture was heated to 50^{o}C for 20h. Evaporation of the solvent followed by column chromatography gave thick brown oil **11** (0.7g, 37% yield).

^{1}H NMR ($CDCl_3$) δ: 5.18 (br s, 1H, N*H*), 3.93-3.82 (m, 1H, *H5*), 3.73 (s, 3H, OC*H*$_3$), 3.54-3.50 (m, 3H, *H6*, Boc-NH-C*H*$_2$), 3.05-2.99 (m, 1H, *H*6') 2.75-2.50 (m, 3H, *H*2, Boc-NH-CH$_2$ -C*H*$_2$), 1.90-1.64 (m, 4H, *H3*, *H3', H4, H4'*), 1.45 (s, 9H, C(C*H*$_3$)$_3$).

^{13}C NMR ($CDCl_3$) δ: 175.11(*CO*OCH$_3$), 161.18 (*C*OOC(CH$_3$)$_3$), 79.23 (*C*(CH$_3$)$_3$), 64.96 (*C*$_5$), 62.85 (O*C*H$_3$), 55.34(*C*$_6$), 55.11(*C*$_4$), 51.77(*C*$_3$), 40.58 (*C*$_2$), 37.18(*C*H$_2$-*C*H$_2$-NH-Boc), 28.28 ((*C*H$_3$)$_3$).

MS: (ESI) 302 $(M)^+$

1-(N-Boc-aminoethyl)-5-(R)-(N3-benzoylthymin-1-yl)-2-(S)-pipecolic acid methyl ester (12)

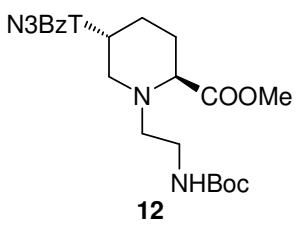

12

To a stirred solution of 1-(*N*-Boc-aminoethyl)-5-(*R*)-hydroxy-2-(*S*)-pipecolic acid methyl ester **11** (0.55g, 1.82mmol), N3-benzoylthymine (0.84g, 3.64mmol) and triphenyl phosphine (0.95g, 3.64mmol) in dry THF (10ml) at room temperature, was added dropwise diethylazodicarboxylate (DEAD, 0.47ml, 3.64mmol). After completion of the reaction as indicated by TLC (24h), the solvent was removed *in vacuo* and residue purified by silica gel column chromatography to get the pure product **12** (0.3g, 32% yield). $[\alpha]_D^{25}$ = +10.0 (c=0.1, MeOH).

^{1}H NMR ($CDCl_3$) δ: 7.92 (s, 1H, *T-H*6), 7.88 (s, 1H, Bz, *p*-C*H*), 7.62-7.44 (m, 4H, Bz, *o*-C*H, m*-C*H*) 5.28 (br s, N*H*), 3.74 (s, 1H, *H5*), 3.72 (s, 3H, OCH_3), 3.48-3.22 (m, 3H, Boc-NH-CH_2, *H6*), 2.94-2.69 (m, 3H, Boc-NH-CH_2-CH_2, *H*2) 2.14-2.00 (m, 1H, *H6'*), 2.00 (s, 3H, T-CH_3), 2.00-1.63 (m, 4H, *H4*, *H4'*, *H3*, *H3'*), 1.42 (s, 9H, C(CH_3)$_3$).

^{13}C NMR ($CDCl_3$) δ: 175.28 (*C*OOCH_3)**,** 169.09 (*C*OOC(CH_3)$_3$), 163.24 (*T-C*2), 156.01 (Ph-*C*O), 150.31 (*T-C*4), 142.58 (*T-C*6), 138.87, 131.65, 130.36, 129.13 (arom), 109.50 (*T-C*5), 79.55 (*C*(CH_3)$_3$), 66.60 (*C5*), 64.70 (*C6*), 56.00 (Boc-NH-*C*H_2), 52.24 (C2), 51.25 (OCH_3), 39.73 (Boc-NH-CH_2-*C*H_2), 29.41 (*C4*), 28.39 (C(*C*H_3)$_3$), 27.75 (*C3*), 12.27 (T-*C*H_3).

FAB-MS: (100%, dibenzofulvalene), 515 $(M+H)^+$

MS: (ESI) 514 $(M)^+$

1-(N-Boc-aminoethyl)-5-(R)-(thymin-1-yl)-2-(S)-pipecolic acid (13)

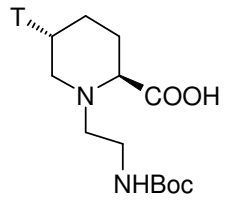

13

To a solution of 1-(*N*-Boc-aminoethyl)-5(*S*)-(N3-benzoylthymin-1-yl)-2(*S*)-pipecolic acid methyl ester **12** (0.36g, 0.70mmol) in methanol (2ml) was added aqueous 2M NaOH (2ml). TLC analysis after 10min. indicated the absence of the starting material as a result of hydrolysis of the methyl ester function. The reaction mixture was further stirred overnight, when TLC indicated the presence of a lower moving spot. The excess NaOH was neutralized by Dowex-50 H^+ resin, which was then, filtered off. The methanol from the filtrate was removed under vacuum and the residue was taken up in water. This was washed with ethyl acetate before concentrating it to dryness to obtain the product **13** (0.25g, quantitative yield) as white solid foam.

^{1}H NMR (D_2O) δ: 7.50 (1H, *T-H*6) 4.52-4.44 (m, 1H, *H*5), 4.21-3.94 (m, 3H, Boc-NH-CH_2, *H2*) 3.50-3.45 (m, 4H, Boc-NH-CH_2-CH_2, *H6*, *H6'*), 2.34-2.24 (m, 4H, *H4*, *H4'*, *H3*, *H3'*), 1.89 (s, 3H, T-CH_3), 1.45 (s, 9H, C(CH_3)$_3$).

MS: (ESI) 396 $(M)^+$

N-Boc-2-aminoethanol (15)

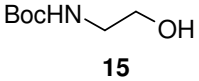

15

To a cooled, stirred solution of 2-aminoethanol **14** (5.1ml, 84mmol) in water-dioxane (1:1), was added triethylamine (11.7 ml, 84mmol) and stirred for 10-15min at 0^0C. To this reaction mixture at 0^0C was addred drop-wise Boc-azide (10g, 70mmol). The reaction was stirred at room temperature overnight. The dioxane was then removed under vacuum, and the water layer extracted several times with ethyl acetate. The organic layer was dried over

sodium sulphate and then, evaporated to dryness under vacuum to get the product 2-*N*-Boc-aminoethanol **15** (6.5g, 58% yield), which was used in further steps without purification.

^{1}H NMR ($CDCl_3$) δ: 5.09 (br s, 1H, N*H*), 3.69-3.64 (m, 2H, (CH_2)), 3.28-3.23 (t, 2H, (CH_2)), 2.65 (br s, 1H, O*H*), 1.42 (s, 9H, C(CH_3)$_3$)

2-N-Boc-aminoethylmesylate (16)

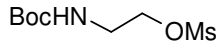

16

To an ice-cooled solution of 2-*N*-Boc-aminoethanol **15** (2.8g, 17.4mmol) in dry dichloromethane (25ml), was added dry pyridine (1.7ml, 20.9mmol). To this reaction mixture was added methane sulphonyl chloride (2ml, 26.1mmol) in small portions over 10-15min. The reaction was kept at 0^0C overnight. After that solvent was evaporated and the product immediately purified by silica gel column chromatography to get 2-*N*-Boc-aminoethylmesylate **16** (2.6g, 62% yield).

^{1}H NMR ($CDCl_3$) δ: 4.91(br s, 1H, N*H*), 4.29-4.24 (t, 2H, (CH_2)), 3.45 (m, 2H, (CH_2)), 3.02 (s, 3H, OSO_2CH_3), 1.43 (s, 9H, C(CH_3)$_3$)

N-benzyloxycarbonyl-D-glutamic acid

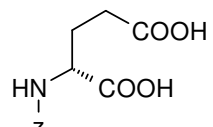

17a

To a solution of D-glutamic acid **17** (68mmol, 10g) in 1,4-dioxan was added a 2N sodium hydroxide solution and cooled to 0^0C. After stirring for 5min at 0^0C a 50% solution of benzylchloroformate in toluene (81.6mmol, 23.3ml) was added dropwise to the above solution. After complete addition, reaction mixture was stirred overnight at rt. The reaction mixture was concentrated to remove 1,4-dioxan and then washed with diethyl

ether to remove unreacted benzylchloroformate. Then reaction mixture was acidified with conc. HCl to pH 2.0 and extracted with ethyl acetate. The organic layer was dried with sodium sulfate and concentrated in *vacuum*, resulting in white solid **17a** (18g, 94% yield).

^{1}H NMR ($CDCl_3$) δ: 7.34 (s, 5H, Ar-*H*), 5.67-5.63 (d, 1H, N*H*), 5.11 (s, 2H, Ph-CH_2), 4.51-4.39 (m, 1H, *H1*), 2.50-2.19 (m, 4H, *Hα*, *Hα'*, *Hβ*, *Hβ'*).

(R)-3-benzyloxycarbonyl-5-oxo-4-oxazolidine propanoic acid (18)

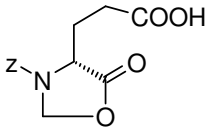

18

A mixture containing *N*-benzyloxycarbonyl-L-glutamic acid **17a** (64.06mmol, 16g), paraformaldehyde (160.15mmol, 4.80g) and *p*-toluenesulphonic acid monohydrate (3.84mmol, 0.731g) in benzene was heated at reflux for 3-4 hrs, with removal of water with a dean stark setup. The solution was allowed to cool to room temperature and to it ethyl acetate was (100ml) added, the solution was washed with 0.3M aqueous potassium carbonate (10ml), water (10ml x 2) and dried with sodium sulfate. The solvent was evaporated to give colourless syrup **18** (13.63g, 82% yield). $[\alpha]_D^{25}$ = +67.27 (c=2.2, MeOH).

^{1}H NMR ($CDCl_3$) δ: 7.40 (s, 5H, Ar-*H*), 5.60 (br s, 1H, *H2*), 5.30-5.25 (d, 1H, *H2'*), 5.20 (s, 2H, Ph-CH_2), 4.45-4.35 (m, 1H, *H4*), 2.55-2.05 (m, 4H, *Hα*, *Hα'*, *Hβ*, *Hβ'*).

N-benzyloxy-D-glutamic acid α-methyl ester (19)

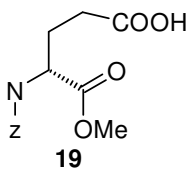

19

Oxazolidinone **18** (40.96mmol, 12g) was added to a solution of sodium methoxide (49.15mmol, 2.65g) in methanol at 0 to -10^0C with stirring under an atmosphere of nitrogen. After stirring for

60min, the solution is warmed to room temp and partitioned between ethyl acetate (200 ml) and saturated solution of potassium hydrogen sulphate (50ml) and organic layer worked up to give ester as clear oil **19** (11.2g, 93% yield). $[\alpha]_D^{25}$ = -7.5 (c=2.0, MeOH).

^{1}H NMR ($CDCl_3$) δ: 7.35 (s, 5H, Ar-*H*), 5.56-5.52 (d, 1H, N*H*), 5.12 (s, 2H, Ph-CH_2), 4.50-4.40 (m, 1H, *H1*), 3.75 (s, 3H, OCH_3), 2.46-1.95 (m, 4H, *Hα*, *Hα*', *Hβ*, *Hβ*').

N-benzyloxycarbonylamino-6-diazo-5-oxo-D-glutamic acid-2-methyl ester (20)

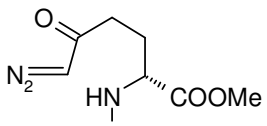

20

To a cooled solution of N-benzyloxy-D-glutamic acid α-methyl ester **19** (33.90mmol, 10g) in THF (40ml) was added triethylamine (37.29mmol, 5.2ml) and stirred for 5-10min. After that ethylchloroformate (37.29mmol, 3.6ml) was added slowly and stirred for 15-20min at 0 to -10^0C, resulting in white thick suspension. To this mixed anhydride was added previously generated diazomethane (339.0mmol) in ether and reaction kept at -20^0C, for overnight. Evaporation of the solvent followed by column chromatography gave thick yellow oil **20** (7.0g, 65% yield).

^{1}H NMR ($CDCl_3$) δ: 7.35 (s, 5H, Ar-*H*), 5.59-5.55 (d, 1H, N*H*), 5.24 (s, 1H, *H1*), 5.11 (s, 2H, Ph-CH_2), 4.39-4.31 (m, 1H, N=N-C*H*), 3.74 (s, 3H, OCH_3), 2.40-1.94 (m, 4H, *Hα*, *Hα*', *Hβ*, *Hβ*').

IR (neat) cm^{-1}: 2140, 1728 and others.

5-oxo-N-benzyloxycarbonyl-2-(R)-pipecolic acid methyl ester (21)

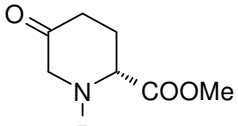

21

A concentrated solution of the diazoketone **20** (21.22mmol, 6.77g) in benzene was added dropwise to a solution of

rhodium (II) acetate (89.50mg, 1mol %) at reflux in benzene (360ml, final concentration 0.02mol/ml). The solution was heated for a further 30 min. Evaporation of the solvent followed by column chromatography gave as a colourless oil **21** (3.2g, 52% yield). $[\alpha]^{25}_{D}$ +11.7 (c=0.5, $CHCl_3$).

^{1}H NMR ($CDCl_3$) δ: 7.33 (s, 5H, Ar-*H*), 5.4-5.0 (m, 2H, C*H*$_2$-Ar), 4.7 (m, 1H, *H2*), 4.3-4.0 (m, 3H, *H6*, *H5*), 3.4 (s, 3H, COOC*H*$_3$), 2.6-2.3 (m, 2H, *H4*).

^{13}C NMR ($CDCl_3$) (major rotamer) δ: 198.3 (*C*5), 170.4 (*CO*OCH$_3$), 155.8, 135.6, 128.3, 128.0 (Ar) 68.0 (*C*H$_2$-Ar), 62.4 (*C*6), 54.9(*C*3), 33.2 (*C*4), 21.8 (O*C*H$_3$).

IR (neat) cm^{-1}: 1728 and others.

5-(R)-hydroxy-N-benzyloxycarbonyl-2-(R)-pipecolic acid methyl ester (22)

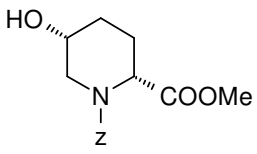

22

A cooled (0^0C) solution of 5-oxo-N-benzyloxycarbonyl-2-(*R*)-pipecolic acid methyl ester **21** (3.44mmol, 1.0g) in methanol (20ml) was treated with sodium borohydride (4.13 mmol, 0.160g). After being stirred for 2h, the reaction mixture was concentrated *in vacuuo* and the residue was dissolved in ethyl acetate (50ml). The organic solution was washed with 10% ammonium chloride solution, brine, and dried over sodium sulfate and concentrated. The resulting residue was chromatographed to give colourless oil **22** (0.95g, 95% yield). $[\alpha]_D^{25}$ = +15.38 (c=0.26, MeOH).

^{1}H NMR ($CDCl_3$) δ: 7.35 (s, 5H, Ar-*H*), 5.15 (s, 2H, Ph-C*H*$_2$), 4.89-4.77 (m, 1H, *H2*), 4.27-4.21 (m, 1H, *H5*), 3.73-3.65 (m, 4H, OC*H*$_3$, *H6*), 2.85-2.71 (m, 1H, *H6'*), 2.48-2.26 (m, 2H, *H3, H3'*) 1.98-1.73 (m, 2H, *H4, H4'*).

5-(R)-hydroxy-2-(R)-pipecolic acid methyl ester (23)

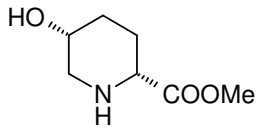

23

Deprotection of 5-(*R*)-hydroxy-N-benzyloxycarbonyl-2-(*R*)-pipecolic acid methyl ester **22** (3.24mmol, 0.95g,) using hydrogenation (Pd/C, 10%) gave 5-(*R*)-hydroxy-2-(*R*)-pipecolic acid methyl ester **23** (0.48g, 93% yield).

^{1}H NMR ($CDCl_3$) δ: 3.83-3.81 (m, 1H, *H2*), 3.74 (s, 3H, OC*H*$_3$), 3.40-3.33 (t, 1H, *H5*), 3.08-3.00 (dd, 1H, *H6*) 2.88-2.80 (dd, 1H, *H6'*), 1.90-1.83 (m, 3H, *H4*, *H4'*, *H3*), 1.74-1.61 (m, 1H, *H3'*).

1-(N-Boc-aminoethyl)-5-(R)-hydroxy-2-(R)-pipecolic acid methyl ester (24)

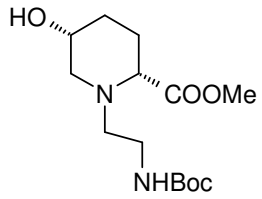

24

To a cooled solution of 5-(*R*)-hydroxy-2-(*R*)-pipecolic acid methyl ester **23** (3.02mmol, 0.48g), DMAP (0.604mmol, 0.074g) in dry DMF:Acetonitrile (1:1) (10ml) was added *N,N*-diispropyl ethylamine (7.55mmol, 1.3ml). Stirring was continued for 15min and then to this N-Boc amino mesylate (3.02mmol, 0.721g) in DMF (3ml) was added. Reaction mixture was heated to 50^{o}C for 20h. Evaporation of the solvent followed by column chromatography gave thick brown oil **24** (0.4g, 44% yield). $[\alpha]_D^{25}$ = +11.9 (c=0.42, MeOH).

^{1}H NMR ($CDCl_3$) δ: 5.34 (br s, 1H, N*H*), 3.96-3.93 (m, 1H, *H2*), 3.75 (s, 3H, OC*H*$_3$), 3.41-3.25 (m, 3H, *H5*, Boc-NH-C*H*$_2$), 3.16-3.13 (m, 1H, *H*6) 2.69-2.63 (m, 3H, *H6'*, Boc-NH-CH$_2$ -C*H*$_2$), 1.96-1.66 (m, 4H, *H3*, *H3', H4, H4'*), 1.45 (s, 9H, C(C*H*$_3$)$_3$).

^{13}C NMR ($CDCl_3$) δ: 173.47(*CO*OCH$_3$), 156.26 (*C*OOC(CH$_3$)$_3$), 79.13 (*C*(CH$_3$)$_3$), 65.67 (*C*$_5$), 64.90 (O*C*H$_3$), 55.69(*C*$_6$), 54.98(*C*$_4$), 51.55(*C*$_3$), 40.60 (*C*$_2$), 37.70(*C*H$_2$-*C*H$_2$-NH-Boc), and 28.43 ((*C*H$_3$)$_3$).

MS: (ESI) 302 $(M)^+$

1-(N-Boc-aminoethyl)-5-(S)-(N3-benzoylthymin-1-yl)-2-(R)-pipecolic acid methyl ester (25)

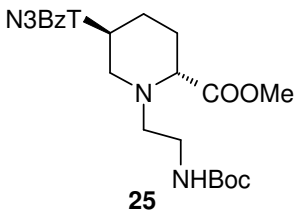

25

To a stirred solution of 1-(*N*-Boc-aminoethyl)-5-(*R*)-hydroxy-2-(*R*)-pipecolic acid methyl ester **24** (0.40g, 1.32mmol), N3-benzoylthymine (0.61g, 2.64mmol) and triphenyl phosphine (0.69g, 2.64 mmol) in dry THF (5ml) at room temperature, was added dropwise diethylazodicarboxylate (DEAD, 0.34ml, 2.64mmol). After completion of the reaction as indicated by TLC (24h), the solvent was removed *in vacuo* and residue purified by silica gel column chromatography to get the pure product **25** (0.22g, 32% yield). $[\alpha]_D^{25}$ = -12.0 (c=0.25, MeOH).

^{1}H NMR ($CDCl_3$) δ: 7.90-7.89 (m, 2H, *T-H*6, Bz, *p*-C*H*), 7.68-7.45 (m, 4H, Bz, *o*-C*H, m*-C*H*) 5.24 (br s, N*H*), 3.75(s, 1H, *H2*), 3.72 (s, 3H, OCH_3), 3.46-3.22 (m, 3H, Boc-NH-CH_2, *H5*), 3.00-2.68 (m, 3H, Boc-NH-CH_2-CH_2, *H6*) 2.16-2.00 (m, 1H, *H6'*), 2.00 (s, 3H, T-CH_3), 1.96-1.67 (m, 4H, *H4*, *H4'*, *H3*, *H3'*), 1.43 (s, 9H, C(CH_3)$_3$).

^{13}C NMR ($CDCl_3$) δ: 175.55 (*C*OOCH_3), 169.36 (*C*OOC$(CH_3)_3$), 163.50 (*T-C*2), 156.27 (Ph-*C*O), 150.57 (*T-C*4), 142.84 (*T-C*6), 135.13, 131.91, 130.62, 129.39 (Ar), 109.76 (*T-C*5), 79.82 (*C*$(CH_3)_3$), 66.87 (*C5*), 64.97 (*C6*), 56.26 (Boc-NH-*C*H_2), 52.50 (C2), 51.51 (O*C*H_3), 39.99 (Boc-NH-CH_2-*C*H_2), 29.67 (*C4*), 28.66 (C(*C*H_3)$_3$), 28.02 (*C3*), 12.53 (T-*C*H_3).

MS: (ESI) 514 $(M)^+$

1-(N-Boc-aminoethyl)-5-(S)-(thymin-1-yl)-2-(R)-pipecolic acid (26)

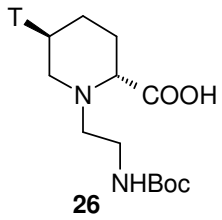

26

To a solution of 1-(*N*-Boc-aminoethyl)-5(*S*)-(N3-benzoylthymin-1-yl)-2(*R*)-pipecolic acid methyl ester **25** (0.22g, 0.43mmol) in methanol (2ml), was added aqueous 2M NaOH (2ml). TLC analysis after 10min. indicated the absence of the starting material as a result of hydrolysis of the methyl ester function. The reaction mixture was further stirred overnight, when TLC indicated the presence of a lower moving spot. The excess NaOH was neutralized by Dowex-50 H^+ resin, which was then, filtered off. The methanol from the filtrate was removed under vacuum and the residue was taken up in water. This was washed with ethyl acetate before concentrating it to dryness to obtain the product **26** (0.12g, quantitative yield) as white solid foam.

^{1}H NMR (D_2O) δ: 7.55 (1H, *T-H*6) 4.55-4.48 (m, 1H, *H2*), 4.26-3.94 (m, 3H, Boc-NH-C*H*2, *H5*) 3.54-3.42 (m, 4H, Boc-NH-CH2-C*H*2, *H6*, *H6'*), 2.50-2.32(m, 3H, *H4*, *H4'*, *H3*), 1.81-1.72 (m, 1H, *H3'),* 1.96 (s, 3H, T-CH_3), 1.51 (s, 9H, C(CH_3)$_3$).

MS: (ESI) 396 $(M)^+$

N3-benzoylthmine[35] (2)

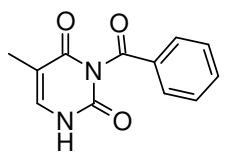

2

To a stirred solution of thymine (5.0g, 40mmol) in dry acetonitrile (40ml) and dry pyridine (10ml) in an ice-bath, benzoyl chloride (11.2ml, 96mmol), was added dropwise. Stirring was continued at room temperature overnight, when dibenzoyl thymine (**1**) was found to be present. This was converted to the monobenzoyl derivative **2** by treating with 0.25M K_2CO_3 in dioxane: water, 1:1 (75ml) and monitored by TLC. The

dioxane was removed under vacuum. The solid obtained was filtered and washed with water. The pure product **2** was obtained upon desiccation.

N^4-benzyloxycarbonylcytosine[36] (3)

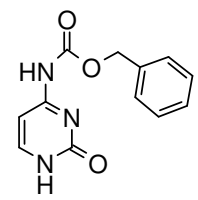

3

Cytosine (1.0g, 9.0mmol) was suspended in dry pyridine (100ml) at 0°C. CBz-Cl (3.2ml, 22.5mmol) was added and the reaction was stirred under nitrogen overnight. The pyridine suspension was evaporated to dryness. Water (10ml) and dilute HCl was added to bring the pH to 4.0. The resulting white precipitate was filtered off, washed with water and partially dried under vacuum. The wet precipitate was boiled in absolute ethanol (10ml), cooled to 0°C, filtered, washed thoroughly with ether and dried under vacuum (1.1g, 50% yield).

N1-(Boc)-1,2-diaminoethane (28)

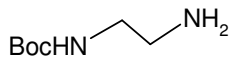

28

1,2-diaminoethane **27** (20g, 0.33mol) was taken in dioxane: water (1:1, 500ml) and cooled in an ice-bath. Boc-azide (5g, 35mmol) in dioxane (50ml) was slowly added with stirring and the pH was maintained at 10.0 by continuous addition of 4M NaOH. The mixture was stirred for 8h and the resulting solution was concentrated to 100ml. The *N*1, *N*2-di-Boc derivative not being soluble in water, precipitated, and it was removed by filtration. The corresponding *N*1-mono-Boc derivative was obtained by repeated extraction from the filtrate in ethyl acetate. Removal of solvents yielded the mono-Boc-diaminoethane **28** (3.45g, 63% yield).

^{1}H NMR ($CDCl_3$) δ: 5.21 (br s, 1H, N*H*), 3.32 (t, 2H, J=8 Hz), 2.54 (t, 2H, J=8 Hz), 1.42 (s, 9H, C(C*H*$_3$)$_3$).

Ethyl N-(2-Boc-aminoethyl)-glycinate (29)

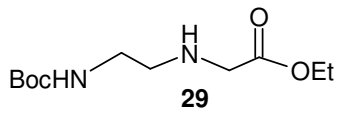

29

The *N1*-(Boc)-1,2-diaminoethane **28** (3.2g, 20mmol) was treated with ethylbromoacetate (2.25ml, 20mmol) in acetonitrile (100ml) in the presence of K_2CO_3 (2.4g, 20mmol) and the mixture was stirred at ambient temperature for 5h. The solid that separated was removed by filtration and the filtrate was evaporated to obtain the ethyl *N*-(2-Boc-aminoethyl)-glycinate **29** (4.3g, 83% yield) as a colourless oil.

^{1}H NMR ($CDCl_3$) δ: 5.02 (br s, 1H, N*H*), 4.24-4.20 (q, 2H, J=8Hz), 3.35 (s, 2H), 3.24-3.20 (t, 2H, J=6Hz), 2.80-2.76 (t, 2H, J=6Hz), 1.46 (s, 9H, C(C*H*$_3$)$_3$), 1.34-1.28 (t, 3H, J=8Hz).

Ethyl N-(Boc-aminoethyl)-N-(chloroacetyl)-glycinate (30)

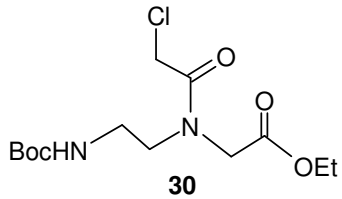

30

The ethyl *N*-(2-Boc-aminoethyl)-glycinate **29** (4.0g, 14mmol) was taken in 10% aqueous Na_2CO_3 (75ml) and dioxane (60ml). Chloroacetyl chloride (6.5ml, 0.75mmol) was added in two portions with vigorous stirring. The reaction was complete within 5 min. The reaction mixture was brought to pH 8.0 by addition of 10% aqueous Na_2CO_3 and concentrated to remove the dioxane. The product was extracted from the aqueous layer with dichloromethane and was purified by column chromatography to obtain the ethyl *N*-(Boc-aminoethyl)-*N*-(chloroacetyl)-glycinate **30** as a colourless oil in good yield (4.2g, 80% yield).

^{1}H NMR ($CDCl_3$) δ: 5.48 (br s, 1H), 4.25-4.14 (m, 2H), 4.03 (s, 2H), 3.54 (t, 2H), 3.33-3.28 (q, 2H), 1.45 (s, 9H, C(C*H*$_3$)$_3$), 1.34-1.26 (t, 3H, J=8Hz).

N-(Boc-aminoethylglycyl)-thymine ethyl ester (31)

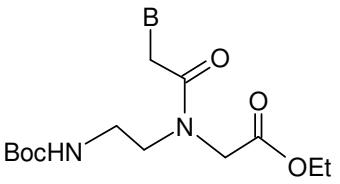

31 B = T
32 B = C^{CBz}
33 B = A
34 B = 2-amino-6-chloropurine

Ethyl *N*-(Boc-aminoethyl)-*N*-(chloroacetyl)-glycinate **30** (4.0g, 11.6mmol) was stirred with anhydrous K_2CO_3 (1.56g, 11.8mmol) in DMF with thymine (1.4g, 11.2mmol) to obtain the desired compound **31** in good yield. DMF was removed under reduced pressure and the oil obtained was purified by column chromatography.

^{1}H NMR ($CDCl_3$) δ: 8.75 (br s, 1H, *T*-N*H*), 7.97 (maj) (s, 1H, *T*-*H*6), 5.66 (maj) & 5.09 (min) (br s, 1H, N*H*), 4.55 (maj) & 4.40 (min) (s, 1H, *T*-C*H*$_2$), 4.20 (m, 2H, OC*H*$_2$), 3.48 (m, 2H), 3.28 (m, 2H), 1.85 (s, 3H, *T*-C*H*$_3$), 1.39 (s, 9H), 1.23 (m, 3H).

^{13}C NMR ($CDCl_3$) δ: 170.8, 169.3, 167.4, 164.3, 156.2, 151.2, 141.1, 110.2, 79.3, 61.8, 61.2, 48.5, 48.1, 47.7, 38.4, 28.1, 13.8, 12.2.

N-(Boc-aminoethylglycyl)-(N^4-benzyloxycarbonyl cytosine)ethyl ester (32)

A mixture of NaH (0.25g, 6.2mmol) and N^4-benzyloxycarbonyl cytosine **3** (1.24g, 6.2mmol) was taken in DMF and stirred at 75^{o}C till the effervescence ceased. The mixture was cooled and ethyl *N*-(Boc-aminoethyl)-*N*-(chloroacetyl)-glycinate **30** (2.0g, 6.2mmol) was added. Stirring was then continued at 75^{o}C to obtain the cytosine monomer, *N*-(Boc-aminoethylglycyl)-(N^4-benzyloxycarbonyl cytosine)ethyl ester **32**, in moderate yield (1.62g, 50% yield).

^{1}H NMR ($CDCl_3$) δ: 7.63 (d, 1H, *C-H6*, J=8Hz), 7.32 (s, 5H, Ar), 7.22 (d, 1H, *C-H*5, J=8Hz), 5.68 (br s, 1H, N*H*), 5.20 (s, 2H, Ar-CH_2), 4.69 (maj) & 4.22 (min) (br s, 2H), 4.12 (q, 2H), 4.01 (s, 2H), 3.49 (m, 2H), 3.29 (m, 2H), 1.44 (s, 9H, C(CH_3)$_3$), 1.23 (t, 3H).

N-(Boc-aminoethylglycyl)-adenine ethyl ester (33)

NaH (0.25g, 6.1mmol) was taken in DMF (15ml) and adenine (0.8g, 6.1mmol) was added. The mixture was stirred at 75^{o}C till the effervescence ceased and the mixture was cooled before adding ethyl *N*-(Boc-aminoethyl)-*N*-(chloroacetyl)-glycinate **30** (2.0g, 6.1mmol). The reaction mixture was heated once again to 75^{o}C for 1h, when TLC analysis indicated the disappearance of the starting ethyl *N*-(Boc-aminoethyl)-*N*-(chloroacetyl)-glycinate. The DMF was removed under vacuum and the resulting thick oil was taken in water and the product, extracted in ethyl acetate. The organic layer was then concentrated to obtain the crude product, which was purified by column chromatography to obtain the pure *N*-(Boc-aminoethylglycyl)-adenine ethyl ester **33**.

^{1}H NMR ($CDCl_3$) δ: 8.34 (s, 1H), 7.97 (min) & 7.93 (maj) (s, 1H), 5.82 (maj) & 5.75 (min) (br, 2H), 5.11 (maj) & 4.96 (min), 4.27 (min) & 4.07 (maj) (s, 2H), 4.22 (m, 2H), 3.66 (maj) & 3.56 (min) (m, 2H), 3.41 (maj) & 3.54 (min) (m, 2H), 1.42 (s, 9H, C(CH_3)$_3$), 1.27 (m, 3H).

N-(Boc-aminoethylglycyl)-2-amino-6-chloropurine ethyl ester (34)

A mixture of 2-amino-6-chloropurine (1.14g, 6.8mmol), K_2CO_3 (0.93g, 7.0mmol) and ethyl *N*-(Boc-aminoethyl)-*N*-(chloroacetyl)-glycinate **30** (2.4g,

7.0mmol) were taken in dry DMF (20ml) and stirred at room temperature for 4h. K_2CO_3 was removed by filtration, and the DMF, by evaporation under reduced pressure. The resulting residue was purified by column chromatography to obtain the *N*-(Boc-aminoethylglycyl)-2-amino-6-chloropurine ethyl ester (**34**) in excellent yield (2.65g, 98% yield).

^{1}H NMR ($CDCl_3$) δ: 7.86 (min) & 7.82 (maj) (s, 1H), 7.30 (s, 1H), 5.76 (br s, 1H, N*H*), 5.18 (br, 2H), 4.96 (maj) & 4.81 (min) (s, 2H), 4.17 (min) & 4.02 (maj) (s, 2H), 3.58 (maj) & 3.48 (min) (m, 2H), 3.36 (maj) and 3.26 (min) (m, 2H), 1.38 (s, 9H, $C(CH_3)_3$), 1.22 (m, 3H).

Hydrolysis of the PNA ethyl ester monomers

General method

The ethyl esters were hydrolyzed using 2N aqueous NaOH (5ml) in methanol (5ml) and the resulting acid was neutralized with activated Dowex-H^+ till the pH of the solution was 7.0. The resin was removed by filtration and the filtrate was concentrated to obtain the resulting Boc-protected acid (**35** - **38**) in excellent yield (>85%).

Picric Acid Estimation of Resin Functionalization

The typical procedure for estimation of the loading value of the resin was carried out with 5mg of the resin and comprised the following steps:

The resin was swollen in dry CH_2Cl_2 for at least 30min. The CH_2Cl_2 was drained off and a 50% solution of TFA in CH_2Cl_2 was added (1ml x 2), 15min each. After washing thoroughly with CH_2Cl_2, The TFA salt was neutralized with a 5% solution of DIPEA in CH_2Cl_2 (1ml x 3, 2min each). The free amine was treated with a

0.1M picric acid solution in CH_2Cl_2 (2ml x 2, 3min each). The excess picric acid was eliminated by extensively washing the resin with CH_2Cl_2. The adsorbed picric acid was displaced form the resin by adding a solution of 5% DIPEA in CH_2Cl_2. The eluant was collected and the volume was made up to 10ml with CH_2Cl_2 in a volumetric flask. The absorbance was recorded at 358nm in ethanol and the concentration of the amine groups on the resin was calculated using the molar extinction coefficient of picric acid as 14,500$cm^{-1}M^{-1}$ at 358nm.

Kaiser's Test

Kaiser's test was used to monitor the Boc-deprotection and amide coupling steps in the solid phase peptide synthesis. Three solutions were used, viz. (1) ninhydrin (5.0g) dissolved in ethanol (100ml), (2) phenol (80g dissolved in ethanol (20ml) and (3) KCN: 2ml of a 0.001M aqueous solution of KCN in 98ml pyridine).

To a few beads of the resin to be tested taken in a test tube, were added 3-4 drops of each of the three solutions desribed above. The tube was heated at 100^oC for ~5min, and the colour of the beads was noted. A blue colour on the beads and in the solution indicated successful deprotection, while colourless beads were observed upon completion of the amide coupling reaction. The blank solution should remain yellow.

Cleavage of the PNA oligomers from the solid support

A typical cleavage reaction was carried out with 5 or 10mg of resin-bound PNA oligomer. The resin-bound PNA oligomer (10mg) was stirred in an ice-bath with thioanisole (20µl) and 1,2-ethanedithiol (8µl) for 10min, TFA (120µl) was added and stirring was continued for another 10min. TFMSA (16µl) was added and stirring continued for 2h. The reaction mixture was filtered through a sintered funnel. The residue was washed with TFA (3 x 2ml) and the combined filtrate and washings were

evaporated under vacuum and co-evaporated with ether, avoiding heating during this process. The residue was precipitated using dry ether and centrifuged to obtain a white pellet. The pellet was re-dissolved in methanol (~0.1ml) and re-precipitated by adding ether. The pellet collected after centrifugation was subjected to this re-precipitation process at least thrice, when a white precipitate was obtained of the crude PNA oligomer.

Gel Filtration

The crude PNA oligomer obtained after ether precipitation was dissolved in water (~0.5ml) and loaded on a gel filtration column. This column consisted of G25 Sephadex and had a void volume of 0.5/1ml. The oligomer was eluted with water and six fractions of 0.5/1ml volume each were collected. The presence of the PNA oligomer was detected by measuring the absorbance at 260nm. The fractions containing the oligomer were freeze-dried. The purity of the cleaved crude PNA oligomer was determined by RP HPLC on a C18 column. If found to be above 90%, the oligomers were sued as such for experiments without further purification. If the purity was not satisfactory, the oligomers were purified by HPLC/FPLC.

FPLC

The crude PNA oligomers were dissolved in water containing 0.1% TFA, the starting buffer for injection. The polypyrimidine T_8 sequences were purified using a gradient of 0 to 60% buffer B in 40min at a flow rate of 1.0ml/min, where buffer A = water with 0.1% TFA and buffer B = 60% CH_3CN in water containing 0.1% TFA. The mixed sequence PNAs eluted earlier and hence had to be purified using a gradient of 0 to 30% B in 30min at a flow rate of 1.0ml/min, when good resolution of the

peaks was obtained. The purity of the oligomer after FPLC was ascertained by HPLC on a C18 RP column.

HPLC

The purity of the PNA oligomers was ascertained on an analytical RP C18 column using a gradient of 5 to 50% CH_3CN in water containing 0.1% TFA at a flow rate of 1.5ml/min.

MALDI-TOF Mass Spectrometry

Literature reports the analysis of PNA purity by MALDI-TOF mass spectrometry[52] in which several matrices have been explored, *viz*. sinapinic acid (3,5-dimethoxy-4-hydroxycinnamic acid), CHCA (α-cyano-4-hydroxycinnamic acid) and DHB (2,5-dihydroxybenzoic acid). Of these, sinapinic acid was found to give the best signal to noise ratio with all the other matrices typically producing higher molecular ion signals.

For all the MALDI-TOF spectra recorded for the *aepip*PNAs reported in this Chapter, sinapinic acid was used as the matrix and was found to give satisfactory results.

2.8.1. UV studies

All the UV spectrophotometric studies were performed either on a Perkin Elmer λ15 UV-VIS spectrophotometer equipped with a Julabo temperature programmer and a Julabo water circulator or Perkin Elmer λ35 UV-VIS spectrophotometer with peltier to maintain the temperature. The samples were degassed by purging nitrogen or argon gas through the solution for 2-3min prior to the start of the experiments. Nitrogen gas was purged through the cuvette chamber below 15^{o}C to prevent the condensation of moisture on the cuvette walls.

2.8.2. UV-titration

To a solution of DNA **53** in 0.01M sodium phosphate at pH 7.4, were added fixed portions of the complementary PNA oligomer **40**. The temperature of the circulating water was maintained at 10^{o}C (i. e., well below the melting temperature of the complexes) and the absorbance at each step was recorded at 260nm. This was plotted as a function of the PNA mole fraction.

2.8.3. UV-T_m

The PNA oligomers and the appropriate DNA oligomers were mixed together in stoichiometric amounts (2:1, PNA:DNA for oligothymine-T_8 PNAs or 1:1 for the duplex forming PNAs, *viz.*, the mixed base sequences) in 0.01M sodium phosphate buffer, pH 7.4 to achieve a final strand concentration of either 0.5 or 1μM each strand. For the AT-rich PNAs, antiparallel complexes were constituted by employing DNA **56** while parallel complexes were constituted using DNA **57**. The samples were heated at 85^{o}C for 5min followed by slow cooling to room temperature. They were allowed to remain at room temperature for at least half an hour and refrigerated overnight prior to running the melting experiments. Each melting experiment was repeated at least thrice. The absorbance or the percent hyperchromicity at 260nm was plotted as a function of the temperature. The Tm was determined from the peaks in the first derivative plots and is accurate to ±1^{o}C.

For the salt-dependence experiments, 50mM sodium chloride was added to the buffer before annealing the samples. In the pH-dependence experiments, the PNA:DNA complexes were constituted in 0.01M phosphate buffers of different pH values prior to annealing. In order to study the relative rates of melting and re-association, the complexes were held at 85^{o}C for 5min upon completion of the heating

process and then cooled to 5^{o}C at a rate of 0.2^{o}C/min. As for the heating process, the absorbance values were recorded every minute and plotted as a function of the temperature along with the heating profile.

Hyperchromicity observations

A useful parameter of interest is the hyperchromicity changes accompanying the melting transitions that can be measured from UV-melting curves. This data can be derived from the UV-T_m plots and suggests the hyperchromicity for PNAs containing two modified *aepip* units and homopyrimidine PNAs containing cytosine and thymine nucleobases was found to be more than other sequences. The duplexes of *aepip*PNAs having purines generally exhibited higher hyperchromicity with antiparallel DNA than with parallel DNA. Generally higher Tms were accompanied by larger % hyperchromicities though the hyperchromicity changes could not always be directly correlated with the thermal stabilities. However, in maximum cases, these were slightly higher than the control *aeg*PNAs. Since these reflect the extent of base-stacking, the observed pattern of changes suggest variable base stacking effects depending on the base type, stereochemistry and relative orientations of strands in duplexes and triplexes. The percent hyperchromicity accompanying the melting of the mismatched PNA:DNA complexes were very much lower than that accompanying the melting of the fully complementary duplexes.

2.8.4. Mismatch studies

DNA **54** was used to probe the specificity of the PNA-oligothymine-T_8 interaction with DNA. The relevant PNA and DNA strands were mixed together in a 2:1 molar ratio and subjected to UV-melting.

2.8.5. CD

CD spectra were recorded on a Jasco J-715 spectropolarimeter. The CD spectra of the PNA:DNA complexes and the relevant single strands were recorded in 0.01M sodium phosphate buffer, pH 7.4. The temperature of the circulating water was kept below the melting temperature of the PNA:DNA complexes, i. e., at 10^{o}C.

The CD spectra of the oligothymine T_8 single strands were recorded as an accumulation of 10 scans from 320 to 195nm using a 1cm cell, a resolution of 0.1nm, band-width of 1.0nm, sensitivity of 2mdeg, response 2sec and a scan speed of 100nm/min. for the PNA_2:DNA complexes, spectra were recorded as an accumulation of 10 scans, response of 1sec and a scan speed of 200nm/min.

The CD spectra of the mixed base PNAs and the derived PNA:DNA duplexes were recorded as an accumulation of 5 scans and a scan speed of 200nm/min.

2.8.6. Gel shift experiments

The PNA (**39**, **42, 45**) and DNA oligomers (**53**) utilized in the gel mobility shift assays were mixed together in the desired ratios in water. The sample was lyophilized to dryness and re-suspended in 10µl 0.01M sodium phosphate buffer, pH 7.4. The sample was annealed as described earlier by heating at 85^{o}C for 5min followed by slow cooling to room temperature and refrigeration overnight. Prior to loading, 10µl sucrose solution in Tris buffer, pH 8.3, the gel-running buffer, was added and the sample, loaded on the gel. Bromophenol blue was used as the tracer dye, but was loaded in an adjacent well and not mixed with the sample.

Gel electrophoresis was performed on a 15% non-denaturing polyacrylamide gel (acrylamide:*bis*-acrylamide, 29:1) until the BPB migrated to three-fourths of the gel length. During electrophoresis, the temperature was maintained ~10^{o}C. Bands of

the single stranded PNA/DNA and the PNA:DNA complexes were visualized as dark bands by UV-shadowing, i.e., by illuminating the gel placed on a fluorescent thin-layer silica gel chromatographic plate, F_{254}, 20cm x 20cm using UV light.

2.9. APPENDIX

- Compound **9**, ^{1}H NMR
- Compound **10**, ^{1}H NMR
- Compound **11**, ^{1}H, ^{13}C NMR, DEPT and ESI-MASS
- Compound **12**, ^{1}H, ^{13}C NMR, DEPT and ESI-MASS
- Compound **13**, ^{1}H NMR and ESI-MASS
- Compound **22**, ^{1}H NMR
- Compound **24**, ^{1}H, ^{13}C NMR, DEPT and ESI-MASS
- Compound **25**, ^{1}H, ^{13}C NMR, DEPT and ESI-MASS
- Compound **26**, ^{1}H NMR and ESI-MASS

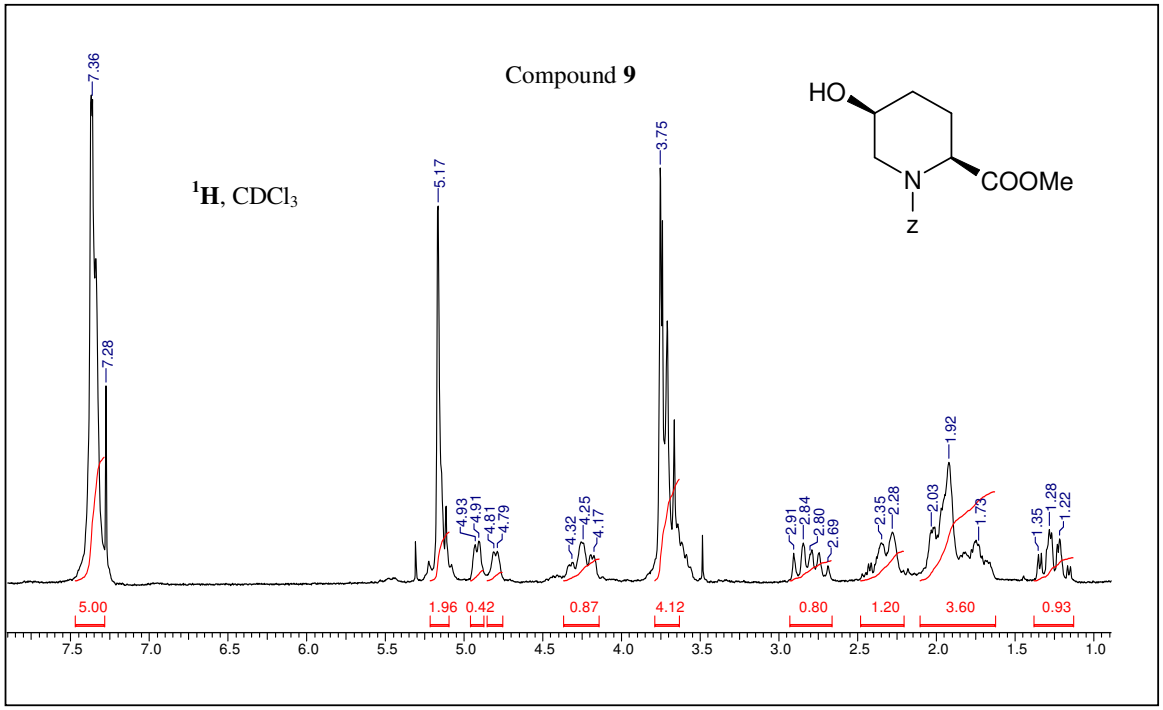
Compound **9**
^{1}**H**, $CDCl_3$
HO
N
Z
COOMe
7.36
7.28
5.17
4.93
4.91
4.81
4.79
4.32
4.25
4.17
3.75
2.91
2.84
2.80
2.69
2.35
2.28
2.03
1.92
1.73
1.35
1.28
1.22
5.00
1.96
0.42
0.87
4.12
0.80
1.20
3.60
0.93

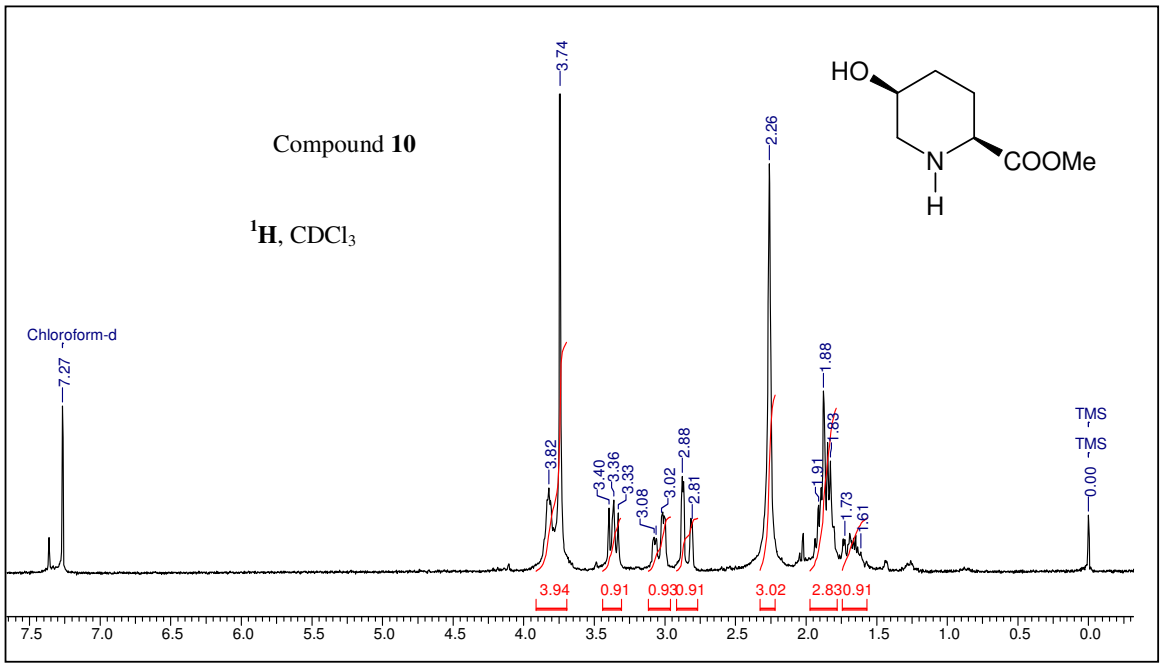
Compound **10**
^{1}**H**, $CDCl_3$
HO
N
H
COOMe
Chloroform-d
7.27
3.74
3.82
3.40
3.36
3.33
3.08
3.02
2.88
2.81
2.26
1.91
1.88
1.73
1.61
TMS
TMS
0.00
3.94
0.91
0.93
0.91
3.02
2.83
0.91

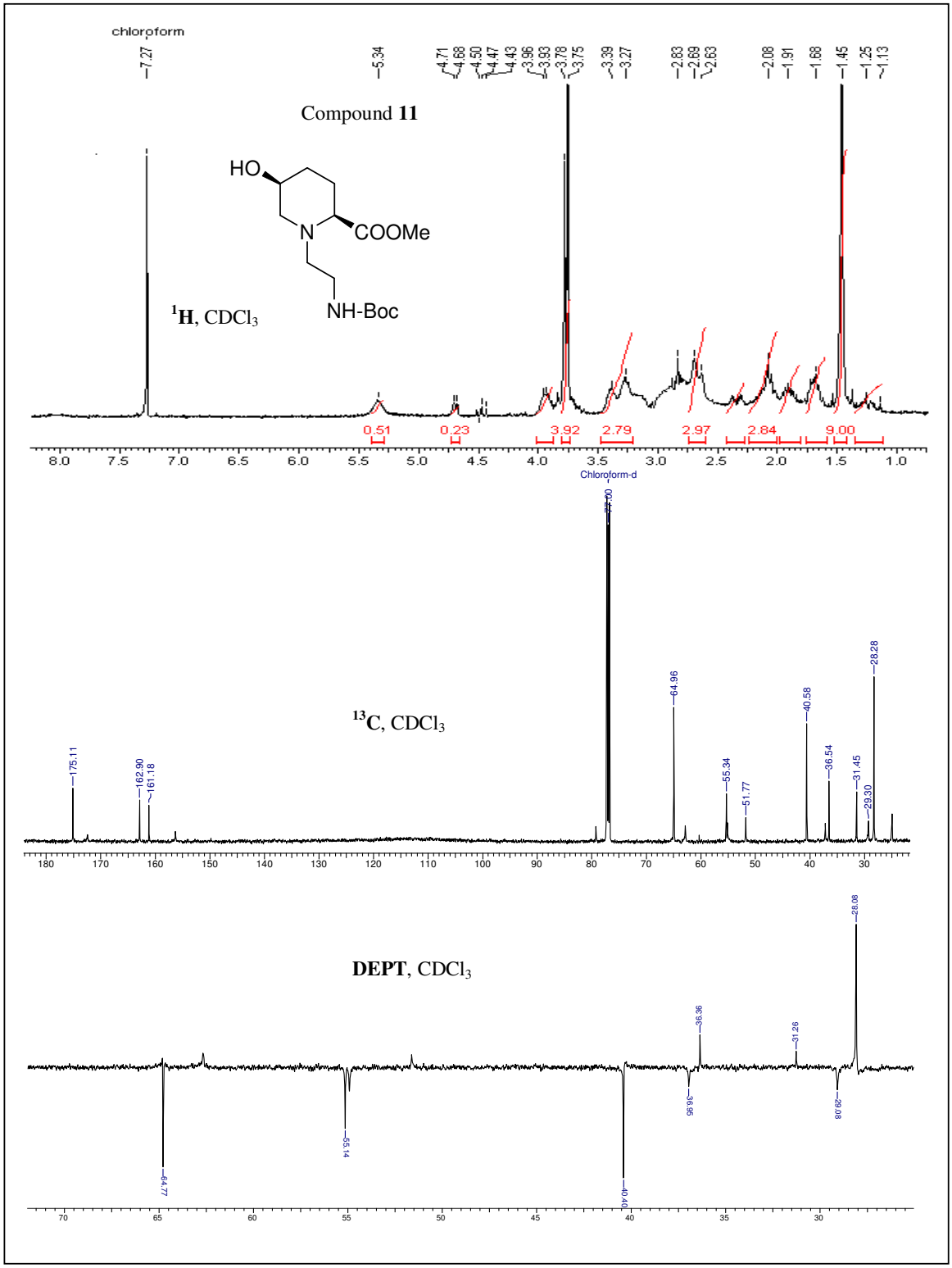
Compound **11**
HO
N
COOMe
NH-Boc
^{1}H, $CDCl_3$
chloroform
7.27
5.34
4.71
4.68
4.50
4.47
4.43
3.96
3.93
3.78
3.75
3.39
3.27
2.83
2.69
2.63
2.08
1.91
1.68
1.45
1.25
1.13
0.51
0.23
3.92
2.79
2.97
2.84
9.00
Chloroform-d
^{13}C, $CDCl_3$
175.11
162.90
161.18
77.00
64.96
55.34
51.77
40.58
36.54
31.45
29.30
28.28
DEPT, $CDCl_3$
64.77
55.14
40.40
36.36
31.26
29.08
28.08

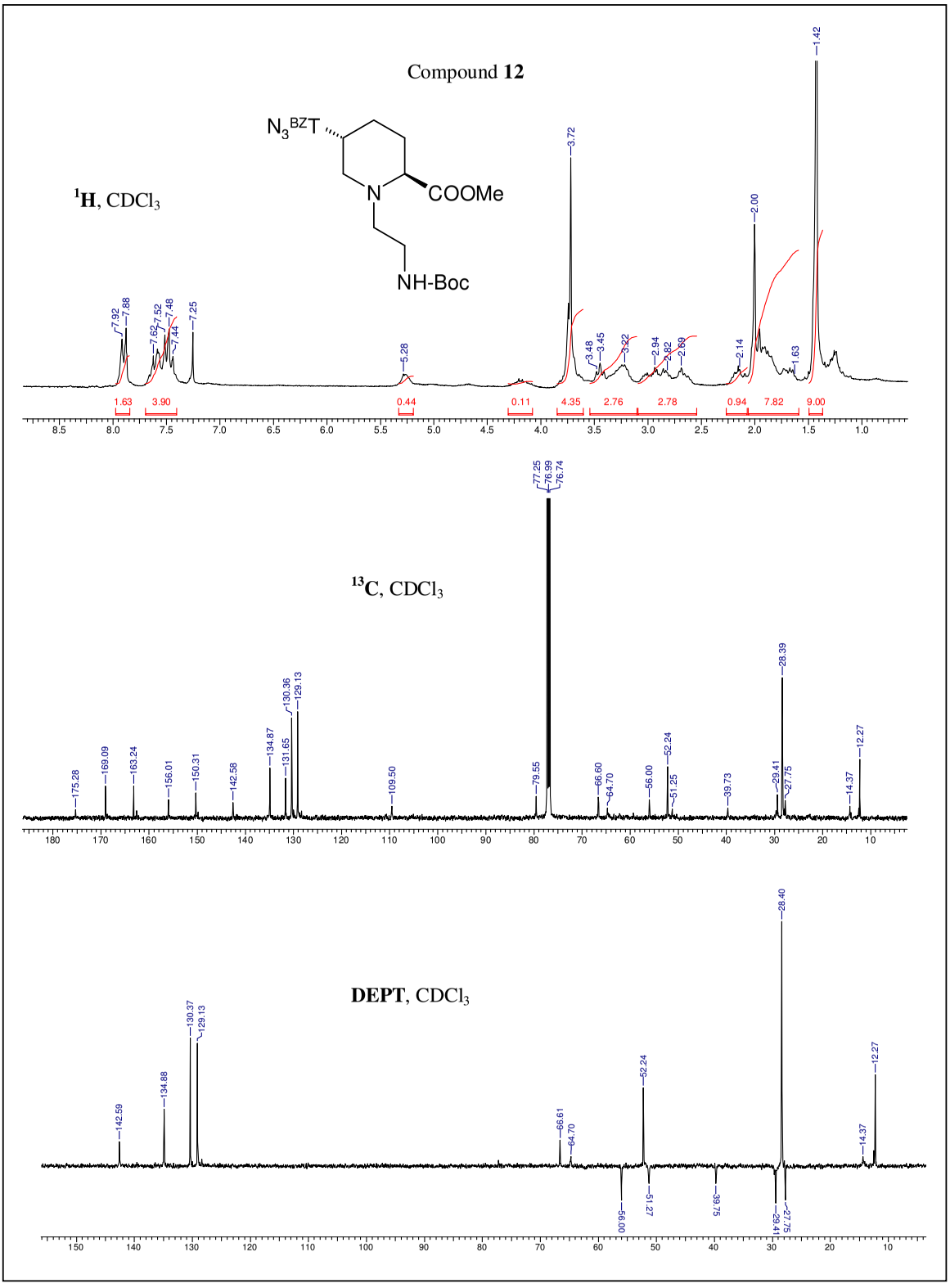
Compound **12**
N_3^{BZT}
COOMe
NH-Boc
^{1}H, $CDCl_3$
^{13}C, $CDCl_3$
DEPT, $CDCl_3$

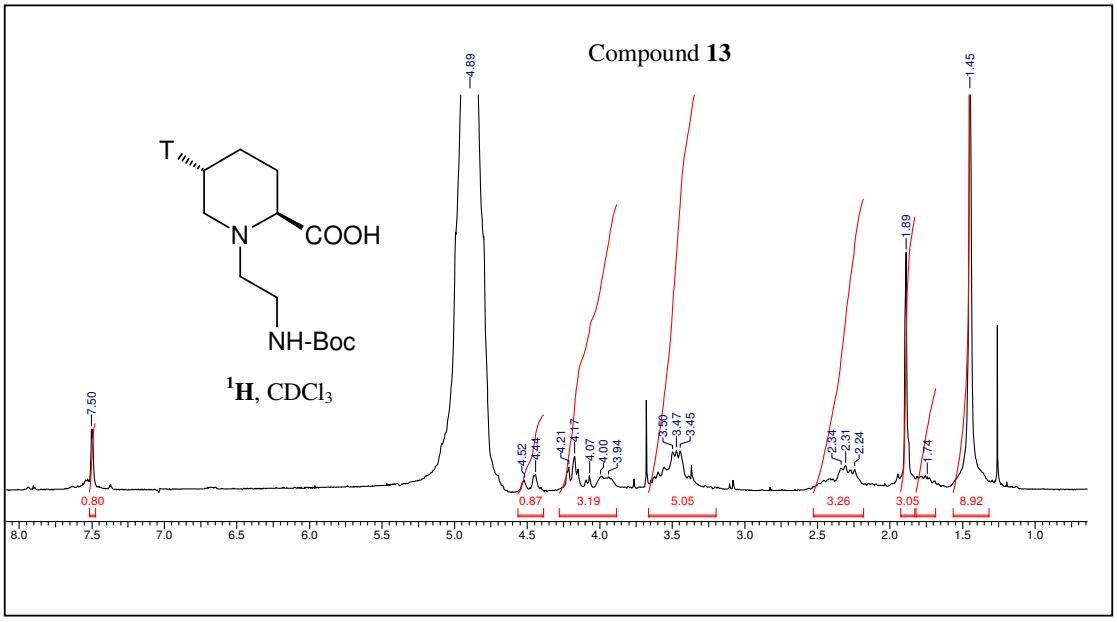
Compound **13**
T
N
COOH
NH-Boc
^{1}**H**, $CDCl_3$
7.50
4.89
4.52
4.44
4.21
4.17
4.07
4.00
3.94
3.50
3.47
3.45
2.34
2.31
2.24
1.89
1.74
1.45
0.80
0.87
3.19
5.05
3.26
3.05
8.92

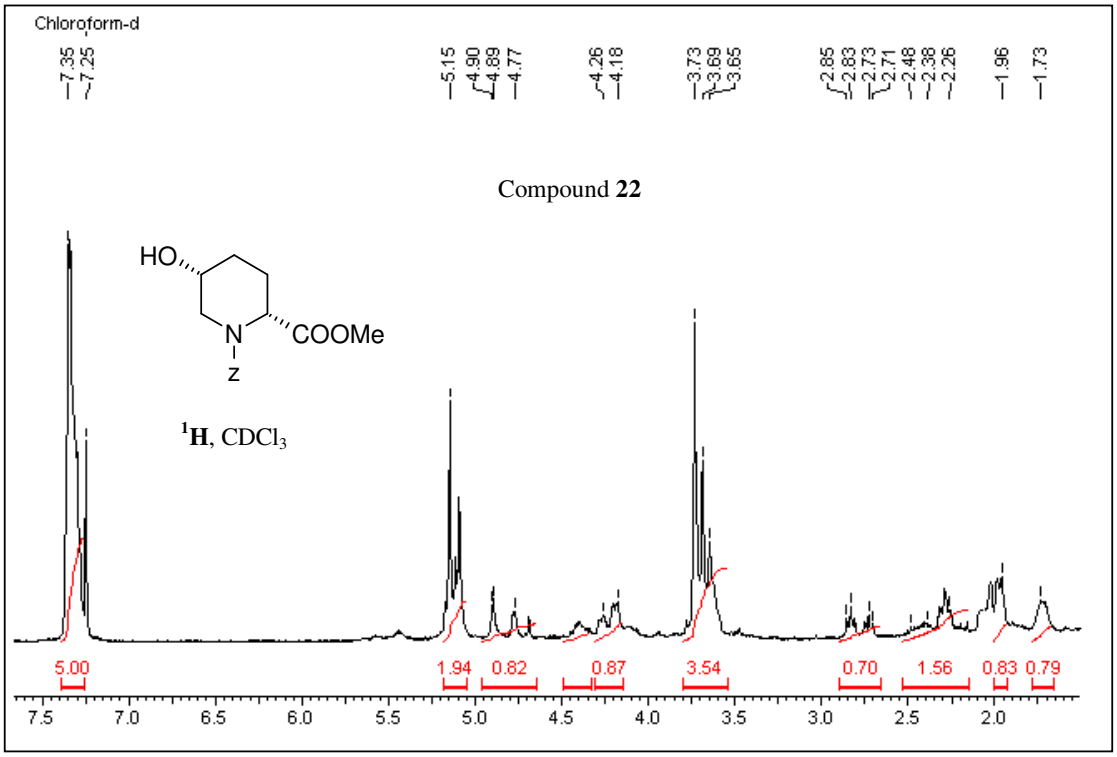
Chloroform-d
7.35
7.25
5.15
4.90
4.89
4.77
4.26
4.18
3.73
3.69
3.65
2.85
2.83
2.73
2.71
2.48
2.38
2.26
1.96
1.73
Compound **22**
HO
N
COOMe
Z
^{1}**H**, $CDCl_3$
5.00
1.94
0.82
0.87
3.54
0.70
1.56
0.83
0.79

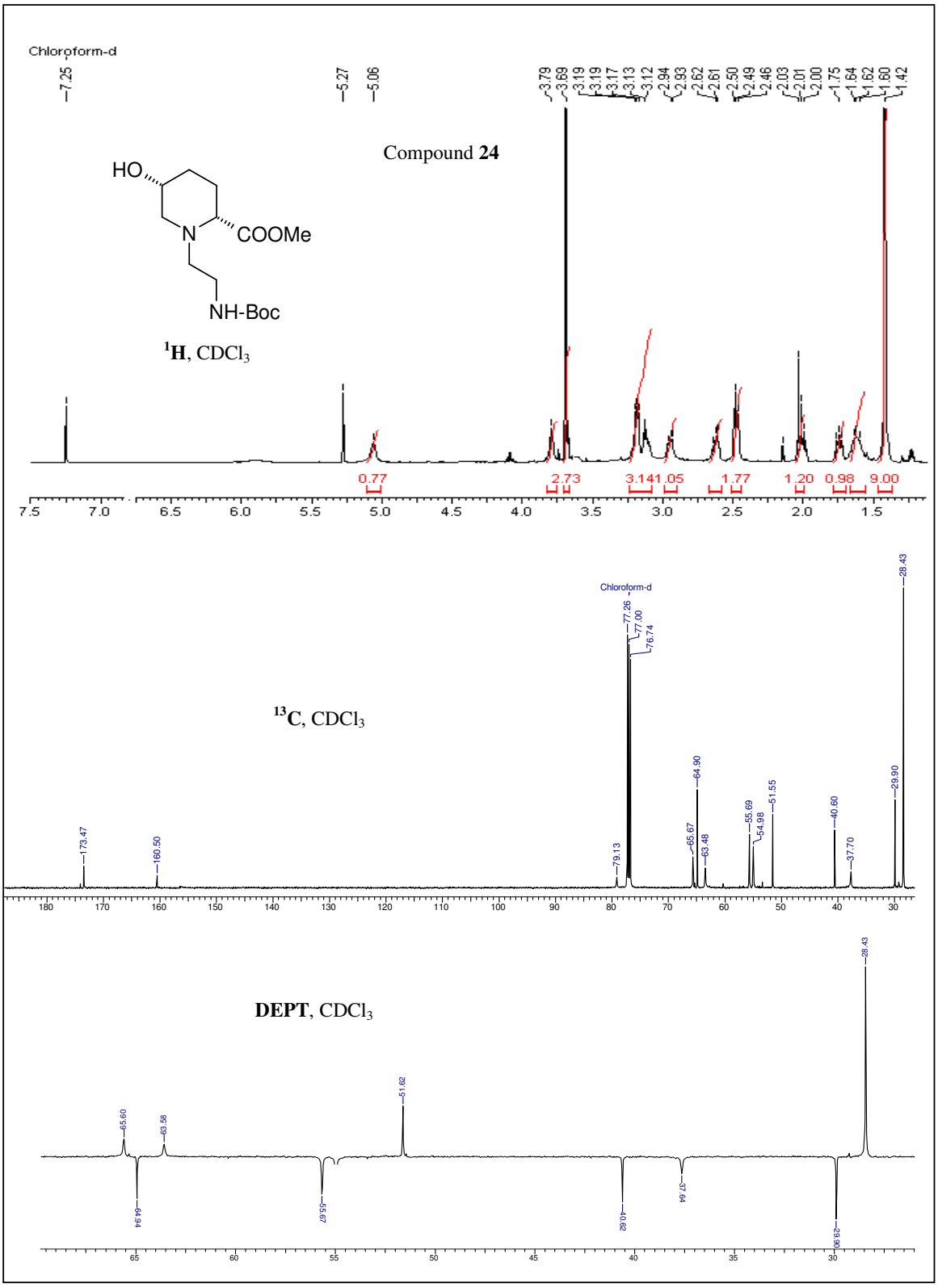
Chloroform-d
7.25
5.27
5.06
3.79
3.69
3.19
3.19
3.17
3.13
3.12
2.94
2.93
2.62
2.61
2.50
2.49
2.46
2.03
2.01
2.00
1.75
1.64
1.62
1.60
1.42
Compound 24
HO
N
COOMe
NH-Boc
1H, CDCl3
0.77
2.73
3.14
1.05
1.77
1.20
0.98
9.00
7.5
7.0
6.5
6.0
5.5
5.0
4.5
4.0
3.5
3.0
2.5
2.0
1.5
13C, CDCl3
Chloroform-d
77.26
77.00
76.74
173.47
160.50
79.13
64.90
65.67
63.48
55.69
54.98
51.55
40.60
37.70
29.90
28.43
180
170
160
150
140
130
120
110
100
90
80
70
60
50
40
30
DEPT, CDCl3
65.60
63.58
51.62
64.94
55.67
29.62
27.64
28.43
29.90
65
60
55
50
45
40
35
30

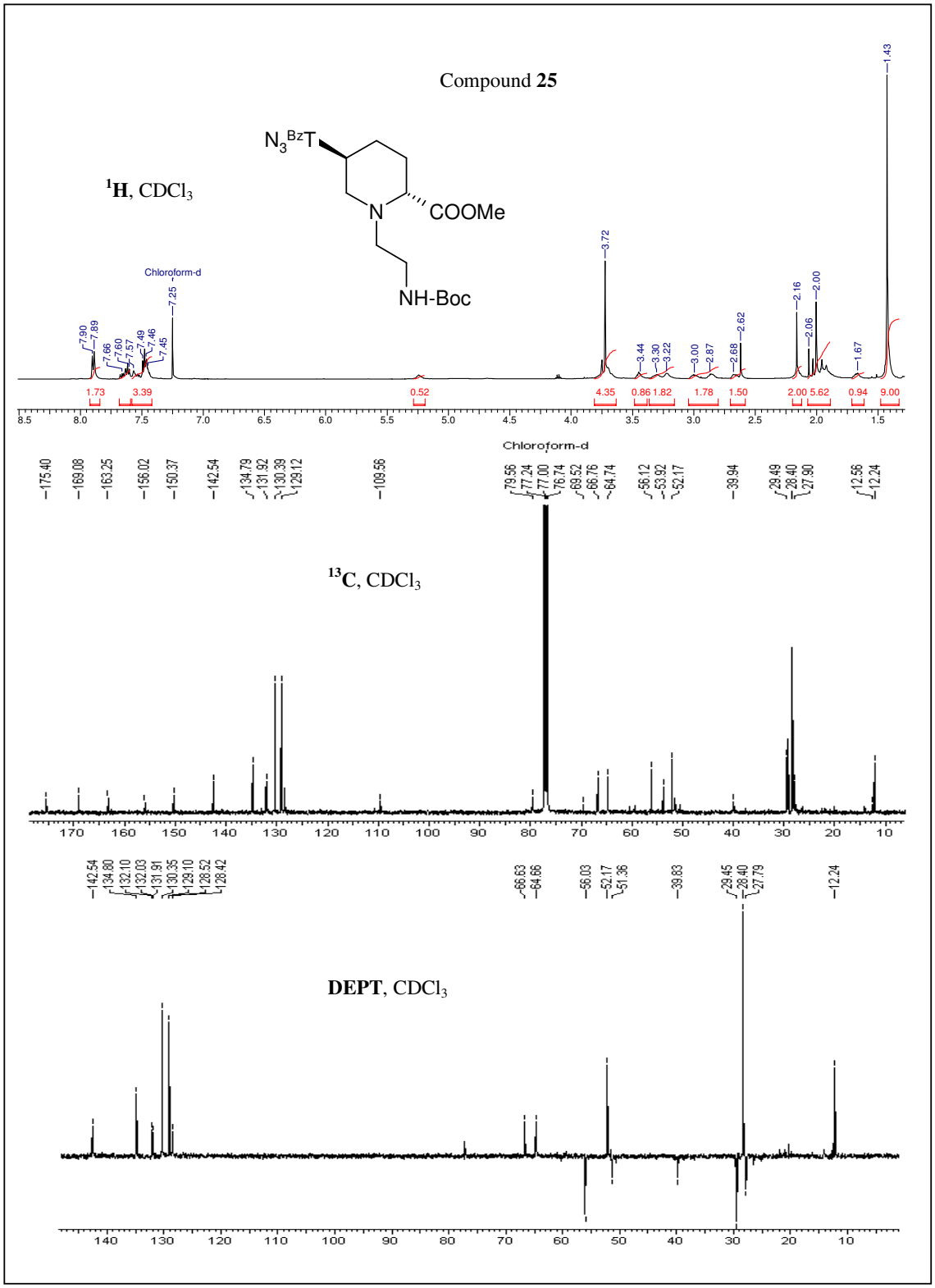
Compound **25**
$N_3^{Bz}T$
COOMe
NH-Boc
^{1}H, $CDCl_3$
Chloroform-d
7.90
7.89
7.66
7.60
7.57
7.49
7.46
7.45
7.25
3.72
3.44
3.30
3.22
3.00
2.87
2.68
2.62
2.16
2.06
2.00
1.67
1.43
1.73
3.39
0.52
4.35
0.86
1.82
1.78
1.50
2.00
5.62
0.94
9.00
^{13}C, $CDCl_3$
Chloroform-d
175.40
169.08
163.25
156.02
150.37
142.54
134.79
131.92
130.39
129.12
109.56
79.56
77.24
77.00
76.74
69.52
66.76
64.74
56.12
53.92
52.17
39.94
29.49
28.40
27.90
12.56
12.24
DEPT, $CDCl_3$
142.54
134.80
132.10
132.03
131.91
130.35
129.10
128.52
128.42
66.63
64.86
56.03
52.17
51.36
39.83
29.45
28.40
27.79
12.24

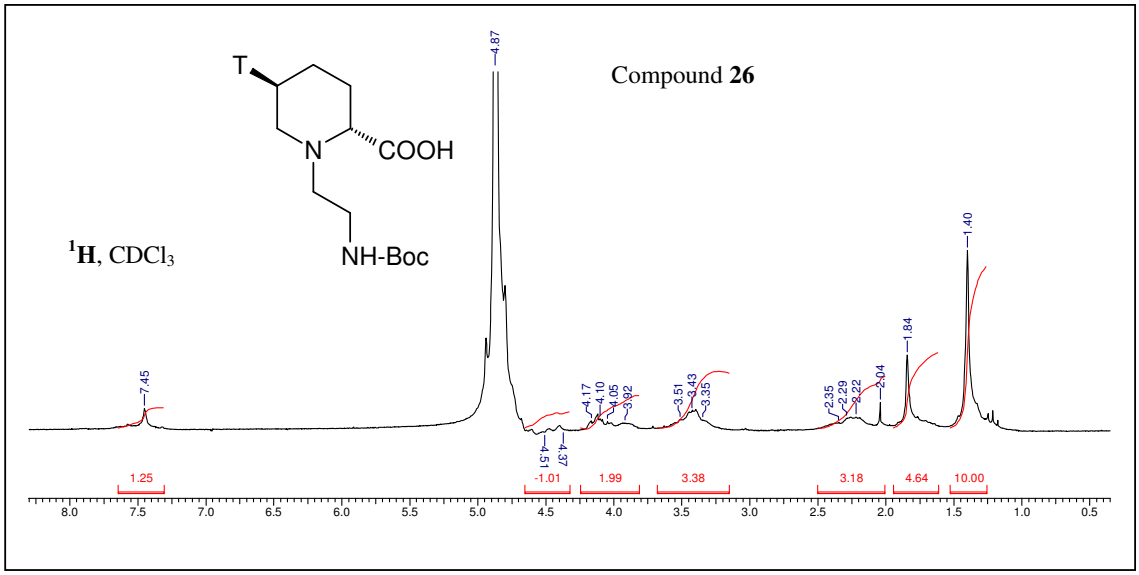
T
N
COOH
NH-Boc
Compound **26**
^{1}**H**, $CDCl_3$
4.87
7.45
4.17
4.10
4.05
3.92
3.51
3.43
3.35
2.35
2.29
2.22
2.04
1.84
1.40
4.51
4.37
1.25
1.01
1.99
3.38
3.18
4.64
10.00

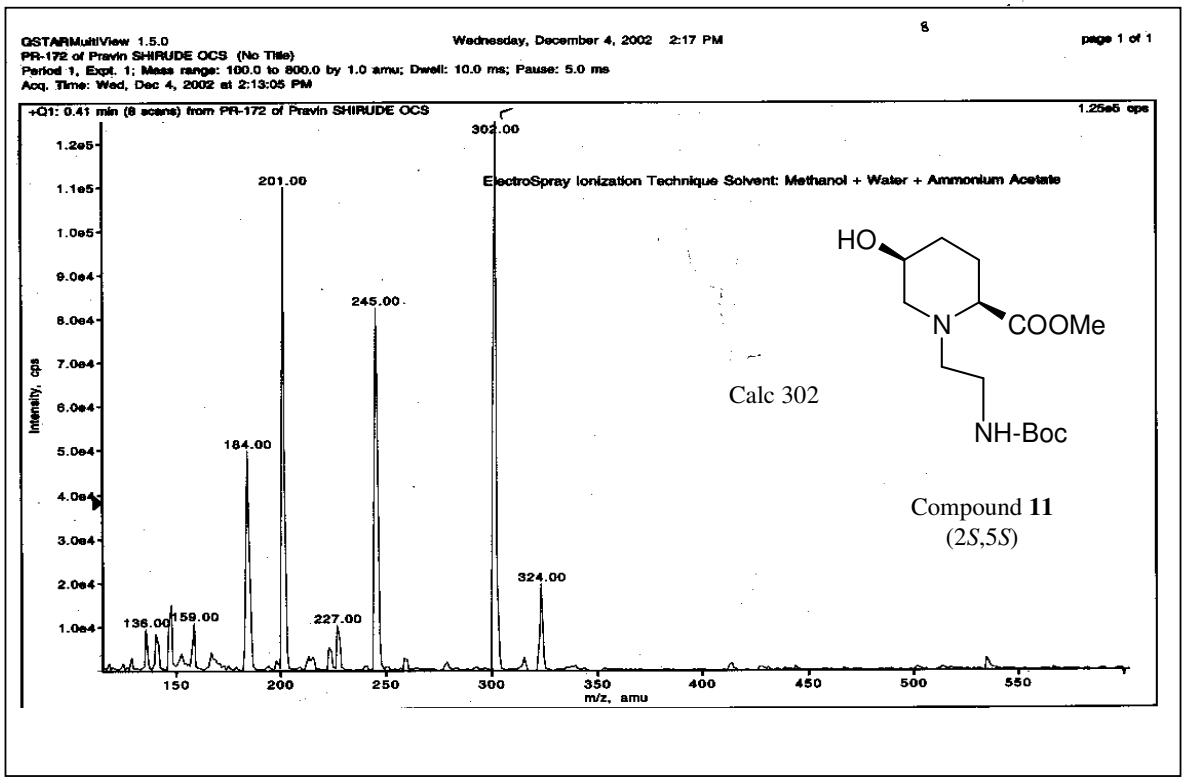
QSTARMultiView 1.5.0
Wednesday, December 4, 2002 2:17 PM
page 1 of 1
PR-172 of Pravin SHIRUDE OCS (No Title)
Period 1, Expt. 1; Mass range: 100.0 to 800.0 by 1.0 amu; Dwell: 10.0 ms; Pause: 5.0 ms
Acq. Time: Wed, Dec 4, 2002 at 2:13:05 PM
+Q1: 0.41 min (8 scans) from PR-172 of Pravin SHIRUDE OCS
1.25e5 cps
ElectroSpray Ionization Technique Solvent: Methanol + Water + Ammonium Acetate
Intensity, cps
m/z, amu
302.00
201.00
245.00
184.00
324.00
136.00
159.00
227.00
HO
N
COOMe
NH-Boc
Calc 302
Compound **11**
(2*S*,5*S*)

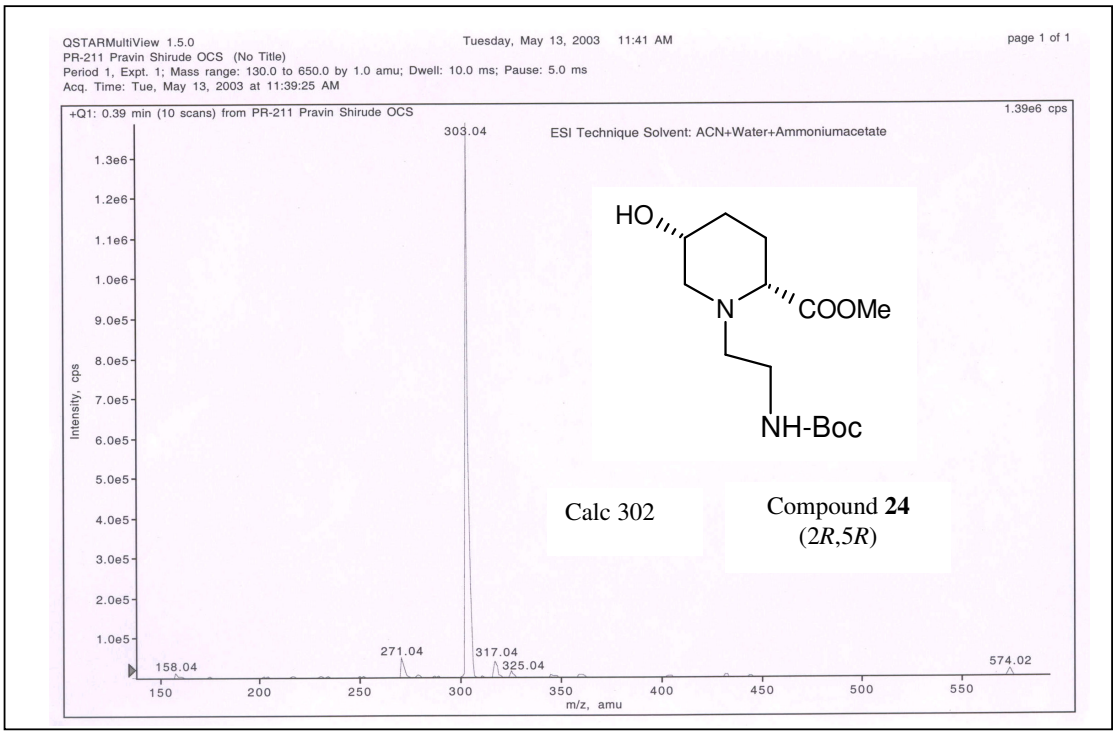
QSTARMultiView 1.5.0
Tuesday, May 13, 2003 11:41 AM
page 1 of 1
PR-211 Pravin Shirude OCS (No Title)
Period 1, Expt. 1; Mass range: 130.0 to 650.0 by 1.0 amu; Dwell: 10.0 ms; Pause: 5.0 ms
Acq. Time: Tue, May 13, 2003 at 11:39:25 AM
+Q1: 0.39 min (10 scans) from PR-211 Pravin Shirude OCS
1.39e6 cps
303.04
ESI Technique Solvent: ACN+Water+Ammoniumacetate
Intensity, cps
m/z, amu
158.04
271.04
317.04
325.04
574.02
HO
N
COOMe
NH-Boc
Calc 302
Compound 24
(2R,5R)

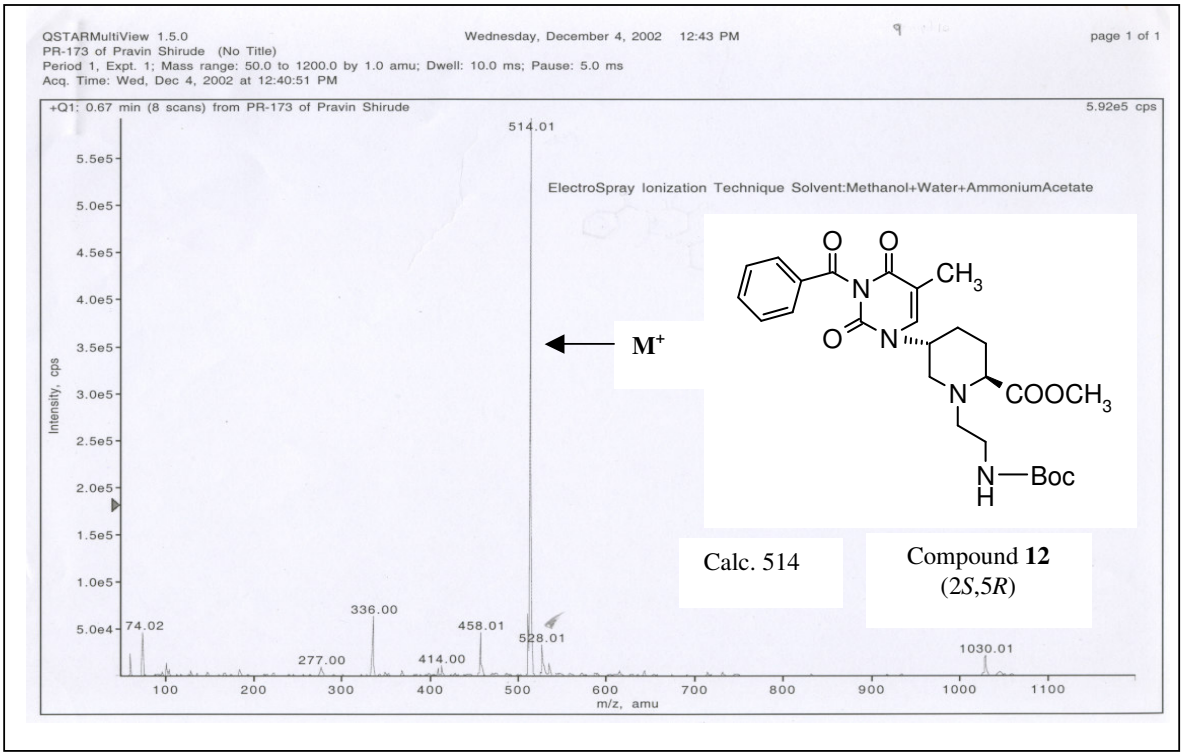
QSTARMultiView 1.5.0
Wednesday, December 4, 2002 12:43 PM
page 1 of 1
PR-173 of Pravin Shirude (No Title)
Period 1, Expt. 1; Mass range: 50.0 to 1200.0 by 1.0 amu; Dwell: 10.0 ms; Pause: 5.0 ms
Acq. Time: Wed, Dec 4, 2002 at 12:40:51 PM
+Q1: 0.67 min (8 scans) from PR-173 of Pravin Shirude
5.92e5 cps
514.01
ElectroSpray Ionization Technique Solvent:Methanol+Water+AmmoniumAcetate
M+
Intensity, cps
m/z, amu
74.02
277.00
336.00
414.00
458.01
528.01
1030.01
CH3
COOCH3
N—Boc
H
Calc. 514
Compound 12
(2S,5R)

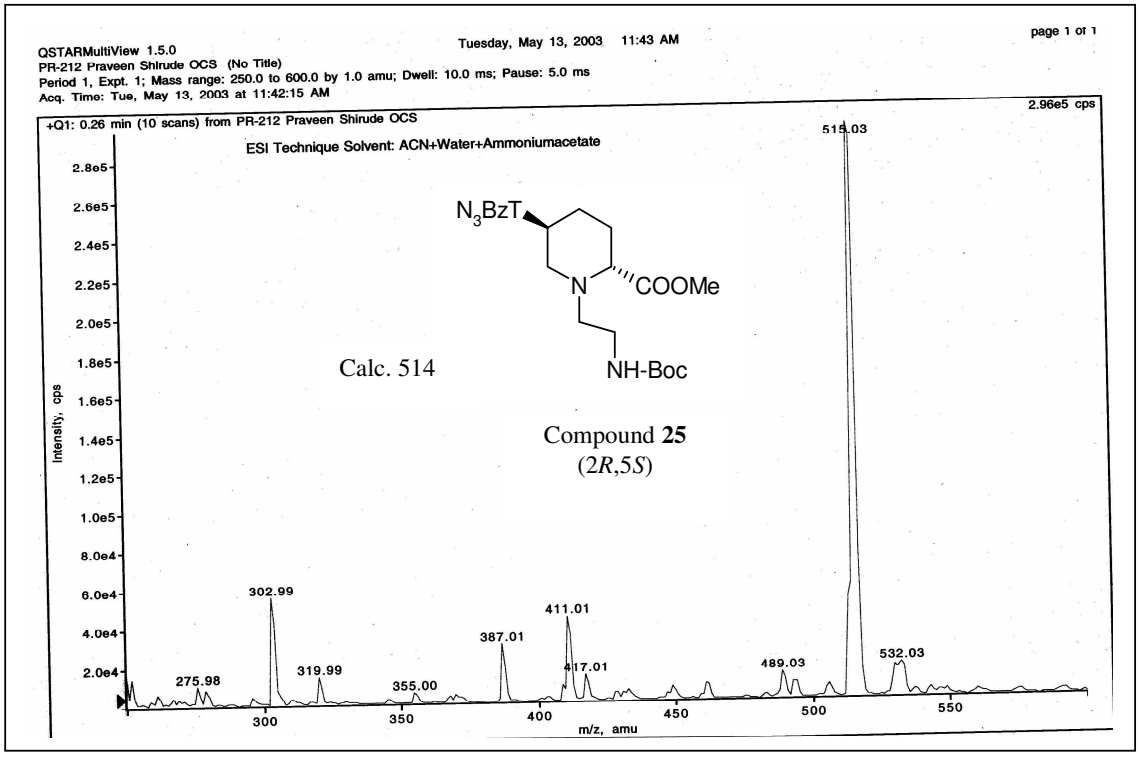
QSTARMultiView 1.5.0
PR-212 Praveen Shirude OCS (No Title)
Period 1, Expt. 1; Mass range: 250.0 to 600.0 by 1.0 amu; Dwell: 10.0 ms; Pause: 5.0 ms
Acq. Time: Tue, May 13, 2003 at 11:42:15 AM
Tuesday, May 13, 2003 11:43 AM
page 1 of 1
+Q1: 0.26 min (10 scans) from PR-212 Praveen Shirude OCS
2.96e5 cps
ESI Technique Solvent: ACN+Water+Ammoniumacetate
Intensity, cps
m/z, amu
515.03
302.99
411.01
387.01
319.99
275.98
355.00
417.01
489.03
532.03
N3BzT
COOMe
NH-Boc
Calc. 514
Compound 25
(2R,5S)

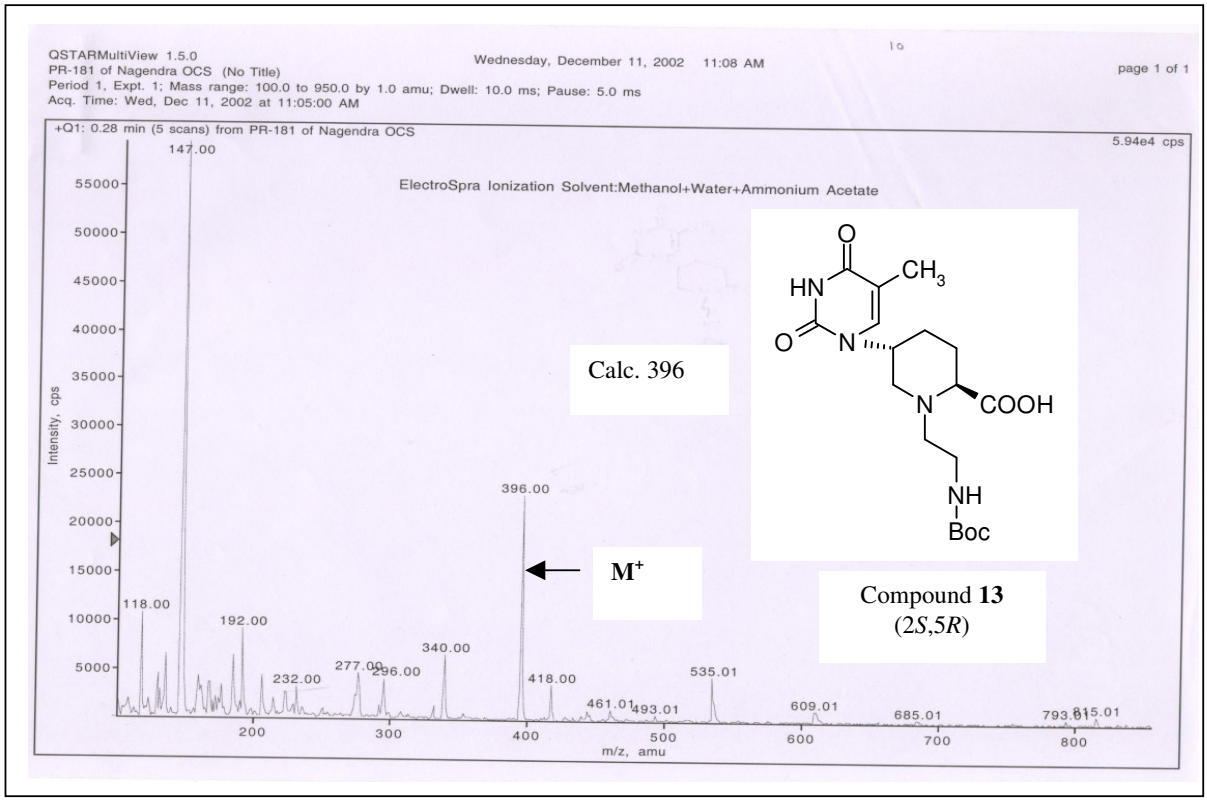
QSTARMultiView 1.5.0
PR-181 of Nagendra OCS (No Title)
Period 1, Expt. 1; Mass range: 100.0 to 950.0 by 1.0 amu; Dwell: 10.0 ms; Pause: 5.0 ms
Acq. Time: Wed, Dec 11, 2002 at 11:05:00 AM
Wednesday, December 11, 2002 11:08 AM
page 1 of 1
+Q1: 0.28 min (5 scans) from PR-181 of Nagendra OCS
5.94e4 cps
ElectroSpra Ionization Solvent:Methanol+Water+Ammonium Acetate
Intensity, cps
m/z, amu
147.00
396.00
118.00
192.00
340.00
277.00
296.00
232.00
418.00
535.01
461.01
493.01
609.01
685.01
793.61
815.01
Calc. 396
M+
Compound 13
(2S,5R)

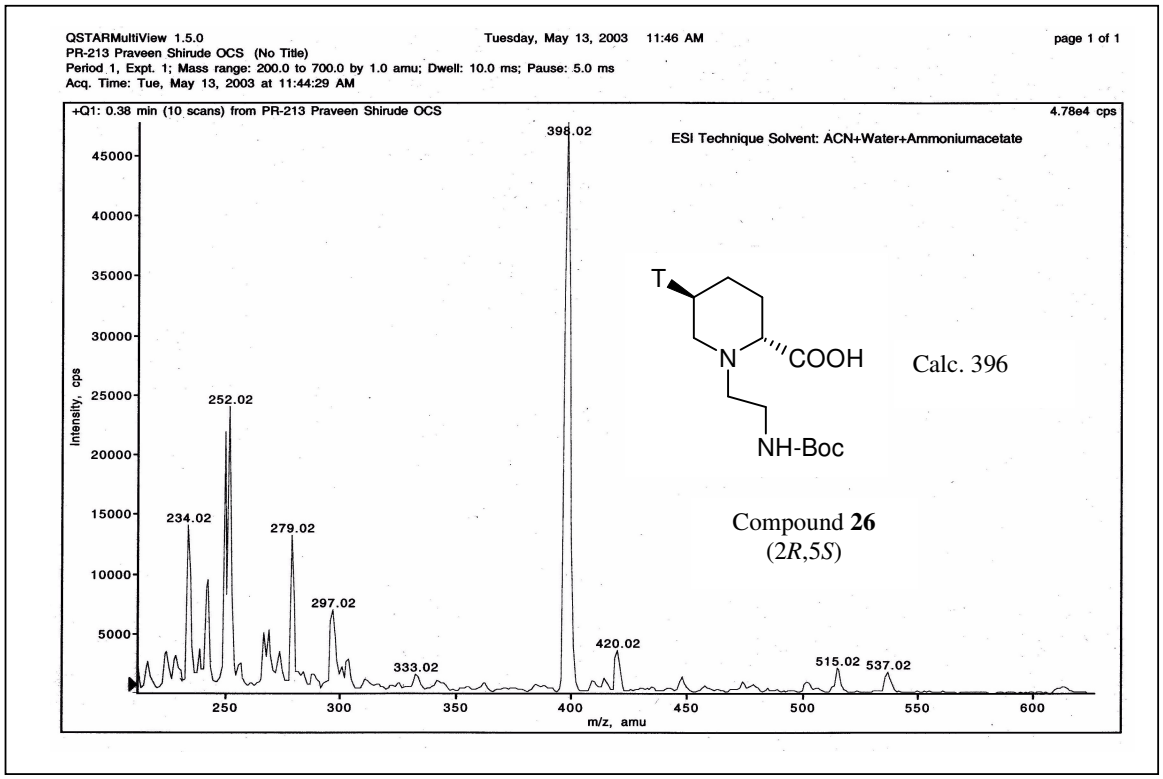
QSTARMultiView 1.5.0
Tuesday, May 13, 2003 11:46 AM
page 1 of 1
PR-213 Praveen Shirude OCS (No Title)
Period 1, Expt. 1; Mass range: 200.0 to 700.0 by 1.0 amu; Dwell: 10.0 ms; Pause: 5.0 ms
Acq. Time: Tue, May 13, 2003 at 11:44:29 AM
+Q1: 0.38 min (10 scans) from PR-213 Praveen Shirude OCS
4.78e4 cps
ESI Technique Solvent: ACN+Water+Ammoniumacetate
Intensity, cps
m/z, amu
398.02
252.02
234.02
279.02
297.02
333.02
420.02
515.02
537.02
T
N
COOH
NH-Boc
Calc. 396
Compound 26
(2R,5S)

3.0. REFERENCES

[1] Uhlmann, E.; Peyman, A. Antisense oligonucleotides: A new therapeutic principle. *Chem. Rev*. **1990**, *90*, 543-584.

[2] *Antisense Research and Applications* (Eds.: Crooke, S. T.; Lebleu, B.), CRC Press, Boca Raton, FL, 1993.

[3] Uhlmann, E.; Peyman, A. Antisense Oligonucleotides - Chemical Modifications. In *Encyclopaedia of Molecualr Biology and Biotechnology* (Ed.: Meyer, E.), VCH, New York, 1995.

[4] De Mesmaeker, A.; Haner, R.; Mertin, P.; Moser, H. E. Antisense Oligonucleotides. *Acc. Chem. Res.* **1995**, *28*, 366-374

[5] *Methods in Molecular Biology, Vol. 20: Protocols for Oligonucleotides and Analogs* (Ed.: Agrawal, S.), Humana Press, New Jersey, Totowa, Chapter 16, 1993, pp. 355-389.

[6] Nielsen, P. E. DNA analogues with nonphosphodiester backbones. *Annu. Rev. Biophys. Biomol. Struct.* **1995**, *24*, 167-183.

[7] De Mesmaeker, A.; Altmann, K. -H.;Waldner, A.; Wendeborn, S. Backbone modifications in oligonucleotides and peptide nucleic acid systems. *Curr. Opin. Struct. Biol.* **1995**, *5*, 343-355.

[8] Stirchak, E. P.; Summerton, J. E.; Weller, D. D. Uncharged stereoregular nucleic acid analogs: 2- Morpholino nucleoside olgiomers with carbamate internucleoside linkages. *Nucleic Acids Res.* **1989**, *17*, 6129-6141.

[9] Nielsen, P. E.; Egholm, M.; Berg, R. H.; Buchardt, O. Sequence-selective recognition of DNA by strand displacement with thymine-substituted polyamide. *Science,* **1991**, *254*, 1497-1500.

[10] Nielsen, P. E.; Egholm, M.; Buchardt, O. Peptide nucleic acid (PNA). A DNA mimic with a peptide backbone. *Bioconj. Chem.* **1994**, *5*, 3-7.

[11] Hyrup, B.; Egholm, M.; Buchardt, O.; Nielsen, P. E. A flexible and positively charged PNA analogue with an ethylene-linker to the nucleobase: Synthesis and hybridization properties. *Bioorg. Med.Chem. Lett.* **1996**, *6*, 1083-1088.

[12] Good, L.; Nielsen, P. E. Progress in developing PNA as a gene-targeted drug. *Antisense & Nucleic Acids Drug Dev.* **1997**, *7*, 431-437.

[13] Nielsen, P. E.; Haaima, G. Peptide nucleic acid. A DNA mimic with a pseudopeptide backbone. *Chem. Soc. Rev.* **1997**, 73-78.

[14] Uhlmann, E.; Peyman, A.; Breipohl, G.; Will, D. W. PNA: Synthetic Polyamide Nucleic Acids with Unusual Binding Properties. *Angew. Chem. Int. Ed. Engl.* **1998, *37*,** 2796-2823.

[15] Egholm, M.; Buchardt, O.; Christensen, L.; Behrens, C.; Freier, S. M.; Driver, D. A.; Berg, R. H.; Kim, S. K.; Norden, B.; Nielsen, P. E. PNA hybridizes to complementary oligonucleotides obeying the Watson-Crick hydrogen-bonding rules. *Nature,* **1993**, *365*, 566-568.

[16] Hanvey, J. C.; Peffer, N. J.; Bisi, J. E.; Thomson, S. A.; Cadilla, R.; Josey, J. A.; Ricca, D. J.; Hassman, C. F.; Bonham, M. A.; Au, K. G.; Carter, S. G.; Bruckenstein, D. A.; Boyd, A. L.; Noble, S. A.; Babiss, L. E. Antisense and antigene properties of peptide nucleic acids. *Science,* **1992**, *258*, 1481- 1485.

[17] D'Costa, M.; Kumar, V. A.; Ganesh, K. N. Aminoethylprolyl peptide nucleic acids (aepPNA): Chiral PNA analogues that form highly stable DNA: aepPNA$_2$ triplexes. *Org. Lett.* **1999**, *1*, 1513-1516.

[18] D'Costa, M.; Kumar, V. A.; Ganesh, K. N. Aminoethylprolyl (*aep*) PNA: Mixed purine/pyrimidine oligomers and binding orientation preferences for PNA:DNA duplex formation. *Org. Lett.* **2001**, *3*, 1281-1284.

[19] Kumar, V. A. Structural preorganization of peptide nucleic acids: Chiral cationic analogues with five- or six-membered ring structures. *Eur. J. Org. Chem.* **2002**, 2021-2032.

[20] (i).Vilaivan, T.; Lowe, G. A novel pyrrolidinyl PNA showing high sequence specificity and preferential binding to DNA over RNA. *J. Am. Chem. Soc*. **2002**, 124, 9326-9327. (ii) Hickman, D. T.; King, P. M.; Cooper, M. A.; Slater, J. M.; Mickelfield, J. Unusual RNA and DNA binding properties of a novel pyrrolidine-amide oligonucleotide mimic (POM). *Chem. Comm*un. **2000**, 2251-2252. (iii). Puschl, A.; Boesen, T.; Zuccarello, G.; Dahl, O.; Pitsch, S.; Nielsen, P. E. Synthesis of pyrrolidinone PNA: A novel conformationally restricted PNA analogue. *J. Org. Chem*. **2001**, *66*, 707-712.

[21] Bailey, P. D.; Bryans, J. S. Chiral synthesis of 5-hydroxy-(L)-pipecolic acids from (L)-glutamic acid. *Tetrahedron Lett.* **1988**, *29*, 2231-2234.

[22] Adams, D. R.; Bailey, P. D.; Heffernan, J. H.; Stokes, S. An efficient route to the a-methyl ester of L-glutamic acid, and its conversion into *cis*-5-hydroxy-L-pipecolic acid. *Chem. Commun.* **1996**, 349-350

[23] Cruickshank, K. A.; Jiricny, J.; Reese, C. B. The benzoylation of uracil and thymine. *Tetrahedron Lett.* **1984**, *25*, 681.

[24] Brown, D. M.; Todd, A.; Varadarajan, S. *J. Chem. Soc.* **1956**, 2384.

[25] Lowe, G.; Vilaivan, T. Amino acids bearing nucleobases for the synthesis of novel peptide nucleic acids. *J. Chem. Soc. Perkin Trans I,* **1997**, 539-546.

[26] Buchardt, O.; Egholm, M.; Nielsen, P. E.; Berg, R. H. *Int. PCT Appl. wo 92/20702* **1992**.

[27] Ando, T.; Yamawaki, J. Potassium fluoride on Celite: A versatile reagent for C-, N-, O-, and S-alkylations. *Chem. Lett.* **1979**, 45-46.

[28] Christensen, L.; Fitzpatrick, R.; Gildea, B.; Petersen, K.; Hansen, H. F.; Koch, C.; Egholm, M.; Buchardt, O.; Nielsen, P. E.; Coull, J.; Berg, R. H. Solid-phase synthesis of peptide nucleic acids. *J. Peptide Sci.* **1995**, *3*, 175-183.

[29] Dueholm, K. L.; Egholm,M.; Behrens, C.; Christensen, L.; Hansen, H. F.; Vulpius T.; Petersen, K. H.; Berg, R.; H.; Nielsen, P. E.; Buchardt, O. Synthesis of peptide nucleic acid monomers containing the four natural nucleobases: Thymine, cytosine, adenine, and guanine and their oligomerization. *J. Org. Chem.* **1994**, *59*, 5767-5773.

[30] Gisin, B. F. The monitoring of reactions in solid-phase peptide synthesis with picric acid. *Anal. Chim. Acta* **1972,** *58*, 248-249.

[31] Merrifield, R. B.; Stewart, J. M.; Jernberg, N. Instrument for automated synthesis of peptides. *Anal. Chem.* **1966**, *38*, 1905-1914.

[32] Erickson, B. W.; Merrifield, R. B. 1976, in *Solid Phase Peptide Synthesis. In the Proteins* Vol. II, 3rd ed.; Neurath, H. and Hill, R. L. eds., Academic Press, New York, pp 255

[33] Kaiser, E.; Colescott, R. L.; Bossinger, C. D.; Cook, P. I. Color test for detection of free terminal amino groups in the solid-phase synthesis of peptides. *Anal. Biochem.* **1970**, *34*, 595-598.

[34] Fields, G. B.; Fields, C. G. Solvation effects in solid-phase peptide synthesis. *J. Am. Chem. Soc.* **1991**, *113*, 4202-4207.

[35] Barawkar, D. A.; Rajeev, K. G.; Kumar, V. A.; Ganesh, K. N. Triplex formation at physiological pH by 5-Me-dC-N4-(spermine) [X] oligodeoxynucleotides: Non protonation of N3 in X of X*G:C triad and effect of base mismatch/ionic strength on triplex stabilities. *Nucleic Acids Res.* **1996**, *24*, 1229-1237.

[36] Puglisi, J. D.; Tinoco, I. Jr. Absorbance melting curves of RNA. *Methods Enzymol.* **1989**, *180*, 304-325.

[37] Barawkar, D. A.; Bruice, T. C. Deoxynucleic guanidines/PNA (DNG/PNA) chimeras: Oligonucleoside analogue containing cationic guanidinium and neutral amide linkages. *J. Am. Chem. Soc.* **1999**, *121*, 10418.

[38] Egholm, M.; Buchardt, O.; Nielsen, P. E.; Beg, R. H. Recognition of guanine and adenine in DNA by cytosine and thymine containing peptide nucleic acids (PNA). *J. Am. Chem. Soc.* **1992**, *114*, 9677-9678.

[39] Gray, D. M.; Ratliff, R. L.; Vaughan, M. R. Circular dichroism spectroscopy of DNA. *Methods Enzymol.* **1992**, *211*, 389-396.

[40] Gray, D. M.; Hung, S. –H.; Johnson, K. H. Absorption and circular dichroism spectroscopy of nucleic acid duplexes and triplexes. *Methods Enzymol.* **1995**, *246*, 19-34.

[41] Wittung, P.; Nielsen, P. E.; Buchardt, O.; Egholm, M.; Nordén, B. DNA-like double helix formed by peptide nucleic acid. *Nature,* **1994**, *368*, 561-563.

[42] Linkletter, B. A.; Szabo, I. E.; Bruice, T. C. Solid-Phase synthesis of deoxynucleic guanidine (DNG) oligomers and melting point and circular dichroism analysis of binding fidelity of octameric thymidyl oligomers with DNA oligomers. *J. Am. Chem. Soc.* **1999**, *121*, 3888-3896.

[43] Sforza, S.; Haaima, G.; Marchelli, R.; Nielsen, P. E. Chiral peptide nucleic acids (PNAs):helix handedness and DNA recognition. *Eur. J. Org. Chem.* **1999,** 197-204.

[44] Wittung, P.; Nielsen, P.; Norden, B. Extended DNA-recognition repertoire of peptide nucleic acid (PNA): PNA-dsDNA triplex formed with cytosine-rich homopyrimidine PNA. *Biochemistry,* **1997**, *36*, 7973-7979.

[45] Kim, S. H.; Nielsen, P. E. ; Egholm, M.; Buchardt, O. Right-handed triplex formed between peptide nucleic acid PNA-T8 and poly(dA) shown by linear and circular dichroism spectroscopy. *J. Am. Chem. Soc*. **1993**, *115*, 6477.

[46] Eschenmoser, A.; Dobler, M. Why pentose and not hexose nucleic acids? Part I. Introduction to the problem, conformational analysis of oligonucleotide single strands containing 2',3'-dideoxyglucopyranosyl building blocks ('homo-DNA') and reflections on the conformation of A- and B-DNA. *Helv. Chim. Acta* **1992**, *75***,** 218–259.

[47] Lescrinier, E; Esnouf, R.; Schraml, J.; Busson, R.; Heus, H. A; Hilbers, C. W.; Herdewijn. P. Solution structure of a HNA-RNA hybrid. *Chem. Biol.* **2000**, *7*, 719–731.

[48] Lonkar, P. S.; Kumar, V. A. Design and synthesis of conformationally frozen peptide nucleic acid backbone: chiral piperidine PNA as a hexitol nucleic acid surrogate. *Bioorg. Med. Chem. Lett.* **2004**, *14*, 2147-2149.

[49] Püschl, A.; Boesen, T.; Tedeschi, T.; Dahl, O.; Nielsen, P. E. Synthesis of (3*R*,6*R*)- and (3*S*,6*R*)-piperidinone PNA. *J. Chem. Soc., Perkin Trans.1* **2001**, *21*, 2757-2763.

[50] Egholm, M.; Buchardt, O.; Christensen, L.; Behrens, C.; Freier, S. M.; Driver, D. A.; Berg, R. H.; Kim, S. K.; Nordén, B.; Nielsen, P. E. PNA hybridizes to complementary oligonucleotides obeying the Watson-Crick hydrogen-bonding rules. *Nature,* **1993**, 566-568.

[51] Koch, T.; Naesby, M.; Wittung, P.; Jorgensen, M.; Larsson, C.; Buchardt, O.; Stanley, C. J.; Nordén, B.; Nielsen, P. E.; Ørum, H. PNA-Peptide Chimerae. *Tetrahedron Lett.* **1995**, *36*, 6933-6936.

[52] Bergmann, F.; Bannwarth, W.; Tam, S. Solid phase synthesis of directly linked PNA-DNA-hybrids. *Tetrahedron Lett.* **1995,** *36*, 6823-6826.

[53] Petersen, K. H.; Jensen, K. D.; Buchardt, O.; Nielsen, P. E.; Buchardt, O. PNA-DNA linker synthesis of *N*-((4,4'-dimethoxytrityloxy)ethyl)-*N*-(thymin-1-ylacetyl)glycine. *Bioorg. Med.Chem. Lett.* **1995**, *5*, 1119-1124.

[54] Petersen, K. H.; Buchardt, O.; Nielsen, P. E. Synthesis and oligomerization of N^{δ}-Boc-N^{α}-(thymin-1-ylacetyl)ornithine. *Bioorg. Med. Chem. Lett.* **1996**, *6*, 793.

[55] Finn, P. J.; Gibson, N. J.; Fallon, A.; Hamilton, A.; Brown, T. Synthesis and properties of DNA-PNA chimeric oligomers. *Nucleic Acids Res.* **1996**, *24*, 3357-3363.

[56] Uhlmann, E.; Peyman, A.; Breipohl, G.; Will, D. W. PNA: Synthetic Polyamide Nucleic Acids with Unusual Binding Properties. *Angew. Chem. Int. Ed. Engl.* **1998**, *37*, 2796-2823.

[57] van der Laan, A. C.; Brill, R.; Kulimelis, R. G.; Kuyl- Yeheskiely, E.; van Boom, J. H.; Andrus, A.; Vinayak, R. A convenient automated solid-phase synthesis of PNA-(5')-DNA-(3')-PNA chimera. *Tetrahedron Lett.* **1997**, *38*, 2249-2252.

[58] Haaima, G.; Lohse, A.; Buchardt, O.; Nielsen, P. E. Peptide nucleic acids (PNAs) containing thymine monomers derived from chiral amino acids: Hybridization and solubility properties of D-lysine PNA. *Angew. Chem. Int. Ed. Engl.* **1996**, *35*, 1939-1942.

[59] Kosynkina, L.; Wang, W.; Liang, T. C. A convenient synthesis of chiral peptide nucleic acid (PNA) monomers. *Tetrahedron Lett.* **1994**, *35*, 5173-5176.

[60] Dueholm, K. L.; Petersen, K. H.; Jensen, D. K.; Nielsen, P. E.; Egholm, M.; Buchardt, O. Peptide nucleic acid (PNA) with a chiral backbone based on alanine. *Bioorg. Med. Chem. Lett.* **1994**, *4*, 1077-1080.

[61] Lowe, G.; Vilaivan, T. Solid-phase synthesis of novel peptide nucleic acids. *J. Chem. Soc. Perkin Trans I,* **1997**, 555-560.

[62] Gangamani, B. P.; Kumar, V. A.; Ganesh, K. N. Chiral analogues of peptide nucleic acids: Synthesis of 4-aminoprolyl nucleic acids and DNA complementation studies using UV/CD spectroscopy. *Tetrahedron,* **1999**, *55*, 177-192.

[63] Howarth, N. M.; Wakelin, L. P. G. α-PNA: A novel peptide nucleic acid analogue of DNA. *J. Org. Chem.* **1997**, *62*, 5441-5450.

[64] Altmann, K–H.; Chiesi, C. S.; Garciá- Echeverría, C. Polyamide based nucleic acid analogs — synthesis of δ-amino acids with nucleic acid bases bearing side chains. *Bioorg. Med. Chem. Lett.* **1997**, *7*, 1119-1122.

[65] Zhang, L.; Min, J.; Zhang, L. Studies on the synthesis and properties of new PNA analogs consisting of L- and D-lysine backbones. *Bioorg. Med. Chem. Lett.* **1999**, *9*, 2903-2908.

[66] van der Laan, A. C.; van Amsterdam, I.; Tesser, G. I.; van Boom, J. H.; Kuyl-Yeheskiely, E. Synthesis of chirally pure ornithine based PNA analogues. *Nucleosides & Nucleotides,* **1998**, *17*, 219-231.

[67] Fujii, M.; Yoshida, M.; Hidaka, J.; Ohtsu, T. Hybridization properties of nucleic acid analogs containing β-aminoalanine modified with nucleobases. *Chem. Commun.* **1998**, 717.

[68] Sforza, S.; Haaima, G.; Marchelli, R.; Nielsen, P. E. Chiral peptide nucleic acids (PNAs): Helix handedness and DNA recognition. *Eur. J. Org. Chem.* **1999**, 197-204.

[69] Norden, B. *Chem. Scr.* **1975**, *7*, 14.

[70] Norden, B. *Acta Chem. Scand.* **1972**, *26*, 111.

[71] Wittung, P.; Eriksson, M.; Lyng, R.; Nielsen, P. E.; Norden. B. Induced Chirality in PNA-PNA Duplexes. *J. Am. Chem. Soc.* **1995**, *117*, 10167-10173.

[72] Hunziker, J.; Priestley, E. S.; Brunar, H.; Dervan, P. B. Design of an N7-Glycosylated Purine Nucleoside for Recognition of GC Base Pairs by Triple Helix Formation. *J. Am. Chem. Soc.* **1995**, *117*, 2661-2662.

CHAPTER 3:

APPLICATIONS OF BIS-PNA FOR TARGETTING COMPLEMENTARY DNA: EFFECT OF N7G IN *aeg*/*aep* PNA BACKBONE

3.1. INTRODUCTION

Novel molecules designed to bind effectively with high sequence specificity to desired double-stranded DNA (dsDNA) targets are of major interest in medicine as gene therapeutic agents and in molecular biology as 'genetic tools'.[1] The unique properties of peptide nucleic acids (PNAs)[2,3] have attracted considerable interest in this respect, not least due to the unexpected duplex invasion binding mode that has opened a novel avenue to target dsDNA. Thus a further characterization of PNAs and their binding mode(s) are warranted.

The acyclic, neutral and achiral aminoethyl glycyl PNAs hybridize with high affinity and specificity to oligonucleotides. It supervenes the Watson-Crick base pairing rules and thus, are true mimics in terms of base-pair recognition.[4] PNA can bind to complementary nucleic acids in both antiparallel (Figure 1, *ap*, with the PNA 'N' terminus towards the 3'-end and the 'C' terminus towards the 5'-end of the complementary DNA/RNA oligonucleotide) and parallel (Figure 1, *p*, with the PNA 'N' terminus towards the 5'-end and the 'C' terminus towards the 3'-end of the complementary DNA/RNA oligonucleotide) orientation.

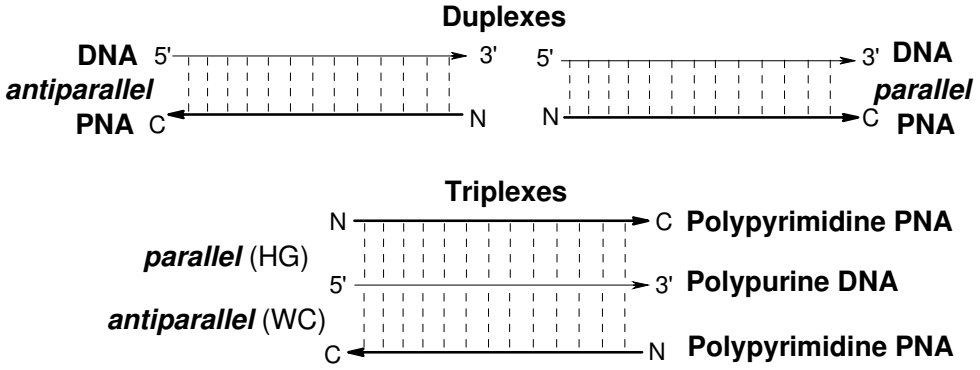

Figure 1. The parallel and antiparallel orientation of the PNA strands in a PNA:DNA duplex and a PNA_2:DNA triplex.

It has been generally observed that antiparallel orientation is slightly preferred. PNAs can bind to both DNA and RNA targets in a sequence-specific manner to form duplex structures. Although the Watson-Crick duplex formation (anti-parallel duplex formation) is the preferred formation for the PNA bindings, parallel duplex structure can still be formed when PNAs bind to the target sequences. While PNA:DNA duplexes are more stable in the antiparallel form, the parallel orientation seems to be preferred for PNA_2:DNA triplexes, if only one species of PNA is employed.[5] PNA_2:DNA triplex formation[6] follows the rules of homopyrimidine DNA triplex formation. Thus, the most stable triplexes are formed when the Watson-Crick base-pairing PNA strand is in the antiparallel orientation relative to the DNA strand and the Hoogsteen strand is in the parallel orientation relative to the DNA strand, i. e., the two strands are antiparallel to each other[4] (Figure 1).

Homopyrimidine PNAs typically bind with a PNA_2:DNA stoichiometry. Such complexes are comprised of a PNA:DNA double helix (formed by Watson- Crick hydrogen bonds) bound with a second PNA strand lying in the major groove of the duplex and paired by Hoogsteen hydrogen bonds. The stability of these triple helix structures are found to be so favourable that strand invasion of DNA:DNA duplex is possible, leading to PNA_2:DNA triplexes (Figure 2).

Figure 2. P-loop structures formed by strand invasion of homopyrimidine mono-PNAs (**A**) or bis-PNAs (**B**) into dsDNA.

To entropically enhance strand invasion efficiency, PNA clamps or bisPNAs are often used (Figure 2). The bisPNAs are two homopyrimidine PNA oligomers that are covalently connected via a flexible linker.[7,8] Linkage of two PNA oligomers offers the possibility to expediently design one PNA strand preferentially for Hoogsteen binding and the other PNA strand preferentially for Watson-Crick binding.[9] This also reduces a trimolecular reaction of PNA to DNA binding to a bimolecular reaction, accelerating the PNA invasion. PNA strand invasion into dsDNA can be additionally accelerated by incorporation of positive charges into PNA or bisPNA oligomers.[9,10]

Homopyrimidine PNAs that are rich in cytosines add to the double stranded target polynucleotides as Hoogsteen strands forming PNA:DNA_2 triplexes[11,6] Oligomers such as PNA-C_{10} or PNA-$(CT)_5$ do not invade double stranded polynucleotides by forming triplexes in a way analogous to that observed with thymine-rich PNAs.[12] These reactions are significantly pH-dependent owing to the requirement of N3-protonation of cytosine in the third strand. In literature, attempts have been made to mimic the C^+ hydrogen-bonding pattern by neutral bases (C^+ mimetics) such as N7-G, 8-oxo-adenine and J base to avoid the necessity of low pH for C-containing PNA oligomers (Figure 3).

One such mimic, 8-oxo-adenine has been employed to recognize guanine in the Hoogsteen mode.[13,14,15] Pseudoisocytosine (ψiC) is another C^+ mimic that has been utilized to achieve pH-independent Hoogsteen binding of the third strand to a G:C base pair.[16,17] Pseudoisocytosine has also been introduced into PNA for pH-independent triplex formation.[18]

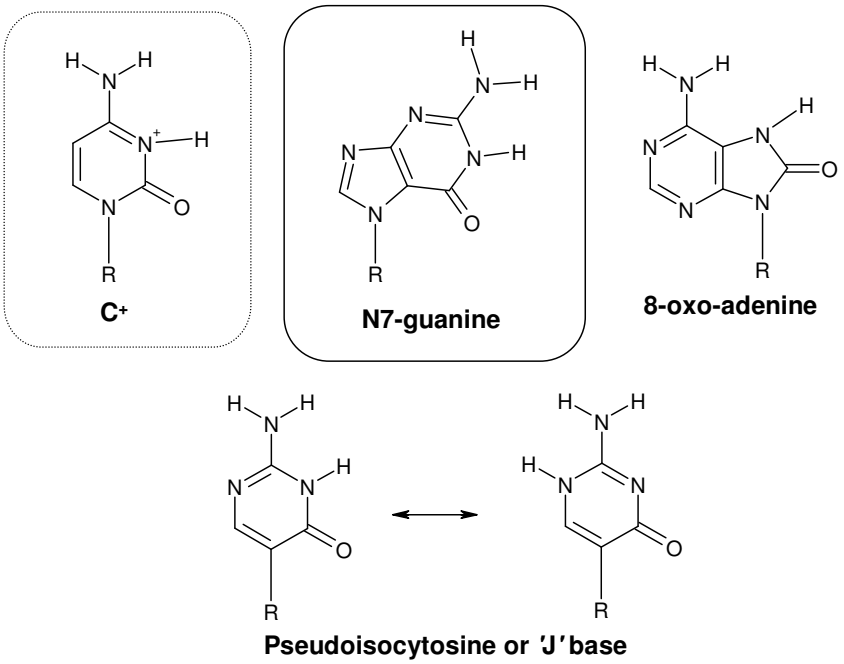

Figure 3. Neutral C^+ hydrogen bonding mimics.

Homopyrimidine PNAs contain only C and T as nucleobases. BisPNAs are two homopyrimidine PNAs connected by a flexible linker molecule. Homopyrimidine mono- and bis-PNAs bind to double-stranded (ds) DNA by strand invasion leading to so-called P-loop complexes. Employing bisPNAs where in the Watson-Crick PNA strand is connected *via* ethylene glycol linkers to the Hoogsteen PNA strand[8,19] leads to an increase in the thermal stability (melting temperature) of the triplexes. Optimal results in terms of pH-independence and thermal stability of the complexes formed were obtained when the cytosines in the Hoogsteen strand were replaced by pseudoisocytosine, as compared to placement of pseudoisocytosine in the Watson-Crick strand. In the complexes where the cytosine PNA strand is antiparallel to the DNA target (Figure 4a) (and thus the pseudoisocytosine strand is parallel), almost no pH dependence of the T_m was observed.

This indicated an orientation-directed selectivity in complex formation to align the Watson-Crick strand in the antiparallel configuration and the Hoogsteen strand in the parallel configuration as in Figure 4b.

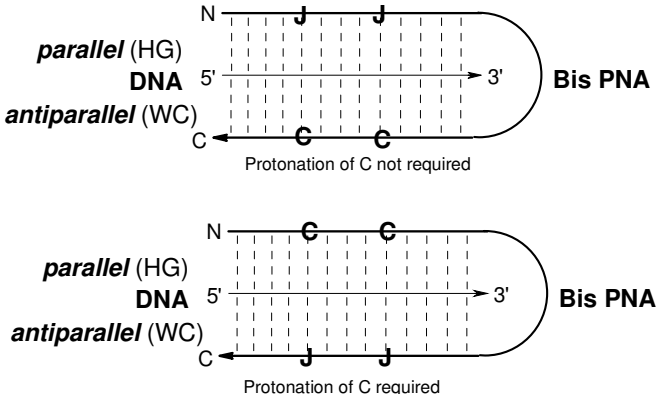

Figure 4. Triplex formation with bisPNAs carrying pseudoisocytosine as a neutral C^+ mimic.

N7-glycosylated guanine, a positional isomer of the naturally occurring N9-guanine is yet another nucleobase that provides bidentate hydrogen bonding to target G:C base pairs (Figure 5, Table 1). It thus, mimics the C^+ hydrogen-bonding pattern, but surpasses the requirement of low pH for complex formation. Nucleoside derivatives of N7-guanine have been demonstrated to be effective in forming base triplets with dG:dC base pair targets.[19,20,21] In DNA triplexes, natural N9G binds in a reverse HG mode to a G:C base pair in a purine motif, with the third strand in an antiparallel orientation[22] (Figure 1a). The pyrimidine motif requires N3-protonation of C and hence acidic conditions for stable triplex formation,[23] even in PNA:DNA triplexes.[24] N7G can replace protonated C (C^+) in the pyrimidine motif as its mimic (Figure 1b) and allows the formation of stable triplexes at neutral pH[21] in HG mode. In PNA_2:DNA triplexes, the two H-bond donor sites of the N7G as a C^+ mimic may recognize G through HG mode in both parallel (Figure 1b) and antiparallel (Figure

1c) orientations, but may not recognize G in WC binding mode (Figure 1d). Incorporation of N7G units in PNA strand may thus stabilize triplexes only when engaged in HG mode of binding (Figure 1c) unlike cytosine or 'J' base- another C^+ mimic.[25]

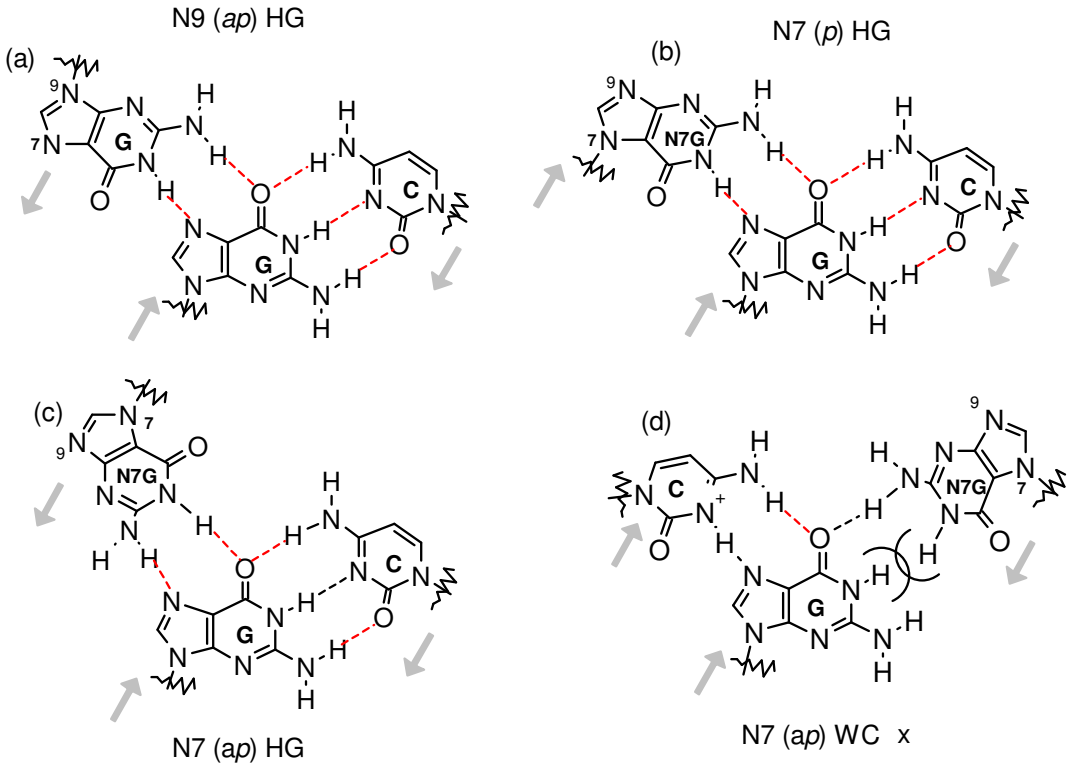

Figure 5. PNA hydrogen bonding schemes: (a) G_{ap}*G:C_{ap} (b) $N7G_p$*G:C_{ap} (c) $N7G_{ap}$*G:C_p (d) C^+_p*G:$N7G_{ap}$ [*p* = parallel, *ap* = antiparallel, * indicates Hoogsteen H-bonding, : indicates WC H-bonding].

Table 1. PNA hydrogen bonding schemes.*

Base	**WC**		**HG**	
	p	***ap***	***p***	***ap***
G-G:C	-	√	-	√
N7G-G:C	√	-	-	√
N7G-G:C	-	√	-	√
C^+-G:N7G	-	√	√	-

*[*p* = parallel, *ap* = antiparallel]

An acyclic nucleoside analogue bearing the N7-guanine nucleobase was also found to be able to form triplexes.[26] This analogue retains the heterocyclic portion of the molecule essential for base-base recognition, but lacks the rigid conformational features of the ribose/deoxyribose sugar (Figure 6). The triplex containing five adjacent acyclic N7G residues exhibited Tm values significantly higher than the triplex containing alternating G-C base pairs.

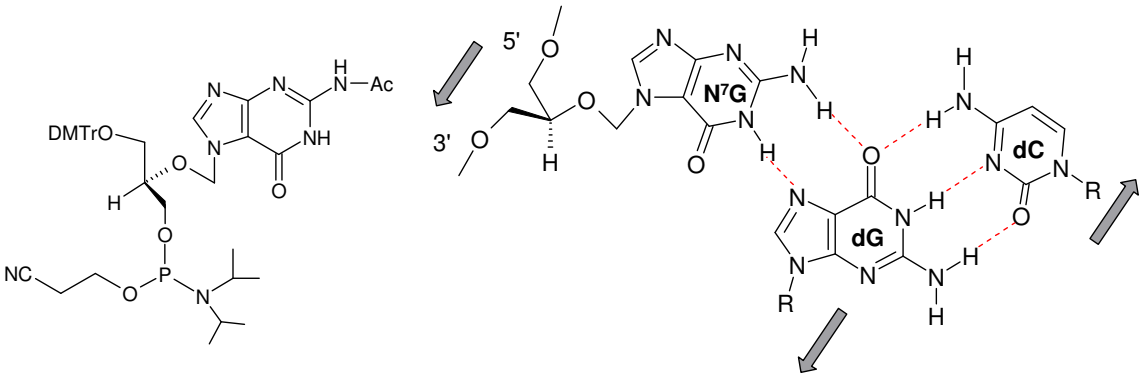

Figure 6. Acyclic N7G nucleoside analogue and its triplex formation.

3.2. RATIONALE FOR THE PRESENT WORK

Homopyrimidine PNA sequences form PNA_2:DNA triplexes in which PNA (parallel or antiparallel) is involved in either Watson-Crick (WC) or Hoogsteen (HG) hydrogen bonding modes with the central polypurine DNA strand. In such PNA_2:DNA triplexes, the DNA strand is engaged in simultaneous binding to two PNA strands and ambiguity persists in establishing the specific correlation among parallel/antiparallel PNA strands with HG or WC binding mode with DNA.[19] In practice, this would lead to the formation of PNA_2:DNA triplexes with different combinations of various parallel/antiparallel strand orientations. The uncertainty in

WC/HG PNA strand orientation with respect to DNA of such mixed PNA_2:DNA complexes can be partially overcome by conjugating the two PNA strands with a linker to construct a bisPNA hairpin that can form only two triplexes with a 1:1 (PNA:DNA) composition.[8] It was thought that introduction of a chiral monomer into one arm of bisPNA may assist in identifying the orientation and towards this aim, the chiral (2*S*,4*S*)-*aep*PNA (C and N7-G) monomer (Figure 7) was introduced into one of the hairpin arms of bisPNA carrying a cationic peptide linker.

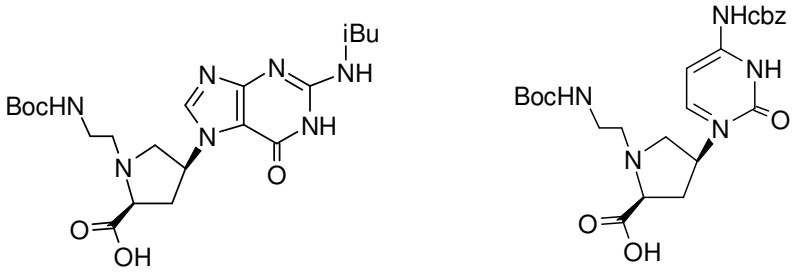

Figure 7. *aep*PNA monomers.

It was found[28] that both *aep*PNA-C and *aep*PNA-N7G containing bisPNAs formed more stable triplexes when the constituent arm had antiparallel orientation with respect to the middle DNA strand, unlike the corresponding *aeg*-bisPNA. As expected, the triplex formation was pH dependent in case of PNA-C oligomers and pH independent with PNA-N7-G oligomers. However, since the peptide linker contained three units of positively charged lysine residues, the protonation of N3 of *aep*PNA-C necessary for triplex formation and that of pyrrolidine ring nitrogen will be severely affected due to electrostatic effects. Further, the positive charges in the linker will also accelerate the PNA:DNA hybridization kinetics and mask the specificity effects.

This can be avoided by replacing the charged peptide linker[28] by a neutral linker (Figure 8) composed of polyethyleneoxy units to examine the true selectivities in hybridization of the two arms of PNA with parallel/antiparallel DNA strand.

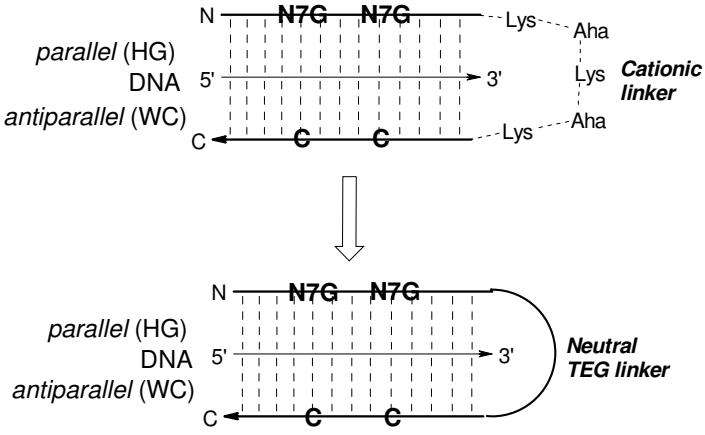

Figure 8. Triplex formation with bisPNAs carrying different linkers.

This chapter describes the synthesis of mixed polypyrimidine bisPNA (H-TTTXTXT-TEG-EG-TCTCTTT-NH-$(CH_2)_2$-COOH) containing *aep*PNA (X=C/N7-G) units and having neutral tetraethylene glycol liker and results on its hybridization with complementary DNA as followed by UV-T_m. A fluorescence-based assay that delineates the kinetics of strand invasion from the thermodynamic stability was used to study the kinetics of bisPNA:DNA complex formation by the use of fluorescence properties of the commonly used intercalator, ethidium bromide.[27,28] In case of the present *teg*-bisPNA, this assay is shown to resolve the independent kinetics of hybridization of the two arms of bisPNA as a function of the DNA orientation.

Homopyrimidine PNA_2:DNA triplex formation is pH-dependent owing to the requirement of N3-protonation of cytosine in the Hoogsteen mode of recognition. N7G being a C^+ mimic, should circumvent the requirement of low pH for triplex formation and make effective triplexes at physiological pH.

3.3. OBJECTIVES

The specific objectives of this Chapter are:

1. Synthesis of amionethylglycyl PNA-N7G monomer bearing N7-guanine as a C^+ mimic.
2. Synthesis of 1-(*N*-Boc-aminoethyl)-4(*S*)-(N^2-isobutyrylguanin-7-yl)-2(*S*)-proline as a chiral N7G monomeric unit.
3. Synthesis of tetraethylene glycol linker.
4. Design and solid phase peptide synthesis of bisPNA oligomers incorporating the *aeg*/*aep*PNA-N7G units.
5. A study of the pH effects on triplex formation.
6. A study of the strand invasion of target DNA duplex by these modified bisPNAs using fluorescence assay and influence of these oligomers on the binding orientation (*ap*/*p*).

3.4. PRESENT WORK

3.4.1. Synthesis of Protected Nucleobases

N^2-isobutyrylguanine[29] (**1**) was synthesized by treating guanine with

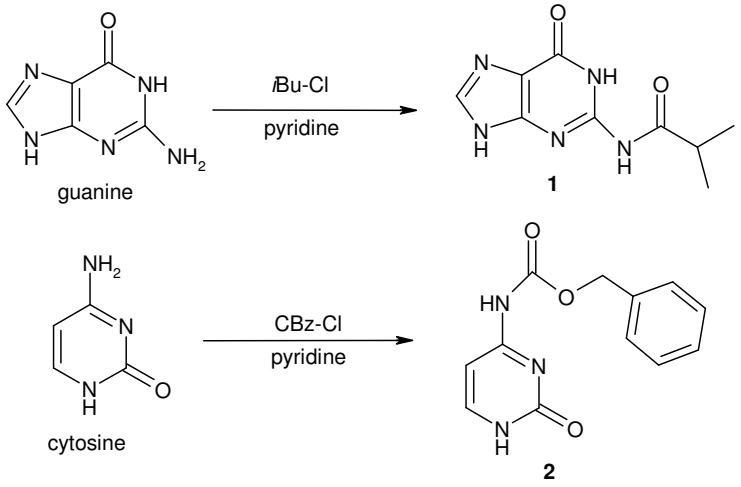

Scheme 1. Protection of the exocyclic amino groups of the nucleobases.

isobutyryl chloride in dry pyridine to yield N^2-isobutyrylguanine (**1**) (Scheme 1). N^4-benzyloxycarbonylcytosine[30] (**2**) was obtained when cytosine was treated with benzyloxycarbonyl chloride in dry pyridine.

3.4.2. Synthesis of Protected Monomeric Aminoethyl Prolyl PNA

The *N*-(Boc-aminoethyl)-(thymin-1-yl)-glycinate (**3**) and *N*-(Boc-aminoethyl)-(N^4-benzyloxycarbonylcytosin-1-yl)glycinate (**5**) (Scheme 2) were synthesized by reported procedures (See Chapter 2). The *N*-(Boc-aminoethylglycyl)-(N^2-isobutyrylguanin-7-yl)ethyl ester (**4**) was prepared by reacting compound **3** with N^2-isobutyrylguanine in the presence of potassium carbonate (Scheme 2).

3.4.2a 1-(N-Boc-aminoethyl)-4(S)-(N^4-benzyloxycarbonyl cytosin-1-yl)-2(S)-proline methyl ester[28] (10). The synthesis pathway for 1-(*N*-Boc-aminoethyl)-4(*S*)-(N^4-benzyloxycarbonyl cytosin-1-yl)-2(*S*)-proline methyl ester (**10**) consisted of four steps. These steps start from esterification of the carboxylic acid moiety followed by alkylation of the proline ring nitrogen with 2-(*N*-Boc)-aminoethyl mesylate (**8**). The next step involved conversion of the C4-hydroxyl group to its corresponding mesyl derivative (**9**) by treatment of **8** with mesyl chloride in pyridine (Scheme 2). 1-(*N*-Boc-aminoethyl)-4(*R*)-O-mesyl-2(*S*)-proline methyl ester (**9**) was reacted with N^4-benzyloxycarbonyl cytosine, in presence of K_2CO_3 and a catalytic amount of 18-crown-6 in DMF to give the 4(*S*)-(N^4-benzyloxycarbonyl cytosin-1-yl) derivative (**10**). This step is accompanied by an inversion of stereochemistry at the C4-stereocenter owing to the S_N2 displacement reaction. The 4(*S*)-(N^4-benzyloxycarbonyl-cytosin-2-yloxy) derivative (not shown) was also obtained as a side-product of the above reaction in 20% yield. The *N*1- and *O*2- substituted products are distinguishable in ^{1}H NMR by the chemical shifts of the H5 and H6 protons of

cytosine, viz. δ7.25 & δ7.60 for H5 and δ8.45 & δ8.35 for H6 in the *N*1- and *O*2-substituted derivatives respectively. The *O*2-substituted product is characterized by a downfield shift of the H4 signal from δ5.20 in the *N*1-substituted derivative to δ5.35. Thus, the synthesis of 1-(*N*-Boc-aminoethyl)-4(*S*)-(N^4-benzyloxycarbonyl cytosin-1-yl)-2(*S*)-proline methyl ester involves the inversion of stereochemistry at one stereocenter, i. e., C4.

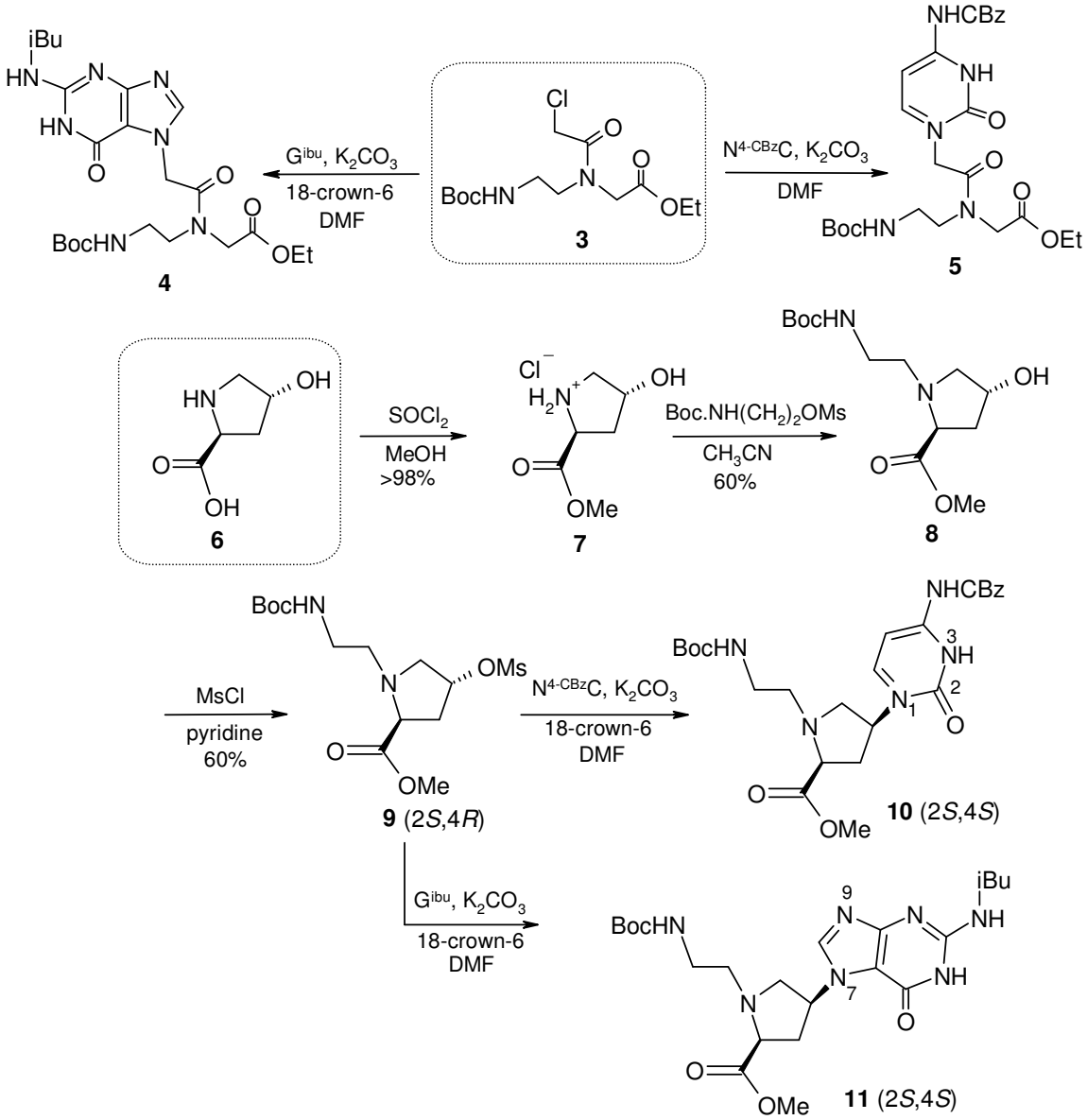

Scheme 2. Synthesis of protected monomeric units.

3.4.2b 1-(N-Boc-aminoethyl)-4(S)-(N^2-isobutyrylguanin-7-yl)-2(S)-proline methyl ester[28] (11). The guanine N7-substituted (2*S*,4*S*) derivative **11** was prepared from 4(*R*)-hydroxy-2(*S*)-proline (**6**) by a similar set of reactions as in Scheme 2, involving a single inversion step. These comprised esterification of the carboxylic acid function, alkylation of the pyrrolidine ring nitrogen, followed by the treatment with mesyl chloride in pyridine to get the 1-(*N*-Boc-aminoethyl)-4(*R*)-*O*-mesyl-2(*S*)-proline methyl ester. This mesylate (**9**) was stirred with N^2-isobutyrylguanine and anhydrous K_2CO_3 in dry DMF, when the 1-(*N*-Boc-aminoethyl)-4(*S*)-(N^2-isobutyrylguanin-7-yl)-2(*S*)-proline methyl ester was obtained as the major product (Scheme 2). The reaction is an S_N2 displacement, which yields the product with inverted stereochemistry at the C4 stereocenter. The more polar 1-(*N*-Boc-aminoethyl)-4(*S*)-(N^2-isobutyrylguanin-9-yl)-2(*S*)-proline methyl ester (not shown) was also isolated as the minor product. The ^{1}H NMR spectrum of **11** showed a downfield shift in the resonance of the H4 proton in from δ5.20 to δ5.65. These two products differed in the ^{1}H NMR spectra mainly in their guanine H8 resonances, *viz*. δ8.40 and δ8.10 in the *N*7- and *N*9-substituted products respectively. Thus, the (2*S*,4*S*) product (**11**) was synthesized from the starting (2*S*,4*R*) hydroxy proline **6** in four steps.

3.4.3. Hydrolysis of Esters

Solid phase synthesis of *aeg*PNA and *aep*PNA requires N-protected free carboxylic acids. Towards this, the methyl ester groups of these PNA monomers were subjected to saponification by sodium hydroxide in a water-methanol mixture to yield the corresponding carboxylic acids (Figure 9).

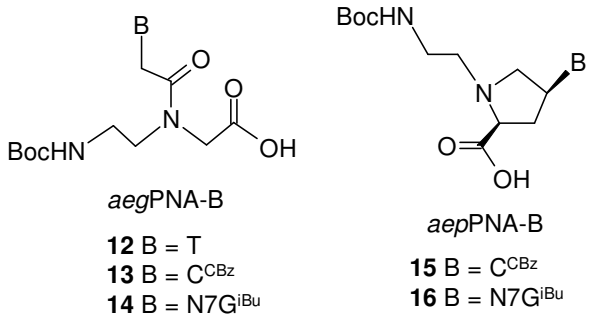

Figure 9. *aeg- aep*PNA monomeric units used in the synthesis of bisPNAs.

3.4.4. Synthesis of Linker

The tetraethylene glycol linker **22** that can be used on-line in PNA synthesis was synthesized according to Scheme 3. Tetraethylene glycol **17** was monotosylated[31] using *p*-toluene sulfonyl chloride, which in its ^{1}H NMR spectrum showed signals in the aromatic region integrating for 10H (Ar-H, tosyl). The resulting monotosylate **18** was treated with sodium azide in DMF to obtain the azide-alcohol **19**. A characteristic peak appearing at 2106 cm^{-1} in the IR spectrum of **19** and the disappearance of aromatic signals corresponding to the tosylate group confirmed the formation of

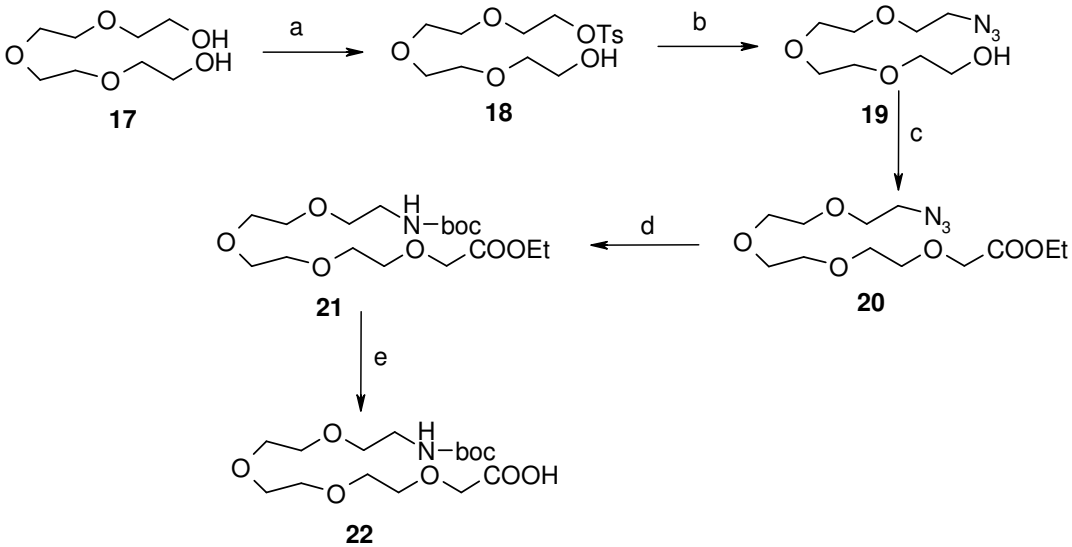

Scheme 3. a) *P*TsCl, NaOH, THF, Water, 0^{0}C, 3 hr. b) NaN_3, DMF, 60^{0}C, 5hr. c) Br-CH_2-COOEt, NaH, DMF, 16hr. d) Ra/Ni, H_2, 40psi, EtOAc, $(Boc)_2O$. e) NaOH (1M), MeOH.

azide. Then this was *O*-alkylated with ethyl bromoacetate using sodium hydride to obtain the ester **20**. A characteristic peak appearing at δ 4.2 in the ^{1}H NMR spectrum for CH_2 of ethyl ester confirmed the formation of **20**. A hydrogenation of $-N_3$ to $-NH_2$ and its simultaneous protection with *t*-Boc was achieved by subjecting compound **20** to pressure hydrogenation for 1 ½ hr in the presence of Raney-Ni/ di-*tert*-butyldicarbonate to give compound **21**. In the ^{1}H NMR of **21**, a peak for 9H appeared at δ 1.5 (*t*-Boc). It was then hydrolyzed to acid **22**.

3.4.5. Design and Synthesis of Hairpin bisPNA Oligomers

The hairpin PNA sequences were designed as shown in the Figure 8. The *aeg*/*aep*PNA-N7G units are present in the arm A of the hairpin and bind to DNA **27** and DNA **28** in the parallel and antiparallel orientations respectively. Thus, arm B of the hairpin binds to DNA **27** and DNA **28** in the antiparallel and parallel orientations respectively. The PNA and DNA oligomers utilized in this study are listed in Tables 1 and 2 respectively.

Figure 10. Design of hairpin bisPNAs.

Table 2. Hairpin bisPNA Oligomer Sequences.

PNA	Sequence Composition
23	H- TTTCTCT -TEG-TEG- TCTCTTT -NH-$(CH_2)_2$-COOH
24	H- TTT c T c T –TEG-TEG- TCTCTTT -NH-$(CH_2)_2$-COOH
25	H- TTT^{7}GT^{7}GT –TEG-TEG- TCTCTTT -NH-$(CH_2)_2$-COOH
26	H- TTT^{7}gT^{7}gT –TEG-TEG- TCTCTTT -NH-$(CH_2)_2$-COOH

T/C/7G = *aeg*PNA-T/C/7G; c/^{7}g = *aep*PNA-C/N7G

Table 3. DNA Oligonucleotide Sequences,

DNA	Oligomer Sequences 5' → 3'	
27	G C A A A G A G A C T	antiparallel DNA
28	T C A G A G A A A C G	parallel DNA
29	A G T C T C T T T G C	DNA complementary to **27** for duplexation
30	C G T T T C T C T G A	DNA complementary to **28** for duplexation

The PNA oligomers were synthesized utilizing the Boc-protection strategy as outlined in Chapter 2. Each coupling cycle involving the deprotection, neutralization and coupling steps was monitored for completion by the Kaiser's test. Tetraethylene glycol linker loop was also coupled using the same procedure employing HBTU, HOBt and diisopropylethylamine as the coupling agents. Merrifield resin derivatized with β-alanine was used as the solid support.

The oligomer synthesis was carried out in a single assembly starting from the first arm (arm B) of the hairpin, the neutral linker loop and the first thymine residue of the second arm (arm A) of the hairpin. At this stage, the resin was partitioned into four portions. The four portions were extended separately to include the *aeg*PNA-C, *aeg*PNA-N7G, *aep*PNA-C and *aep*PNA-N7G monomers respectively at the positions

shown in Figure 8, followed by completion of the synthesis with the other *aeg*PNA monomers.

3.4.6. Cleavage from the Solid Support

The PNA oligomers were cleaved from the solid support using TFMSA[32] to yield oligomers with free 'C' terminal carboxylic acids. During this process, the cytosine exocyclic amino protecting groups, *viz*. the benzyloxycarbamate are cleaved liberating the amine. However, the N^2-isobutyryl groups of the N7-guanine units are left intact and had to be additionally subjected to treatment with aqueous ammonia at 55^{o}C for 16h, or treated with ethylenediamine:ethanol mixture for 20h before cleavage reaction to achieve complete removal of exocyclic amino group protection.

3.4.7. Purification

The fully deprotected oligomers were initially desalted by size-exclusion chromatography over G25 Sephadex. They were subsequently purified by FPLC on a reverse phase C8 column using an ascending gradient of acetonitrile in water containing 0.1% TFA. The purity of the oligomers was re-checked by reverse phase HPLC on a C18 column and confirmed by MALDI-TOF mass spectrometry. Some representative HPLC profiles and mass spectra are shown in above Figures 9 and 10 respectively.

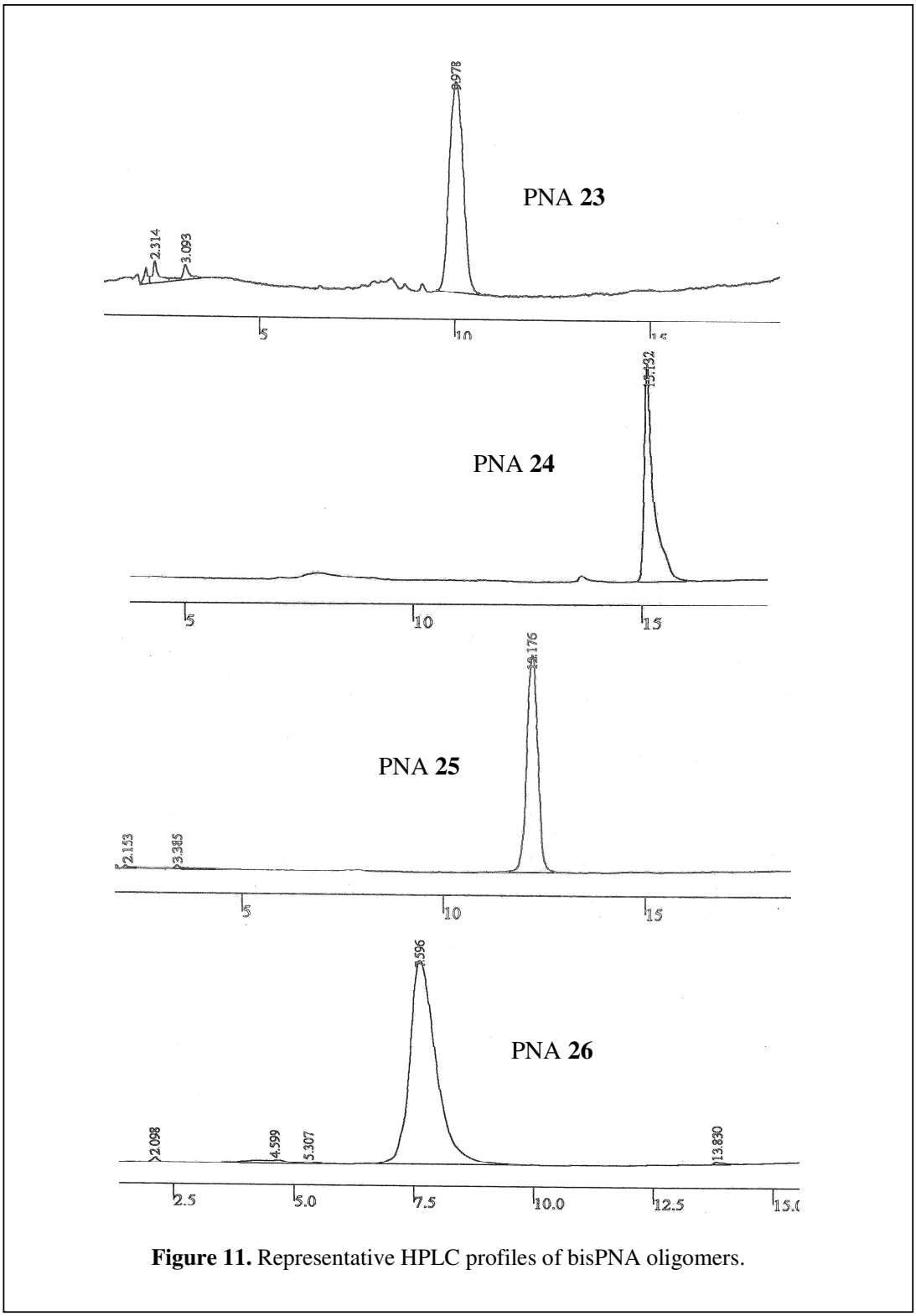

Figure 11. Representative HPLC profiles of bisPNA oligomers.

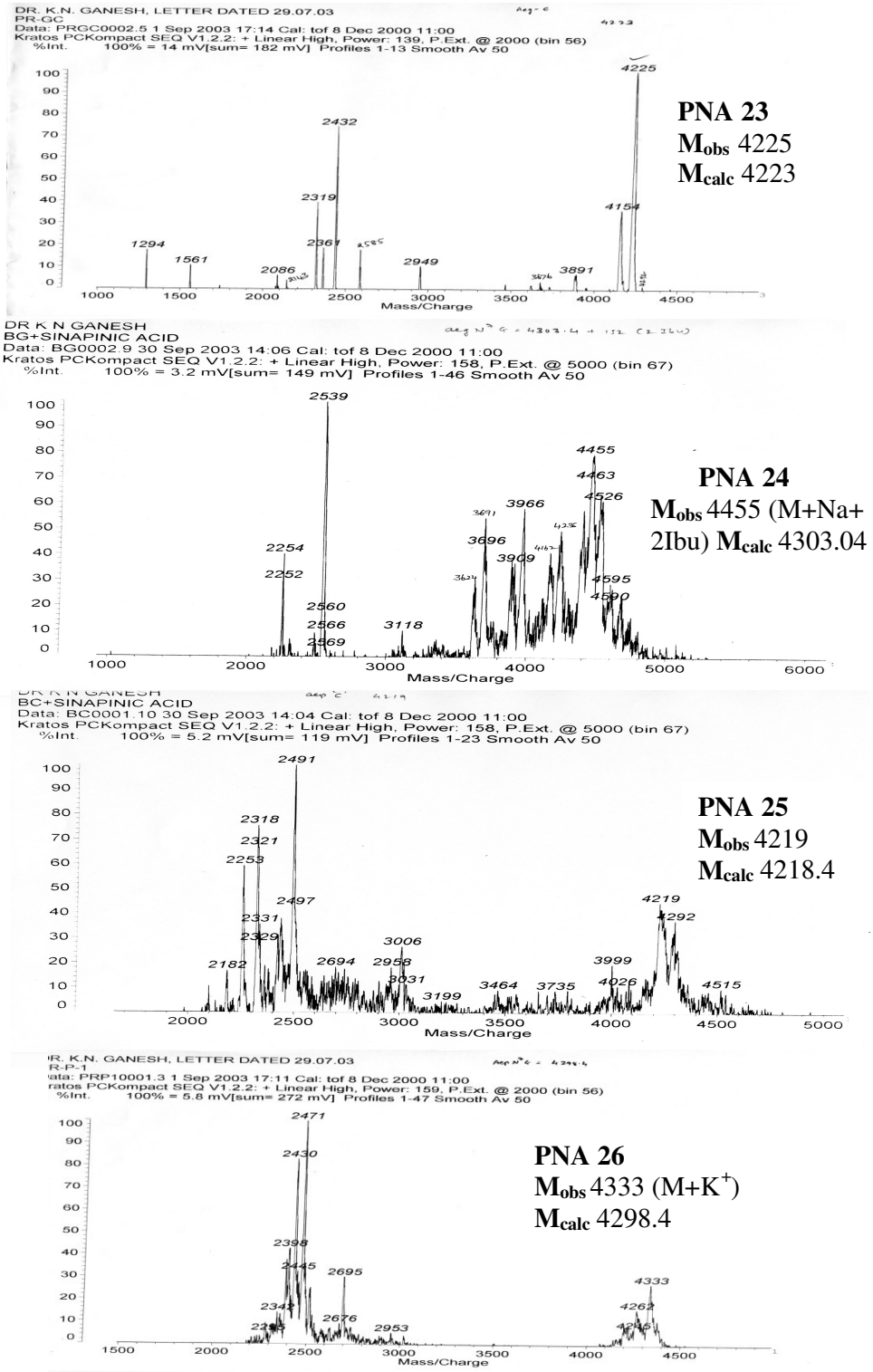

Figure 12. MALDI-TOF spectra of representative bisPNA oligomers.

3.4.8. UV-Melting

The hairpin PNA sequences **23**-**26** were mixed with the appropriate DNA oligomer **27** or **28** in equimolar concentration and annealed prior to melting. The samples were heated at a rate of 0.5°C rise per minute and the absorbance at 260nm was recorded at every minute. The percent hyperchromicity at 260nm was plotted as a function of temperature and the melting temperature was deduced from the peak in the first derivative plots.

3.4.9. Fluorescence: Strand Invasion Assay

The bisPNA oligomers **23-26** are appropriate to study the strand invasion properties by triplex formation when targeted towards duplex DNA. Ethidium bromide upon intercalation into a DNA duplex (**27:29** or **28:30**) shows increase in fluorescence intensity but is known not to interact with PNA_2:DNA or PNA:PNA complexes.[28,33] Strand invasion of the duplex DNA saturated with ethidium bromide by triplex-forming PNA oligomer should therefore cause a decrease in ethidium bromide fluorescence due to the disruption of DNA duplex-ethidium bromide complexation. The loss of ethidium bromide fluorescence as a function of time upon addition of triplex forming PNA oligomers may be used to study the kinetics of duplex strand invasion in this fluorescent intercalator displacement assay (Figure 13).

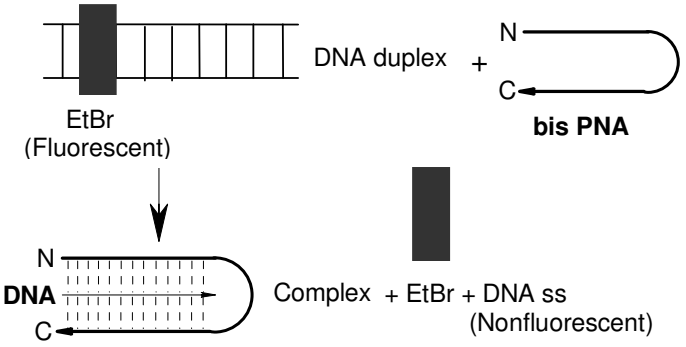

Figure 13. Principle of fluorescence assay for strand invasion.

3.4.10. Gel Electrophoresis

Electrophoretic gel shift assay was used to establish the electrophoretic mobility of a DNA fragment in a native polyacrylamide gel, which is resulted in the presence of a PNA strand displacement complex. The bisPNAs were individually treated with dsDNA and the complexation was monitored by nondenaturing gel electrophoresis at 10°C. The spots were visualized on a fluorescent TLC background. The formation of bisPNA:DNA triplexes is accompanied by displacing one strand of dsDNA and appearance of a lower migrating band due to bisPNA:DNA complexes.

3.5. RESULTS AND DISCUSSION

3.5.1. UV-T_m Studies on Hairpin PNA-DNA Triplexes

The UV-T_m values of the complexes of the bisPNAs with the complementary DNA strands are detailed in Table 4.

Table 4. UV-T_m of bisPNA-DNA complexes.[a]

Entry	**PNA**	DNA **27** (*p*)			DNA**28** (*ap*)		
		pH 7.3	*pH 5.8*	Δ *pH*	*pH 7.3*	*pH 5.8*	Δ *pH*
1	**23**, *aeg*PNA-C	21	29	+8	27 (6)	42 (13)	+15
2	**24**, *aeg*PNA-N7G	32	29	-3	44 (12)	41 (12)	-3
3	**25**, *aep*PNA-C	23	49	+26	42 (19)	52 (3)	+10
4	**26**, *aep*PNA-N7G	38	30	-8	41 (3)	44 (14)	+3

[a] UV T_m data (°C) for PNA:DNA complexes with DNA **27** and **28**. Experiments were performed in 10 mM sodium phosphate buffer, pH 7.3 and 5.8. T_m values are accurate to ±1°C and were obtained from peaks in the first derivative plots of percent hyperchromicity vs temperature. Each experiment was repeated at least twice. Values in brackets ΔT_m (*ap-p*).

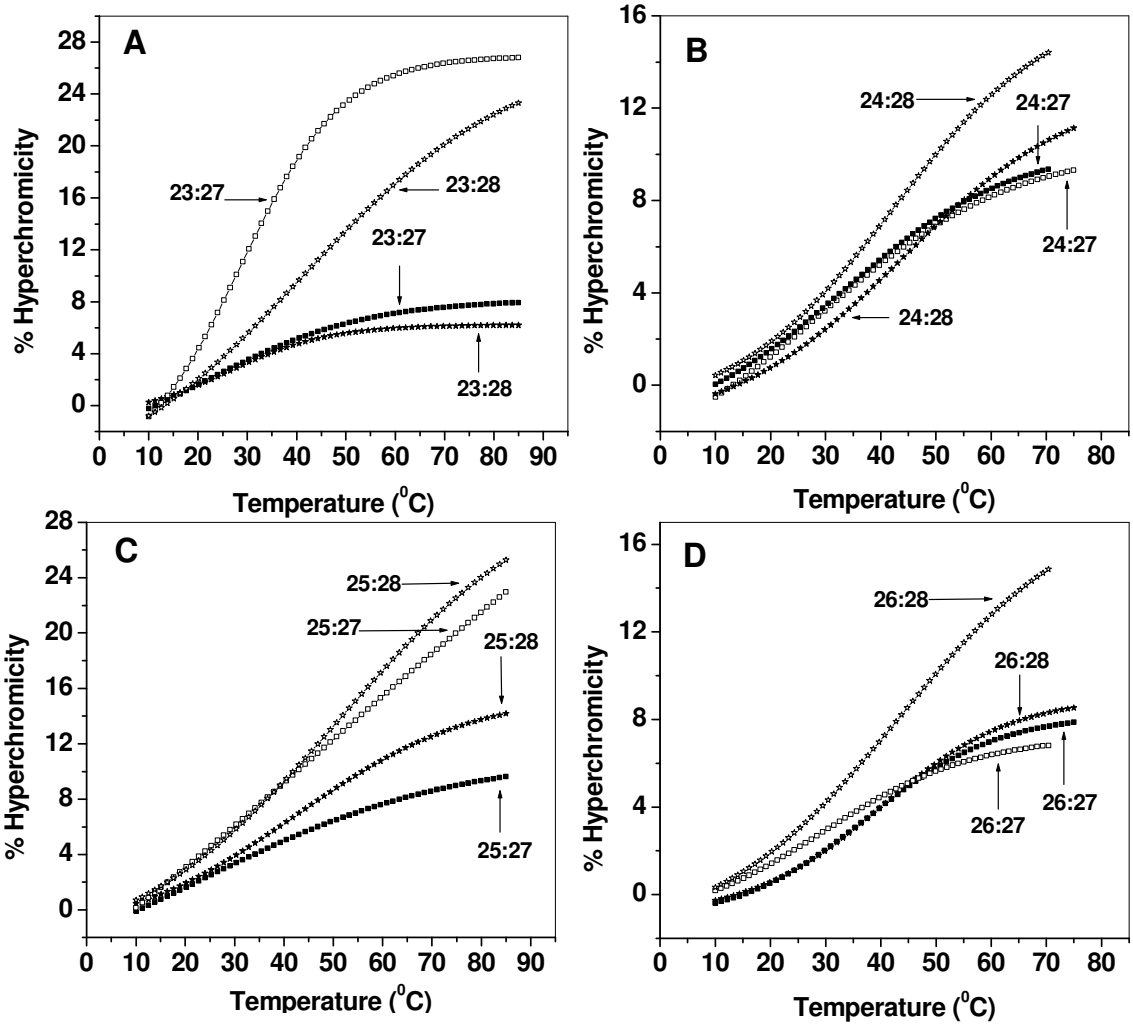

Figure 14. UV-T_m plots of the bisPNA:DNA complexes exhibiting the binding orientation bias with (**A**) *aeg*PNA-C (**B**) *aeg*PNA-N7G (**C**) *aep*PNA-C (**D**) *aep*PNA-N7G and the pH (in)dependence at pH 5.8 (□,■) and 7.4 (✡,✶).

The oligodeoxynucleotides **27** and **28**, identical in sequence but reversed in 5'-3' direction, were used to probe the parallel/antiparallel binding preferences, studied by UV melting experiments at pH 5.8 and 7.4. The control bisPNA **23** having *aeg*PNA-C units as X in arm A binds to either DNA **27** or DNA **28** but only with little different affinity (~21°C & 27°C respectively) at pH 7.3 (entry 1, Table 4). At acidic pH 5.8, a higher *T*m (~42°C) was seen with DNA **28** as expected from N3 protonation of cytosine. This protonation could be on 'C' located either in arm A or arm B of

bisPNA **23** (or both), with the protonated form leading to HG and the non protonated form leading to WC mode of recognition in either orientations (Figure 14). (The protonation of terminal, non-hydrogen bonded 'C' in DNA **27** and **28** does not affect the binding or recognition event). In *aeg*PNA **23,** the two arms of PNA are distinguished slightly in terms of binding in the WC or HG mode at pH 5.8, with DNA **28** binding better than DNA **27** (entry 1).

The replacement of *aeg*PNA-C at X in arm A by the C+ mimic *aeg*PNA-N7G (PNA **24**) also gave complexes of different stabilities (entry 2, Table 4) with the target DNA strands **27** and **28**. At both pHs, a dominant preference for antiparallel orientation of arm A as in complex **24**:**28** was observed compared to the parallel orientation of arm A as in complex **24**:**27** (ΔT_m ~12°C) at pH 7.3 (Figure 5d). Thus the donor-acceptor H-bonding sites of N7G are capable of recognizing G in the HG *ap*-mode with neutral linker, unlike the positively charged linker (Figure 15). However at acidic pH, a slight destabilization was seen suggesting that 'C' protonation is not favourable.

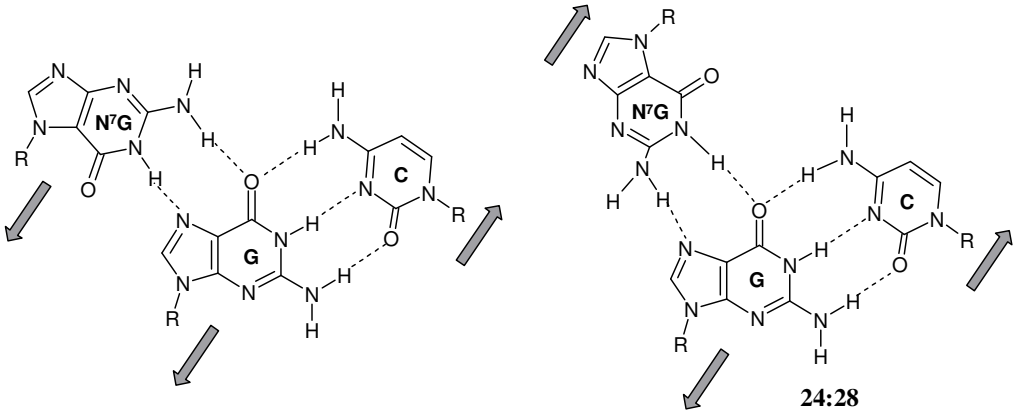

Figure 15. N7G third strand binding in the parallel and antiparallel HG modes.

In contrast to the achiral *aeg*PNA units, introduction of a chiral *aep*PNA-C unit as X in arm A in **25** leads to a stronger binding at pH 7.3 with DNA **28** (T_m ~42°C) as compared to binding with DNA **27** (T_m ~ 23°C) (entry 3, Table 4). This suggests a considerable bias (ΔT_m ~19°C) in the antiparallel DNA binding orientation induced by the chiral *aep* unit. At acidic pH (5.8), the stability was further enhanced in case of both DNA **27** and **28**, as expected from the protonation of N3 in C [$\Delta T_m(\Delta pH)$ ~26°C and ~10°C respectively]. These results indicate that the chiral *aep*PNA-C units in **25** stabilize the PNA:DNA (**25:28**) complex when present in the PNA strand (arm A) oriented antiparallel to the central DNA strand.

PNA **26** containing the chiral *aep*PNA-N7G unit as X in arm A also exhibited a slightly antiparallel preference to bind DNA **28** over parallel DNA **27** at neutral pH conditions (entry 4, Table 4, ΔT_m ~3°C) with more relative stability at acidic pH 5.8 (ΔT_m +11°C). In this case, *aep*PNA-N7G in arm A can bind only in the parallel HG mode (Figure 5d) and as expected, PNA **26:**DNA **28** binding has much lower pH-dependence as compared to *aep*PNA-C **25**: DNA **28** binding. The overall results suggest that hairpin bisPNAs bind to DNA **28** better than DNA **27.**

Thus from UV-T_m we can summarize that ΔpH is more for PNA-C, particularly for *aep*PNA C. As ΔpH is less for PNA-N7G, confirms the pH independence of N7G. In all bisPNAs the preferred binding is *ap* HG and *p* WC at both pH. It means *p* WC is preferred over *ap* WC except for PNA **24**. (at acidic pH)

The pK_a's of cytosine N3 in *aeg*PNA-C (6.91) and *aep*PNA-C (6.81) (Figure 16) were not very different, inspite of the possible protonation of the pyrrolidine ring nitrogen in the *aep*PNA-C at physiological pH, although these were significantly higher than that of N3-C in cytidine (4.34).

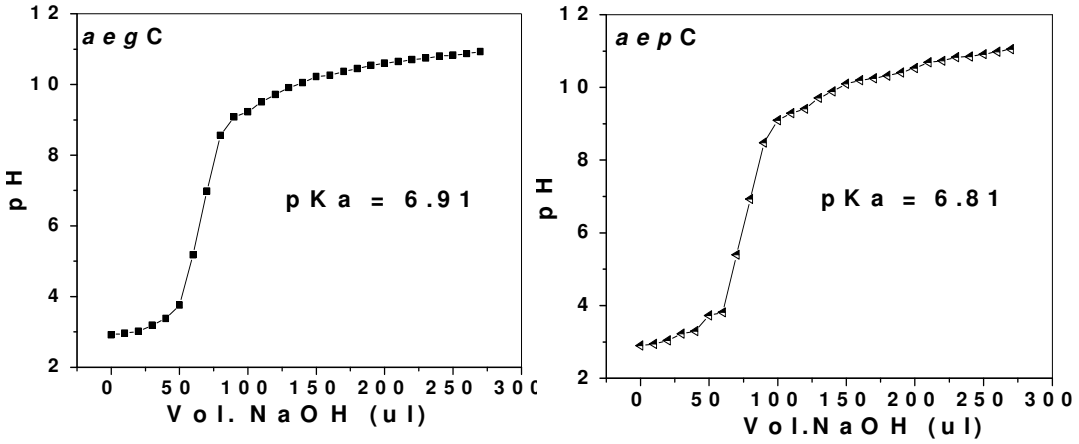

Figure 16. pH Titration of *aeg*C and *aep*C monomers.

3.5.2. Fluorescence Assay for Strand Invasion

The bisPNA oligomers reported in this chapter are appropriate to study the strand invasion properties by triplex formation when targeted towards duplex DNA (Figure 13). We studied the effects of nucleobase and backbone modifications of bisPNAs synthesized here, on the kinetics of strand invasion of both complementary DNA duplex **27:29** and **28:30** by ethidium bromide displacement assay. Thus, after strand invasion, arm A of the bisPNA hairpin having *aeg*/*aep*PNA-N7G binds to DNA **27** and DNA **28** in the parallel and antiparallel orientations respectively.

This study should permit delineation of the effects of chiral, positively charged *aep*PNA backbone with respect to C^+ and the C^+ mimic-N7G unit. [In our earlier studies with bisPNAs containing cationic peptide linker, we noticed that the strand invasion is slower and incomplete in case of *aeg*PNA-N7G and *aep*PNAs at ambient temperature. These effects seems to arise due to conformational distortions induced in the PNA backbone by *aep* chiral monomer units and due to presence of a purine base in a pyrimidine rich strand.] The set of DNA and PNA oligomers for this study comprised DNA duplex **27:29, 28:30** and PNA oligomers **23, 24, 25** and **26**.

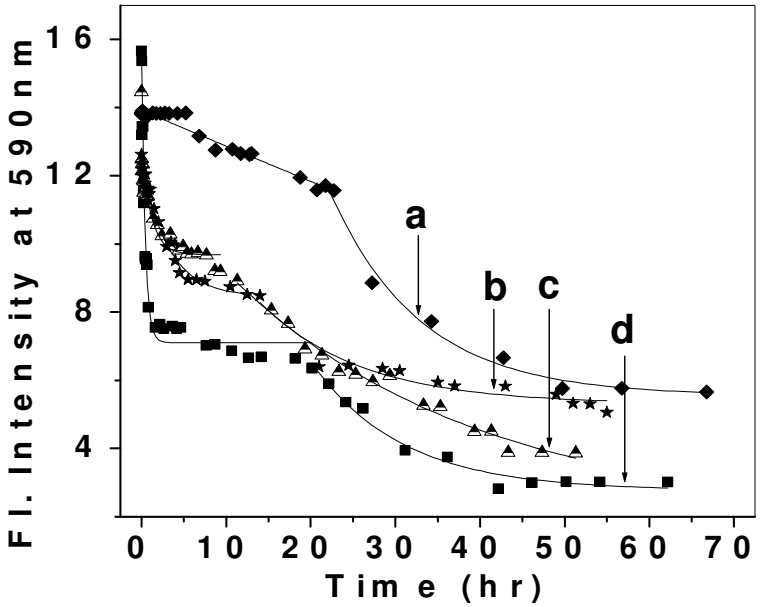

Figure 17. Ethidium bromide fluorescence as a function of time studied for the DNA duplex **27**:**29** after the addition of PNA **23** (d); PNA **24** (b); PNA **25** (c) and PNA **26** (a) at pH 7.3.

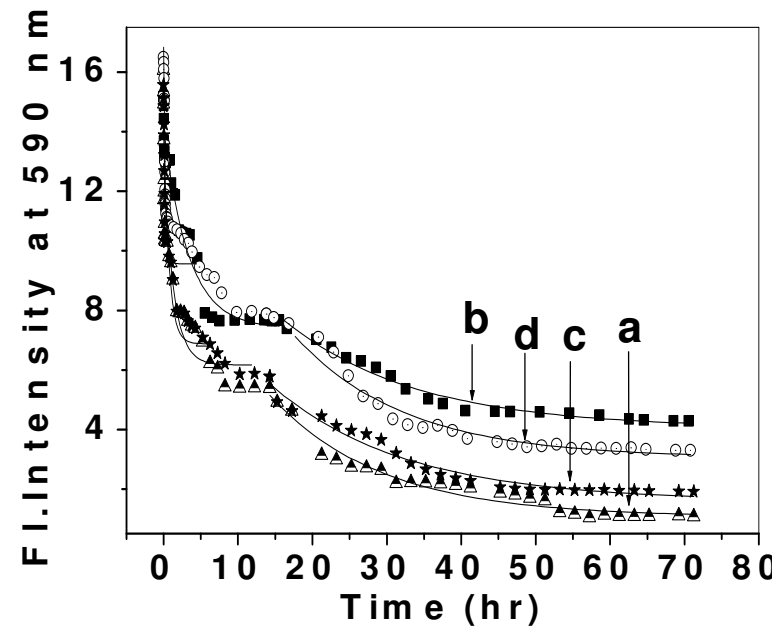

Figure 18. Ethidium bromide fluorescence as a function of time studied for the DNA duplex **28**:**30** after the addition of PNA **23** (a); PNA **24** (b); PNA **25** (c) and PNA **25** (d) at pH 7.3.

The DNA duplexes **27**:**29** and **28:30** were separately saturated with ethidium bromide and the kinetics of the strand invasion process was examined by monitoring the fluorescence emission decay at 590nm (λ_{ex} 490nm) as a function of time after individually adding the four PNAs **23-26** for over 60 hours. The emission intensity monitored in each case over 60h showed exponential decrease at different rates followed by reaching a plateau (Figure 17 and 18).

Table 5. Decay constants for **27:29** duplex invasion by bisPNAs[b]

PNA	T1	T2
23	0.43017	10.64208
24	3.22782	11.89339
25	1.18162	28.78645
26	1.84498	10.62524

[b]Decay constants obtained from figure 17 where results were subjected to Non-linear curve fit: exponential decay 2 in Microcal origin 6.1.

Table 6. Decay constants for **28:30** duplex invasion by bisPNAs[b]

PNA	T1	T2
23	1.36116	14.89386
24	3.33942	17.62497
25	0.74143	17.88327
26	0.22541	14.85553

[b]Decay constants obtained from figure 18 where results were subjected to Non-linear curve fit: exponential decay 2 in Microcal origin 6.1

Interestingly the decay profiles of polyoxyethylene bisPNAs was not monophasic, but could be fitted into biexponential decay. The data in Table 5 and 6 shows the two decay constants T_1 and T_2 computed from the data of Figure 17 and 18 respectively. This is in contrast to the results from cationic peptide linker (Figure 19[28]) wherein the decay profile was monophasic. This suggests that the DNA duplex

invasion by polyoxyethylene-linked *aeg*-bisPNA occurs in two steps in contrast to a single step process observed for cationic peptide linked bisPNA.

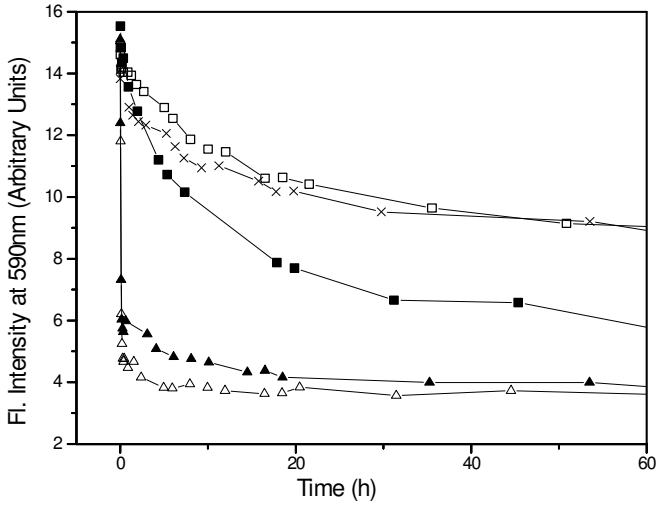

Figure 19[28]. Ethidium bromide fluorescence as a function of time studied for the DNA duplex **27**:**29** after the addition of PNA **23** at pH 5.8 (-Δ-); PNA **23** at pH 7.4 (-▲-); PNA **25** at pH 5.8 (-■-); PNA **26** at pH 7.4 (-□-) and PNA **24** at pH 7.4 (-✕-).

The data in Table 5 indicates that step 1 is fastest with *aeg*-bisPNA-C **23** while slowest for *aeg*-bisPNA-N7G **24**, with intermediate rates for *aep*PNAs **25** and **26**; step 2 is slowest in case of *aep*-bisPNA-C, with other PNAs having similar rates. While the data in Table 6 indicates that step 1 is fastest with *aep*-bisPNA-N7G **26** while slowest for *aeg*-bisPNA-N7G **24**, with intermediate rates for PNAs **23** and **25**; step 2 is having similar decay rates in case of all PNAs. The kinetics follows an order completely different from that seen according to T_m. Thus the thermal stability of bisPNA:DNA duplexes are delinked from their rate of association/dissociation. The faster rates of invasion seen in cationic linker bisPNA may presumably partly due to the electrostatic effects due to the linker, which may repel the ethidium bromide that has positive charges.

In literature, two plausible routes for the strand invasion reaction have been postulated[34,35,36] According to one mechanism, the first stage consists of a fluctuating opening of the DNA double helix and a transient formation of a PNA-DNA Watson-Crick duplex (WC-first mechanism). The second mechanism envisages formation of an unstable PNA-$[DNA]_2$ triplex via Hoogsteen pairing (HG-first mechanism), followed by dissociation of duplex to form PNA_2:DNA triplex. The final result is the same for both mechanisms and the unstable intermediates are very difficult to detect. By using pH dependent gel mobility shift analysis, it was recently demonstrated[35] that at neutral pH, C-containing PNAs undergo strand invasion via the HG-first mechanism (Figure 20).

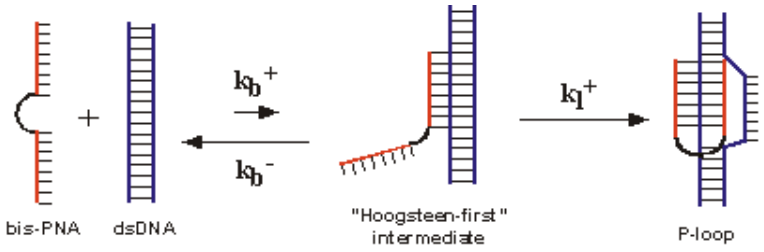

Figure 20. Proposed Hoogsteen-first mechanism at strand invasion of homopyrimidine bisPNAs into dsDNA.

Our present results based on fluorescence assay gives a direct and strong support for a two-step process, as seen by the presence of biexponential decay constants. The first, kinetically faster process has decay constant T1 in the range 0.2-3.4h while the second slower process has the decay constant T2 in the range 10.6 to 28.7h. Compared to *aeg*-bisPNA **23**, the *aep*-bisPNAs show three times lower T1, perhaps due to the presence of rigid pyrrolidine ring as part of the backbone, which sterically slows down the initial binding of the PNA to DNA duplex. The PNA **24** having *aeg*-PNA-N7G was the slowest, due to energy barrier in interconversion of

syn-anti rotamers in attaining hybridization competent conformation. The *aep*-PNA-N7G monomers having the base directly linked to the rings in PNA **25** and **26** lack such rotamers. The second step of base pair formation is inordinately slow in case of *aep*-bisPNA-C **25,** for which the reasons are not obviously clear from present experiments.

In the first step, DNA **27/28** should form HG pairing with arm A of bisPNAs **23**-**26** in a parallel binding motif while the second step leads to formation of WC pairing in antiparallel fashion. For the duplex invasion of **28:30** by bisPNAs, it was noticed that the *aep*PNAs exhibit faster kinetics for first step, which also leads to more stable hybrids. In these cases first HG-mechanism gives rise to antiparallel binding with DNA duplex, which appears to be a faster process than parallel binding observed in case of **27:29** DNA duplex. Thus our results seem to delineate the invasion process by parallel/antiparallel binding, with the latter being more favourable.

3.5.3. Gel Shift Assays: Competition Binding Experiments

The results of competition binding experiments carried out by adding bis-PNAs to the DNA duplex (**27/29** or **28/30**) followed by annealing and complexation was monitored by non-denaturing gel electrophoresis at 10°C is shown in Figure 21 and 22. Due to a higher binding affinity of bis-PNA:DNA complexes compared with DNA:DNA complexes, the added bisPNA binds to the complementary DNA **27/28** in the DNA triplex, releasing the DNA strand **29/30**. This is clearly seen in the gel electrophoresis in which the DNA complex band (Figure 21, lane 7) is converted into a bisPNA:DNA complex seen as a retarded band and the released DNA strand (Figure 21, lane 1-2, 4-5 and Figure 22, lane 1-3) seen as a faster moving band. The results

indicate that the bisPNAs do successfully compete for binding with the complementary DNA strand.

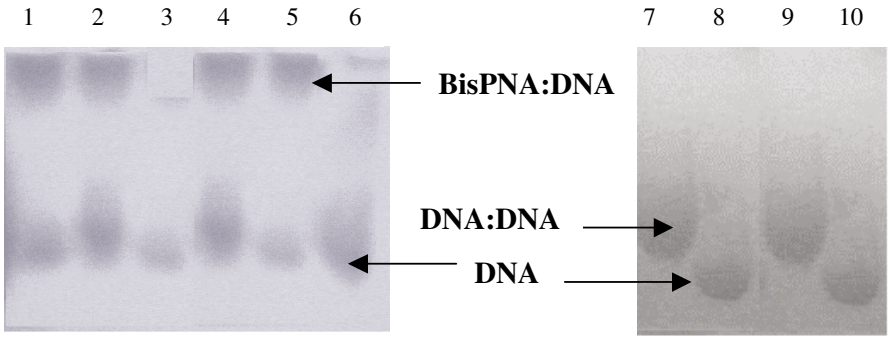

Figure 21. 15% Polyacrylamide Gel Electrophoresis of bisPNA:DNA complexes.

Lane **1**: PNA **23** + DNA **27:29**
Lane **2**: PNA **23** + DNA **28**:**30**
Lane **3**: DNA **29** single strand
Lane **4**: PNA **25** + DNA **27:29**
Lane **5**: PNA **25** + DNA **28**:**30**
Lane **6**: DNA **30** single strand
Lane **7**: DNA **27:29** duplex
Lane **8**: DNA **29** single strand
Lane **9**: DNA **28**:**30** duplex
Lane **10**: DNA **30** single strand

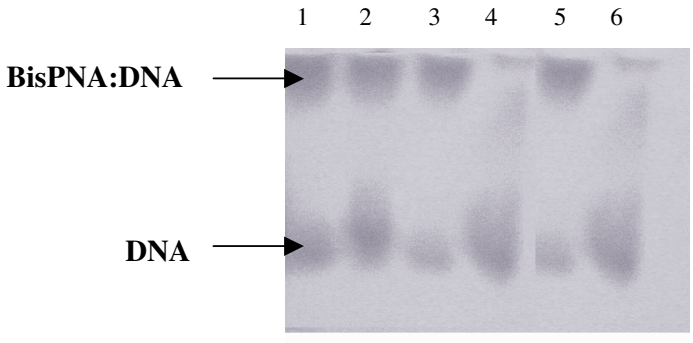

Figure 22. 15% Polyacrylamide Gel Electrophoresis of bisPNA:DNA complexes.

Lane **1**: PNA **24** + DNA **27**:**29**
Lane **2**: PNA **24** + DNA **28**:**30**
Lane **3**: PNA **26** + DNA **27**:**29**
Lane **4**: DNA **29** single strand
Lane **5**: PNA **26** + DNA **28**:**30**
Lane **6**: DNA **30** single strand

3.6. CONCLUSIONS

The N7-guanine nucleobase and neutral TEG linker has been successfully incorporated into PNA using simple chemistry and solid phase peptide synthesis. It has proved to be a good C^+ mimetic at neutral and acidic pH, with difference in T_m being observed with DNA **27** and DNA **28**. The overall results suggest that bisPNAs bind better to DNA **28** than DNA **27**. Thus, triplex formation is pH-dependent when *aeg*/*aep*PNA-C units are used, while *aeg*/*aep*PNA-N7G units permit triplex formation at physiological pH as well as at acidic pH.

In addition, the introduction of *aep*PNA C units in the backbone of the hairpin bisPNAs, which form triplexes, strongly influenced the recognition of DNA in an orientation selective manner. The more stable complexes were formed when the arm A was antiparallel to the central strand.

3.7. EXPERIMENTAL

The synthesis of the *aeg*PNA-T/C monomers was carried out according to the procedures described in Chapter 2.

N^2-isobutyrylguanine[29] (1)

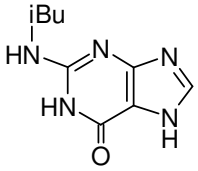

To an ice-cold stirred solution of guanine (1.0g, 6.6mmol) in dry DMF (10ml) and triethyl amine (1.0ml, 3.5mmol) was added dropwise isobutyryl chloride (0.1ml, 6.4mmol). Reaction mixture as heated at 85^0C and stirred for 3h. The solvent was evaporated under vacuum. The residue was precipitated out in boiling isopropanol, filtered and dried to yield the product **1** (0.9g, 61.2% yield).

1-(N-Boc-aminoethyl)-4-(R)-hydroxy-2-(S)-proline methyl ester[28] (8)

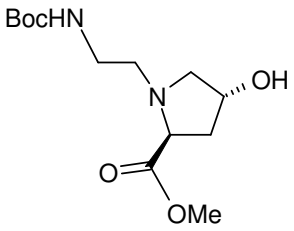

A mixture of 4-(*R*)-hydroxy-2-(*S*)-proline methyl ester hydrochloride **7** (4.0g, 22.1mmol), 2-(*N*-Boc)-aminoethyl-mesylate (chapter 2) (2.64g, 11.04mmol), diisopropyl-ethylamine (DIPEA) (3.8ml, 22.1mmol) DMAP (0.13g, 1.1mmol) were stirred together in DMF:Acetonitrile (1:1) at room temperature for 24h under argon atmosphere. Then reaction mixture was heated at 50^0C for 2h and again stirred at room temperature for 36h. After completion of reaction as indicated by TLC, solvents were removed *in vacuo*. The crude product was purified by silica gel column chromatography. The pure product **8** was obtained in 54% yield.

^{1}H NMR ($CDCl_3$) δ: 5.25(br s, 1H, N*H*), 4.42(m, 1H, *H*4), 3.69(s, 3H, OCH_3), 3.61(t, 1H, *H*5), 3.38(dd, 1H, *H*5'), 3.15(dd, 2H, Boc-NH-CH_2), 2.77(br m, 4H, *H*2, Boc-NH-CH_2-CH_2, O*H*), 2.50(dd, 1H, *H*3), 2.12(m, 1H, *H*3'), 1.42(s, 9H, C(CH_3)$_3$).

1-(N-Boc-aminoethyl)-4-(R)-O-mesyl-2-(S)-proline methyl ester[28] (9)

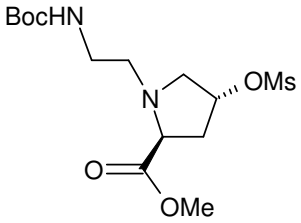

To a stirred ice-cooled solution of 1-(*N*-Boc-aminoethyl)-4-(*R*)-hydroxy-2-(*S*)-proline methyl ester **8** (2.0g, 6.9mmol) in dry DCM (15ml) and triethylamine (1.1ml, 7.6mmol), was added dropwise methane sulphonyl chloride (0.8ml, 10.3mmol). After 2h, upon completion of reaction, more DCM (5 x 15ml) was added to the reaction mixture and washed with water and extracted in DCM. The organic layer was dried over sodium sulphate and concentrated to get the crude product **9**, which was purified by silica gel column chromatography (1.7g, 60% yield).

^{1}H NMR ($CDCl_3$) δ: 5.20(m, 2H, N*H*, *H*4), 3.70(s, 3H, OCH_3), 3.65(t, 1H, *H*5), 3.50(dd, 1H, *H*5'), 3.15(m, 2H, Boc-NH-CH_2), 3.00(s, 3H, SO_2-CH_3), 2.85(dd, 1H, *H*2), 2.75(m, 2H, Boc-NH-CH_2-CH_2), 2.35(m, 2H, *H*3, *H*3'), 1.45(s, 9H, C(CH_3)$_3$).

1-(N-Boc-aminoethyl)-4-(S)-(N^4-benzyloxycarbonyl-cytosin-1-yl)-2-(S)-proline methyl ester[28] (10)

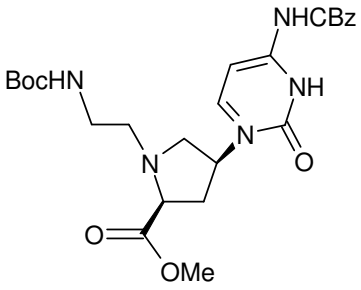

A mixture of 1-(*N*-Boc-aminoethyl)-4-(*R*)-O-mesyl-2-(*S*)-proline methyl ester **9** (1.2g, 3.2mmol), N^4-benzyloxycarbonylcytosine **2** (2.0g, 8.2mmol), anhydrous potassium carbonate (2.2g, 16.4mmol) and 18-crown-6 (0.34g, 1mmol) in anhydrous DMF (6ml) was stirred under nitrogen atmosphere at 70^{o}C for 5h. The solvent was completely removed under vacuum and the residue purified by silica gel column chromatography to get the pure product (0.5g, 30% yield) as the major product.

^{1}H NMR ($CDCl_3$) δ: 8.47(d, 1H, *C-H*6), 7.42(s, 5H, Ph), 7.27(d, 1H, *C-H*5), 5.39(t, 1H, Boc-N*H*), 5.23(s, 3H, Ph-CH_2, *H*4), 3.72(s, 3H, OCH_3), 3.20(br m, 4H, *H*5, *H*5', Boc-NH-CH_2), 2.78(m, 2H, Boc-NH-CH_2-CH_2), 2.59(m, 1H, *H*2), 1.92(m, 2H, *H*3, *H*3'), 1.44(s, 9H, C(CH_3)$_3$).

1-(N-Boc-aminoethyl)-4-(S)-(N^2-isobutyrylguanin-7-yl)-2-(S)-proline methyl ester[28] (11)

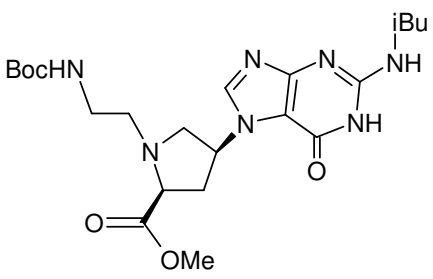

A mixture of 1-(*N*-Boc-aminoethyl)-4-(*R*)-O-mesyl-2-(*S*)-proline methyl ester **9** (0.5g, 1.4mmol), N^2-isobutyrylguanine **1** (0.80g,

3.5mmol), anhydrous potassium carbonate (0.9g, 7.0mmol) and 18-crown-6 (0.25g-0.50g) in dry DMF (5ml) was kept stirring at 80°C for 48h. The solvent was completely removed under vacuum and the pure product obtained (0.28g, 40% yield) after column chromatography.

^{1}H NMR ($CDCl_3$) δ: 12.25 (br s, 1H, *G*-N1*H*), 10.87 (br s, 1H, iBu-N*H*), 8.38 (s, 1H, *G-H*8), 5.63 (m, 1H, *H*4), 5.24 (m, 1H, Boc-N*H*), 3.69 (s, 3H, OCH_3), 3.37 (m, 4H, *H*5, *H*5', Boc-NH-CH_2), 3.21-2.77 (m, 5H, Boc-NH-CH$_2$-CH_2, *H*2, $(CH_3)_2CH$, *H*3), 2.18 (m, 1H, *H*3'), 1.42 (s, 9H, C(CH_3)$_3$), 1.22 (d, 6H, (CH_3)$_2$CH).

^{13}C NMR ($CDCl_3$) δ: 179.6 (*C*OCH(CH_3)$_2$), 173.1 (*C*OOCH_3), 156.4 (G-*C*2), 156.0 (G-*C*4), 153.3 (*C*OOC(CH_3)$_3$), 147.5 (G-*C*6), 142.3 (G-*C*8), 111.5 (G-*C*5), 79.2 (*C*(CH_3)$_3$), 64.7 (*C*H(CH_3)$_2$), 59.5 (*C*4), 57.9 (*C*5), 53.7 (Boc-NH-*C*H$_2$), 52.0 (*C*2), 37.6 (Boc-NH-CH$_2$-*C*H$_2$), 35.9 (*C*3), 28.4 ((*C*H$_3$)$_3$), 19.0 ((*C*H$_3$)$_2$).

N-(Boc-aminoethylglycyl)-(N^2-isobutyryl-N7-guanine)-ethyl ester (4)

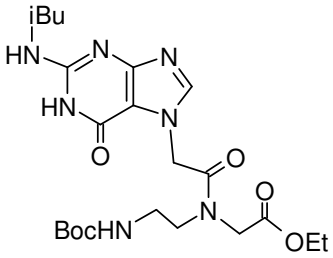

A mixture of N^2-isobutyrylguanine **1** (0.37g, 1.67mmol), K_2CO_3 (0.23g, 1.67mmol) and ethyl *N*-(Boc-aminoethyl)-*N*-(chloroacetyl)-glycinate (Chapter 2) (0.54g, 1.67mmol) were stirred in dry DMF at rt overnight. The reaction mixture was filtered and the filtrate evaporated under reduced pressure. The resulting residue was purified by column chromatography to get the *N*-(Boc-aminoethylglycyl)-(N^2-isobutyryl-N7-guanine) ethyl ester **4** (0.45g, 53% yield).

^{1}H NMR ($CDCl_3$) δ: 12.25 (s, 1H, iBu-N*H*), 10.01 (s, 1H, G-N^1-*H*), 8.11(s, 1H, G-*H*8), 5.80 (m, 1H, Boc-N*H*), 5.40 (maj) & 5.29 (min) (s, 2H, CH_2-G), 4.31 - 4.08 (m, 4H, N-CH_2-COOCH_2CH$_3$), 3.61 (m, 2H, Boc-NH-CH_2), 3.42 (maj) & 3.35 (min) (m,

2H, Boc-NH-CH_2-CH_2), 2.79 (m, 1H, CH(CH_3)$_2$), 1.41 (min) & 1.37 (maj) (s, 9H, (CH_3)$_3$), 1.23 (m, 9H, CH_2CH_3, CH(CH_3)$_2$).

^{13}C NMR ($CDCl_3$) δ: 179.5 (*C*OOCH(CH_3)$_2$), 169.0 (*C*OOEt), 166.6 (G-CH_2-*C*O), 162.3 (G-*C*2), 155.9 (G-*C*4), 153.1 (*C*OOC(CH_3)$_3$), 147.6 (G-*C*6), 144.6 (G-*C*8), 112.0 (G-*C*5), 79.5 (*C*(CH_3)$_3$), 61.3 (*C*H(CH_3)$_2$), 48.8 (N-*C*H_2-COOEt), 46.7 (O*C*H_2CH_3), 38.4 (Boc-NH-*C*H_2), 35.8 (Boc-NH-CH_2-*C*H_2), 28.1 ((*C*H_3)$_3$), 18.7 ((*C*H_3)$_2$), 13.8 (CH_2*C*H_3).

Hydrolysis of the PNA ethyl ester monomers

General method

The ethyl esters were hydrolyzed using 2M aqueous NaOH (5ml) in methanol (5ml) and the resulting acid was neutralized with activated Dowex-H^+ till the pH of the solution was 7.0. The resin was removed by filtration and the filtrate was concentrated to obtain the resulting Boc-protected acid (**4-5** & **10-11**) in excellent yield (>85%).

2-{2-[2-(2-hydroxyethoxy)ethoxy]ethoxy}ethyl 4-methylbenzenesulfonate[31] (18)

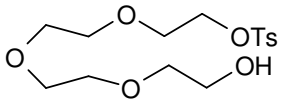

A solution of sodium hydroxide (2.74g, 68.5 mmol) in water (15ml) was added to a mixture of tetraethyleneglycol (**17**) (87.8g, 452mmol) and THF (15ml). After the mixture had cooled down to 0^0C, a solution of toluene *p*-sulfonyl chloride (8.3g, 43.7mmol) in THF (50ml) was added with stirring over 1h. After stirring at 0^0C for 2h, the reaction mixture was poured into an ice-water (250ml). The organic layer was separated, and the aqueous layer was extracted with CH_2Cl_2 (3 x 100ml). The combined organic layers were washed twice

with water (50ml). Drying of the organic layer and evaporation of the solvent under reduced pressure afforded (13.74g, 90% yield with reference to tosyl chloride) of clear oil **18**.

^{1}H NMR ($CDCl_3$) δ: 7.86-7.76 (d, 2H), 7.35-7.31 (d, 2H), 4.17-4.12 (m, 2H), 3.70-3.58 (m, 14H), 2.43 (s, 3H).

2-{2-[2-(2-azidoethoxy)ethoxy]ethoxy}ethanol (19)

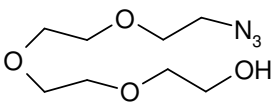

Monotosylate **18** (5g, 14.4mmol) was taken in dry DMF (50ml) and sodium azide (4.67g, 71.85mmol) was added into it. The raction mixture was heated at 60^{0}C with stirring for 5hr. The solvent was removed under vacuum; the residue was taken in water and extracted with CH_2Cl_2 (3 x 50ml). The pooled organic extracts were washed with water and brine. Drying of the organic layer and evaporation of the solvent under reduced pressure afforded azide **19** (2.70g, 87% yield).

^{1}H NMR ($CDCl_3$) δ: 3.69-3.46 (m, 14H), 3.39-3.36 (t, 2H).

^{13}C NMR ($CDCl_3$) δ: 71.41, 69.43, 68.77, 60.28, 59.76, 49.47.

IR ($CHCl_3$) cm^{-1}: 2106 and others.

Ethyl 14-azido-3,6,9,12-tetraoxatetradecan-1-oate (20)

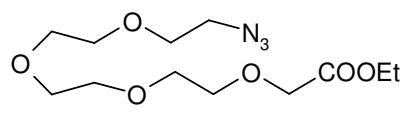

A solution of azide **19** (3.50g, 16mmol) in dry DMF (5ml) was added to a cooled solution of sodium hydride (0.42g, 17.58mmol) in dry DMF (10ml). Reaction mixture was stirred for 30 min and then to it ethylbromoacetate (1.96ml, 17.58mmol) was added dropwise, at 0^{0}C. The reaction mixture was stirred for 16h at room temperature. The

reaction mixture was quenched with ice water and solvent was removed under vacuum; the residue was taken in water and extracted with ethyl acetate (3 x 50ml). The pooled organic extracts were washed with water and brine. Drying of the organic layer and evaporation of the solvent gave crude oil. Purification using column chromatography afforded **20** (2.0 g, 44% yield).

^{1}H NMR ($CDCl_3$) δ: 4.26-4.12 (m, 4H), 3.69-3.46 (m, 14H), 3.39-3.36 (m, 2H), 1.29-1.21 (t, 3H).

Ethyl 14-tert-butoxycarbonylamino-3,6,9,12-tetraoxatetradecan-1-oate (21)

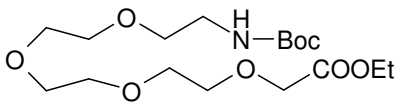

Compound **20** (2g, 6.6mmol) was taken in dry ethyl acetate (2ml) in 250ml hydrogenation flask and di-tert-butyldicarbonate (1.57g, 7.2mmol) was added to it. Raney Ni (1ml, suspension in ethanol) was separately washed thoroughly with ethyl acetate and was added to the hydrogenation flask. It was subjected to hydrogenation at 40-psi pressure for 1.5 hr. The catalyst was filtered and washed with methanol/ethyl acetate mixture. The filtrate was concentrated under vacuum to give crude protected amine. Purification using column chromatography afforded **21** (1.5g, 50% yield).

^{1}H NMR ($CDCl_3$) δ: 5.20 (br s, 1H), 4.24-4.09 (m, 4H), 3.69-3.46 (m, 14H), 3.27-3.24 (m, 2H), 1.38 (s, 9H), 1.26-1.19 (t, 3H).

^{13}C NMR ($CDCl_3$) δ: 170.11, 155.74, 78.69, 70.53, 70.20, 69.87, 68.33, 60.42, 40.10, 28.08, 13.85.

MS: (ESI) 379 $(M)^+$, 279 (M^+- Boc).

14-tert-butoxycarbonylamino-3,6,9,12-tetraoxatetradecan-1-oic acid (22)

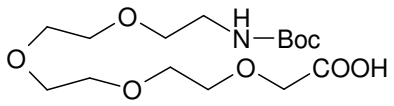

To a solution of Ethyl 14-tert-butoxycarbonylamino-3,6,9,12-tetraoxatetradecan-1-oate **21** (0.4g, 1.0mmol) in methanol (2ml), was added aqueous 2M NaOH (2ml). TLC analysis after 10 minutes indicated the absence of the starting material as a result of hydrolysis of the methyl ester function. The excess NaOH was neutralized by Dowex-50 H^+ resin, which was then, filtered off. The methanol from the filtrate was removed under vacuum and concentrating it to dryness to obtain the product **22** (0.35g, quantitative yield) as brown solid.

^{1}H NMR ($CDCl_3$) δ: 6.00 (br s, 1H), 4.11 (s, 2H), 3.69-3.46 (m, 14H), 3.34-3.24 (m, 2H), 1.39 (s, 9H).

^{13}C NMR ($CDCl_3$) δ: 170.11, 155.74, 79.29, 71.18, 70.56, 70.27, 69.11, 40.35, 28.39.

MS: (ESI) 352 $(M)^+H$, 252 (M^+H- Boc).

3.7.1. UV-melting

The concentration of the PNA oligomers was calculated on the basis of the absorption at 260nm, assuming the molar extinction coefficients of the nucleobases to be as in DNA, i. e., T, 8.8 $cm^2/\mu mol$; C, 7.3 $cm^2/\mu mol$; G, 11.7 $cm^2/\mu mol$ and A, 15.4 $cm^2/\mu mol$. The hairpin bisPNA oligomer (**23**-**26**) and the relevant complementary DNA oligonucleotide (**27**/**28**) were mixed together in a 1:1 molar ratio in 0.01M sodium phosphate buffer, pH 5.8 or 7.4 to get a final strand concentration of 1μM. The samples were annealed by heating at 85^{o}C for 1-2min, followed by slow cooling to room temperature, kept at room temperature for ~30min and then, refrigerated overnight. UV experiments were performed on a Perkin Elmer λ35 UV-VIS

spectrophotometer fitted with a Peltier temperature programmer. The samples were heated at a rate of 0.2^{o}C rise per minute and the absorbance at 260nm was recorded at every minute. The percent hyperchromicity at 260nm was plotted as a function of temperature and the melting temperature was deduced from the peak in the first derivative plots.

3.7.2. Fluorescence assay for strand invasion

Fluorescence measurements were done on a Perkin Elmer model LS-50B spectrometer attached to a Julabo water bath circulator for variable temperature. The DNA duplex **27:29/28:30** (1μM) in 5mM sodium phosphate buffer, pH 7.4 at 20°C was saturated with ethidium bromide (0.5μM) and then excited at 490nm and the emission monitored at 590nm using a spectral bandwidth of 5nm. Then the kinetics of strand invasion process was examined by monitoring the fluorescence decay at 590nm as a function of time after individually adding the four bisPNAs **23-26** (10μM) for over 60h.

3.7.3. pK_a determination

The *aeg*PNA-C and *aep*PNA-C monomers (**13** and **15**) after Boc-deptrotection, were titrated with 0.1M NaOH. The pH titration curve (pH versus volume of NaOH) exhibited the pK_a.

3.8. APPENDIX

- Compound **4**, ^{1}H NMR and ESI-MASS
- Compound **8**, ^{1}H NMR
- Compound **11**, ^{1}H and ESI-MASS
- Compound **18**, ^{1}H NMR
- Compound **19**, ^{1}H NMR
- Compound **20**, ^{1}H NMR
- Compound **21**, ^{1}H, ^{13}C NMR, DEPT and ESI-MASS
- Compound **22**, ^{1}H, ^{13}C NMR and ESI-MASS

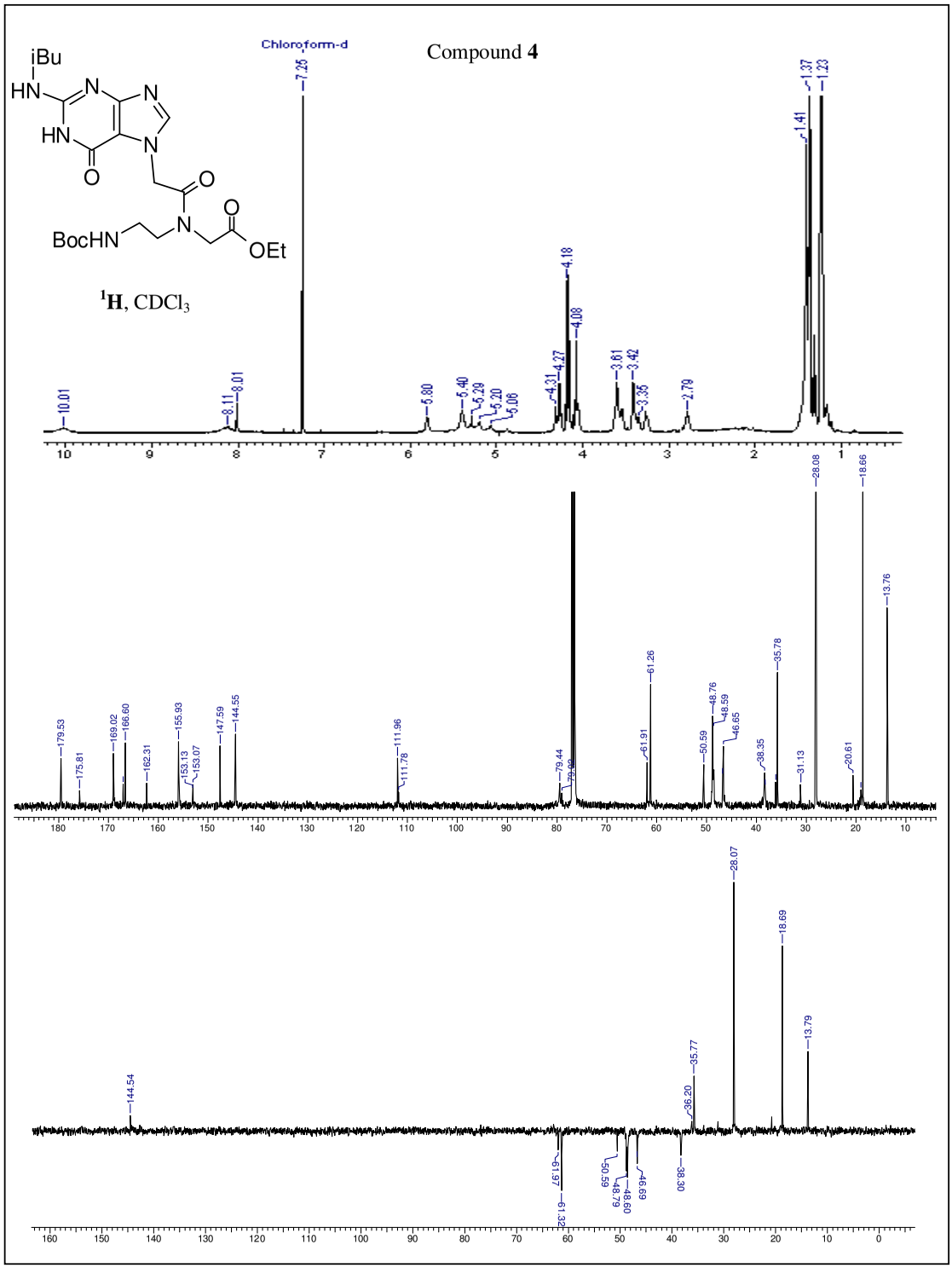
Compound **4**
Chloroform-d
iBu
HN
N
N
HN
N
O
O
O
N
BocHN
OEt
^{1}**H**, $CDCl_3$
7.25
1.41
1.37
1.23
4.18
4.08
4.27
4.31
3.81
3.42
3.35
2.79
5.80
5.40
5.29
5.20
5.06
10.01
8.11
8.01
28.08
18.66
13.76
179.53
175.61
169.02
166.60
162.31
155.93
153.13
153.07
147.59
144.55
111.96
111.78
79.44
61.91
61.26
50.59
48.76
48.59
46.65
38.35
35.78
31.13
20.61
28.07
18.69
13.79
144.54
36.20
35.77
61.97
61.32
50.59
48.79
48.60
46.69
38.30

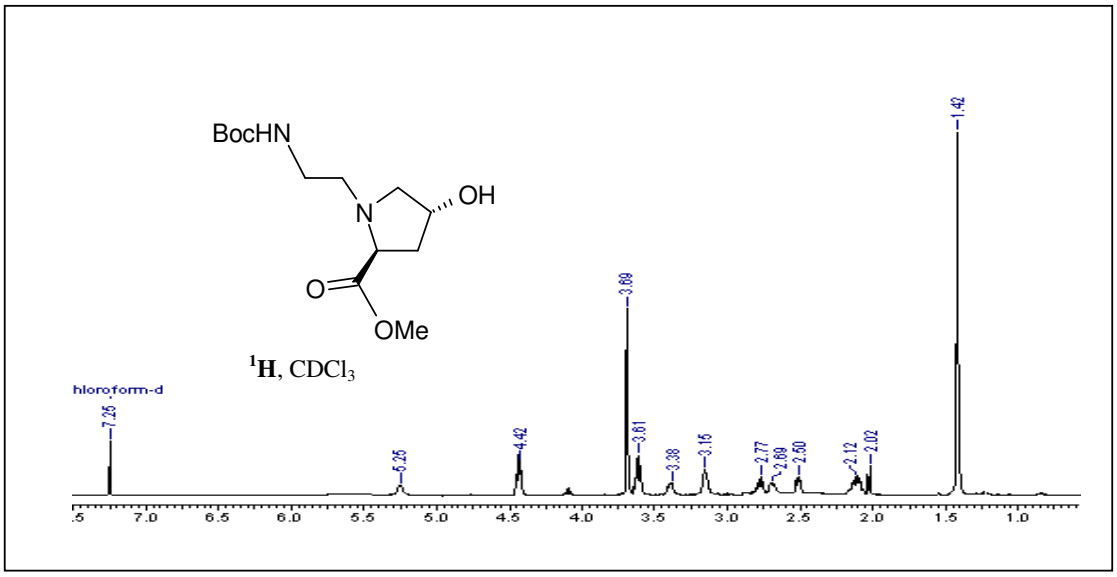

^{1}H, $CDCl_3$

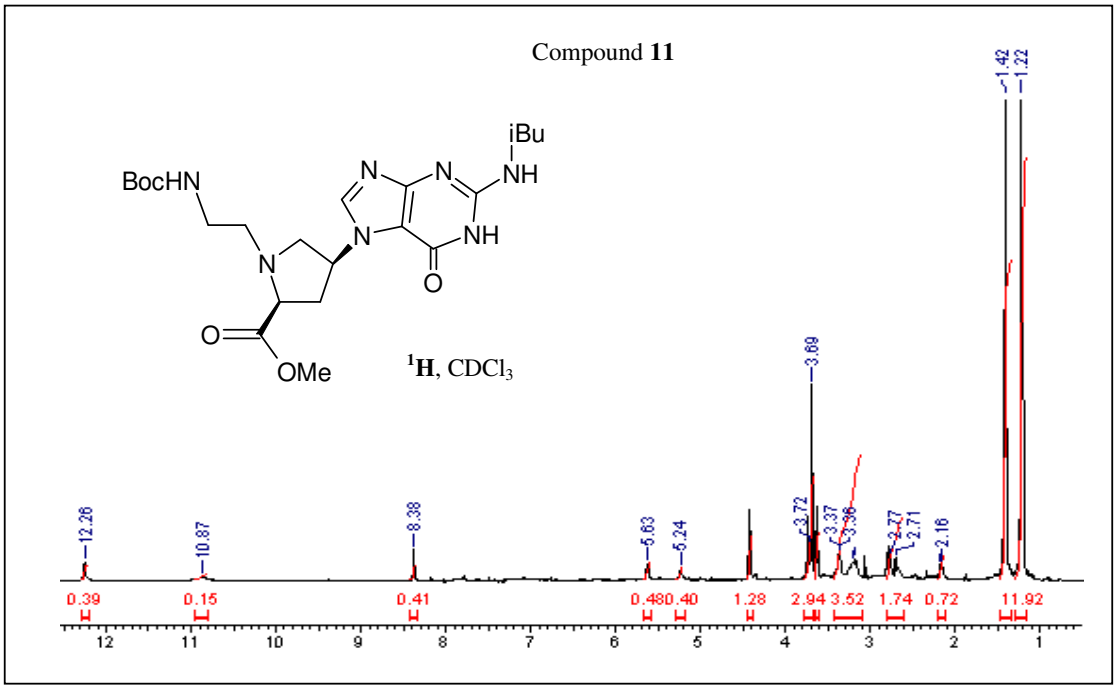

^{1}H, $CDCl_3$

Compound **18**

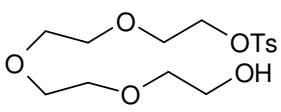

^{1}H, $CDCl_3$

Compound **19**

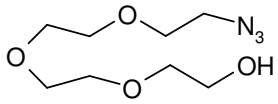

^{1}H, $CDCl_3$

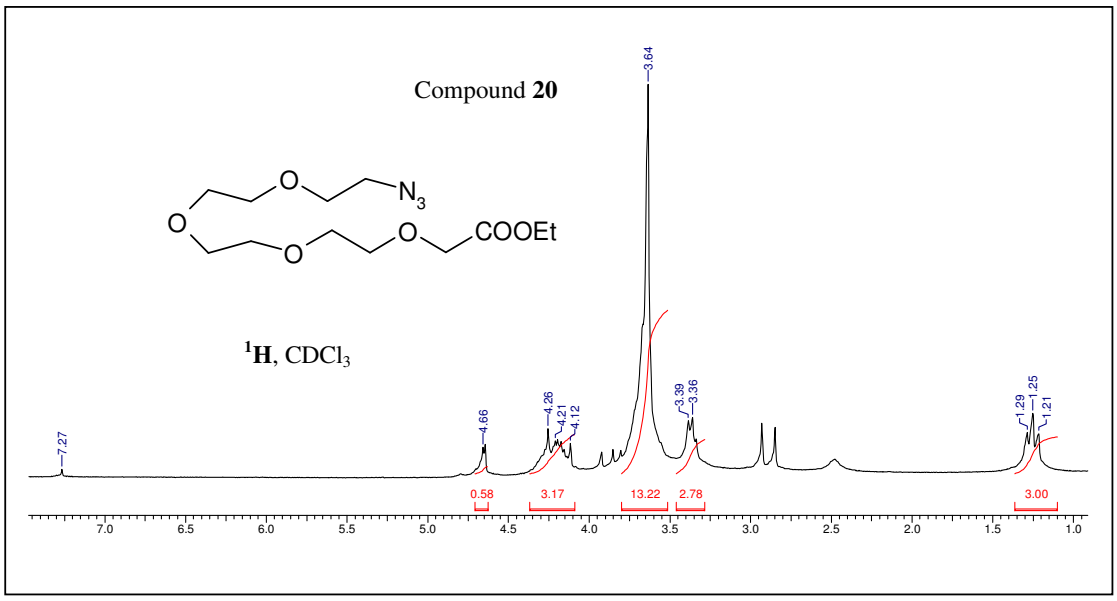
Compound **20**
O
O
O
O
N_3
COOEt
^{1}**H**, $CDCl_3$
7.27
4.66
4.26
4.21
4.12
3.64
3.39
3.36
1.29
1.25
1.21
0.58
3.17
13.22
2.78
3.00
7.0
6.5
6.0
5.5
5.0
4.5
4.0
3.5
3.0
2.5
2.0
1.5
1.0

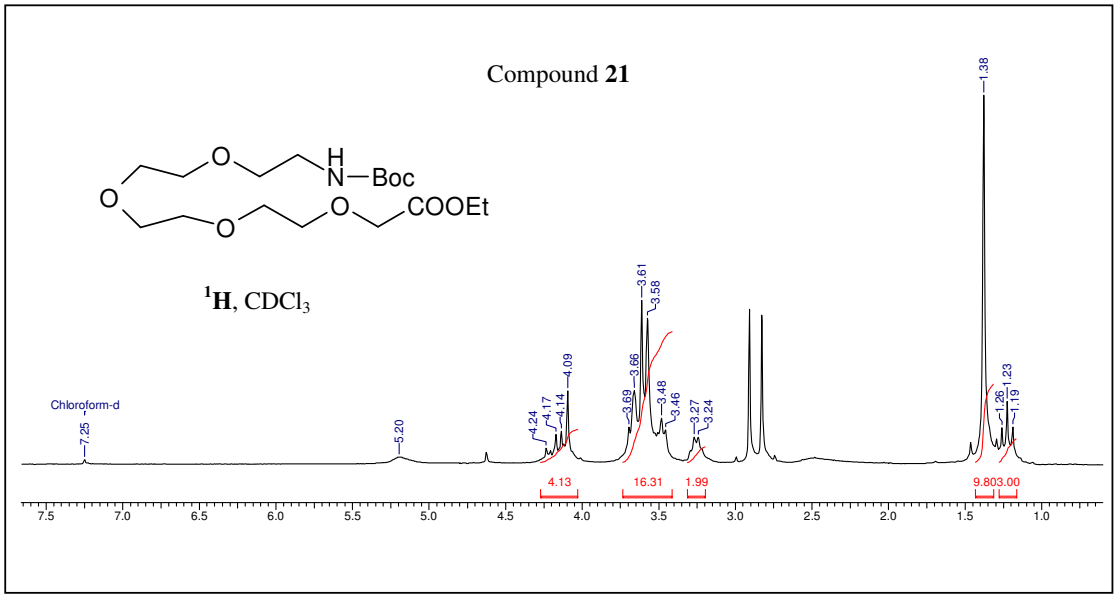
Compound **21**
O
O
O
O
H
N—Boc
COOEt
^{1}**H**, $CDCl_3$
Chloroform-d
7.25
5.20
4.24
4.17
4.14
4.09
3.69
3.66
3.61
3.58
3.48
3.46
3.27
3.24
1.38
1.26
1.23
1.19
4.13
16.31
1.99
9.80
3.00
7.5
7.0
6.5
6.0
5.5
5.0
4.5
4.0
3.5
3.0
2.5
2.0
1.5
1.0

Compound **21**

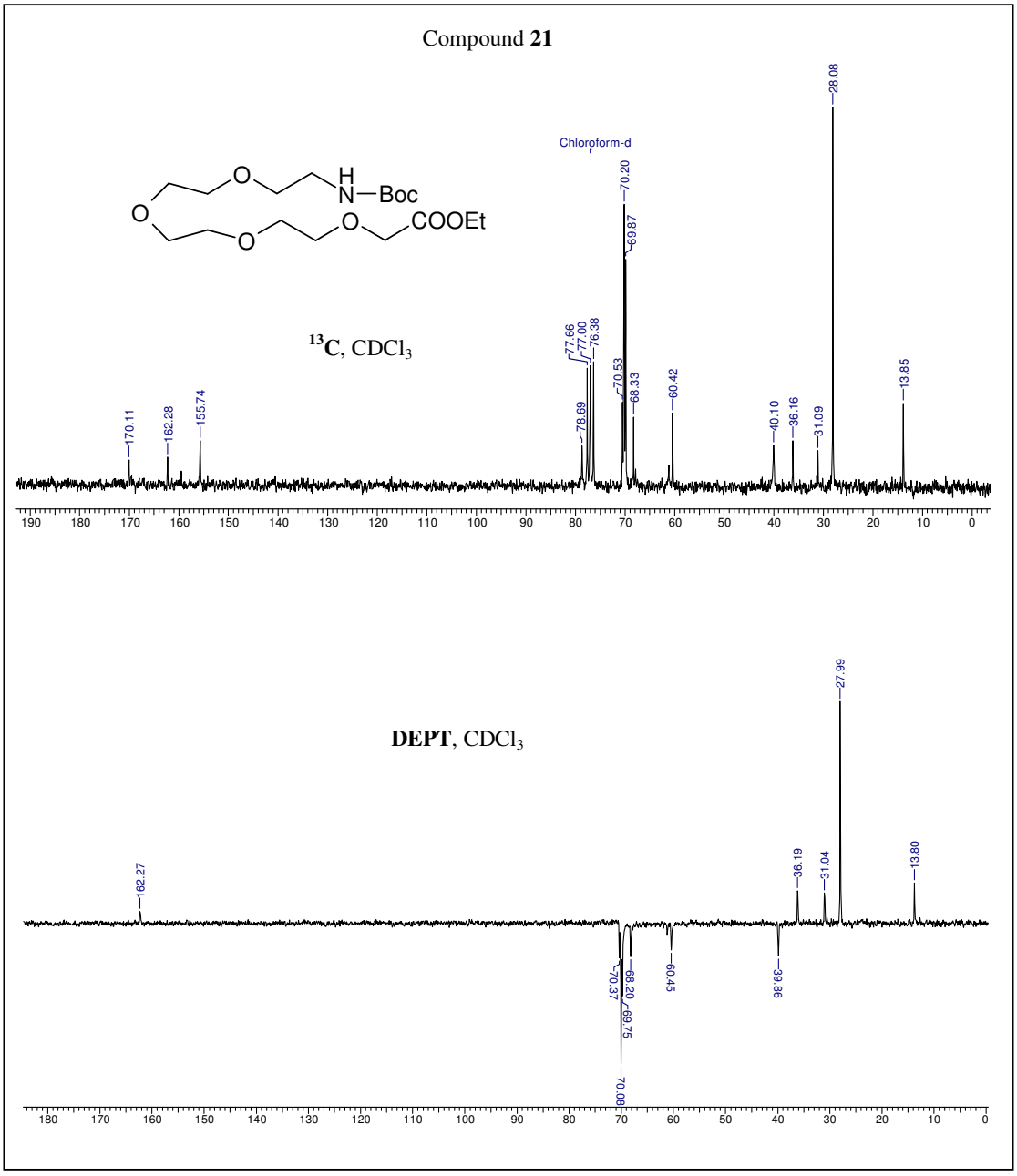
Chloroform-d
28.08
70.20
69.87
77.66
77.00
76.38
70.53
68.33
60.42
78.69
170.11
162.28
155.74
40.10
36.16
31.09
13.85
^{13}C, CDCl$_3$
27.99
36.19
31.04
13.80
162.27
70.37
68.20
69.75
70.08
60.45
39.86
DEPT, CDCl$_3$

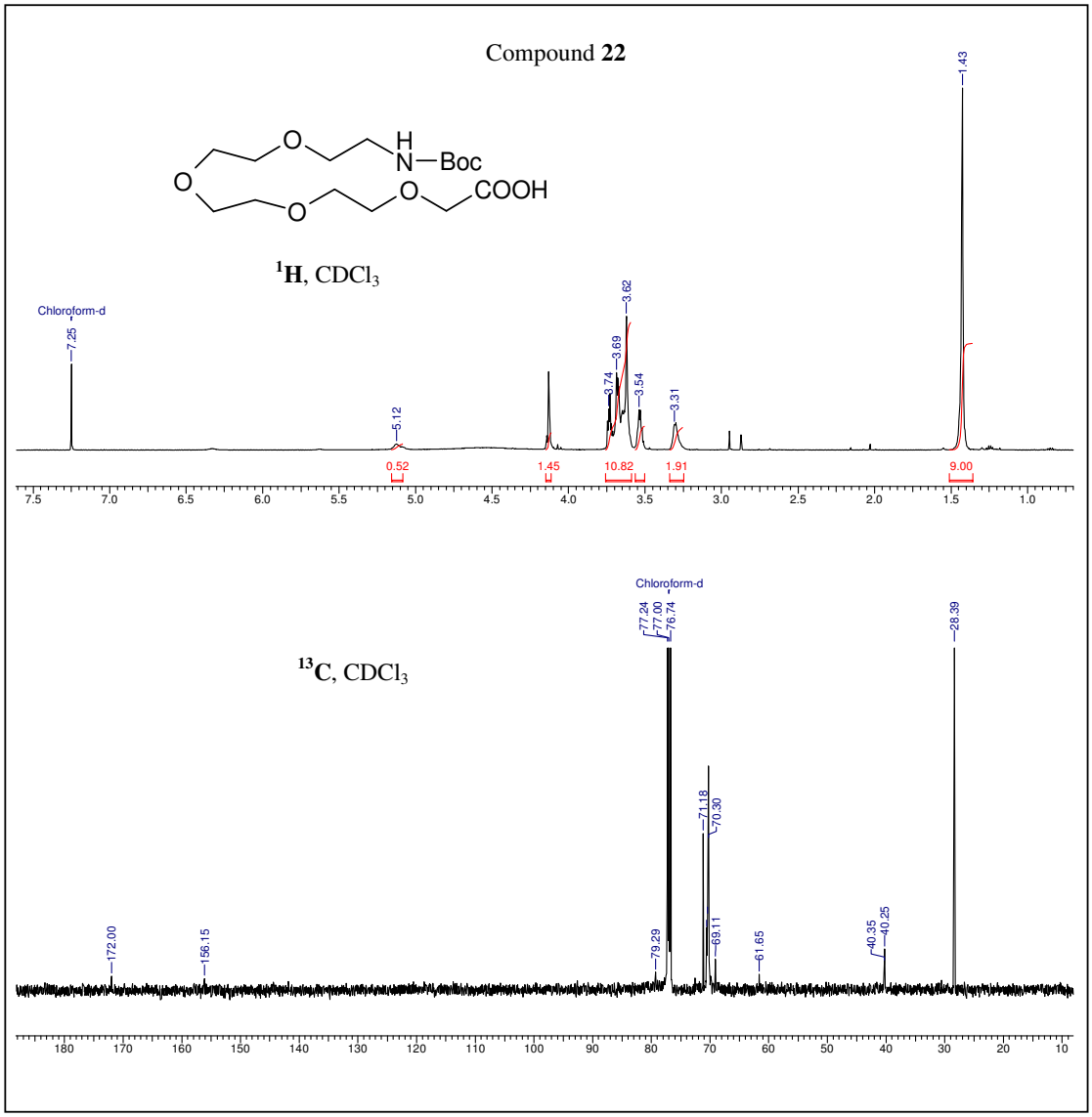
Compound **22**
O
H
N—Boc
O
O
O
COOH
^{1}H, $CDCl_3$
Chloroform-d
7.25
5.12
3.74
3.69
3.62
3.54
3.31
1.43
0.52
1.45
10.82
1.91
9.00
^{13}C, $CDCl_3$
Chloroform-d
77.24
77.00
76.74
172.00
156.15
79.29
71.18
70.30
69.11
61.65
40.35
40.25
28.39

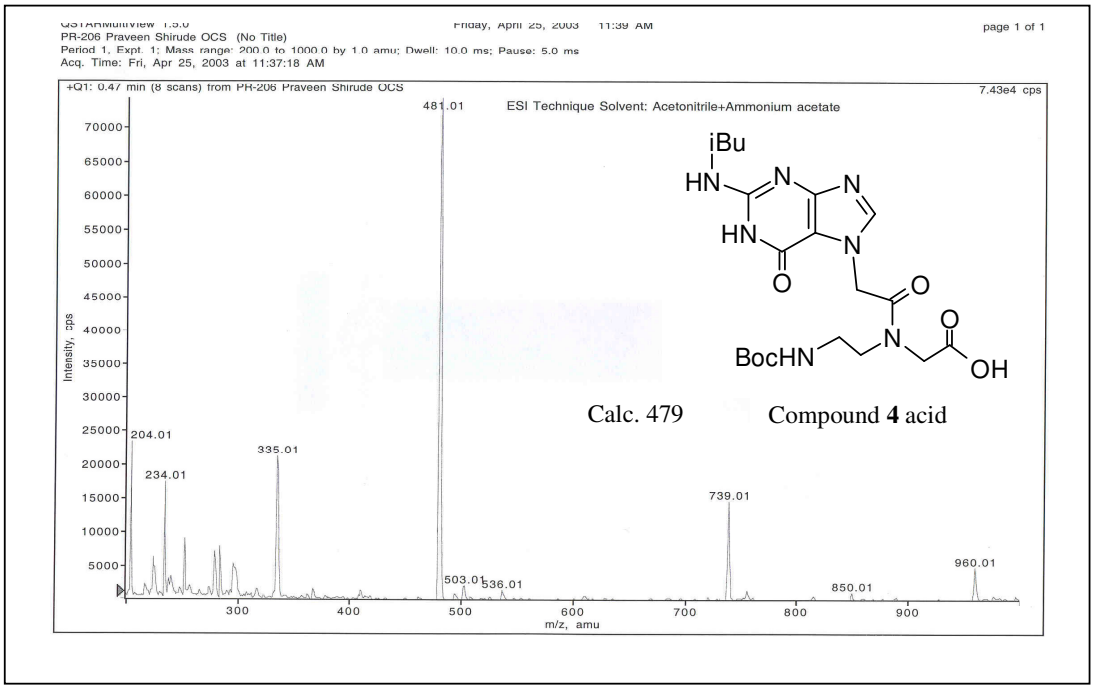

Calc. 479 Compound **4** acid

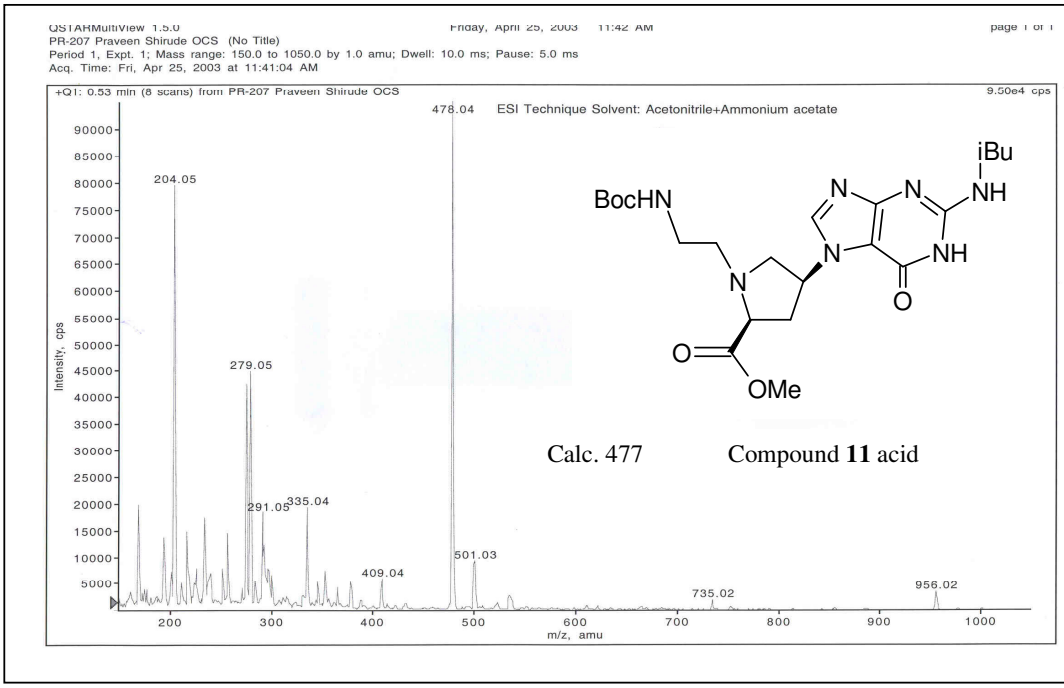

Calc. 477 Compound **11** acid

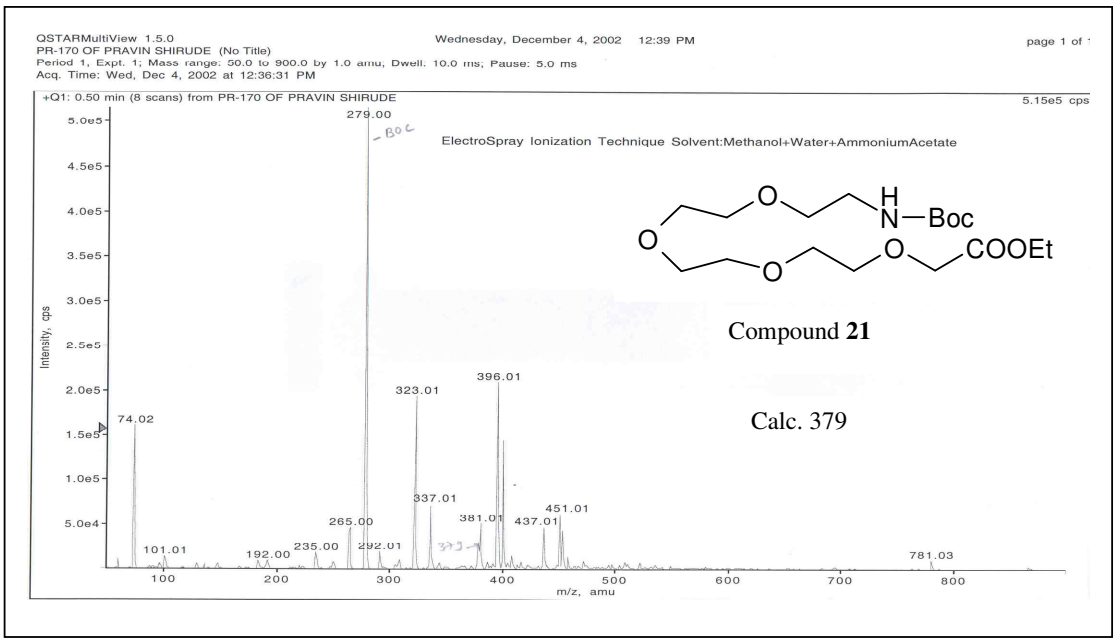

Compound **21**

Calc. 379

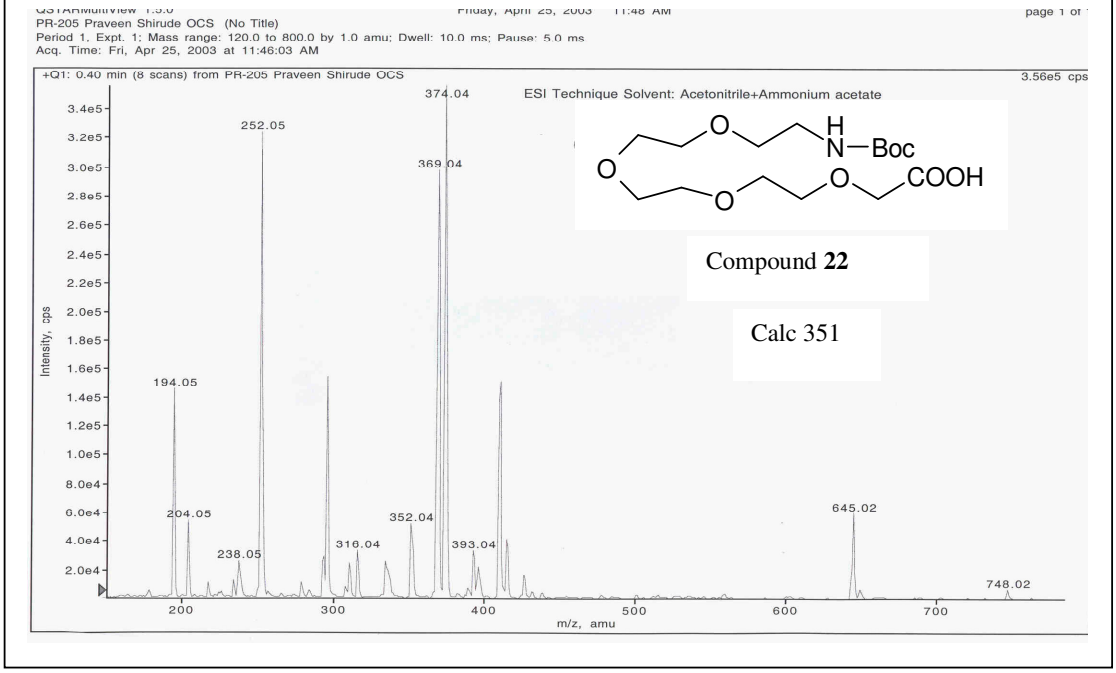

Compound **22**

Calc 351

3.9. REFERENCES

[1] Nielsen, P. E. Design of sequence-specific DNA-binding ligands. *Eur. J. Chem.* **1997**, *3*, 505–508.

[2] Corey, D. R. Peptide nucleic acids: Expanding the scope of nucleic acid recognition. *Trends Biotechnol*. **1997**, *15*, 224–229.

[3] Good, L.; Nielsen, P. E. Progress in developing PNA as a gene-targeted drug. *Antisense Nucleic Acid Drug Dev*. **1997**, *7*, 431–437.

[4] Egholm, M.; Buchardt, O.; Christensen, L.; Behrens, C.; Freier, S. M.; Driver, D. A.; Berg, R. H.; Kim, S. K.; Norden, B.; Nielsen, P. E**.** PNA hybridizes to complementary oligonucleotides obeying the Watson-Crick hydrogen-bonding rules. *Nature,* **1993**, *365*, 566-568.

[5] Egholm, M.; Buchardt, O.; Nielsen, P. E.; Beg, R. H. Recognition of guanine and adenine in DNA by cytosine and thymine containing peptide nucleic acids (PNA). *J. Am. Chem. Soc*. **1992**, *114*, 9677-9678.

[6] Wittung, P.; Nielsen, P.; Norden, B. Extended DNA-recognition repertoire of peptide nucleic acid (PNA): PNA- dsDNA triplex formed with cytosine-rich homopyrimidine PNA. *Biochemistry,* **1997**, *36*, 7973-7979.

[7] Egholm, M.; Christensen, L.; Dueholm, K. L.; Buchardt, O.; Coull, J.; Nielsen, P. E. Effecient pH independent sequence-specific DNA binding by pseudoisocytosine-containing bis-PNA. *Nucleic Acids Res.* **1995**, *23*, 217-222.

[8] Griffith, M. C.; Risen, L. M.; Greig, M. J.; Lesnik, E. A.; Sprankle, K. G.; Griffey, R. H.; Kiely, J. S.; Freier, S. M. Single and bis peptide nucleic acids as triplexing agents: binding and stoichiometry. *J. Am. Chem. Soc.* **1995**, *117*, 831-832.

[9] Kuhn, H.; Demidov, V. V.; Frank-Kamenetskii, M. D.; Nielsen, P. E. Kinetic sequence discrimination of cationic bis-PNAs upon targeting of double-stranded DNA. *Nucleic Acids Res.* **1998**, *26*, 582-587.

[10] Veselkov, A. G.; Demidov, V. V.; Nielsen, P. E.; Frank-Kamenetskii, M. D. A new class of genome rare cutters. *Nucleic Acids Res.* **1996**, *24*, 2483-2488.

[11] Nielsen, P. E.; Egholm, M.; Berg, R. H.; Buchardt, O. Sequence-selective recognition of DNA by strand displacement with thymine-substituted polyamide. *Science,* **1991**, *254*, 1497-1500.

[12] Wittung, P.; Nielsen, P. E.; Norden, B. Direct observation of strand invasion by peptide nucleic acid (PNA) into double-stranded DNA. *J. Am. Chem. Soc.* **1996**, *118*, 7049-7054.

[13] Miller, P. S.; Bhan, P.; Cushman, C. D.; Trapane, T. L. Recognition of a guanine-cytosine base pair by 8-oxoadenine. *Biochemistry,* **1992**, *31*, 6788-6793.

[14] Krawczyk, S. H.; Milligan, J. F.; Wadwani, S.; Moulds, C.; Froehler, B. C.; Matteucci, M. D. Oligonucleotide-mediated triple helix formation using an N3-protonated deoxycytidine analog exhibiting pH-independent binding within the physiological range. *Proc. Natl. Acad. Sci. USA,* **1992b,** *89*, 3761-3764.

[15] Davison, E. C.; Johnsson, K. Triple helix binding of oligodeoxyribonucleotides containing 8-oxo-2'- deoxyadenosine. *Nucleosides Nucleotides,* **1993**, *12*, 237-243.

[16] Ono, A.; Ts'o, P. O. P.; Kan, L. S. Triplex formation of oligonucleotides containing 2'-O-methylpseudoisocytidine in substitution for 2'-deoxycytidine. *J. Am. Chem. Soc.* **1991**, *113*, 4032.

[17] Ono, A.; Ts'o, P. O. P.; Kan, L. S. Triplex formation of an oligonucleotide containing 2'-O-methylpseudoisocytidine with a DNA duplex at neutral pH. *J. Org. Chem.* **1992**, *57*, 3225.

[18] Egholm, M.; Christensen, L.; Dueholm, K.; Buchardt, O.; Coull, J.; Nielsen, P. E. Efficient pH-independent sequence-specific DNA binding by pseudoisocytosine-containing bis-PNA. *Nucleic Acids Res.* **1995**, *23*, 217-222.

[19] Rao, T. S.; Durland, R. H.; Revankar, G. R. Synthesis of oligonucleotides containing 7-(2-deoxy-β-D-erythro-pentofuranosyl) guanine and 8-amino-2'-deoxy-guanosine. *J. Heterocyclic Chem.* **1994**, *31*, 935-940.

[20] Hunziker, J.; Priestley, E. S.; Brunar, H.; Dervan, P. B. Design of an N7-glycosylated purine nucleoside for recognition of GC base pairs by triple helix formation. *J. Am. Chem. Soc.* **1995**, *117*, 2661-2662.

[21] Brunar, H.; Dervan, P. B. Sequence composition effects on the stabilities of triple helix formation by oligonucleotides containing N7-deoxyguanosine. *Nucleic Acids Res.* **1996**, *24*, 1987-1991.

[22] Beal, P.A.; Dervan, P. B. Second structural motif for recognition of DNA by oligonucleotide- directed triple-helix formation. *Science,* **1991**, *251*, 1360-1363.

[23] (a) D'Costa, M.; Kumar, V. A.; Ganesh, K. N. Aminoethylprolyl peptide nucleic acids (aepPNA): Chiral PNA analogues that form highly stable DNA:aepPNA$_2$ triplexes. *Org. Lett.* **1999**, *1*, 1513-1516. (b) D'Costa, M.; Kumar, V. A.; Ganesh, K. N. Aminoethylprolyl (*aep*) PNA: Mixed purine/pyrimidine oligomers and binding orientation preferences for PNA:DNA duplex formation. *Org. Lett.* **2001**, *3*, 1281-1284. (c) Kumar, V. A. Structural preorganization of peptide nucleic acids: Chiral

cationic analogues with five- or six-membered ring structures. *Eur. J. Org. Chem.* **2002**, 2021-2032.

[24] Egholm, M.; Buchardt, O.; Nielsen, P. E.; Berg, R. H. Peptide nucleic acids (PNA). Oligonucleotide analogs with an achiral peptide backbone. *J. Am. Chem. Soc.* **1992**, *114*, 1895-1897.

[25] Kuhn, H.; Demidov, V. V.; Frank-Kamenetskii, M. D.; Nielsen, P. E. Kinetic sequence discrimination of cationic bis-PNAs upon targeting of double-stranded DNA. *Nucleic Acids Res.* **1998**, *26*, 582-587.

[26] St. Clair, A.; Xiang, G.; McLaughlin, L. W. Synthesis and triplex forming properties of an acyclic N7-glycosylated guanine nucleoside. *Nucleosides Nucleotides,* **1998**, *17*, 925-937.

[27] Woods, C. R.; Ishii, T.; Wu, B.; Bair, K. W.; Boger, D. L. Hairpin versus Extended DNA Binding of a Substituted β-Alanine Linked Polyamide. *J. Am. Chem. Soc*. **2002**, *124*, 2148-2152.

[28] D'Costa, M.; Kumar, V. A.; Ganesh, K. N. N7-Guanine as a C^+ mimic in hairpin *aeg*/*aep*PNA-DNA triplex: probing binding selectivity by UV-T_m and kinetics by fluorescence-based strand-invasion assay. *J. Org. Chem.* **2003**, *68*, 4439-4445.

[29] Jenny, T. F.; Schneider, K. C.; Benner, S. A. N2-isobutyryl-O6-[2-(p-nitrophenyl)-ethyl]guanine: A new building block for the efficient synthesis of carbocyclic guanosine analogs. *Nucleosides Nucleotides,* **1992**, *11*, 1257-1261.

[30] Brown, D. M.; Todd, A.; Varadarajan, S. *J. Chem. Soc.* **1956**, 2384.

[31] Smet, M.; Dehaen, W. Synthesis of crown ethers containing a rubicene moiety. *Molecules,* **2000**, *5*, 620-628.

[32] Hodges, R. S.; Merrifield, R. B. Monitoring of solid phase peptide synthesis by an automated spectrophotometric picrate method. *Anal. Biochem.* **1975**, *65*, 241-272.

[33] Tse, W. C.; Boger, D. L. A fluorescent intercalator displacement assay for establishing DNA binding selectivity and affinity *Acc. Chem. Res.* **2004**, *37*, 61-69.

[34] *Antisense Research and Applications* (Eds.: Crooke, S. T.; Lebleu, B.), CRC Press, Boca Raton, FL, 1993.

[35] Demidov, V. V.; Yavnilovich, M. V.; Belotserkovskii, B. P.; Frank-Kamenetskii, M. D.; Nielsen, P. E. Kinetics and mechanism of polyamide ('peptide') nucleic acid binding to duplex DNA. *Proc. Natl Acad. Sci.* USA, **1995**, *92*, 2637-2641.

[36] Kuhn, H.; Demidov, V. V.; Nielsen, P. E.; Frank-Kamenetskii, M. D. An experimental study of mechanism and specificity of peptide nucleic acid (PNA) binding to duplex DNA. *J. Mol. Biol.* **1999,** *286*, 1337-1345.

CHAPTER 4:

SECTION A: SYNTHESIS AND BIOPHYSICAL EVALUATION OF FLUORESCENT PNAs

SECTION B: INDUCTION OF CHIRALITY IN ACHIRAL *aeg*PNA

This chapter has two sections. **Section A** deals with the synthesis and biophysical evaluation of fluorescent PNAs and **Section B** deals with the effect of chiral ligands on *aeg*PNA backbone.

SECTION A: SYNTHESIS AND BIOPHYSICAL EVALUATION OF FLUORESCENT PNAs

4.1 INTRODUCTION

Peptide nucleic acids (PNA) are DNA analogues in which the sugar–phosphate backbone is replaced by a peptide amide bond backbone.[1] PNAs exhibit unique properties that set them apart from other traditional DNA analogues. These properties are: (i) unprecedented strong binding to complementary, mixed DNA/ RNA sequences to form duplexes, (ii) high specificity discrimination of mismatched base pairs and (iii) 'strand invasion' at polypurine/pyrimidine stretches on a DNA duplex to form a PNA_2:DNA triplex.[2] This fact, coupled with their resistance to proteases and nucleases and chemical stability over a wide pH range, has led to the development of novel applications that cannot be satisfactorily executed with other DNA analogues. Such applications include blocking and activation of gene expression *via* D-loop complexes, identification of point mutations by PNA-directed PCR clamping, using fluorophore conjugated PNA as probes to locate individual genes in a DNA map and antisense drug development.[3] Most of the structural changes to improve PNA properties far have centered on backbone modifications to introduce conformational constrain and chirality.[4]

4.2. RATIONALE AND OBJECTIVES FOR THE PRESENT WORK

2-aminopurine (2-AP) is a fluorescent analogue of adenine (6-aminopurine) and has been used as a probe of nucleic acid properties. Incorporating 2AP into DNA quenches its fluorescence, reducing its quantum yield from that of the free nucleoside. This reduction is attributed to stacking interaction with nearest neighbour nucleobases, and therefore, fluorescent properties of 2-AP have been used to probe the equilibrium stacking properties of DNA duplexes containing these mismatched pairs.[5]

The fluorescent 2-aminopurine has frequently been used to study variations in DNA structure since its emission properties are highly sensitive to local conformational changes. It can be substituted for adenine for Watson-Crick base pairing with thymine in opposite strand and as it is an inherently fluorophoric, it minimally perturbs the helix conformation.[6] The anisotropy behaviour can also be used to analyze the restricted angular range of 2-AP motion or 'wobbling' within the duplex. The base 2-AP can selectively excited in the presence of normal bases, making it ideal real-time spectroscopic probe to study the dynamics and local environmental changes due to DNA binding with other molecules.[7,8,9]

Two different tautomeric states of 2-aminopurine are known; the 9-H and 7-H tautomers that have a proton at, respectively, nitrogen number 9 and 7. Both calculations and experiments show that 2-AP in the ground state mainly exists as the

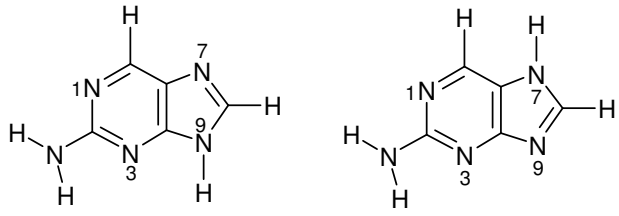

2-aminopurine: 9-H 2-aminopurine: 7-H

9-H tautomer.[10,11] However, recent experiments and calculations suggests that the 7-H tautomer might be present in significant amounts upon excitation.[12,13]

This section presents synthesis and studies on PNA analogue having intrinsic fluorescence due to incorporation of 2-aminopurine.[14]

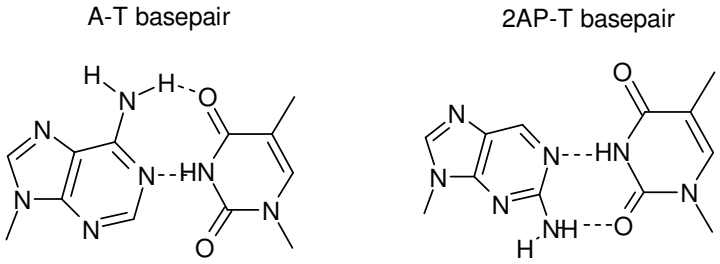

Incorporation of 2-AP into PNA would therefore add a new dimension to the existing repertoire of PNA properties inducing novel and potential applications.[15] In this section PNA–DNA complexation is examined *via* fluorescence changes, with a view to probe conformational changes induced in PNA due to chemical modifications and hybridization events.

4.3. OBJECTIVES

The specific objectives of this section are

1. Synthesis of 2-aminopurine fluorescent PNA monomer.
2. Synthesis of mixed PNA- sequences incorporating 2-aminopurine.
3. Biophysical studies of (2-AP)PNA-DNA hybrids using UV and fluorescence spectroscopic techniques.

4.4. WORK DONE

4.4.1. Synthesis of 2-aminopurine PNA monomer

The ethyl N-(2-amino-6-chloropurin-9-ylacetyl)-N-(2-butoxycarbonylamino-ethyl) glycinate (**1**) (Scheme 1) was synthesized by reported procedures (See Chapter 2). The desired PNA monomer **3** carrying a 2-aminopurine moiety was synthesized in two steps. The 6-chloro group in **1** was first removed by hydrogenation over Pd–C to afford **2**, which was followed by hydrolysis of the ester with aq. NaOH to give the corresponding carboxylic acid **3**. This monomer was used directly for incorporation into PNA oligomers without protecting the 2-amino function, since it is inactive for normal peptide coupling conditions.

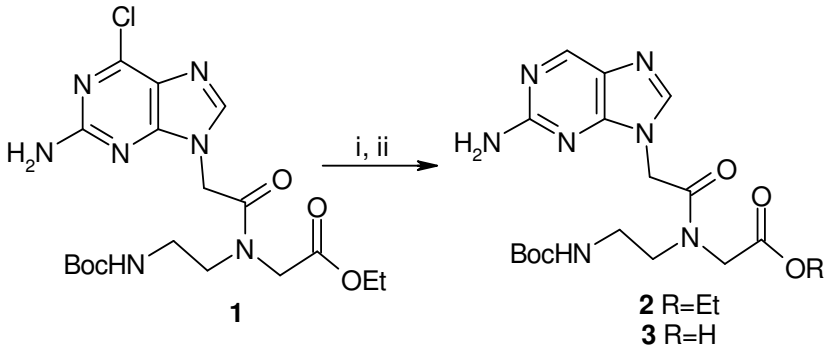

1 **2** **3**

Scheme 1. Synthesis of 2-aminopurine PNA monomer.

4.4.2. Synthesis of PNA Oligomers

All the peptide oligomers were synthesized on Merrifield resin, with β-alanine chosen as the first amino acid linker. The rationale for this is that β-alanine is achiral and hence does not interfere in the spectral properties of PNA. As it has a short alkyl chain, its contribution to hydrophobic nature of the PNA is negligible. Merrifield resin was therefore functionalised with N-Boc-β-alanine following the cesium salt method[16] to obtain the benzyl ester linkage between the resin and the first amino acid.

The functionalised resin was assayed to determine the loading value of first amino acid by picric acid method (Chapter 2).

Table 1. Resin-linked PNA Sequences Synthesized by Solid Phase Protocols.

Entry	Resin-linked PNA Oligomer
1	MF--β-ala-T T **A*** T T A T T A T T A T-Boc
2	MF--β-ala-T T A T T **A*** T T A T T A T-Boc
3	MF--β-ala-T T A T T A T T **A*** T T A T-Boc
4	MF--β-ala-T T A T T A T T A T T **A*** T-Boc

MF = Merrifield resin; T/A = *aeg*PNA-T/A; **A*** = 2-aminopurine PNA monomer.

The stepwise synthesis of fluorescent PNA oligomers was carried out in the C→N direction as described in Chapter 2. The fluorescent probe/base, 2-aminopurine (2-AP), was incorporated at 3rd, 6th, 9th and 12th position into a PNA 13-mer (Table 1) that contains thymines and adenines. The assembly of the PNA oligomers **4** to **11** was performed manually on Merrifield resin prior functionalised with β-alanine (0.180 equiv/gm) by standard solid phase peptide synthesis. The 2-AP monomer **3** was used in place of 'A' monomer in the indicated position *(***A***)*.

4.4.3. Synthesis of Complementary Oligonucleotides

The oligodeoxynucleotides (**12-13**, Table 3) were synthesized on a Pharmacia Gene Assembler Plus DNA synthesizer using the standard β-cyanoethyl phosphoramidite chemistry. The oligomers were synthesized in the 3'-5' direction on a CPG solid support, followed by ammonia treatment.[17] The oligonucleotides were de-salted by gel filtration, their purity ascertained by RP HPLC on a C18 column to be more than 98% and were used without further purification in the biophysical studies of PNA.

Table 2. DNA Oligonucleotide Sequences.

DNA	**Oligomer Sequences** 5' → 3'	
12	A A T A A T A A T A A T A	DNA complementary to **4-11** for duplexation
13	A A T A A T G A T A A T A	mismatch DNA

4.4.4. Cleavage from the Solid Support

The PNA oligomers were cleaved from the solid support using TFMSA[18] to yield oligomers with free 'C' terminal carboxylic acids. The benzyl ester linkage between PNA and resin allows cleavage by an amine to obtain PNAs with C-terminal amides.[19] PNAs carrying an amine or a polyamine at C-terminus is possible by reaction of the resin with diamine or polyamine. The PNA **8-11** were obtained by cleavage of peptide from the MF-resin with spermine via transamidation reaction. In case of spermine the product is expected to arise by the attack of primary amine rather than the secondary amino group due to steric reasons as has been established in earlier studies.[20]

4.4.5. Purification

The fully deprotected oligomers were initially desalted by size-exclusion chromatography over G25 Sephadex. They were subsequently purified by FPLC on a reverse phase C8 column using an ascending gradient of acetonitrile in water containing 0.1% TFA. The purity of the oligomers was re-checked by reverse phase HPLC on a C18 column and confirmed by MALDI-TOF mass spectrometry. Some representative HPLC profiles and mass spectra are shown in Figures 1 and 2 respectively.

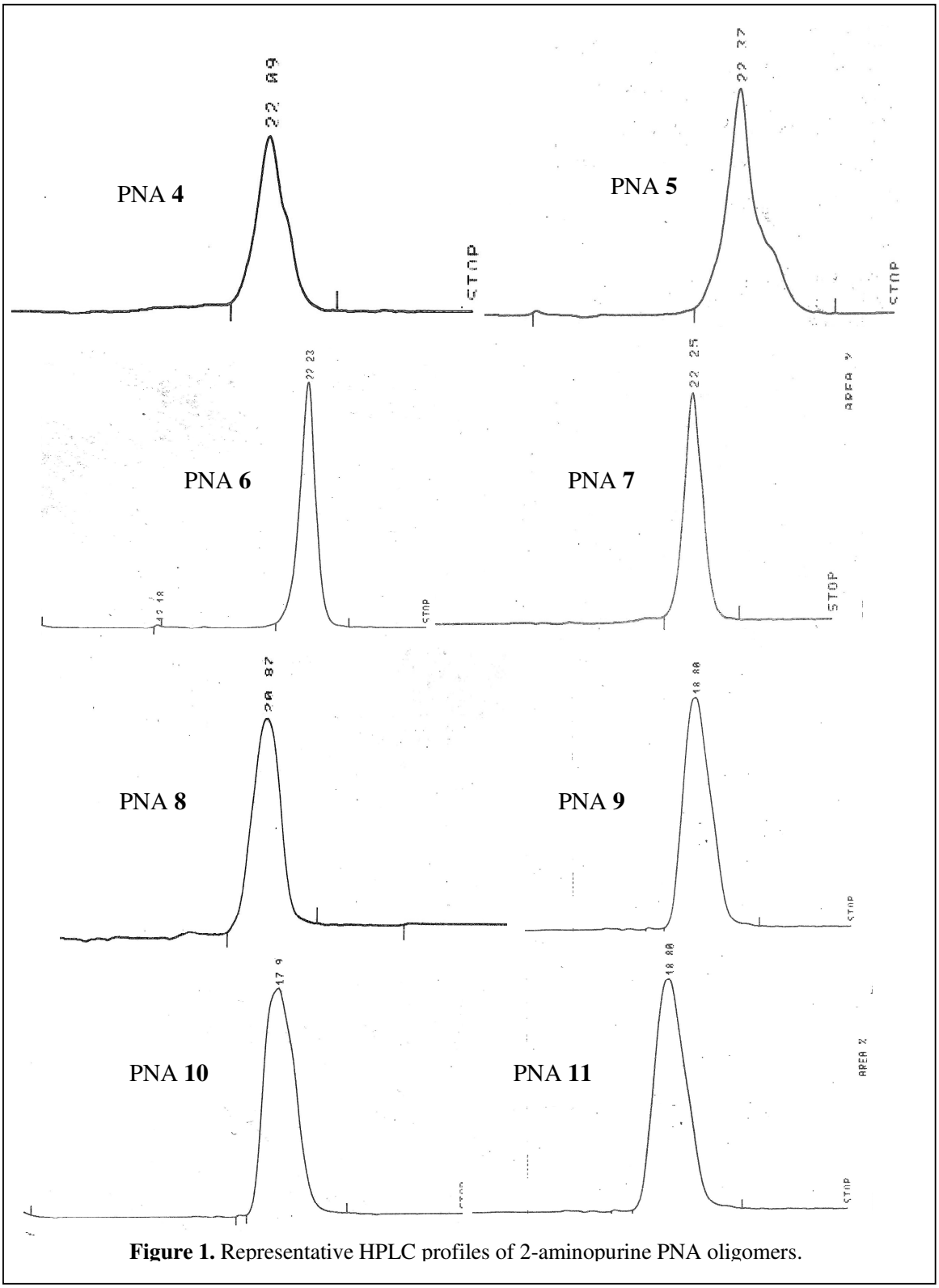

Figure 1. Representative HPLC profiles of 2-aminopurine PNA oligomers.

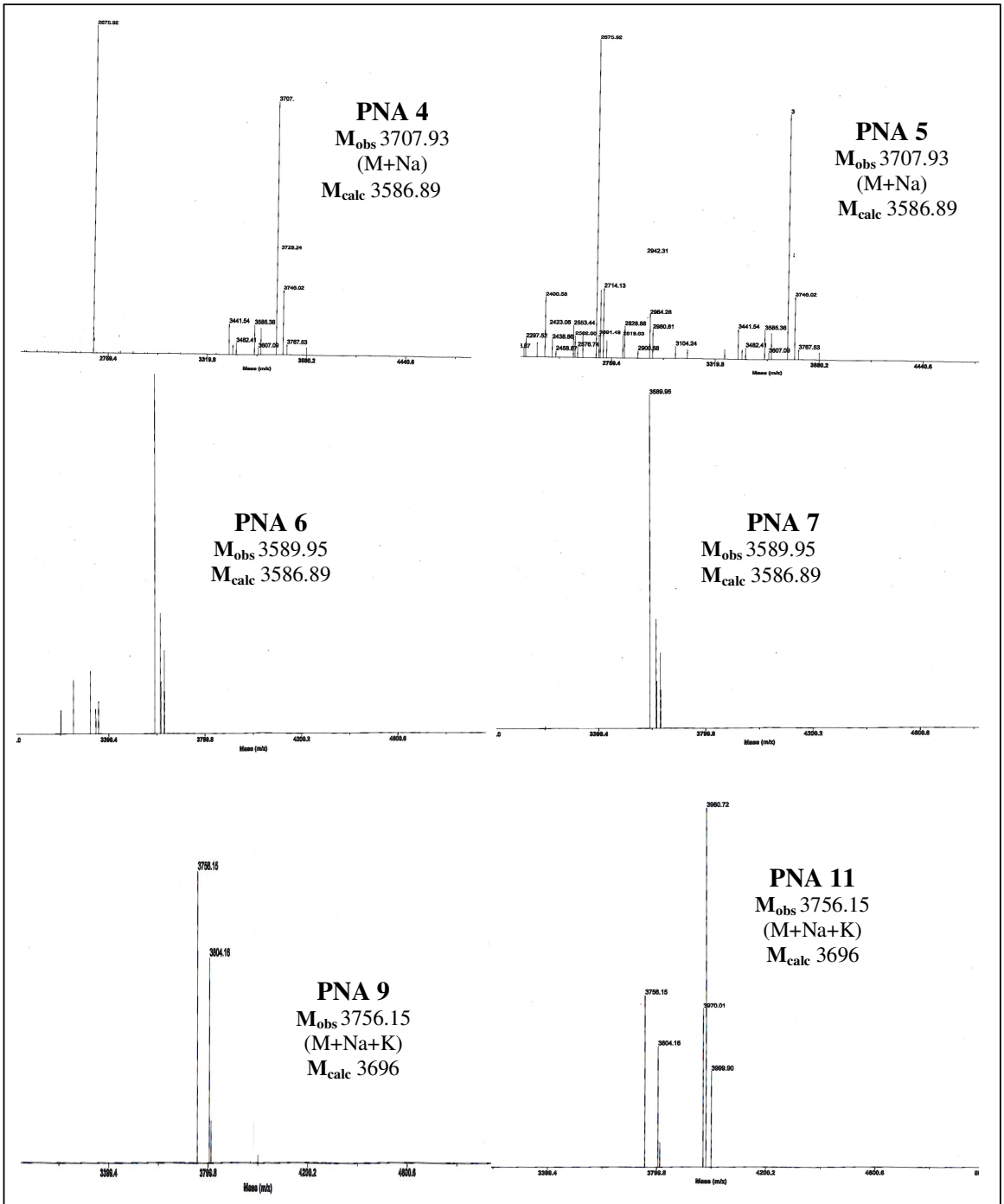

Figure 2. MALDI-TOF spectra of representative 2-aminopurine PNA oligomers.

Table 3. 2-AP PNA Oligomer Sequences.

PNA	Sequence Composition
4	H_2N–T A T T A T T A T T **A*** T T–$CONHCH_2CH_2CO_2H$
5	H_2N–T A T T A T T **A*** T T A T T– $CONHCH_2CH_2CO_2H$
6	H_2N–T A T T **A*** T T A T T A T T– $CONHCH_2CH_2CO_2H$
7	H_2N–T **A*** T T A T T A T T A T T– $CONHCH_2CH_2CO_2H$
8	H_2N–T A T T A T T A T T **A*** T T–CONH-Spermine
9	H_2N–T A T T A T T **A*** T T A T T–CONH-Spermine
10	H_2N–T A T T **A*** T T A T T A T T–CONH-Spermine
11	H_2N–T **A*** T T A T T A T T A T T–CONH-Spermine

T/A = *aeg*PNA-T/A; **A*** = 2-aminopurine PNA monomer.

4.4.6. UV-Melting

The 2-AP PNA sequences **4**-**11** were mixed with the appropriate DNA oligomer **12** or **13** in equimolar concentration and annealed prior to melting. Appropriate oligonucleotides and PNA each at a strand concentration of 1-2μM based on UV absorbance calculated using molar extinction coefficients at 260nm, 2-AP = 6.8, A = 15.4, C =7.3, G =11.7, T = 8.8 $cm^2/\mu M$. The samples were heated at a rate of 0.5^oC rise per minute and the absorbance at 260nm was recorded at every minute. The percent hyperchromicity at 260nm was plotted as a function of temperature and the melting temperature was deduced from the peak in the first derivative plots.

4.4.7. Fluorescence Studies

2-Aminopurine, an isomer of nonfluorescent adenine (6-aminopurine) has intrinsic fluorescence.[21] When present in a DNA double helix it is known to form a stable base pair with thymine without significantly affecting the local and global structure of B-form duplex.[13,14] The incorporation of 2-aminopurine (2-AP) into PNA would lead to fluorescent PNA. The 2-amino purine PNA monomer (**3**) and the PNA

oligomers (**4-11**) exhibited fluorescence emission with maxima at 371nm upon excitation at 308nm (Figure 3). There are a few reports of attaching other fluorophores to PNA mainly at N-terminus and using them as label to detect various properties of PNA.[22,23] The incorporation of intrinsically fluorescent 2-aminopurine into PNA has many advantages.[13] It can be selectively excited in presence of a normal base (A, C, T or G) making it ideal for (i) using as a lable, (ii) studying local environment changes resulting from PNA binding with other molecules and (iii) measuring the kinetics of duplex formation and study dynamics interaction.[24] The incorporation of this base into PNA would therefore add a new dimension to the existing repertoire of PNA properties and potential applications. The fluorescence studies describe PNA-DNA (**4-11:12/13**) hybrid formation by monitoring changes in 2-aminopurine fluorescence.

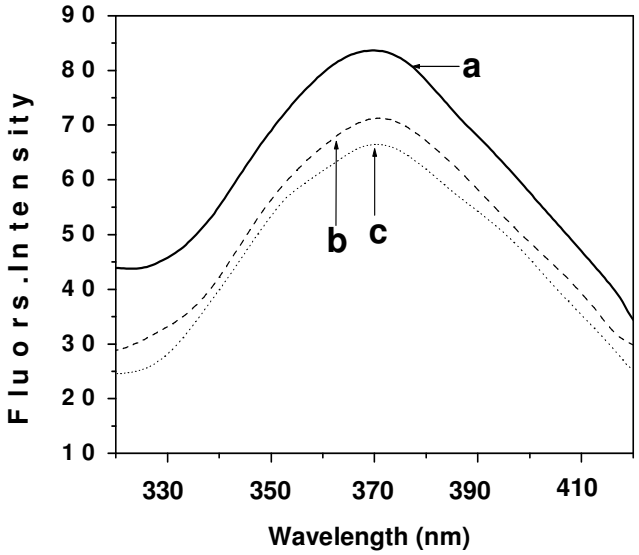

Figure 3. Fluorescent spectra of (a) 2-aminopurine monomer, (b) PNA **4**, (c) **4:12**.

4.5. RESULTS AND DISCUSSIONS

4.5.1 Fluorescent Studies

***4.5.1a PNA:DNA duplex formation: Monitoring by fluorescence*:** The 2-amino purine PNA monomer (**3**) and the PNA oligomers (**4-11**) exhibited fluorescence emission with maxima at 371nm upon excitation at 308nm. The fluorescent PNAs **4-7** upon binding to its cDNA **12** affected a decrease in fluorescence intensity indicating a successful hybridization. Similar behavior was obtained with *sp*-PNA conjugate **8-11** incorporating 2-AP upon addition of cDNA **12**. Hydrogen bond formation between 2-aminopurine and thymine is known to decrease the quantum yield of the 2-aminopurine.[26] The duplex formation was substantiated by a flourescence titration experiment in which stoichiometric addition of cDNA **12** to a fluorescent PNA **4** solution was accompanied by a gradual decrease in flourescence intensity upto an addition of 1 equivalence of DNA, beyond which the intensity did not vary much (Figure 4).

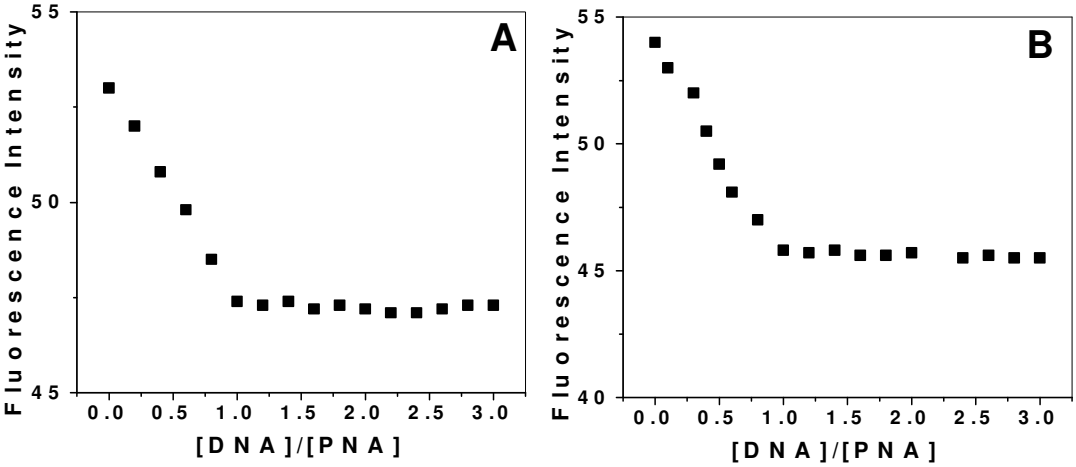

Figure 4. Fluorescence titration of DNA (**12**) with (**A**) PNA **4** and (**B**) PNA **8**. (2µM PNA in 10mM Phosphate at pH 7.3).

The fluorescent 2-AP-*sp*-PNA **8** also showed similar characteristics upon DNA titration. The 2-AP-PNA (**4**) showed a small but significant change in the fluorescence intensity (50-45arb units) on addition of DNA (**12**) and the quenching was saturated with one equivalence of DNA. There was a tremendous change in the quenching of the spermine analogue 2-AP-*sp*-PNA (**8**) where the fluorescence intensity dropped from 50 to 30arb units. The comparatively slow rate of duplex formation in **4** is due to presence of the anionic C-terminal carboxylic acid. As the spermine analogues have terminal positive charges, these interact with the negatively charged DNA to form much stable complexes. These data are similar to the previously reported PNA containing 2-AP.[15]

4.5.1b Temperature dependent fluorescence: The strength of PNA self-organisation and PNA-DNA binding was also studied by temperature dependent fluorescence experiments. Upon heating, both fluorescent intensity of PNA alone and PNA:DNA duplex showed a gradual decrease. The fluorescent intensity reached a saturation around 55-60°C for **4-11**. The percentage decrease in total intensity for PNA-DNA melting (60%) was much larger than that observed for PNA self-melting (25%) under identical temperature range (Figure 5). The monomer **3** did not show any noticeable change (<2%) in fluorescent intensity upon heating in the temperature range of 5-50 °C. The T_ms obtained from temperature dependent absorbance was slightly lower than that from the fluorescence temperature data (Figure 6). The fluorescence T_m values of PNA:DNA hybrids are given in Table 4.

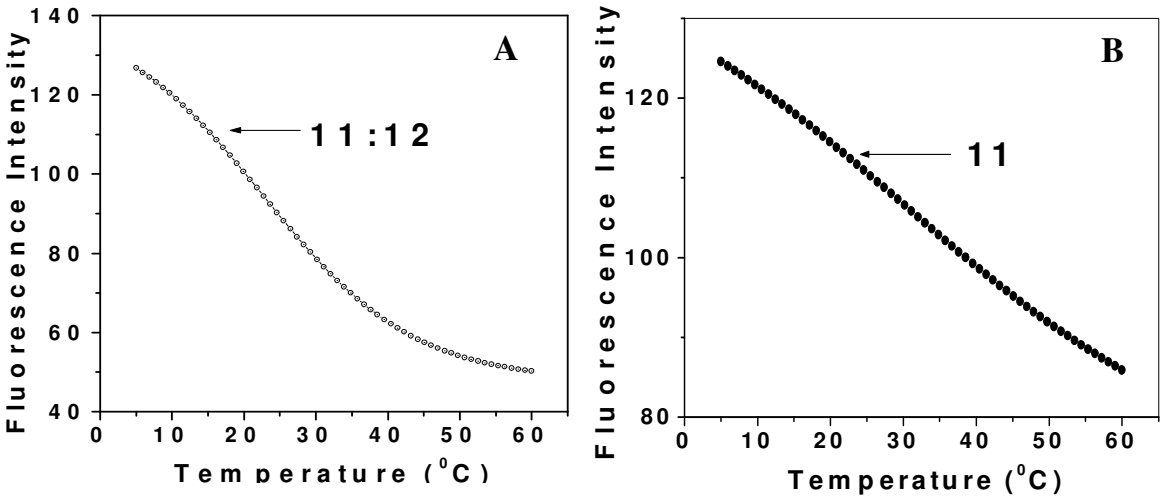

Figure 5. Fluorescence melting isotherm of (**A**) **11:12** duplex and (**B**) **11** single strand.

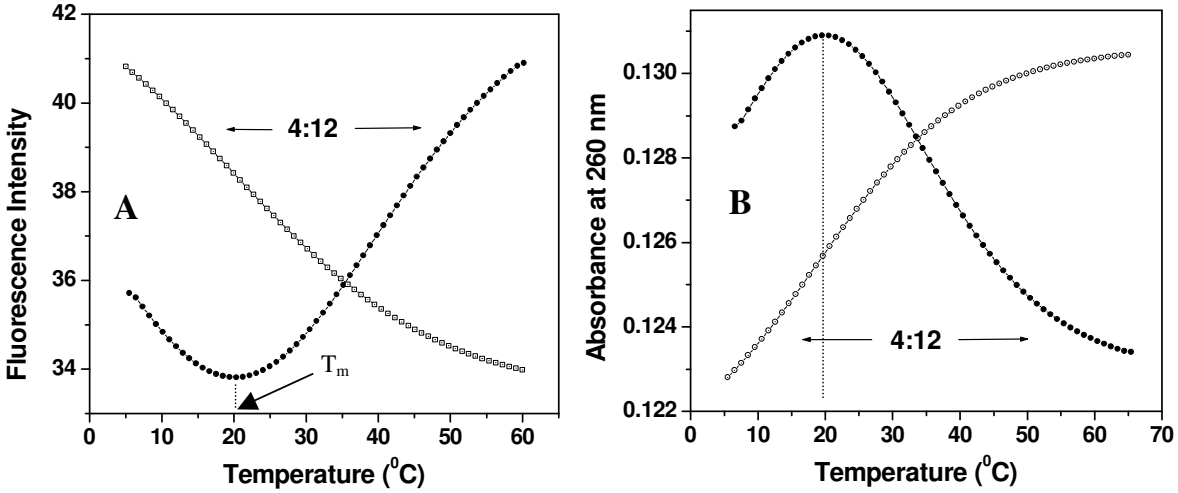

Figure 6. (**A**) Fluorescence melting isotherm and (**B**) UV melting isotherm of PNA:DNA duplex (**4:12**) shown with the first derivative plots.

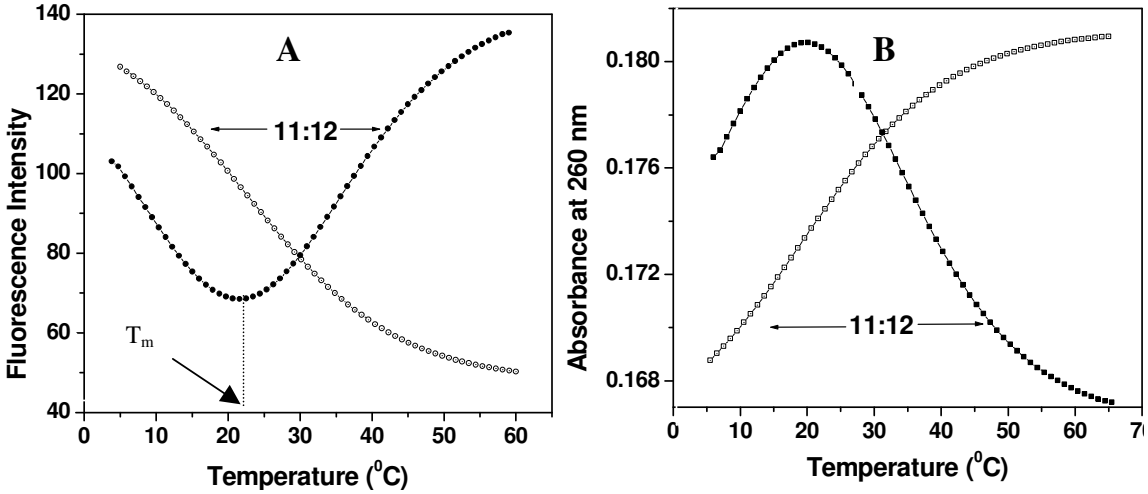

Figure 7. (**A**) Fluorescence melting isotherm and (**B**) UV melting isotherm of PNA:DNA duplex (**11:12**) shown with the first derivative plots.

Table 4. Fluorescence melting T_m of PNA:DNA complexes.[a]

PNA	Sequence	T_m (^{0}C)
4	H_2N–T A T T A T T A T T **A*** T T–$CONHCH_2CH_2CO_2H$	20
5	H_2N–T A T T A T T **A*** T T A T T– $CONHCH_2CH_2CO_2H$	30
6	H_2N–T A T T **A*** T T A T T A T T– $CONHCH_2CH_2CO_2H$	24
7	H_2N–T **A*** T T A T T A T T A T T– $CONHCH_2CH_2CO_2H$	22
8	H_2N–T A T T A T T A T T **A*** T T–CONH-Spermine	22
9	H_2N–T A T T A T T **A*** T T A T T–CONH-Spermine	15
10	H_2N–T A T T **A*** T T A T T A T T–CONH-Spermine	21
11	H_2N–T **A*** T T A T T A T T A T T–CONH-Spermine	23

[a]UV T_m data (^{o}C) for PNA:DNA complexes with DNA **12**. Experiments were performed in 10mM sodium phosphate buffer, pH 7.3. T_m values are accurate to $\pm1^o$C and were obtained from peaks in the first derivative plots of fl. intensity vs temeperature. Each experiment was repeated at least twice.

In consistence with UV-T_m experiments, the T_ms obtained from temperature dependent absorbance (20°C) for spermine PNA:DNA (**11:12**) hybrid was slightly lower than (23°C) that from the fluorescence temperature data (Figure 7).

***4.5.1c Kinetics of PNA:DNA hybridisation*:** The kinetics of PNA:DNA hybridization process was examined by monitoring the fluorescence emission decay at 371 nm as a function of time after mixing 2-AP PNA (**4-11**) with the complementary, antiparallel DNA (**12**). The emission intensity decreased exponentially over a period of 0-20min and there after remained constant (Figure 8A). The time-dependent decrease in fluorescence of PNAs **4-11** immediately upon mixing with DNA may be attributed to specific formation of 2-AP-PNA:DNA hybrid. A similar behaviour was seen in experiments on 2-AP-*sp*-PNA:DNA duplex (**8-11**:**12**). The fluorescence decay curve was exponential. Thus fluorescence from 2AP-PNA is a good monitor of hybridization strength and efficiency. In contrast, PNA (**10**) with mismatch DNA (**13**)

exhibited initial increase in fluorescence and thereafter remained constant over the period (Figure 8B).

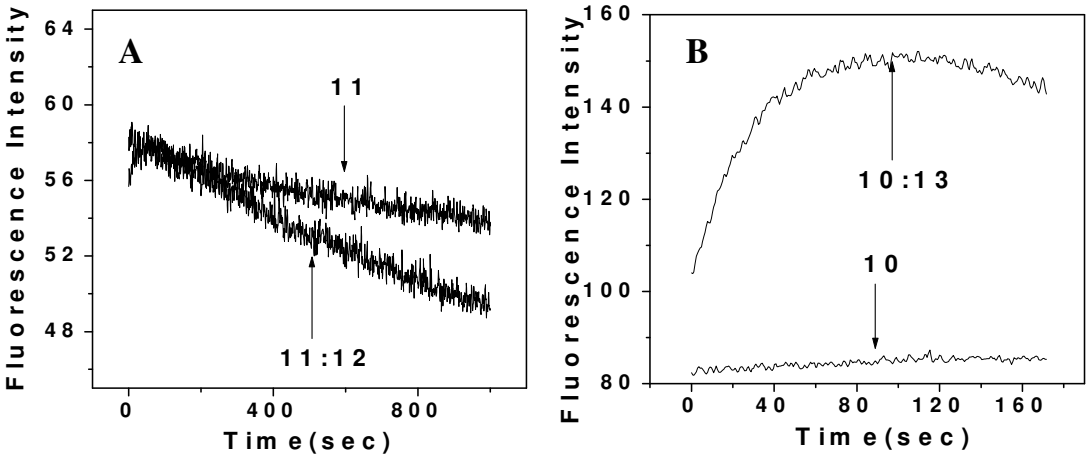

Figure 8: Kinetics of representative (**A**) PNA **11** single strand & their binding with DNA **12** and (**B**) PNA **10** single strand and it's binding with mismatch DNA **13** measured by fluorescence λ_{Ex}(308nm) and λ_{Em}(371nm). Buffer: 10mM Phosphate at pH 7.3.

4.5.1d Fluorescence Anisotropy: Another fluorescence observable parameter capable of giving useful information on molecular environment is fluorescence anisotropy.[25,26] The base 2-AP in **4-11** senses the local changes in conformation/environment accompanying the self-melting of PNA from an ordered chain to a random coil. This process also reorients the fluorophore, leading to a decrease in anisotropy. A higher fluorescence anisotropy and polarization value implies that the fluorophore is more rigid. The polarization and anisotropy values of 2-AP fluorescence was measured as a function of temperature for both PNA **4-11** and PNA:DNA duplex (**4-11**:**13**) and the results are shown in Table 5. An appreciable decrease of both was observed with increasing temperature till about 40^{o}C after which it remained constant. The observed change in anisotropy values in overall suggests that 2-AP base faithfully reports the environment and structural changes in PNA upon mixing with DNA and/or heating,

thus substantiating its utility in monitoring such dynamic events. Thus, the 2-AP residue in **4-11** senses the local changes in conformation/environment accompanying the self-melting of PNA from an ordered chain to a random coil, a process that also reorients the fluorophore.

Table 5. Anisotropy values of PNA single strands and PNA:DNA complexes.

PNA	Anisotropy at temp. (^{0}C)		
	15	**35**	**50**
4	0.80	0.55	0.55
5	0.68	0.64	0.64
6	0.72	0.69	0.69
7	0.89	0.52	0.52
8	0.68	0.43	0.42
9	0.89	0.53	0.53
10	0.68	0.50	0.50
11	0.88	0.71	0.70

PNA:DNA	Anisotropy at temp. (^{0}C)		
	15	**35**	**50**
4:12	0.87	0.78	0.78
5:12	0.83	0.70	0.70
6:12	0.84	0.75	0.75
7:12	0.90	0.87	0.87
8:12	0.69	0.65	0.65
9:12	0.91	0.89	0.89
10:12	0.69	0.66	0.65
11:12	0.89	0.86	0.86

Except for PNAs **5** and **6**, not much difference in anisotropy was noticed upon hybridization with DNA, suggests that PNAs are reasonably ordered even in single stranded form. PNAs **5** and **6** have 2-AP units in the interior of the sequence and hence show increased order (higher anisotropy) upon complementation with DNA. Thus, it is demonstrated that the incorporation of intrinsically fluorescent 2-aminopurine does not affect the binding property of the PNA with the cDNA and further this fluorophore can be used to monitor the structural/conformational variations during hybrid formation and melting. Apart from their utility in diagnostics, these PNA probes may lead to newer capabilities such as study of cellular uptake and intracellular distribution of PNA by employing fluorescence microscopy and as sequence specific DNA biosensors.

4.6 CONCLUSIONS

It is demonstrated that the incorporation of intrinsically fluorescent 2-aminopurine does not affect the binding property of the PNA with the cDNA and further this fluorophore can be used to monitor the structural/conformational variations during hybrid formation and melting. Apart from their utility in diagnostics, these PNA probes may lead to newer capabilities such as study of cellular uptake and intracellular distribution of PNA by employing fluorescence microscopy and as sequence specific DNA biosensors.

SECTION B: INDUCTION OF CHIRALITY IN ACHIRAL *aeg*PNA

4.7. INTRODUCTION

Peptide nucleic acids (PNAs) are DNA mimics in which the deoxyribose phosphate backbone has been replaced by a polyamide skeleton composed of *N*-(2-aminoethyl)glycine units, with the nucleobases linked to the glycine nitrogen via a methylene carbonyl group.[27,28] PNAs bind efficiently and with high sequence selectivity to both single stranded RNA, DNA, and PNA as well as to double stranded DNA.[29] In particular, PNA oligomers bind to complementary DNA oligonucleotides forming helical PNA-DNA duplexes that are in general more stable than the corresponding DNA-DNA duplexes.[30] Furthermore, PNA oligomers of complementary sequences have been shown to hybridize forming helical PNA-PNA duplexes of higher thermal stability's (T_m) than those observed for the PNA-RNA and the PNA-DNA duplexes.[31] The results obtained so far show that PNA has many of the properties required for an antisense or antigene drug including high biological and chemical stability.[32] However, recent structural studies by NMR and X-ray crystallography on PNA complexes (PNA-RNA,[33] PNA form DNA,[34] and especially a PNA-PNA duplex[35] and a PNA_2:DNA triplex,[36] have indicated that the conformation inherently adopted by PNA is not optimal for hybridization to complementary RNA or DNA. PNA seems to prefer a wider helix (28A°) with a much larger pitch (18bp) than DNA or RNA.[35] Since the first reports on PNA, several strategies of structure modification have been explored in order to better understand the chemical and structural features which determine PNA-DNA molecular recognition. The basic structure and the constrained flexibility of the PNA backbone appear to be of

fundamental importance.[32] PNAs are inherently achiral, and therefore PNA-PNA duplexes are racemic mixtures of double helices of opposite handedness.[5] A preferred handedness in the duplex may be induced by linking a chiral amino acid (e.g. L- or D lysine) to the C-terminus of the strand. The process was described as "a seeding of chirality, beginning from the terminal base pair and migrating through the stack of the bases". As expected, helices induced by D- and L-lysine was found to be of opposite helicity.[37] These results indicate that the preferred helical sense of a PNA-PNA duplex is not related in a simple way to the absolute configuration of the amino acid attached to the carboxy-terminus.

4.8. RATIONALE FOR THE PRESENT WORK

More recently, with chiral monomers based on different amino acids inserted into the backbone of the PNA strand, it was found that the type of amino acid side chain and the configuration of the chiral center affect the stability of PNA-DNA duplexes.[38,39] These monomers allow the investigation of having specifically positioned stereogenic centers within the PNA oligomer. Thus, it is of a general interest to investigate how many stereogenic centers inserted at which positions of a PNA oligomer can induce a preferred handedness of the single or double stranded PNA, and if an eventual stereochemical preorganization of PNAs can favor the DNA recognition process. This section presents the effect of stereogenic centers within the backbone on PNA preorganization and DNA binding properties of the PNA-DNA helix. These are studied by means of thermal denaturation measurements (T_m, from which the thermodynamic parameters were derived) and CD spectroscopy. The handedness of PNA helices is discussed on the base of circular dichroism spectra.

Chiral amino acids (D- and L-Proline) (Figure 9) are inserted distally in a PNA 8-mer by means of a standard procedure on a solid phase.[40]

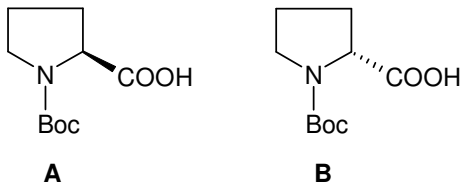

Figure 9. A) L-Proline, B) D-proline.

4.9. OBJECTIVES

The specific objectives of this section are

1. Synthesis of N-protected L-proline and D-proline.
2. Synthesis of PNA- sequences incorporating chiral amino acids.
3. Biophysical studies of chiral PNA-DNA hybrids using UV and CD Spectroscopy.

4.10. WORK DONE

4.10.1. Synthesis of Protected Amino Acids

The N-Boc-L-proline and N-Boc-D-proline were synthesized by reported protection/deprotection chemistry (See Chapter 3). This chiral monomer was used directly for incorporation into PNA oligomers.

4.10.2. Synthesis of PNA Oligomers

All the peptide oligomers were synthesized on Merrifield resin, with β-alanine chosen as the first amino acid linker. The rationale for this is that β-alanine is achiral and hence does not interfere in the spectral properties of PNA. Merrifield resin was

therefore functionalised with N-Boc-β-alanine following the cesium salt method[41] to obtain the benzyl ester linkage between the resin and the first amino acid. The functionalised resin was assayed to determine the loading value of first amino acid by picric acid method (Chapter 2).

Table 6. Resin-linked PNA Sequences Synthesized by Solid Phase Synthesis.

Entry	Resin-linked PNA Oligomer
1	MF--β-ala-**LP**-T T T T T T T T -Boc
2	MF--β-ala-**DP**-T T T T T T T T -Boc
3	MF--β-ala-T T T T T T T T-**LP**-Boc
4	MF--β-ala-T T T T T T T T-**DP**-Boc
5	MF--β-ala-T T T T T T T T-Boc

MF = Merrifield resin; T = *aeg*PNA-T; LP= Boc protected L-proline; DP= Boc protected D-proline monomer.

The stepwise synthesis of chiral PNA oligomers were carried out in the C→N direction as described in Chapter 2. The chiral amino acid, Boc protected proline (LP/DP), has been incorporated at 'C' and 'N' terminal position into PNA 8-mer that otherwise contain thymine monomer. The control aminoethylglycyl (*aeg*) PNA T_8 oligomer was also synthesized. The assembly of the PNA oligomers **1-5** was performed manually on Merrifield resin prior functionalised with β-alanine (0.180equiv/gm) by standard solid phase peptide synthesis.

4.10.3. Synthesis of Complementary Oligonucleotides

The oligodeoxynucleotide (**6**, Table 7) was synthesized on a Pharmacia Gene Assembler Plus DNA synthesizer using the standard β-cyanoethyl phosphoramidite chemistry. The oligomers were synthesized in the 3'-5' direction on a CPG solid support, followed by ammonia treatment.[42] The oligonucleotides were de-salted by

gel filtration, their purity ascertained by RP HPLC on a C18 column to be more than 98% and were used without further purification in the biophysical studies of PNA.

Table 7. DNA Oligonucleotide Sequences.

DNA	**Oligomer Sequences** 5' → 3'		
6	G C A A A A A A A A C G	Complementary to PNA-T_8 with CG clamps	**1-5**

4.10.4. Cleavage from the Solid Support

The PNA oligomers were cleaved from the solid support using TFMSA[43] to yield oligomers with free 'C' terminal carboxylic acids.

4.10.5. Purification

The fully deprotected oligomers were initially desalted by size-exclusion chromatography over G25 Sephadex. They were subsequently purified by FPLC on a reverse phase C8 column using an ascending gradient of acetonitrile in water containing 0.1% TFA. The purity of the oligomers was re-checked by reverse phase HPLC on a C18 column and confirmed by MALDI-TOF mass spectrometry. Some representative HPLC profiles and mass spectra are shown in Figures 10 and 11 respectively.

Table 8. Chiral PNA Oligomer Sequences.

PNA	Sequence Composition
1	H_2N–T T T T T T T T -**LP**–$CONHCH_2CH_2CO_2H$
2	H_2N–T T T T T T T T -**DP**–$CONHCH_2CH_2CO_2H$
3	H_2N–**LP**-T T T T T T T T –$CONHCH_2CH_2CO_2H$
4	H_2N–**DP**-T T T T T T T T –$CONHCH_2CH_2CO_2H$
5	H_2N–T T T T T T T T –$CONHCH_2CH_2CO_2H$

T = *aeg*PNA-T; LP= Boc protected L-proline; DP= Boc protected D-proline monomer.

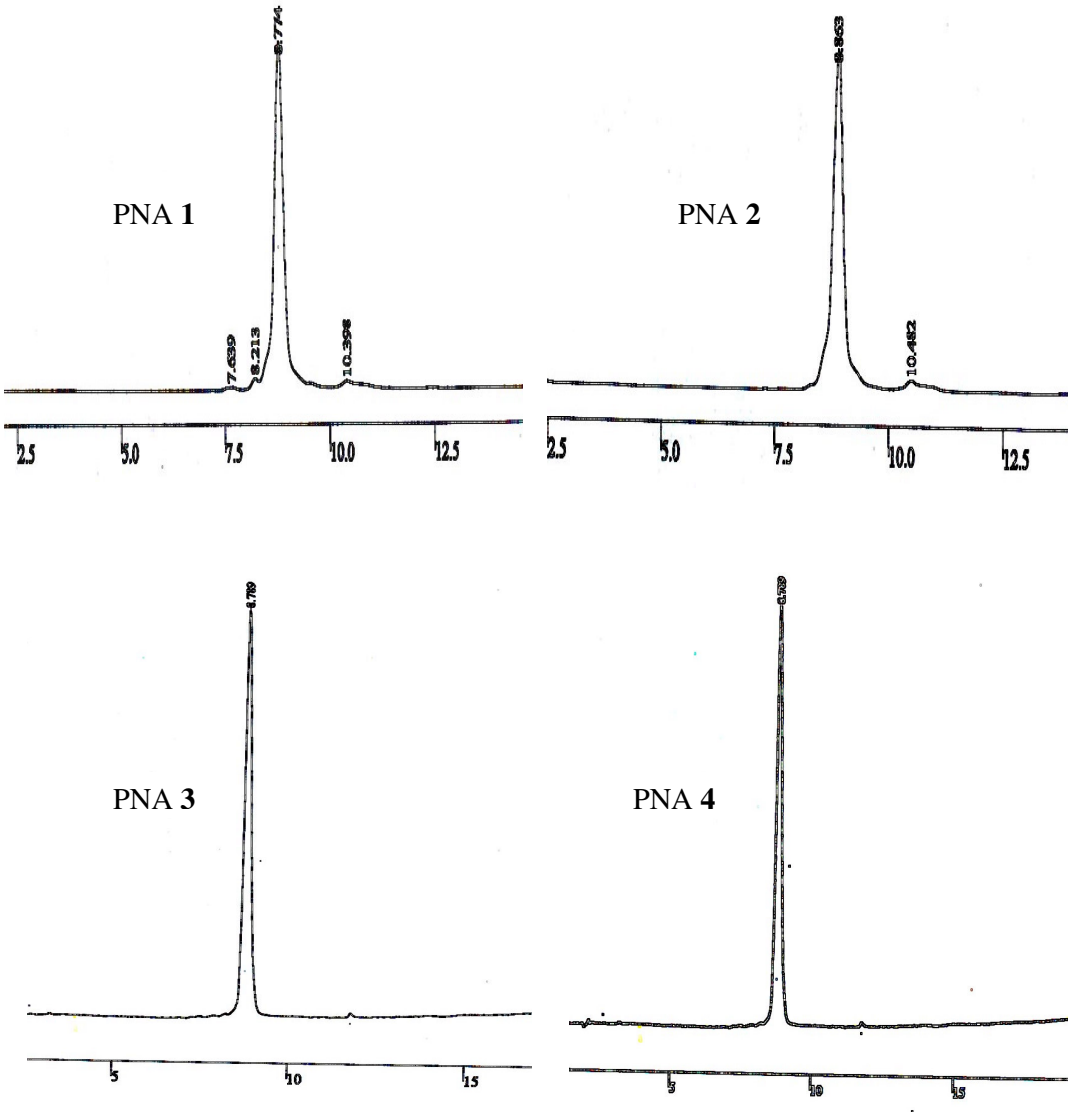

Figure 10. Representative HPLC profiles of chiral PNA oligomers.

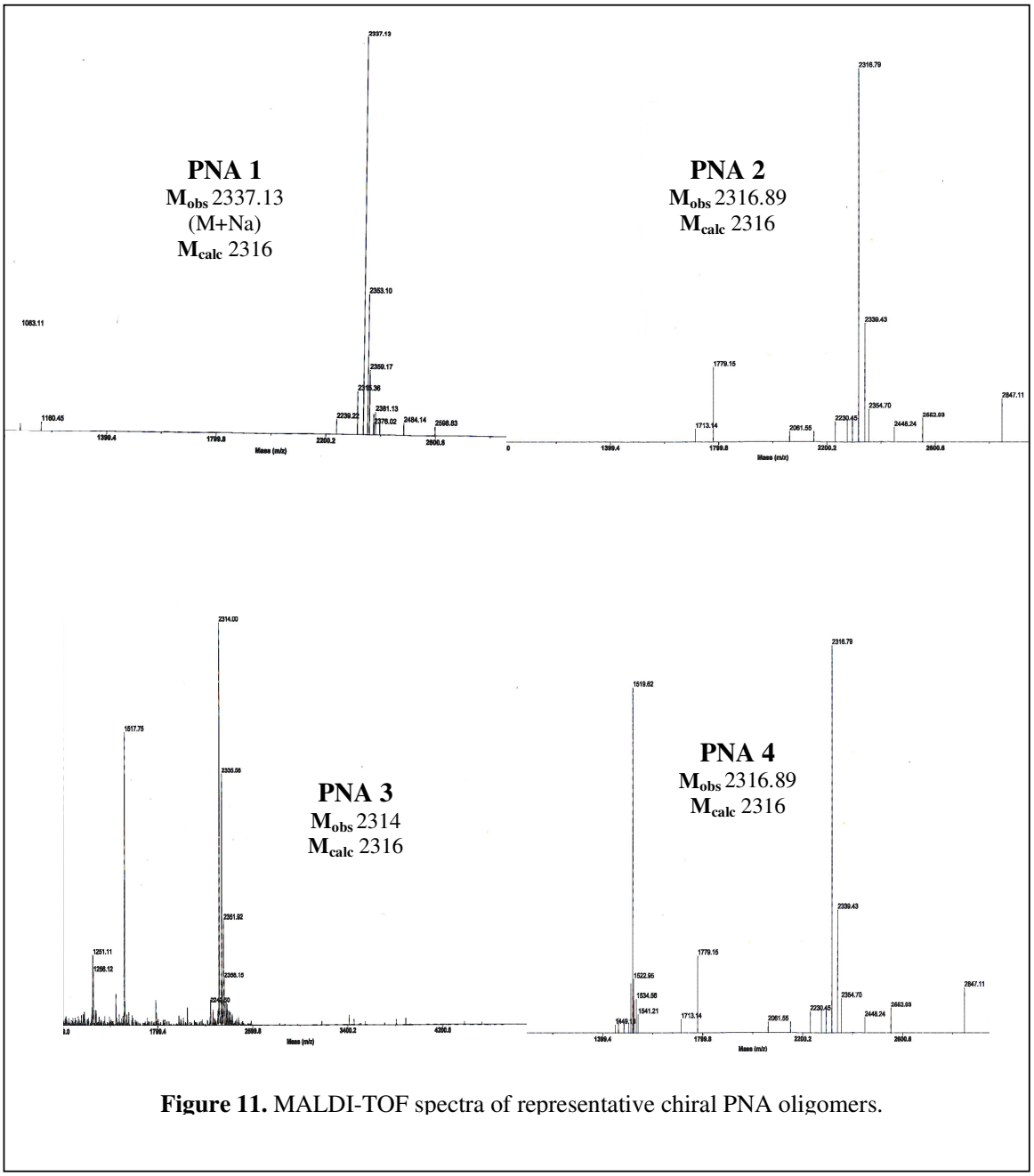

Figure 11. MALDI-TOF spectra of representative chiral PNA oligomers.

4.10.6. UV-Melting

The PNA sequences **1**-**5** were mixed with the appropriate DNA oligomer **6** in 2:1 concentration and annealed prior to melting. The samples were heated at a rate of 0.5^{o}C rise per minute and the absorbance at 260nm was recorded at every minute. The percent hyperchromicity at 260nm was plotted as a function of temperature and the melting temperature was deduced from the peak in the first derivative plots.

4.10.7. CD-Spectroscopy

CD spectra were recorded on a JASCO J715 spectropolarimeter. Each spectrum was recorded with a scan-speed of 200nm/min from 320nm to 195nm keeping a resolution of 0.1nm, a bandwidth of 1.0nm, sensitivity of 2mdeg and response 2s as an accumulation of 10 scans. The samples for CD were prepared in the manner used for UV-T_m studies by heating at 85^{o}C for 5min, followed by slow cooling to room temperature and refrigeration overnight prior to recording the CD spectra. The temperature was maintained below the Tm of the complexes as determined by UV measurements, i.e., at 10^{o}C.

4.11. RESULTS AND DISCUSSIONS

4.11.1 UV-T_m Studies

PNAs (**1-4**) containing L-Proline and D-Proline were hybridized to the complementary DNA (**6**). Thermal stabilities (T_m) of the hybrids were determined by UV spectroscopy and compared with those obtained for the achiral 8-mer PNA of the same sequence (**5**) hybridized to the same targets. The results are summarized in Table 9 and Figure 12.

Table 9. UV-T_m of PNA-DNA complexes.[a]

PNA	Sequence Composition	T_m (^{0}C)
1	H_2N–T T T T T T T T -**LP**–$CONHCH_2CH_2CO_2H$	41
2	H_2N–T T T T T T T T -**DP**–$CONHCH_2CH_2CO_2H$	41
3	H_2N–**LP**-T T T T T T T T –$CONHCH_2CH_2CO_2H$	45
4	H_2N–**DP**-T T T T T T T T –$CONHCH_2CH_2CO_2H$	42
5	H_2N–T T T T T T T T –$CONHCH_2CH_2CO_2H$	43

[a]UV T_m data (^{o}C) for PNA:DNA complexes with DNA **6**. Experiments were performed in 10mM sodium phosphate buffer, pH 7.3. T_m values are accurate to ±1^{o}C and were obtained from peaks in the first derivative plots of percent hyperchromicity vs temeperature. Each experiment was repeated at least twice.

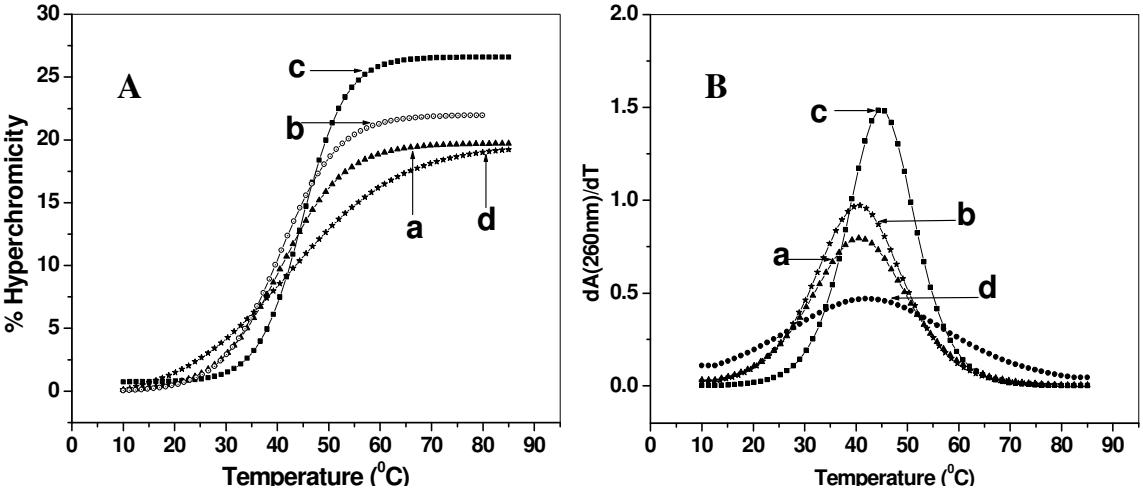

Figure 12. A) UV-Melting profiles of PNA_2:DNA complexes. **B) UV**-Melting first derivative curves of PNA_2:DNA complexes. a**. 1:6**; b. **2:6**, c. **3:6**, d. **4:6.**

The presence of chiral monomers at C-terminus in the strands, both L-proline and D-proline in the PNAs (**1-2**), caused a little decrease of stability (-2^{0}C) for the PNA-DNA hybrids, whereas one chiral L-proline monomer inserted at the N-terminus exerted a positive effect (+2^{0}C). In case of PNA **4** where D-proline is inserted at the N-terminus did not show any significant change as compared to control PNA-DNA hybrids. From these results, it appears that for PNA-DNA hybrids, the stability may depend on the position of chiral monomer in the strand and on the stereochemistry of the amino acid. In particular, with the PNA (**3**), it is certain that the configuration of

the stereogenic center can influence the binding orientation, thus exerting a certain degree of direction control.

4.11.2. CD Spectroscopy

The CD spectra of the single strand PNAs and the PNA-DNA hybrids were recorded in order to obtain information about the helix characteristics. The single stranded chiral PNAs did not show significant CD signals (Figure 13), indicating that the chiral centers are not effective in giving a defined preferred handedness. However, PNAs **1** and **3** with L-proline linked at C/N-terminus induced opposite signs in CD signals in the region 260-280nm (though not entirely mirror images), suggests that these may have opposite helicities. The difference was not so obvious for corresponding D-proline linked PNAs. In contrast, the PNA-DNA hybrids showed strong signals of opposite signs (Figure 14).

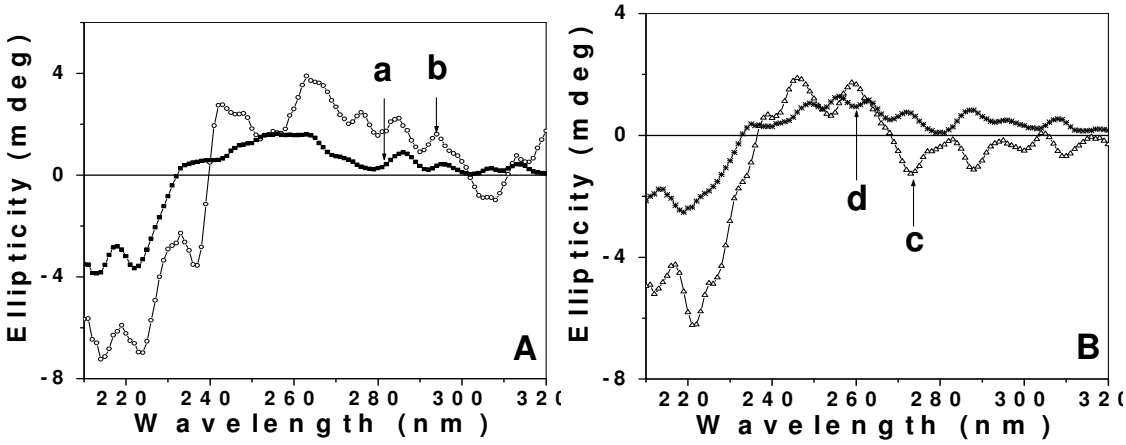

Figure 13. CD spectra of single strand PNAs (A) a:**1**, b:**2**, (B) c:**3**, d:**4**

In the case of the PNA containing L-proline monomer in the strand (**1**), the shape and the intensity of the spectra of the PNA-DNA hybrids were very similar to the PNA containing D-proline monomer in the strand (**2**), indicating that the

handedness was conferred by the chiral monomer inserted at C-terminus. Similarly, the CD spectra of the PNA-DNA hybrids containing L-proline and D-proline at N-terminus induced opposite signs.

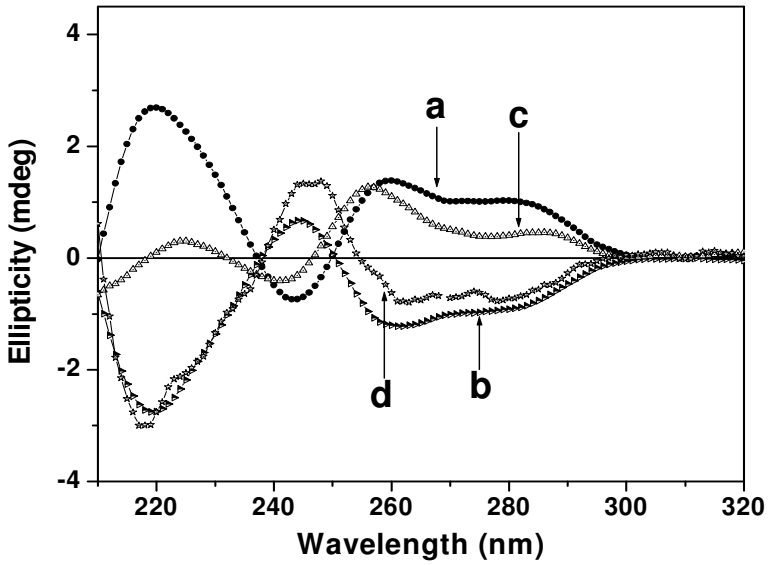

Figure 14. CD profiles of PNA_2:DNA hybrids, a. **1:6**, b. **2:6,** c. **3:6** & d. **4:6**.

It is known that for the right-handed helix, the "L-substituent" is positioned to interact with the major groove, while the "D-substituent" is "pointing directly into solution".[39] For the left-handed helix, the situation is naturally reversed. Thus, the chemical functionality on the amino acid is important. In case of PNA-DNA duplexes the effects are dominated by the DNA strand and are right-handed with both D- and L- ligand linking PNAs.[39]

We can deduce that the induced conformational changes are transmitted to the closest base, thus modifying the stacking interactions and affecting the helical preference. In the single strand same helical preference is present, although less pronounced because of the much weaker stacking interactions.

4.12. CONCLUSIONS

Chiral charged monomers introduced in a PNA strand induce a preferred handedness in the PNA-DNA hybrids. The extent of the induced chirality depends upon stereochemistry of chiral monomers and their position in the strand. The helix propagation most probably occurs through base stacking, since the preference becomes more pronounced in the PNA-DNA complex than in the single strand. The presence of charged chiral monomers only slightly preorganizes the single stranded PNAs, but it enhances significantly the helical preference of the PNA-DNA hybrids, particularly when present at C-terminus, as shown by circular dichroism. The examples shown here are for PNA_2:DNA triplexes, where the two PNA strands are antiparallel. It would be interesting to study the effects of chiral PNAs on PNA:DNA duplexes. Further, the effect of other chiral ligands such as BINAP, biphenyl or allene may throw light on origin of chiral helicity on biopolymers. Therefore, the introduction of chiral amino acid monomers in PNAs should be an efficient way of enhancing the performance of PNA probes in diagnostic and molecular biology applications.

4.13. EXPERIMENTAL

The synthesis of the *aeg*PNA-T/A monomers was carried out according to the procedures described in Chapter 2.

*2-aminopurine PNA monomer (**3**)*

The desired PNA monomer **3** carrying a 2-aminopurine moiety was synthesized in two steps starting from the previously known compound ethyl N-(2-amino-6-chloropurin-9-ylacetyl)-N-(2-butoxycarbonylaminoethyl) glycinate **1**

(Chapter 2). The 6-chloro group in **1** was first removed by hydrogenation over Pd–C to afford **2**, which was followed by hydrolysis of the ester with aq. NaOH to give the corresponding carboxylic acid **3**.

^{1}H NMR of **2** ($CDCl_3$) δ: 8.65 (s, 1H, Ar-*H8*), 7.92–7.88 (s, 1H, Ar-*H6*), 5.88 (br s, 1 H, N*H*), 5.38 (br s, 1H), 5.04–4.89 (s, 2H, glyCH_2), 4.30–4.07 (m, 4H, N–CH_2, OCH_2), 3.64–3.29 (m, 4H), 1.42 (s, 9H), 1.25 (m, 3H).

^{13}C NMR of **2** ($CDCl_3$) δ: 169.6–169.3 (CO_2Et), 167.3–166.9 (*C*ONH), 159.9 (*C*2), 156.2 (Boc: O*C*ON), 153.4 (*C*8), 148.6 (*C*6), 143.7 (*C*4), 126.8 (*C*5), 79.7 (Me_3CO), 62.1, 61.5, 48.4, 38.6, 28.3 (all CH_2), 13.9 (Me_3C).

BOC protected L-and D-proline monomers

The desired chiral amino acid monomers (Figure 1) were synthesized in two steps starting from the easily available L-proline and D-proline. The acid group in L- and D-proline was first esterified to afford methyl esters of L- and D-proline, which was followed by N-BOC protection and further hydrolysis of the ester with aq. NaOH to give the corresponding carboxylic acid.

^{1}H NMR of **A** ($CDCl_3$) δ: 9.79 (br s, 1H), 4.34-4.23 (m, 1H), 3.52-3.36 (m, 2H), 2.25-1.89 (m, 4H), 1.40 (d, 9H).

^{1}H NMR of **B** ($CDCl_3$) δ: 8.00 (br s, 1H), 4.20-4.16 (m, 1H), 3.43-3.34 (m, 2H), 2.16-1.84 (m, 4H), 1.43 (s, 9H).

4.13.1. Aminolysis: Cleavage with Spermine

The peptide resin (20mg) after *t*-Boc deprotection (unless otherwise mentioned) was taken along with 80mg of the amine (spermine) in a 0.5ml screw-

capped vial and heated at 60°C for 42h. The reaction mixture was diluted with water and filtered through sintered funnel and concentrated. The crude mixture was passed through G15/G25 sephadex column and eluted with water to remove the excess amine and further purified by FPLC as described earlier.

4.13.2. Melting experiments

Duplex melting experiments were carried out in the 10mM sodium phosphate.buffer. Appropriate oligonucleotides and PNA each at a strand concentration of 1-2μM based on UV absorbance calculated using molar extinction coefficients at 260nm, A = 15.4, C =7.3, G =11.7, T = 8.8 $cm^2/\mu M$, were mixed, heated to 85°C for 2min, cooled to room temperature and then stored at 4°C overnight. The A_{260} at various temperature were recorded using Perkins Elmer Lambda 35 UV/VIS spectrometer, fitted with temperature programmable peltier, with a heating rate of 0.5°C/min over the rage 5-80°C. Dry nitrogen gas was flushed in the spectrophotometer chamber to prevent condensation at low temperature. Microcal Origin software was used for data analysis. All the curves were fitted with a Boltzmann sigmoidal fit and the melting temperature determined from the peak of the differential curves.

4.13.3. Fluorescent Spectroscopy

Fluorescence measurements were done on a Perkin Elmer model LS-50B spectrometer attached to a Julabo water bath circulator for variable temperature. The fluorescent DNA samples dissolved in the buffer were excited at 308nm and the emission monitored at 367nm using a spectral bandwidth of 5nm. The kinetic data were collected for 15-30min with a time constant of 1s and 5nm bandwidth at 20°C.

The temperature was kept constant by circulating water through water-jacketed cuvette holder. Emission wavelength was fixed at 367nm with excitation at 308nm. For fluorescence polarization and anisotropy measurements, the sample was prepared with a ratio of PNA:DNA 1:2 to ensure complete binding. The samples were excited at 308nm and fluorescence signal at 367nm monitored through crossed polarizers. The experiment was repeated at different temperature (15, 35 and 50°C).

4.13.4. CD Spectroscopy

CD spectra were recorded on a JASCO J715 spectropolarimeter. Each spectrum was recorded with a scan-speed of 200nm/min from 320nm to 195nm keeping a resolution of 0.1nm, a bandwidth of 1.0nm, sensitivity of 2mdeg and response 2s as an accumulation of 10 scans. The samples for CD were prepared in the manner used for UV-T_m studies by heating at 85^oC for 5min, followed by slow cooling to room temperature and refrigeration overnight prior to recording the CD spectra. The temperature was maintained below the T_m of the complexes as determined by UV measurements, i.e., at 10^oC.

4.14. APPENDIX

- Compound **2**, ^{1}H NMR
- Compound **3**, ESI-MASS
- Polarization values for PNAs **4**-**11**
- Compound **A**, ^{1}H NMR
- Compound **B**, ^{1}H NMR

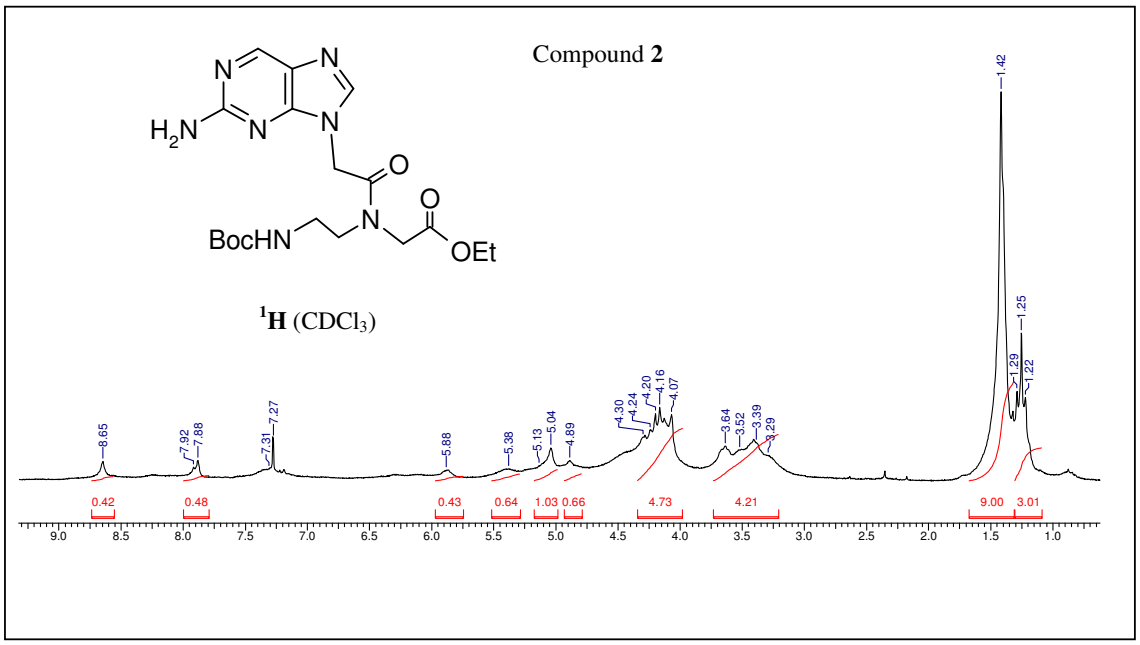
Compound **2**
^{1}**H** ($CDCl_3$)
8.65
7.92
7.88
7.31
7.27
5.88
5.38
5.13
5.04
4.89
4.30
4.24
4.20
4.16
4.07
3.64
3.52
3.39
3.29
1.42
1.25
1.29
1.22
0.42
0.48
0.43
0.64
1.03
0.66
4.73
4.21
9.00
3.01

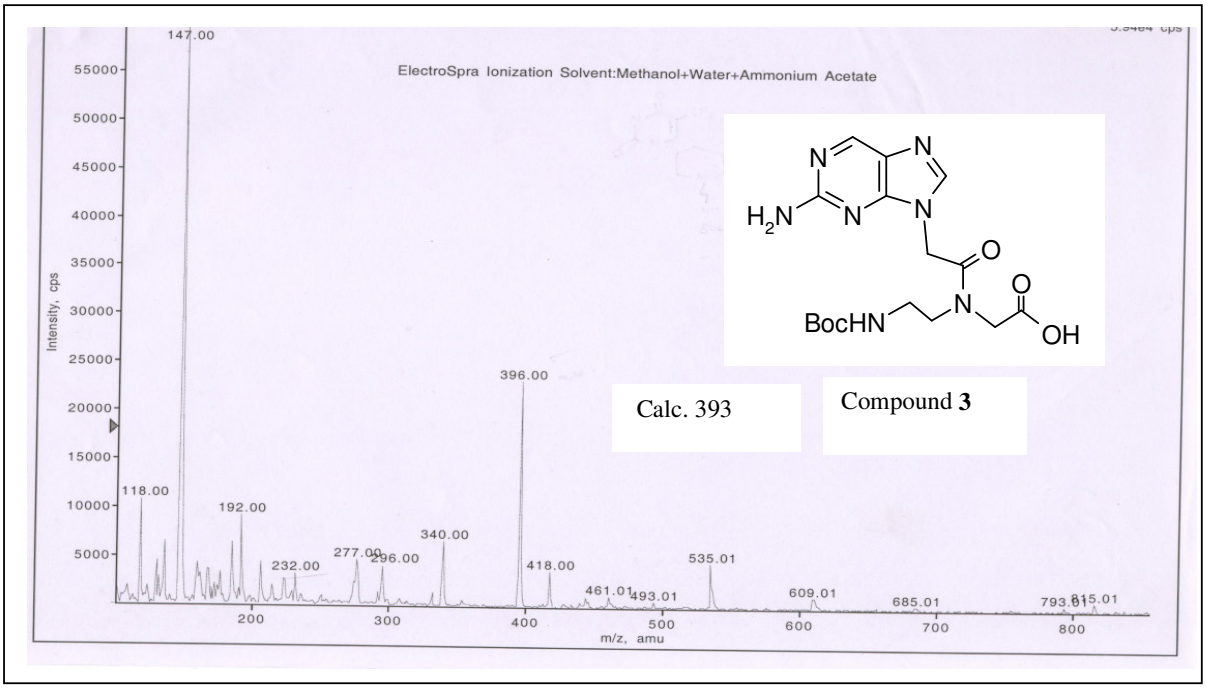
ElectroSpra Ionization Solvent:Methanol+Water+Ammonium Acetate
Intensity, cps
m/z, amu
147.00
396.00
118.00
192.00
232.00
277.00
296.00
340.00
418.00
461.01
493.01
535.01
609.01
685.01
793.01
815.01
Calc. 393
Compound **3**

Table 1. Polarization values of PNA single strands and PNA:DNA complexes.

PNA	Polarization at temp. (^{0}C)		
	15	**35**	**50**
4	0.85	0.62	0.62
5	0.84	0.80	0.80
6	0.73	0.71	0.71
7	0.85	0.60	0.60
8	0.77	0.61	0.61
9	0.89	0.62	0.62
10	0.82	0.66	0.66
11	0.91	0.84	0.84

PNA: DNA	Polarization at temp. (^{0}C)		
	15	**35**	**50**
4:12	0.89	0.84	0.84
5:12	0.83	0.82	0.82
6:12	0.93	0.86	0.86
7:12	0.91	0.89	0.89
8:12	0.78	0.75	0.75
9:12	0.94	0.87	0.87
10:12	0.85	0.75	0.75
11:12	0.95	0.92	0.92

Compound **A**

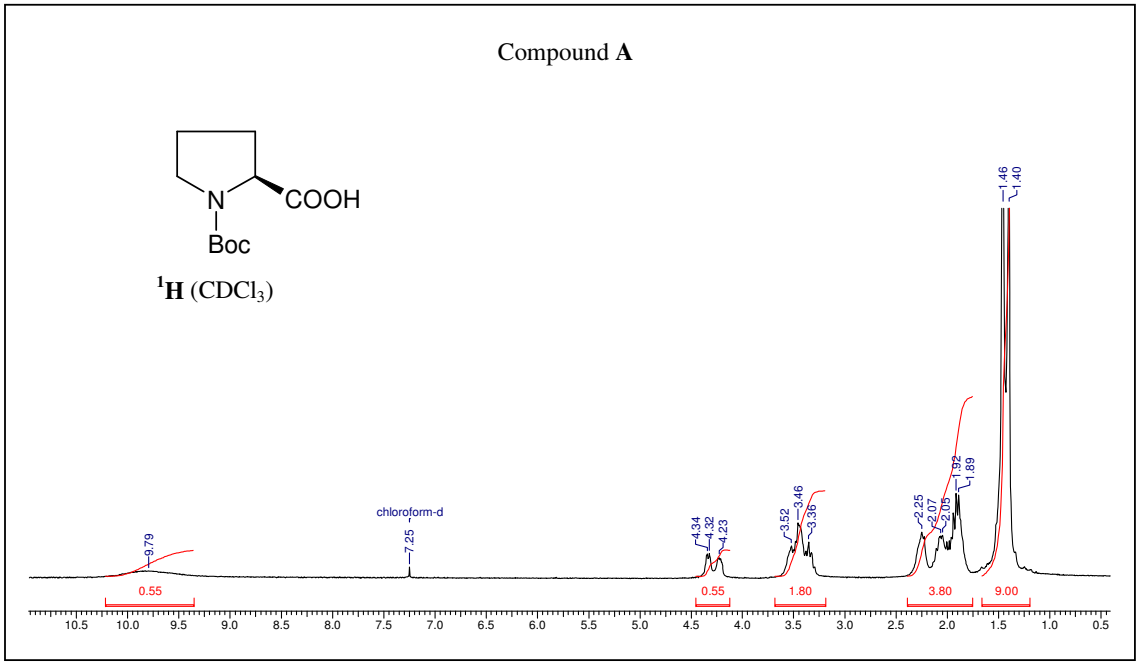

^{1}H ($CDCl_3$)

Compound **B**

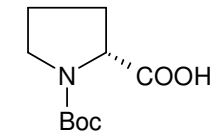

^{1}H ($CDCl_3$)

4.15. REFERENCES

[1] Nielsen, P. E. DNA analogues with nonphosphodiester backbones. *Annu. Rev. Biophys. Biomol. Struct.* **1995**, *24*, 167-183.

[2] Hyrup, B.; Nielsen, P. E. Peptide nucleic acids (PNA): Synthesis, properties and potential applications. *Bioorg. Med. Chem. Lett.* **1996**, *4*, 5-23.

[3] Corey, D. R. Peptide nucleic acids: Expanding the scope of nucleic acid recognition. *Trends Biotechnol.*, **1997**, *15*, 224-229.

[4] (a) Haaima, G.; Lohse, A.; Buchardt, O.; Nielsen, P. E. Peptide nucleic acids (PNAs) containing thymine monomers derived from chiral amino acids: Hybridization and solubility properties of D-lysine PNA. *Angew. Chem. Int. Ed. Engl.* **1996**, *35*, 1939-1942; (b) Gangamani, B. P.; Kumar, V. A.; Ganesh, K. N. Synthesis of N(α)-(pyrinyl/pyrimidinyl acetyl)-4-aminoproline diastereomers with potential use in PNA synthesis. *Tetrahedron,* **1996**, *52*, 15 017-15030.

[5] Jean, J. M.; Hall, K. B. 2-Aminopurine fluorescence quenching and lifetimes: Role of base stacking. *Proc. Natl. Acad. Sci. USA.* **2001**, *98*, 37-41.

[6] Rai, P.; Cole, T. D.; Thompson, E.; Millar, D. P.; Linn, S. Steady-state and time-resolved fluorescence studies indicate an unusual conformation of 2-aminopurine within ATAT and TATA duplex DNA sequences. *Nucl. Acid. Res.* **2003**, *31*, 2323-2332.

[7] (a) Xu, D.; Evans, K. O.; Nordlund, T. M. Melting and premelting transitions of an oligomer measured by DNA base fluorescence and absorption. *Biochemistry*, **1994**, *33*, 9592-9599; (b) Law, S. M.; Eritja, R.; Goodman, M. F.; Breslauer, K. J. Spectroscopic and calorimetric characterizations of DNA duplexes containing 2-aminopurine. *Biochemistry*, **1996**, *35*, 12329-12337.

[8] (a) Millar, D. P. Fluorescence studies of DNA and RNA structure and dynamics. *Curr. Opin. Struct. Biol.*, **1996**, *6*, 322-326; (b) Hochstrasser, R. A.; Carver, T. E.; Sowers, L. C.; Millar, D. P. Melting of a DNA helix terminus within the active site of a DNA polymerase. *Biochemistry*, **1994**, *33*, 11971-11979;

[9] Frey, M. W.; Sowers L. C.; Millar, D. P.; Benkovic, S. J. The nucleotide analog 2-aminopurine as a spectroscopic probe of nucleotide incorporation by the klenow fragment of Escherichia coli polymerase I and bacteriophage T4 DNA polymerase. *Biochemistry*, **1995**, *34*, 9185-9192.

[10] Holmen, A.; Norden, B.; Albinsson, B. Electronic transition moments of 2-aminopurine. *J. Am. Chem. Soc.* **1997**, *119*, 3114-3121.

[11] Broo, A.; Holmen, A. Ab initio MP2 and DFT calculations of geometry and solution tautomerism of purine and some purine derivatives**.** *Chem. Phys.* **1996**, *211*,147-161.

[12] Broo, A. A theoretical investigation of the physical reason for the very different luminescence properties of the two isomers adenine and 2-aminopurine. *J. Phys. Chem.* **1998**, *102*, 526-531.

[13] Santhosh, C.; Mishra, P. C. Electronic spectra of 2-aminopurine and 2,6-diaminopurine: phototautomerism and fluorescence reabsorption. *Spectrochim. Acta.* **1991**, *47A*, 1685-1693.

[14] Ward, D. C.; Reich, E.; Stryer, L. Fluorescence studies of nucleotides and polynucleotides. I. Formycin, 2-aminopurine riboside, 2,6-diaminopurine riboside, and their derivatives. *J. Biol. Chem.* **1969**, *244*, 1228-1237.

[15] Gangamani, B. P.; Kumar, V. A.; Ganesh, K. N. 2-Aminopurine peptide nucleic acids (2-*ap*PNA): intrinsic fluorescent PNA analogues for probing PNA–DNA interaction dynamics. *Chem. Commun.* **1997**, 1913-1914.

[16] Gisin, B. F. The monitoring of reactions in solid-phase peptide synthesis with picric acid. *Anal. Chim. Acta* **1972,** *58*, 248-249.

[17] Barawkar, D. A.; Rajeev, K. G.; Kumar, V. A.; Ganesh, K. N. Triplex formation at physiological pH by 5-Me-dC-N4-(spermine) [X] oligodeoxynucleotides: Non protonation of N3 in X of X*G:C triad and effect of base mismatch/ionic strength on triplex stabilities. *Nucleic Acids. Res.* **1996**, *24*, 1229-1237.

[18] Hodges, R. S.; Merrifield, R. B. Monitoring of solid phase peptide synthesis by an automated spectrophotometric picrate method. *Anal. Biochem.* **1975**, *65*, 241-272.

[19] Yeh, S-R.; Falvey, D. E. Model studies of DNA photorepair: Energetic requirements for the radical anion mechanism determined by fluorescence quenching. *J. Am. Chem. Soc.* **1992,** *114*, 7313-7314.

[20] Kanavarioti, A.; Baird, E. E.; Smith, P. J. Use of phosphoimidazolide-activated guanosine to investigate the nucleophilicity of spermine and spermidine. *J. Org. Chem.* **1995**, *60*, 4873-4883.

[21] Evans, K.; Xu, D.; Kim, Y.; Nordlund, T. M. 2-Aminopurine optical spectra: solvent, pentose ring, and DNA helix melting dependence. *J. Fluoresc.* **1992**, *2,* 209-216.

[22] Nielsen, P. E.; Egholm, M.; Berg, R. H.; Buchardt, O. Sequence-selective recognition of DNA by strand displacement with thymine-substituted polyamide. *Science*, **1991**, *254*, 1497-1500.

[23] Kremsky, J. N.; Pluskal, M.; Casey, S.; Perry-O'Keefe, H.; Kates, S. A.; Sinha, N. D. Biotin and fluorescein labeling of biomolecules by active esters of 1-phenylpyrazolin-5-ones. *Tetrahedron lett.* **1996**, *37*, 4313-4316.

[24] Nordlund, T. M.; Andersson, S.; Nisson, L.; Rigler, R.; Graslund, A.; McLaughlin, L. W. Structure and dynamics of a fluorescent DNA oligomer containing the EcoRI recognition sequence: Fluorescence, molecular dynamics, and NMR studies. *Biochemistry*, **1989**, *28*, 9095-9103.

[25] Guest, C. R.; Hochstrasser, R. A.; Sowers, L. C.; Millar, D. P. Dynamics of mismatched base pairs in DNA. *Biochemistry,* **1991**, *30,* 3271-3279.

[26] Larsen, O. F.A.; Stokkum, Ivo H. M. V.; Groot, M. L.; Kennis, John T. M.; Grondelle, R. V.; Amerongen, H. V. Electronic states in 2-aminopurine revealed by ultrafast transient absorption and target analysis. *Chem. Phys. Lett.* **2003**, *371*, 157–163.

[27] Nielsen, P. E.; Egholm, M.; Berg, R. H.; Buchardt, O. Sequence-selective recognition of DNA by strand displacement with thymine-substituted polyamide. *Science,* **1991**, *254*, 1497-1500.

[28] Egholm, M.; Buchardt, O.; Nielsen, P. E.; Berg, R. H. Peptide nucleic acids (PNA). Oligonucleotide analogs with an achiral peptide backbone. *J. Am. Chem. Soc.* **1992**, *114*, 1895-1897.

[29] Eriksson, M.; Nielsen, P. E. PNA-nucleic acid complexes. Structure, stability and dynamics. *Quart. Rev. Biophysics.* **1996**, *29*, 369-394.

[30] Egholm, M.; Buchardt, O.; Christensen, L.; Behrens, C.; Freier, S. M.; Driver, D. Berg, R. H.; Kim, S. K.; Norden, B.; Nielsen, P. E. PNA hybridizes to complementary

oligonucleotides obeying the Watson-Crick hydrogen-bonding rules. *Nature,* **1993**, *365*, 566-568.

[31] Wittung, P.; Nielsen, P. E.; Buchardt, O.; Egholm, M.; Norden, B. DNA-like double helix formed by peptide nucleic acid. *Nature,* **1994**, *368*, 561-563.

[32] Hyrup, B.; Nielsen, P. E. Peptide nucleic acids (PNA): Synthesis, properties and potential applications. *Bioorg. Med. Chem.* **1996**, *4*, 5-23.

[33] Brown, S. C.; Thomson, S. A.; Veal, J. M.; Davis, D. G. NMR solution structure of a peptide nucleic acid complexed with RNA**.** *Science*, **1994**, *265*, 777-780.

[34] Eriksson, M.; Nielsen, P. E. Solution structure of a peptide nucleic acid-DNA duplex. *Nature Struct. Biol.* **1996**, *3*(5), 410-413.

[35] Rasmussen, H.; Kastrup, J. S.; Nielsen, J. N.; Nielsen, J. M.; Nielsen, P. E. Crystal structure of a peptide nucleic acid (PNA) duplex at 1.7 A^0 resolution. *Nature Struct. Biol.* **1997**, *4*, 98-101.

[36] Betts, L.; Josey, J. A.; Veal, J. M.; Jordan, S. R. A nucleic acid triple helix formed by a peptide nucleic acid-DNA complex. *Science,* **1995,** *270*, 1838-1841.

[37] Wittung, P.; Eriksson, M.; Lyng, R.; Nielsen, P. E.; Norden, B. Induced chirality in PNA-PNA duplexes. *J. Am. Chem. Soc.* **1995**, *117*, 10167-10173.

[38] Haaima, G.; Lohse, A.; Buchardt, O.; Nielsen, P. E. Peptide nucleic acids (PNAs) containing thymine monomers derived from chiral amino acids: Hybridization and solubility properties of D-lysine PNA. *Angew. Chem. Int. Ed. Engl.* **1996**, *35*, 1939-1942.

[39] Sforza, S.; Haaima, G.; Marchelli, R.; Nielsen, P. E. Chiral peptide nucleic acids (PNAs):helix handedness and DNA recognition. *Eur. J. Org. Chem.* **1999**, 197-204.

[40] Christensen, L.; Fitzpatrick, R.; Gildea, B.; Petersen, K. H.; Hansen, H. F.; Koch, T.; Egholm, M.; Buchardt, O.; Nielsen, P. E.; Coull, J.; Berg, R. H. Solid-phase synthesis of peptide nucleic acids. *J. Pept. Sci.* **1995**, *3*, 175-183.

[41] Gisin, B. F. The monitoring of reactions in solid-phase peptide synthesis with picric acid. *Anat. Chim. Acta* **1972,** *58*, 248-249.

[42] Barawkar, D. A.; Rajeev, K. G.; Kumar, V. A.; Ganesh, K. N. Triplex formation at physiological pH by 5-Me-dC-N4-(spermine) [X] oligodeoxynucleotides: Non protonation of N3 in X of X*G:C triad and effect of base mismatch/ionic strength on triplex stabilities. *Nucleic Acids Res.* **1996**, *24*, 1229-1237.

[43] Hodges, R. S.; Merrifield, R. B. Monitoring of solid phase peptide synthesis by an automated spectrophotometric picrate method. *Anal. Biochem.* **1975**, *65*, 241-272.

CHAPTER 5:

APPLICATIONS OF ISOTHERMAL TITRATION CALORIMETRY TO STUDY BIOMOLECULAR INTERACTIONS: *aeg/aep/aepip* PNA:DNA HYBRIDS, ENZYME/NUCLEOSIDES BINDING TO NANOPARTICLES, AND CHIRAL RECOGNITION OF DNA BY AMINO ACID-MODIFIED GOLD NANOPARTICLES

This chapter has four sections. These sections deal with the applications of isothermal titration calorimetry (ITC).

5.1. INTRODUCTION TO ISOTHERMAL TITRATION CALORIMETRY AND APPLICATIONS

Molecular recognition is a complex, but fundamental process, which is essential for life. Understanding the thermodynamics that underlie such a process is of enormous interest to biochemists, but still remains a difficult challenge. Due to significant improvements in instrument sensitivity, isothermal titration calorimetry (ITC) is now becoming a routine method for the generation of thermodynamic data relating to biomolecular association. In a single experiment, ITC measures the association constant (Ka), stoichiometry (n), free energy (ΔG°), enthalpy (ΔH°) and entropy (ΔS°) of binding. Relating these parameters to physical processes at the molecular level is more difficult, but it is in combination with structural information that ITC may help to tackle this challenge.[1]

5.2. MEASUREMENT OF THERMODYNAMIC PARAMETERS BY ITC

5.2.1. ITC Instruments

Most of the commonly used isothermal titration calorimeters are based on a cell feedback network, which measures the differential heat effects between a sample and reference cell. This is known as differential power compensation, and is used in both Microcal Inc. (www.microcalorimetry.com) and Calorimetry Sciences Corp. (www.calorimetrysciences.com) instruments (Figure 1).[2] The temperature difference between these two cells is constantly monitored and a constant power is applied to the

reference cell, which activates the feedback circuit to apply a variable power to the sample cell in order to maintain very small temperature difference between the cells. This feedback power is the baseline level in the absence of any reaction. When a reaction occurs, there will be a temperature change in the sample cell, which leads to a temperature difference between the sample and reference cell. This is detected by the calorimeter, and the power applied by cell feedback is adjusted. Exothermic reactions will trigger a temporary decrease in the feedback power, and conversely, endothermic reactions will produce an increased feedback. The heat evolved, or absorbed by the reaction is then obtained by integration of these deflections from baseline, with respect to time.

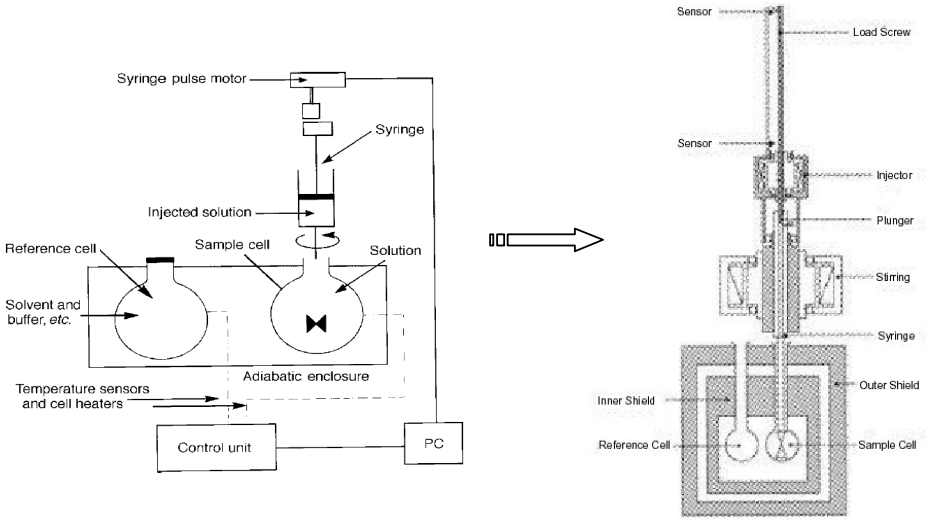

Figure 1. Schematic of syringe mechanism and calorimeter cell.

ITC is the only technique which allows direct measurement of the values of Ka, n, and ΔH° in a single experiment. It should be recognised that ΔH° is actually an apparent (or observed) value since the binding reaction may be accompanied by many linked equilibria yielding heat changes. For example, the observed value of ΔH must be corrected for the heat of ionization of the buffer, when the binding interaction is

associated with changes in protonation. The magnitudes of ΔG° and ΔS° are then obtained from the relationship:

$$\Delta G^\circ = \Delta H^\circ - T\Delta S^\circ = -RT\ In\ K_a$$

ITC also allows measurement of a central thermodynamic parameter, ΔCp, the change in heat capacity (also known as specific heat). ΔCp is an important thermodynamic parameter as it governs the magnitudes of both ΔH° and ΔS°:

$$\Delta Cp = d(\Delta H^\circ)/dT = T.d(\Delta S^\circ)/dT$$

In order to characterize the thermodynamics of a binding interaction fully it is necessary to measure, not only ΔG°, ΔH°, and ΔS°, but also ΔCp, since this parameter allows the prediction of the change of the other three parameters with temperature. ΔCp is usually measured from the change in enthalpy with temperature, using the relationship:

$$\Delta Cp = (\Delta H^\circ_{T2} - \Delta H^\circ_{T1})/\ T2 - T1 = (\Delta S^\circ_{T2} - \Delta S^\circ_{T1})/\ In\ (T2\ /\ T1)$$

Where T1 and T2 are two temperatures at which separate determinations have been made.

5.2.2. Interpretation of Thermodynamics: Binding Parameters

The standard Gibb's free energy change, ΔG°, is the most important energetic parameter measured by ITC. ΔG° determines the direction in which biomolecular binding equilibria will spontaneously proceed, with more negative values of ΔG° favouring higher binding. It is important to realise that ΔG° and its enthalpic and entropic constituents depend upon differences between free and bound states for both of the interacting partners. The standard enthalpy change, ΔH°, reflects changes in the

interactions between atoms. An overall increase in bonding is associated with the release of heat, or a negative enthalpy change, and the reaction is termed exothermic. A negative value of $\Delta H°$ is hallmark of a favourable reaction. Although the meaning of $\Delta H°$ appears simple, the bond energy changes associated with a particular binding reaction, is actually the resultant value of formation and breakage of many individual bonds. These individual changes may produce positive or negative contributions, which means that the observed enthalpy represents the sum of many of these individual components.[3] The standard entropy change, $\Delta S°$, is associated with the disorder in a system, with an increase in bonding tending to decrease disorder. A positive value of $\Delta S°$ is favourable. It can be seen that increased bonding tends to produce negative $\Delta H°$ values, and negative $\Delta S°$ values, which lead to opposing contributions to $\Delta G°$. This enthalpy/entropy compensation, which appears due to effects of perturbing the weak intermolecular bonding occurring in solvent water, may lead to smaller changes in $\Delta G°$. The change in heat capacity, ΔCp controls how $\Delta H°$ and $\Delta S°$, and hence how $\Delta G°$ change with temperature.[4,5]

5.2.2a. Hydrophobic Interactions

The classical understanding of hydrophobic interactions is that non-polar groups associate with each other, minimising contact with polar solvent molecules. Hydrophobic binding interactions often are characterized by small (frequently positive) enthalpy changes, large positive entropy changes, and often a negative contribution to ΔCp.[6,7] This may be understood by considering the interactions of solvent water around a non-polar solute. In the presence of a non-polar compound, the normal hydrogen bond network of water is reorganised. In an effort to maintain the

number of hydrogen bonds, water molecules align themselves around the apolar compound. The binding thermodynamics of hydrophobic interactions are thus

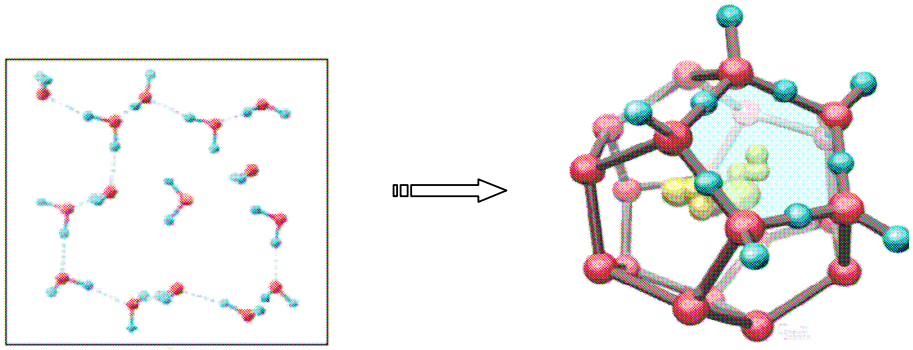

Ordered water surrounding a nonpolar molecule.

explained by the increase in entropy, which results from the release of relatively highly ordered water molecules surrounding the apolar surfaces of the two interacting molecules. These water molecules return to bulk where they form weaker bonds a process that is entropically favourable and slightly endothermic.[5]

Hydrophobic effect in DNA. Similar to hydrophobic side chains in proteins, the hydrophobic groups in nucleic acids (the aromatic bases) are buried, and the hydrophilic groups (the sugar and phosphates) are exposed.

5.2.2b. Electrostatic Interactions

Electrostatic interactions are defined here as those occurring between charged or dipolar ligands and the counter-charged binding site on a macromolecule. The dielectric constant at a binding site may be considerably lower than the dielectric constant of bulk solvent, and would thus favour strong charge-charge interactions upon binding, but transferring a charged group to a low dielectric environment is unfavourable. This is because buried charged groups must be stabilised by local dipoles.[8] Binding of charged groups to macromolecules often is entropically driven,

with low values of ΔH°.[9] An entropic advantage is also expected for displacement of the water molecules solvating the free charged groups.

5.2.2c. Hydrogen Bonds

Hydrogen bond formation is thought to be particularly important in biological binding interactions. However, it is often overlooked that for a hydrogen bond to form between a macromolecule and ligand, similar hydrogen bonds between the macromolecular binding site and water, and also between the ligand and water will have to be broken. Thus, a hydrogen-bonding group makes similar interactions as both a reactant and product, and so there may be a relatively small contribution to binding thermodynamics.[10] The energy of a single hydrogen bond has been estimated to be around 21 kJ/mol (5 kcal/mol), but contributions to binding thermodynamics often are much smaller than this due to the nature of hydrogen bond exchange. However, a single hydrogen bond may contribute from 10 to around 10,000 fold to affinity.[10] This illustrates that it is extremely difficult to make generalisations regarding the contribution of a single hydrogen bond to binding affinity, or to characterise the enthalpy of hydrogen bond formation. Properties of the hydrogen bond donor and acceptor, as well as their local surroundings in both the free and complexed states must be taken into account in order to assign parameterizations.[11]

Base pairing in DNA. Each base pair makes two or three hydrogen bonds. Since these are shielded from solvent, they should stabilize DNA base pairing. However, there's an entropy cost to adopting this very ordered state, and the enthalpy gain is partially offset by an entropy penalty.

5.2.2d. Conformational Changes

Ligand induced conformational changes are important in many binding interactions, and are responsible for several significant functional roles. Conformational changes may be responsible for correct orientation of active site residues involved in catalysis, or may facilitate the subsequent binding of ligands such as other substrates or allosteric effectors.[5] It is likely that conformational changes occurring on ligand binding are subtle changes rather than the large changes exemplified by unfolding or refolding reactions. These subtle changes are therefore expected to exhibit relatively low magnitudes for both ΔH° and ΔS° (usually with strong enthalpy-entropy compensation), with negative values anticipated for ΔCp.[12]

5.2.2e. The Role of Water in Binding Interactions

It is evident from the discussion above that solvent water plays a key role in governing biomolecular-binding interactions. Water molecules interact with both the free partners and the complex, and any changes in the number of water molecules located at a binding interface may have a dominant effect on binding affinity. These locally structured water molecules can potentially be retained or released during a binding interaction with very different thermodynamic consequences. Release of bound waters from a binding interface is associated with a favourable gain in entropy as these molecules are displaced back into bulk. However this is an enthalpically unfavourable process as the strong bonds are made with the macromolecule. Conversely, retention of water may be associated with a favourable enthalpy resulting from increased hydrogen bonding, but an unfavourable entropy penalty.[5]

5.2.2f. Enthalpy-Entropy Compensation

The phenomenon of enthalpy-entropy compensation appears in many, if not all biochemical thermodynamic binding studies. Enthalpy-entropy compensation is characterised by the linear relationship that is observed between the enthalpy change and the entropy change in a binding interaction. Hence, large changes in ΔH° are compensated by large and opposing changes in ΔS°, which almost cancel leading to much smaller variations in the observed ΔG°. Enthalpy-entropy compensation in these systems, seems at first to be connected to the properties of solvent water, but actually appears to be an almost inescapable general consequence of perturbing most weak intermolecular interactions.[13,14]

At the thermodynamic level, the binding affinity is dictated by the Gibbs free energy (ΔG), which in turns depends on the enthalpy and entropy changes, associated with binding. In principle, many combinations of enthalpy and entropy changes are consistent with any ΔG, and therefore, any binding affinity. In reality, the situation is different because ΔH and ΔS reflect different types of interactions and, for small molecules binding to proteins, the ensemble of interactions is finite and dictated by the type of interactions that can be established between the constituent atoms. Enthalpic contributions reflect the strength of H-bonds, van der Waals interactions relative to those with the solvent (water). Entropic contributions to the binding affinity, on the other hand, are mainly due to a large increase in solvent entropy arising from the burial of hydrophobic groups upon binding, and the loss of conformational degrees of freedom associated with binding. In this regard, it must be noted that the binding of conformationally constrained, highly hydrophobic ligands is entropically driven because their binding affinity is dominated by the burial of

hydrophobic groups coupled to a minimal loss of conformational degrees of freedom.[15,16,17]

This chapter deals with the applications of ITC to the following problems.

Section I describes the thermodynamic study of *aeg*PNA, *aep*PNA and *aepip*PNA/DNA interactions.

Section II presents interactions between nucleosides and keggin ion nanoparticles.

Section III describes the chiral recognition of DNA by amino acid-modified gold nanoparticles.

Section IV describes the study of funagal protease binding on gold nanoparticles.

SECTION I: THERMODYNAMIC STUDY OF PNA/DNA INTERACTIONS.

5.3. PRESENT WORK: RATIONALE

A significant amount of PNA research has been focused on the characterization of PNA interactions with other nucleic acids using UV-T_m,[18,19,20] linear and circular dichroism,[21] NMR spectroscopy,[19] X-ray crystallography,[22] and mass spectrometry. [23]Despite much research in characterizing PNA/DNA interactions, the thermodynamic data on PNA/DNA hybridization interactions have been largely determined so for indirectly from UV-melting studies. Thermodynamic data on PNA/DNA binding interactions are not only important in understanding PNA/DNA interactions but also are necessary for the development of thermodynamic models for the design of PNA sequences with specific DNA hybridization properties.

Preorganizing the *aeg*PNA backbone into hybridization competent conformations should be associated with entropic advantages for binding DNA/RNA. It was reported previously from our laboratory, that the chiral aminoethylprolyl (*aep*) PNA (Figure 2) analogue with positively charged tertiary amine in the backbone,

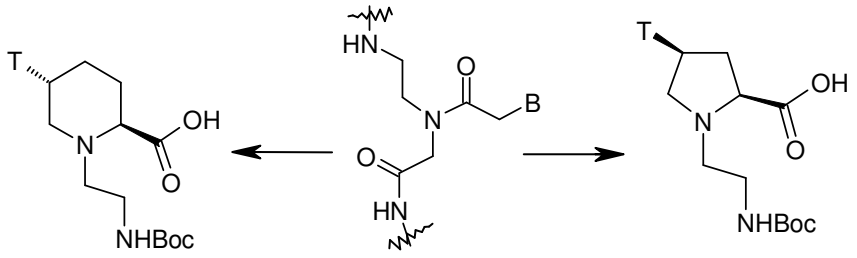

2*S*,5*R* *aepip*PNA *aeg*PNA 2*S*,4*S* *aep*PNA

along with conformational constraint due to the five-membered pyrrolidine ring significantly improved the solubility, affinity and selectivity in DNA:PNA binding. As described in chapter 2, in case of aminoethylpipecolyl (*aepip*) PNA, the conformations in the six-membered ring structures are rigidly locked into chair/boat

forms in contrast to the relatively flexible five-membered ring structures and contributed towards the stability of the resulting PNA-DNA complexes.

In this section, the aim is to evaluate the different thermodynamic parameters [enthalpy (ΔH), binding entropy (ΔS), binding constant (k), and Gibb's free energy (ΔG)] for interactions of unmodified and modified PNAs with cDNA by ITC.

5.4. RESULTS AND DISCUSSIONS

The isothermal titration calorimetry experiments were done with *aepip*PNAs synthesized in chapter 2 and *aep*PNAs. The *aep*PNAs[24] (Table 1) were synthesized and characterized similarly as described in chapter 2.

Table 1. PNA sequences used for ITC.*

PNA	***aepip*PNA (2S,5R)**
1	H-**t**TTTTTTT–(β-Ala)-OH
2	H-TTTTTTT**t**–(β-Ala)-OH
3	H-TTTTTTTT–(β-Ala)-OH
4	H-**t**TCTCTTT–(β-Ala)-OH
5	H-TTCTCTTT–(β-Ala)-OH
6	H-ATG**t**TCTCTTT–(β-Ala)-OH
7	H-ATGTTCTCTTT–(β-Ala)-OH
	***aep*PNA (2S,4S)**
8	H-***t t t t t*** –(β-Ala)-OH
9	H-TTTTT–(β-Ala)-OH
10	H-***t t t t t t t*** –(β-Ala)-OH
11	H-TTTTTTT–(β-Ala)-OH
12	H-***t***TTTTT–(β-Ala)-OH
13	H-TTT***t*** TT–(β-Ala)-OH
14	H-TTTTT***t*** –(β-Ala)-OH
15	H-TTTTTT–(β-Ala)-OH

* T/A/G/C = *aeg*PNA monomers, **t** = *aepip*PNA T, ***t*** **=** *aep*PNA T.

The HPLC and MALDI-TOF spectra of *aep*PNAs are shown in Figure 2, 3 and 4.

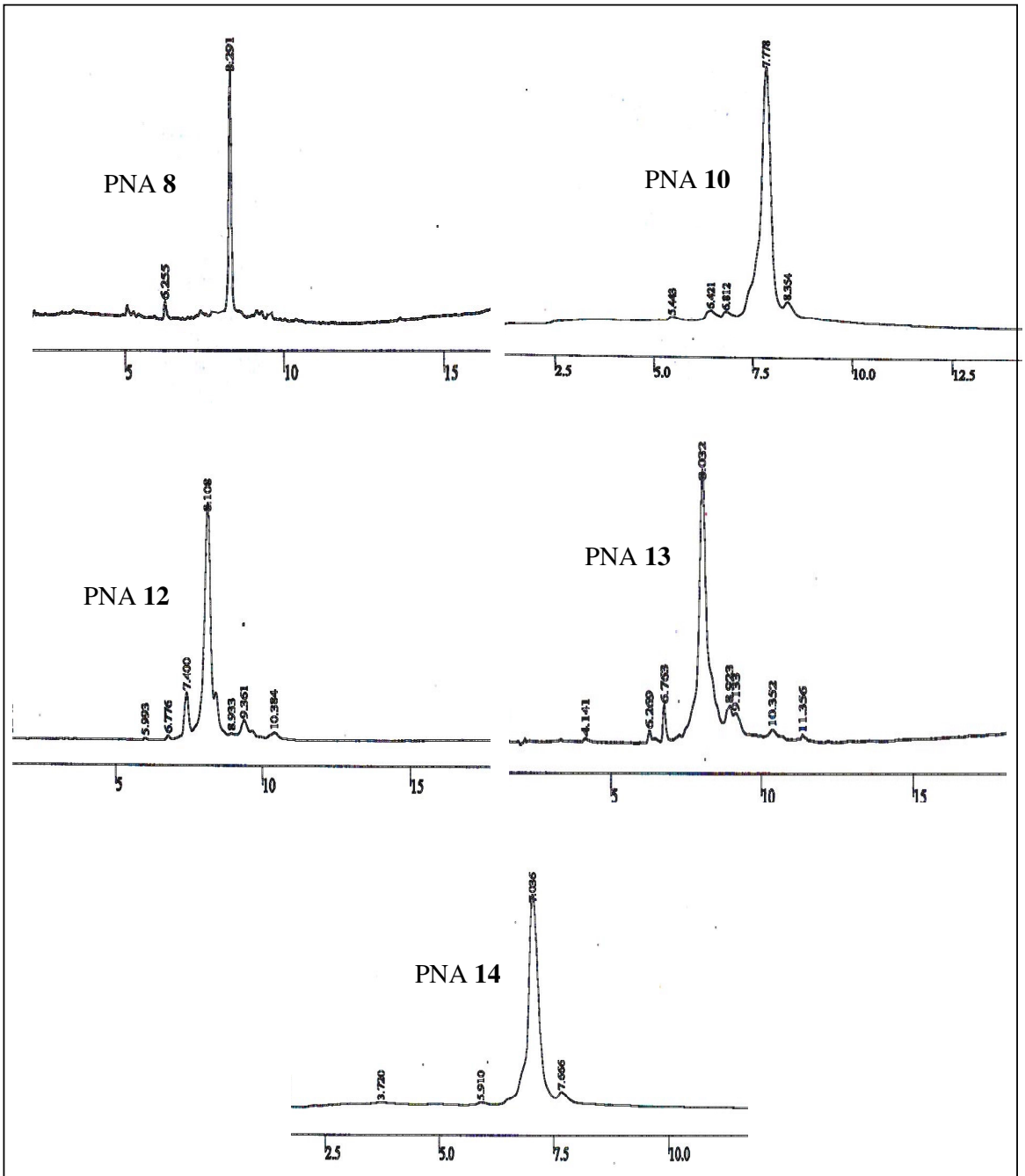

Figure 2. Representative HPLC profiles of *aep*PNA oligomers.

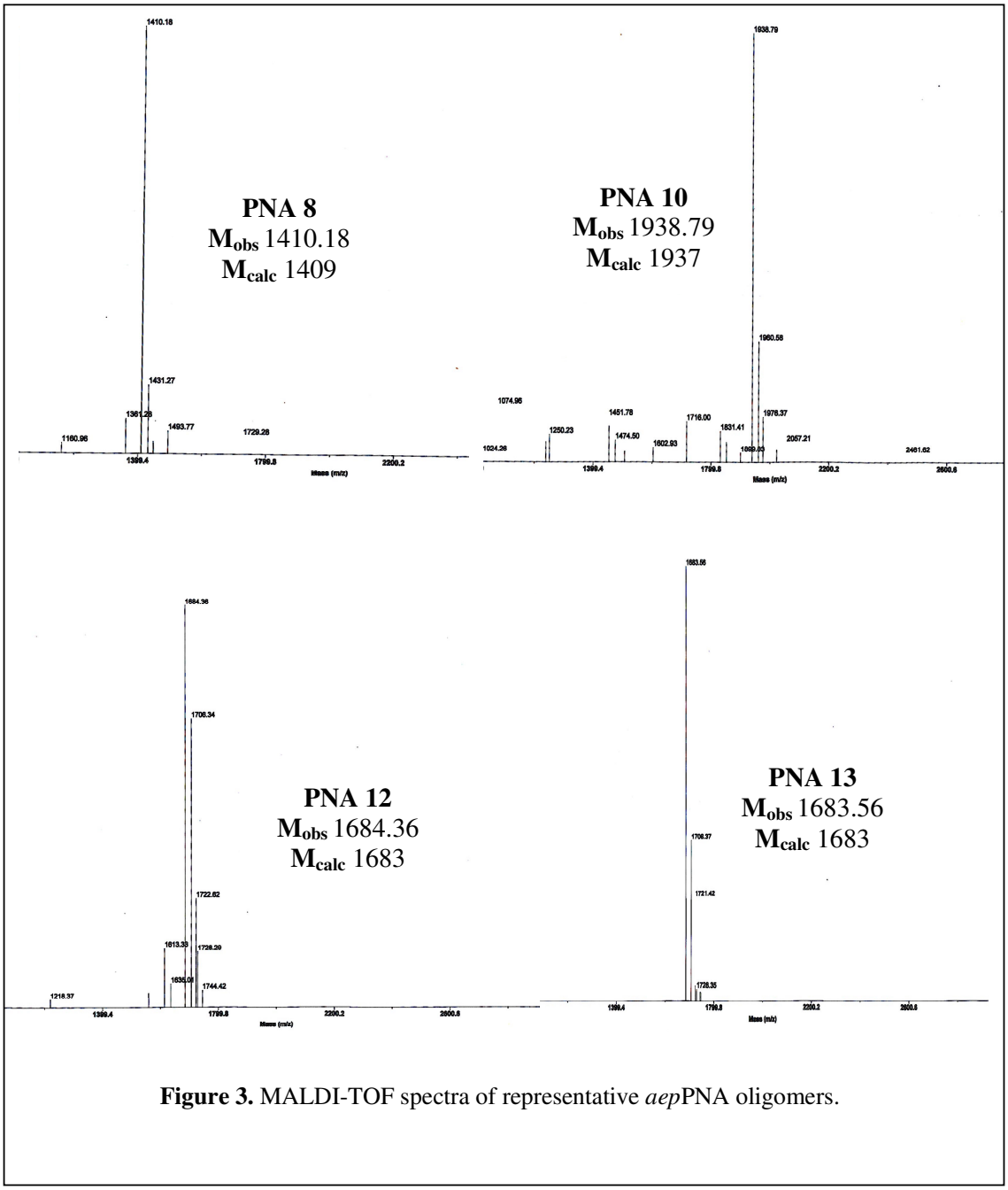

Figure 3. MALDI-TOF spectra of representative *aep*PNA oligomers.

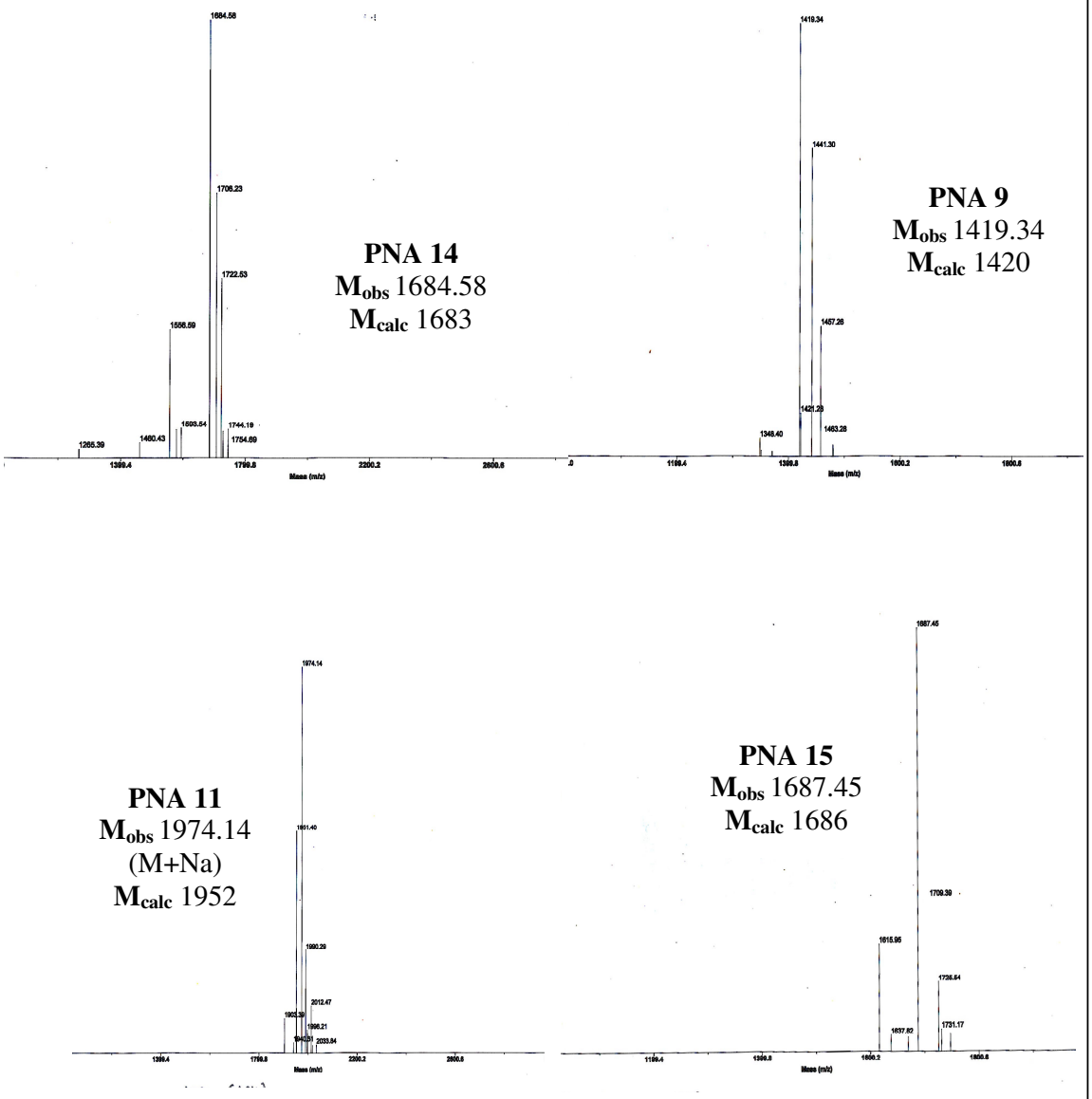

Figure 4. MALDI-TOF spectra of representative *aep*PNA oligomers.

The thermal stabilities of PNA:DNA complexes were studied by temperature dependent UV absorbance measurements. Table 2 shows the Tm values for PNA:DNA complexes derived for various *aeg*PNA, *aep*PNA and *aepip*PNA sequences with different degree of modification.

Table 2. UV-T_m (^{0}C) of PNA-DNA complexes*

PNA	***aepip*PNA (2S,5R)**	**UV-T_m (^{0}C)**
1	H-**t**TTTTTTT–(β-Ala)-OH	43.0
2	H-TTTTTTT**t**–(β-Ala)-OH	48.0
3	H-TTTTTTTT–(β-Ala)-OH	43.0
4	H-**t**TCTCTTT–(β-Ala)-OH	60.0
5	H-TTCTCTTT–(β-Ala)-OH	51.0
6	H-ATG**t**TCTCTTT–(β-Ala)-OH	57.8
7	H-ATGTTCTCTTT–(β-Ala)-OH	51.2
	***aep*PNA (2S,4S)**	
8	H-***t t t t t*** –(β-Ala)-OH	37.5
9	H-TTTTT–(β-Ala)-OH	21.0
10	H-***t t t t t t t*** –(β-Ala)-OH	>85
11	H-TTTTTTT–(β-Ala)-OH	32.6
12	H-***t***TTTTT–(β-Ala)-OH	42.5
13	H-TTT***t*** TT–(β-Ala)-OH	45.2
14	H-TTTTT***t*** –(β-Ala)-OH	42.4
15	H-TTTTTT–(β-Ala)-OH	26.2

*Buffer: 10mM sodium phosphate, pH 7.4. T_m values are accurate to (±) 0.5°C. Experiments were repeated at least thrice and the T_m values were obtained from the peaks in the first derivative plots

ITC Studies

The interaction between *aeg*PNA/*aep*PNA/*aepip*PNA single strand with its complementary DNA were studied directly using isothermal titration calorimetry (ITC). The calorimeter consists of two cells: a reference cell filled with pure solvent (buffer) and a sample titration cell filled with 1.47ml of PNA in sodium phosphate buffer, pH 7.3 (1.33μM). A 5μM DNA solution in same buffer was added from the

syringe into the titration cell containing the PNA in small steps of 10µl at an interval of 120s. The heat evolved/absorbed during hybridization of PNA with DNA was measured.

Each negative peak shown in the heat signal curves from PNA-DNA (Figure 5, 6, 7) represents an exothermic process, which denotes the heat released in one injection of the DNA into the PNA solution as a function of time. The upper panel in Figures 5, 6 and 7 correspond to the raw calorimetric data obtained during titration, while lower panel in Figures 5, 6 and 7 are plots of the integrated enthalpy response obtained from the raw data plotted against the total volume of DNA solution added to the reaction vessel containing the PNA solution. It should be pointed out that the data shown here (and in all subsequent measurements) has been corrected for effects arising due to dilution of the DNA during titration.

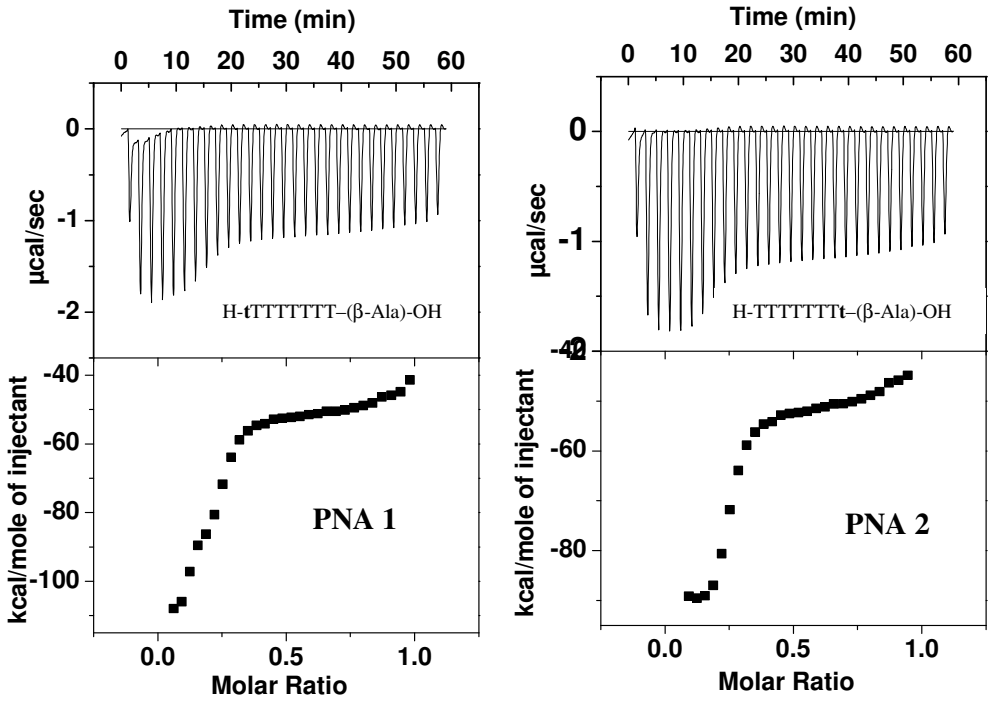

Figure 5. Representative ITC profiles of *aepip*PNA oligomers.

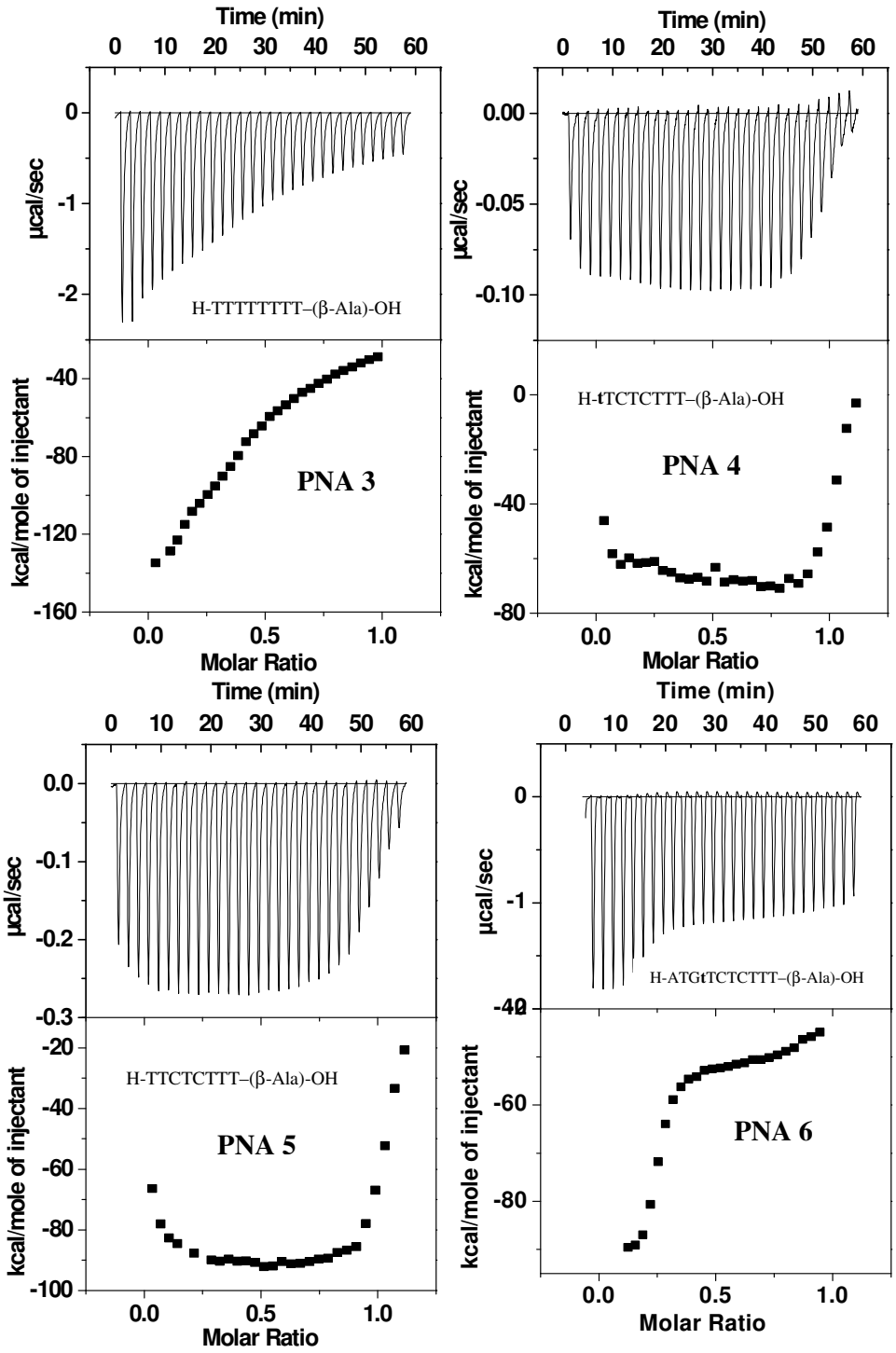

Figure 6. Representative ITC profiles of *aepip*PNA and *aeg*PNA oligomers.

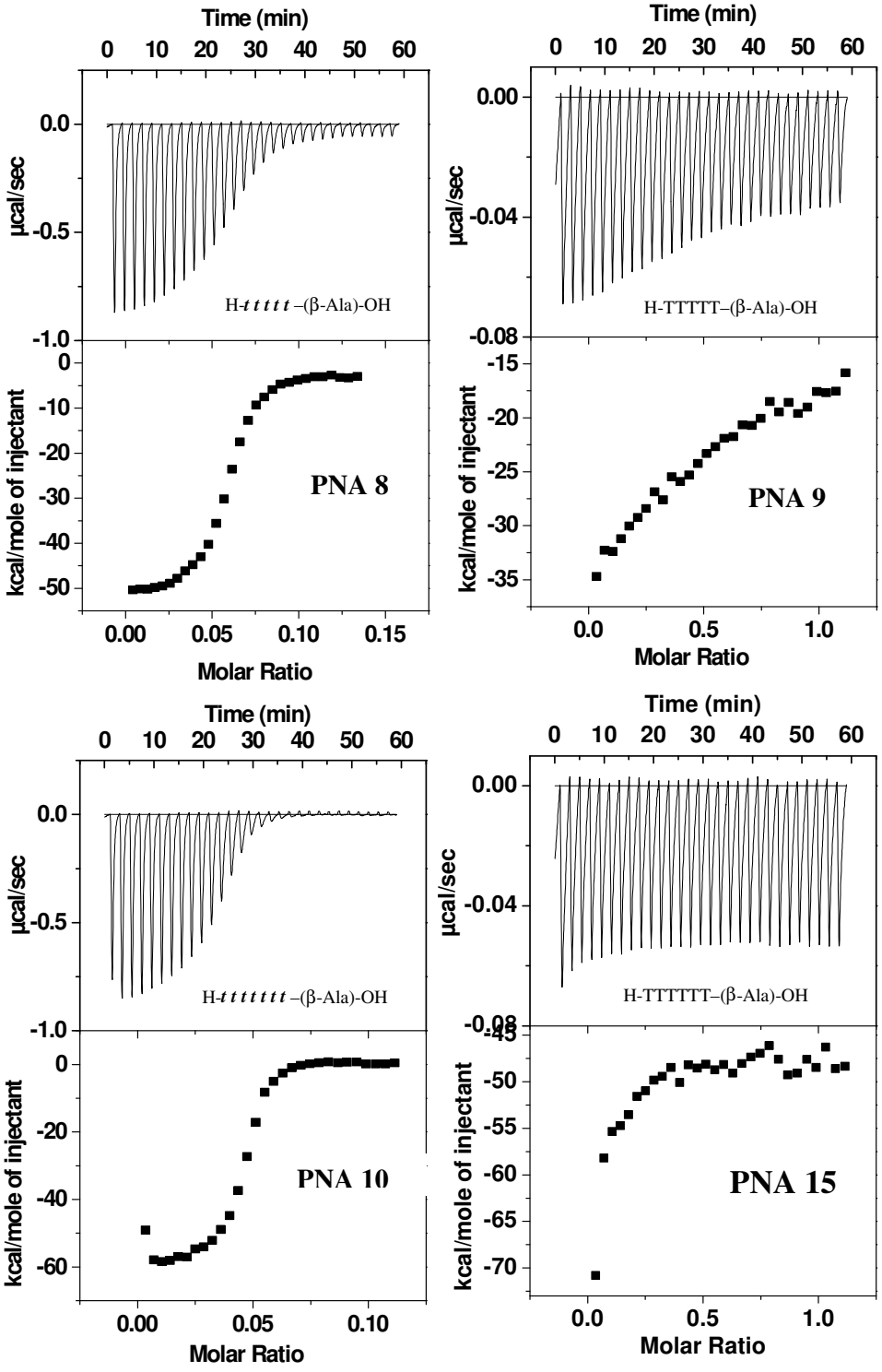

Figure 7. Representative ITC profiles of control *aep*PNA and *aeg*PNA oligomers.

It is well known that the calorimetric response during dilution of the injectant can be quite prominent and capable of obscuring the calorimetric response during reaction and must be carefully taken into account. Lower panels in Figures 5, 6 and 7 would thus correspond to binding isotherms of the PNA with their complementary DNA.

A non-linear, least squares minimization software program (Origin 5.0 from Microcal Inc.) was used to fit the data using one set of binding model for PNA:DNA duplexes and two set of binding model for PNA_2:DNA triplexes.

The ITC results show that the PNA binding affinities (K) are in the range of 1.02 x 10^6 M^{-1} to 2.03 x 10^9 M^{-1} (Lit.[25] 1.8 x $10^6 M^{-1}$ to 4.15 x 10^7 M^{-1} for PNA 10-mers). Thermodynamic parameters for PNAs with its complementary DNA follow a different dependence on sequence and different modifications (Table 3).

Table 3. Thermodynamic quantities for PNA/DNA hybridization reactions from ITC measurements.*

PNA	***aepip*PNA (2*S*,5*R*)**	UV-T_m (^{0}C)	ITC (kcal/mole)		
			-ΔH	**-ΔG**	**TΔS**
1	H-tTTTTTTT–(β-Ala)-OH	43.0	108	44.9	-63
2	H-TTTTTTTt–(β-Ala)-OH	48.0	89	45.6	-43
3	H-TTTTTTTT–(β-Ala)-OH	43.0	134	44.9	-89
4	H-tTCTCTTT–(β-Ala)-OH	60.0	61	47.4	-14
5	H-TTCTCTTT–(β-Ala)-OH	51.0	89	46.0	-43
6	H-ATGtTCTCTTT–(β-Ala)-OH	57.8	89	47.0	-42
7	H-ATGTTCTCTTT–(β-Ala)-OH	51.2	90	46.1	-43
	***aep*PNA (2*S*,4*S*)**				
8	H-t t t t t –(β-Ala)-OH	37.5	50	44.1	-6
9	H-TTTTT–(β-Ala)-OH	21.0	35	41.8	7
10	H-t t t t t t t –(β-Ala)-OH	>85	60	50.9	-9
11	H-TTTTTTT–(β-Ala)-OH	32.6	72	43.4	-28
12	H-tTTTTT–(β-Ala)-OH	42.5	13	44.9	32
13	H-TTTt TT–(β-Ala)-OH	45.2	28	45.2	17
14	H-TTTTTt –(β-Ala)-OH	42.4	13	44.8	32
15	H-TTTTTT–(β-Ala)-OH	26.2	64	42.5	-21

* T/A/G/C = *aeg* PNA monomers, **t** = *aepip* PNA T, ***t*** = *aep* PNA T.

As UV-T_m of *aepip*PNA **2** having C-terminus modification, is stabilized over unmodified *aeg*PNA **3**, the enthalpy (ΔH) is lowered from 134 kcal/mole to 89 kcal/mol. But the entropy (ΔS) for PNA **2** is gained over PNA **3** (high or TΔS). This suggests that, entropy-enthalpy compensations have occurred in *aepip*PNA:DNA binding. Similar entropy-enthalpy compensations have occurred in *aepip*PNA **1**, but to the lesser extent, as there is no change in UV-T_m compared to *aeg*PNA **3**.

In case of mixed pyrimidine sequence i.e. *aepip*PNA **4**, loss in enthalpy of binding is compensated by gain in entropy confirming the UV-T_m stabilization over unmodified *aeg*PNA **5**. The mixed purine-pyrimidine sequence, *aepip*PNA **6**, shows less entropy-enthalpy compensation although larger UV-T_m stabilization has occurred as compared to *aeg*PNA **7**. This suggests that *aepip*PNA modification preorganizes the PNA backbone to hybridization competent conformation leading to stable complexes with DNA.

In all *aeg*/*aep*/*aepip*PNAs the ΔG (free energy) value ranges from 44-47 kcal/mol (except in fully modified PNA **10**). Thermodynamic parameters also depend on the length of sequence. As fully modified 5-mer *aep*PNA **8**, shows increase in enthalpy compensated by decrease in entropy. In contrast a fully modified 7-mer *aep*PNA **10**, shows decrease in enthalpy compensated by increase in entropy. In case of single *aep* unit modification at different positions (PNA **12**-**14**) showed decrease in enthalpy compensated by increase in entropy, confirming the larger UV-T_m stabilization compared to *aeg*PNA.

5.5. CONCLUSIONS

It is demonstrated that isothermal titration calorimetry may be successfully employed to study the thermodynamic parameters of PNA:DNA complexes. The UV-T_m stabilization of modified PNA (*aepip*PNA, *aep*PNA) over *aeg*PNA confirms with the entropy-enthalpy compensation suggesting the preorganization of modified PNA.

SECTION II: NUCLEOSIDES BINDING ON KEGGIN NANOPARTICLES.

5.6. PRESENT WORK: RATIONALE

DNA-based nanotechnology has generated considerable interest in a number of applications due to the specificity, programmability and reproducibility of DNA interaction with nanoparticles. Gold nanoparticles (Au-NPs) modified with DNA find use in diverse fields such as DNA chips,[26] DNA sensors,[27] drug/DNA delivery,[28] imaging,[29] biodiagnostics[30] and in the generation of structured nanoparticle assemblies in electronics.[31] Significant efforts have focused on binding oligonucleotides to metal surfaces and colloids for a variety of important fundamental studies and applications, including the electron transfer through DNA[32] and the development of novel DNA detection technologies.[33]

Keggin ions form a subset of polyoxometalates and have the general formula $(XM_{12}O_{40})^{(8-n)}$, where M stands for W or Mo and X stands for heteroatoms such as P, Si, and Ge with *n* being the valency of X.[34] They participate in catalytic redox processes as electron relays. Similar applications can be envisaged for the keggin ions interacting with DNA nucleosides. This Section presents the use of ITC to directly observe the energetics of interaction of the DNA nucleosides with keggin ions. The observed differential binding strengths of the four nucleosides may be useful to develop suitable strategies of designing oligonucleotides for interaction with ligands.

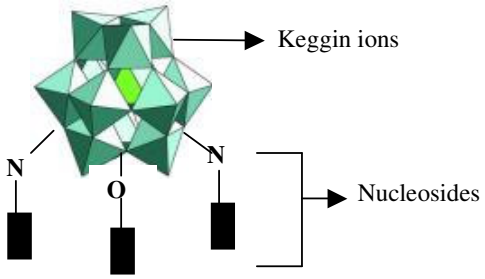

Figure 8. Schematic representation of binding of keggin ions and nucleosides.

5.7. RESULTS AND DISCUSSIONS

TEM images recorded from the Keggin-Cytosine, Keggin-Adenine and Keggin-Guanine nanoparticles are shown in Figure 9. The SEM images also recorded from the as prepared, Keggin-Cytosine, Keggin-Adenine, Keggin-Guanine and Keggin-Thymine nanoparticles. Further, the comparison of the SEM images shows that the morphology of the particles is different, for keggin-adenine spherical, Keggin-guanine square, for keggin-cytosine broom shaped and for keggin-thymine there is no particular morphology. The degree of aggregation of the particles is different in each of the experiments.

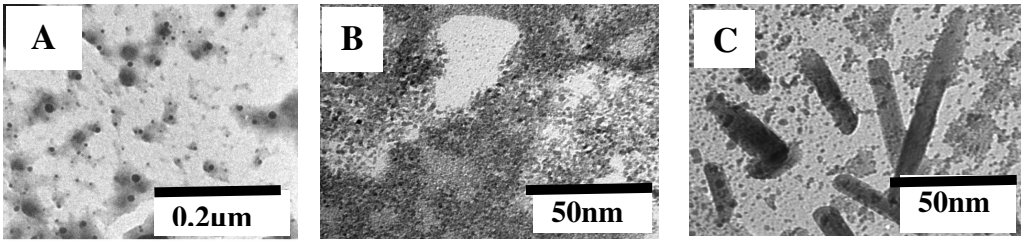

Figure 9. (A), (B), and (C) TEM images from the keggin-Cytosine, keggin-Adenine and keggin-Guanine nucleosides respectively.

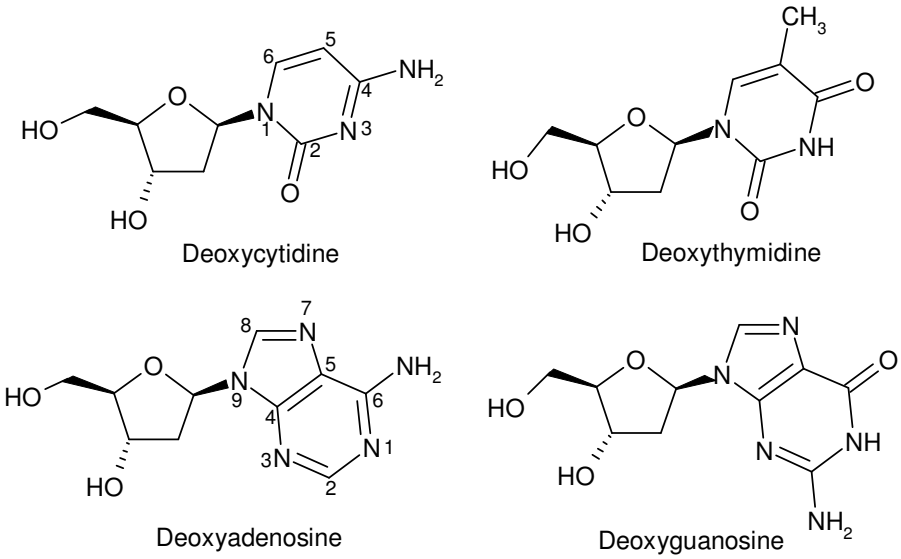

Figure 10. Structures of Nucleosides.

The upper panels in Figure 11 show the ITC calorimetric response recorded during titration of the different DNA nucleobases with an aqueous solution of phosphotungstic acid (10^{-3} mM) ($H_3PW_{12}O_{40}$; obtained from Aldrich and used as-received, PTA). In an ITC measurement, the heat evolved (exothermic reaction) or absorbed (endothermic reaction) is measured during each injection of the reactant (upper panels in Figure 11). Please note that the data shown here (and in all subsequent measurements) has been corrected for effects arising due to dilution of the nucleosides during titration (data in red).

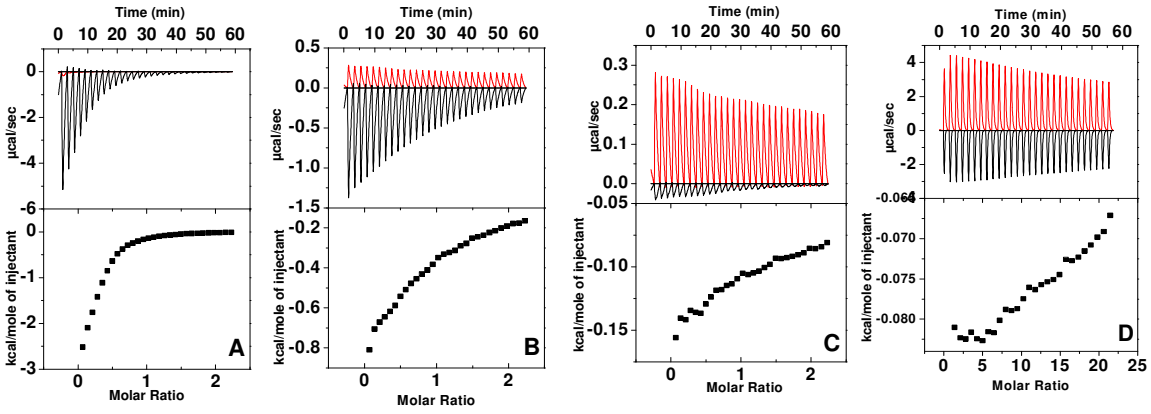

Figure 11. ITC response recorded during titration of DNA nucleosides with aqueous phosphotungstic acid solution. The upper panels in A–D correspond to raw ITC data for Keggin ion interaction with dC, dA, dG and dT respectively. The curves in red are ITC experiments of dilution of the nucleobases in water at pH 3. These measuremtns were performed in a Micro-Cal VP-ITC instrument at 25°C, wherein 300µl of 10^{-2}mM aqueous solution of DNA nucleosides were injected in equal steps of 10µl into 1.47ml of 10^{-3}mM Keggin ion solution.

Integration of the heat evolved/absorbed during each injection plotted against the molar ratio of the reactants in the titration cell results in a 'binding isotherm' and as the binding sites available in the Keggin ions become progressively occupied during titration, the exothermicity of the peaks decreases and eventually saturates (upper panels in Figure 11). From Figure 11, it is observed that the calorimetric response is quite different in each case. Furthermore, the exothermicity of reaction

with the first three nucleobases is quite different. The first injection data for some nucleobases is quite different and is conventionally neglected.[35]

The heat pulses of all the injections can be summed up to define an integral heat. The ratio of the summed up heat (area) at the i'th injection divided by the total heat (area normalized to unity) gives the fractional loading of the total moles of the Keggin ions. From the fractional loading, the free ligand concentration may be computed using a transformation. The binding isotherm chosen in this work is the Michaelis-Menton-Langmuir type model where,

$\phi = \beta K_A C_A / 1 + K_A C_A$

ϕ = Fractional loading of keggin ions

$1-\phi$ = Free unbound fraction of keggin ions

β = geometric or capacity factor

This provides an excellent fit in 3 cases, viz. dA, dG, dC (Figure 12A-C). For dT,

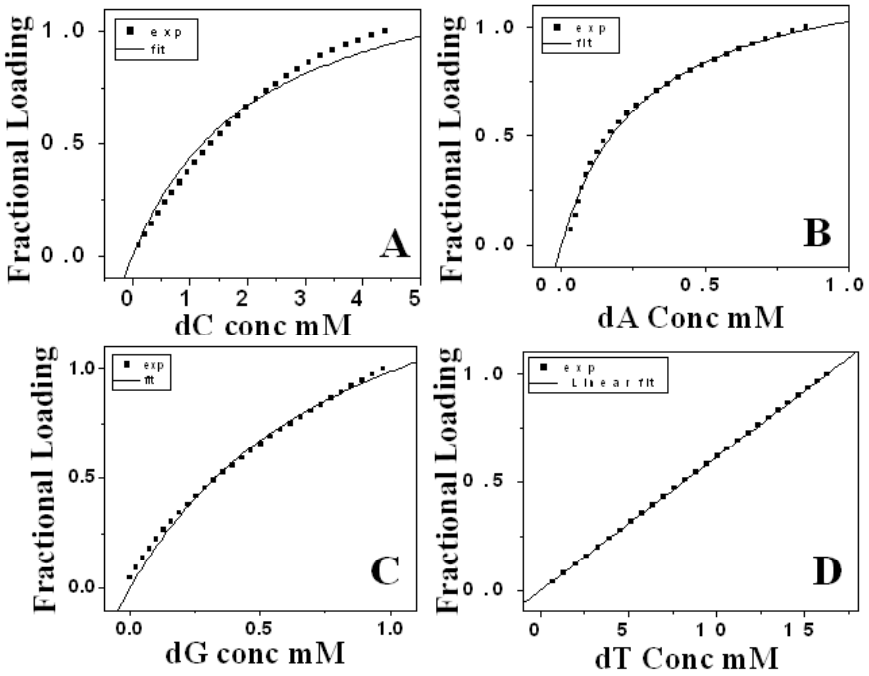

Figure 12. The binding isotherms of different nucleosides with keggin ions obtained from raw ITC data which is fitted using Michaelis-Menton-Langmuir type model.

since the binding is rather weak, a linear isotherm is quite adequate (Figure 12D).

Once the binding constants are known, the free energies are computed using standard thermodynamics. The molar integral heat of binding is computed from the slope of the linear integral heat vs fractional loading plot. All the thermodynamic parameters obtained from the fits shown in Figure 12 are presented in Table 4. The affinity spectrum for binding of the nucleosides follows the order : dA > dG > dC > dT. The contribution of entropy is significant and for two systems, viz., dA and dG the binding with Keggin ions is entropically driven.

Table 4. Thermodynamic of nucleoside binding with Keggin ions.

Nucleoside	**ΔG^a**	**K (M^{-1})**	**ΔH^a**	**$\Delta S/R$ e.u.**	**pK_a***	**β**
Cytosine	-3.6233	$(4.53 \pm 0.52) \times 10^2$	-2.1815	2.4337	4.17 (N-3)	1.41 ± 0.0761
Adenine	-4.8346	$(3.50 \pm 0.18) \times 10^3$	-0.3885	7.5048	3.52 (N-1)	1.32 ± 0.0268
Guanine	-4.1701	$(1.14 \pm 0.79) \times 10^3$	-0.1131	6.8480	3.3 (N-7)	1.85 ± 0.0742
Thymine	-2.4403	$(6.15 \pm 0.01) \times 10^1$	-0.0763	3.9897	9.93 (N-3)	1.00

* Literature values (values in parentheses represents site of protonation). [a]ΔH and ΔG in kcal/mol.

The pK_a values of the sites of protonation in the DNA nucleosides are listed in Table 2, except for dA (which would be zwitterionic at pH 3), the other nucleobases are expected to be cationic under the pH of reaction with Keggin ions (pH = 3) and therefore, capable of electrostatic complextion with the Keggin anions. That there is no meaningful trend based on purely electrostatic considerations on the exothermicity of reaction clearly indicates that entropic effects may dominate the interaction of nucleobases with Keggin ions.

Nucleosides contain two characteristic ligating regions which are capable of metal binding: (1) the heterocyclic ring N atoms and the exocyclic functional groups of the purine and pyrimidine bases, and (2) the hydroxy 'O' atoms of the deoxyribose sugar moiety. For nucleoside-transition metal complexes, X-ray structure studies have shown these two modes of binding to predominate.[36] However, in the case of Keggin ion binding with DNA nucleosides, the binding sites could be much different from those observed in transition metal complexes. Fourier transform infrared spectroscopy studies were carried out on the nucleoside-Keggin ion complexes and indicate the absence of peaks in the range of 3300-3400 characteristic of N-H stretch vibrations in amine groups while other vibrational modes were unchanged relative to the pure nucleosides. This indicates that the nucleosides bind to Keggin ions through the amine groups in agreement with previous observations on the binding of alkylamines[37] and amino acids[38] with gold nanoparticles. The W- O, $(W\text{-}O\text{-}W)_{imter}$ and P-O vibrational modes characteristic of the Keggin structure in the range 800-1200cm^{-1} were also unaltered[39] suggesting no change in the PTA ion structure consequent to binding with the nucleosides.

5.8. CONCLUSIONS

It is demonstrated that isothermal titration calorimetry may be successfully employed to study the interaction of nucleobases with inorganic complexes such as Keggin ions. The nucleobases interact differently with Keggin ions and suggest the exciting possibility of designing oligonucleotide sequences for formation of DNA-based bionconjugates. One possibility could be to use the UV-switchable reducing

capacity of the Keggin ions in such bioconjugates to study electron trasnfer processes in DNA.

SECTION III: CHIRAL RECOGNITION OF DNA BY AMINO ACID-MODIFIED GOLD NANOPARTICLES.

5.9. PRESENT WORK: RATIONALE

DNA-based nanotechnology has generated considerable interest in a number of applications due to the specificity, programmability and reproducibility of DNA interaction with nanoparticles. Gold nanoparticles (Au-NPs) modified with DNA finds use in diverse fields such as DNA chips,[18] DNA sensors,[19] drug/DNA delivery,[20] imaging,[21] biodiagnostics[22] and in the generation of structured nanoparticle assemblies in electronics.[23] DNA is an attractive biomaterial for use as a template in programmed nanoparticle assembly. The ability to synthesize oligonucleotide sequences of predesigned shapes and composition, the versatile biocatalytic transformations that can be performed on DNA, for example, ligation, scission, or polymerization, enable "cut and paste" procedures to be carried out on the template DNA, thus enabling us to design and manipulate the DNA mold.[40]

As part of ongoing investigation into the use of ITC in nanobioconjugate chemistry, this section addresses the following question: Can ITC differentiate between recognition interactions occurring on the surface of nanoparticles based on

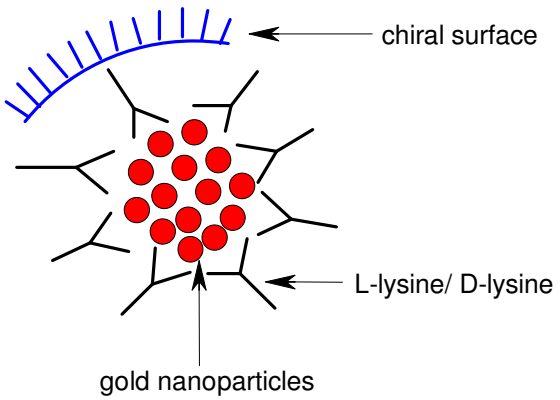

Figure 13. Schematic representation of chiral nanoparticles.

the chirality of the nanoparticle surface? A preferred handedness (chirality) on the surface of gold nanoparticles may be induced by modifying the surface of the nanoparticles through chiral capping ligands such as L or D-lysine (Figure 13). This section presents the interaction of chiral DNA templates with the L- and D-lysine modified gold nanoparticles by ITC and circular dichroism CD spectroscopy.

5.10. RESULTS AND DISCUSSIONS

Figure 14 shows the UV-visible spectra recorded from the gold nanoparticles with and without capped with L- and D-lysine. Curve 1 in the figure corresponds to the spectrum of the gold colloidal solution obtained by borohydride reduction of aqueous chloroauric acid; curve 2 is the superimposed spectra for gold colloidal solutions capped with L and D-lysine. A strong absorption in curve 1 at ca. 530nm observed corresponds to excitation of surface plasmon vibrations in the gold nanoparticles. When the gold nanoparticles are capped with L-lysine or D-lysine, a

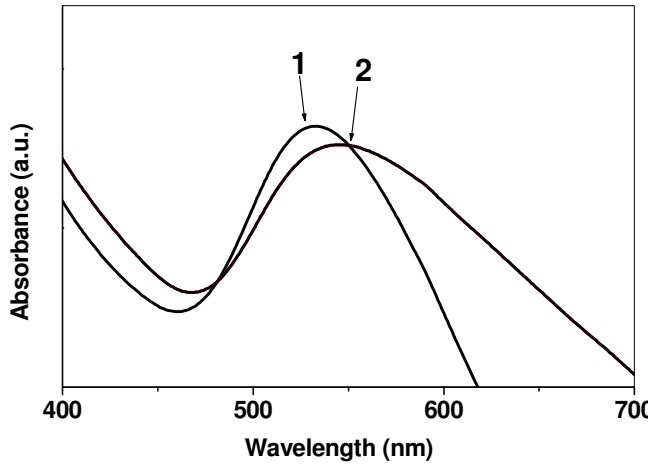

Figure 14. UV-visible spectra recorded from dialysed borohydride reduced gold (curve 1), capped Au-L-lys and Au-D-lys (curve 2).

broadening and red shift of the surface plasmon band is observed (curve 2) which indicates surface-complexation of the amino acids and possibly some aggregation of the gold nanoparticles consequent to surface modification.

The TEM images recorded from Au-L-lys-DNA and Au-D-lys-DNA nanoparticles, (at pH 7) are shown in Figures 15A-B respectively. A comparison of the images shows that DNA interaction with Au-L-lys and Au-D-lys is different consequent to surface modification of gold nanoparticles.

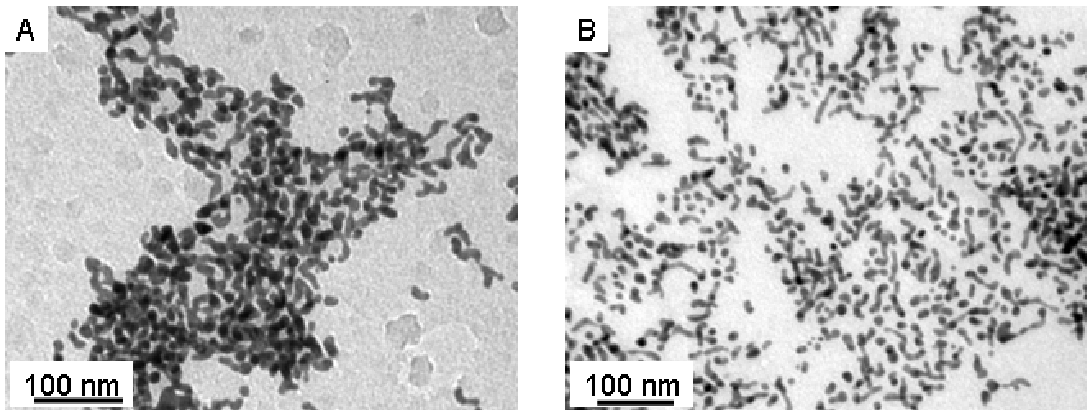

Figure 15. TEM images of lysine capped Au-NP interaction with DNA. Image A corresponds to L-lysine capped Au-NPs interaction with the DNA (5'-GCAAAAAAAACG-3'). Image B corresponds to D-lysine capped Au-NPs interaction with the DNA (5'-GCAAAAAAAACG-3').

The interaction between DNA single strand with gold nanoparticles capped with L-lysine and D-lysine were studied directly using isothermal titration calorimetry (ITC). Each negative peak in the heat signal curves from Au-L-lys-DNA and Au-D-lys-DNA (Figure 16A, 16B) represents an exothermic process, corresponding to the heat released in injection of the aqueous DNA into the gold nanoparticles capped with L-lysine and D-lysine solution respectively as a function of time. While Figure 16A and 16B correspond to the raw calorimetric data obtained for titration of DNA solution with the aqueous gold nanoparticles capped with L-lysine and D-lysine.

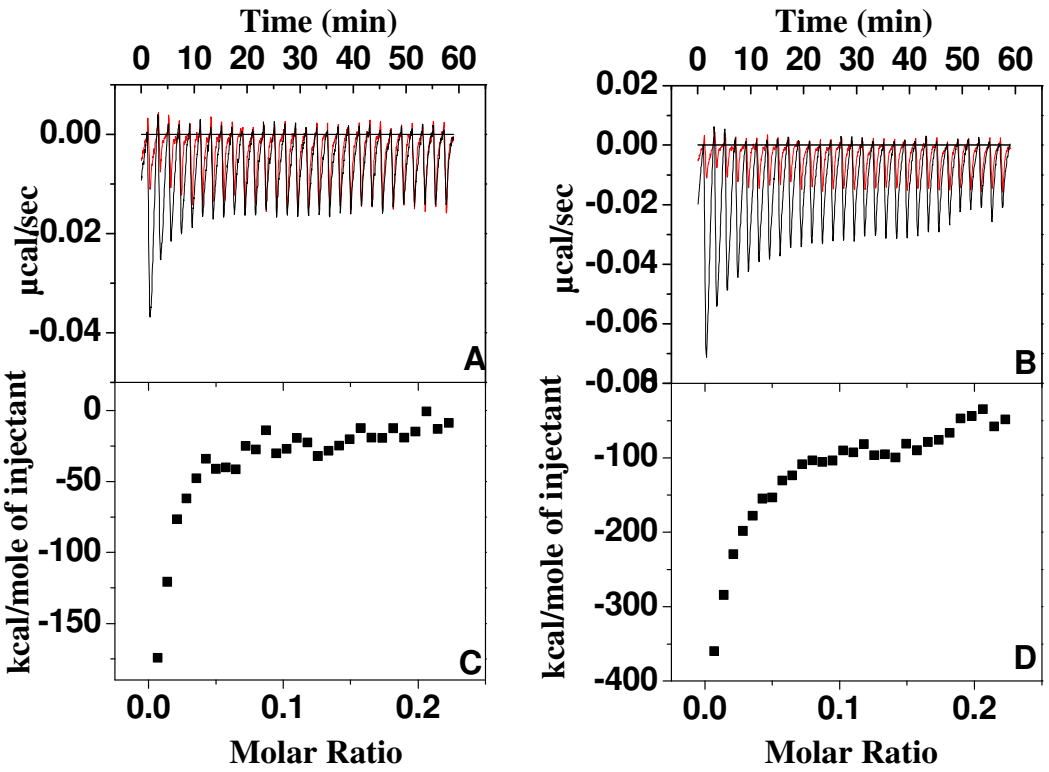

Figure 16. Representative ITC titration data describing the interaction of DNA (5'-GCAAAAAAAACG-3') with gold nanoparticles capped with L-lysine and D-lysine at physiological pH. Panels A and B show the raw calorimetric data obtained during injection of 10^{-6}M aqueous DNA solution into the calorimetric cell containing 1.47ml of 10^{-6}M gold nanoparticles capped with L-lysine and D-lysine, respectively. Panels C and D show the integrated enthalpies of the curves in panels A and B respectively plotted as a function of molar ratio of the DNA solution added to the reaction cell.

Figure 16C and 16D are plots of the integrated enthalpies response obtained from the raw data plotted against the total volume. Please note that the data shown here (and in all subsequent measurements) has been corrected for effects arising due to dilution of the DNA during titration (data in red). It is well known that the calorimetric response during dilution of the injectant can be quite prominent and capable of obscuring the calorimetric response during reaction and must be carefully taken into account. Figure 16C and 16D would thus correspond to binding isotherms of the DNA on the gold surface with different induced chirality.

The exothermicity of the calorimetry peaks is believed to be due to the strong interaction between the gold nanoparticles capped with L-lysine and D-lysine and the

DNA. As the sites available on the surface of the gold nanoparticles capped with L-lysine and D-lysine become progressively occupied during titration, the exothermicity of the peaks decreases and eventually saturates. In case of gold nanoparticles capped with D-lysine, the intense exothermic peaks indicate strong binding during injection of the DNA. It is interesting to note that the intensity of binding of DNA with gold nanoparticles capped with L-lysine is less as compared to gold nanoparticles capped with D-lysine (Table 5).

Table 5. Thermodynamic Parameters obtained from ITC studies of DNA binding with lysine capped Au

Entry	DNA Sequence	-ΔH (Kcal/mol)		Δ(ΔH)
		Au-D-lys	Au-L-lys	
1	5'-GCAAAAAAAACG-3'	359.73	173.98	185.75
2	5'-CCCCCCCCCCCC-3'	537.44	191.88	345.56
3	5'-CCCCCCCCCCCCCCCCCCCCCCCC-3'	300.18	181.88	118.3
4	5'-GCAAAAAAAACG-3' 3'-GCTTTTTTTTCG-5'	177.02	131.05	45.97

It is also found that Δ(ΔH) is more for the interaction of single stranded DNA as compared to DNA duplex (entry 4) with lysine capped gold nanoparticles. Among the single stranded DNAs, it is interesting to note that, Δ(ΔH) is more for the DNA containing cytosine bases (entry 2). But as the length of DNA containing cytosine bases increases, Δ(ΔH) decreases. In contrast to DNA single strands, the interaction between DNA duplex and lysine capped gold naoparticles, Δ(ΔH) is very less.

Circular Dichroism (CD) is a well-established tool used to study the conformational aspects of nucleic acids.[41,42] In comparison with reference samples, CD spectra can provide reliable and useful data concerning the conformational states of the system under study. However, CD does not give detailed structural data as

obtained from X-ray crystallography or NMR. Here it has been shown that upon complexation with aminoacids, which is a chiral molecule, Au-L-lys and Au-D-lys exhibit strong CD signals in the range of gold nanoparticle absorption. Since L and D-lysine are enantiomers, their complexes with gold nanoparticles show opposite signals in the range of 480-580nm (Figure 17). Similarly complexes of Au-L-lys and Au-D-lys with one of the represenative DNA (5'-GCAAAAAAAACG-3') also exhibit opposite signals in CD spectroscopy.

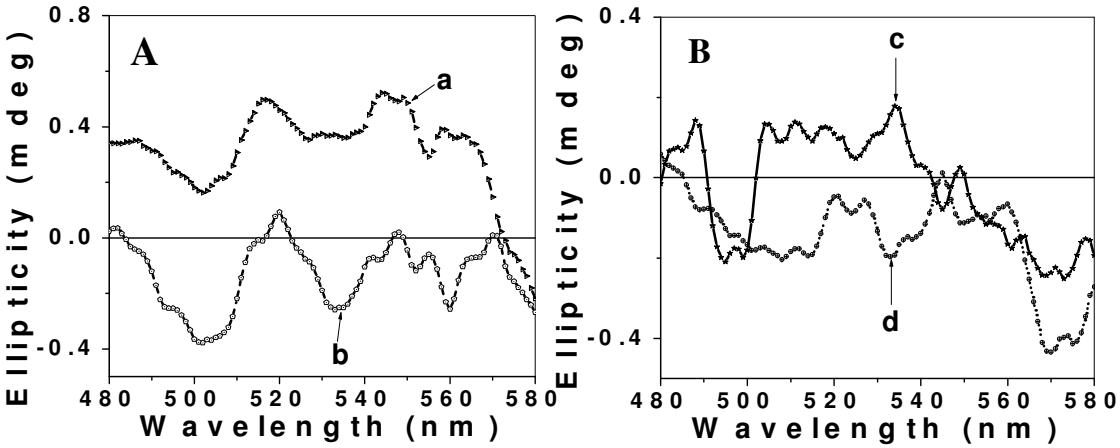

Figure 17. CD spectra of A: Au capped with L-lysine (**a**), Au capped with D-lysine (**b**), B: Complex of Au capped with L-lysine and DNA (5'-GCAAAAAAAACG-3') (**c**) Complex of Au capped with D-lysine and DNA (5'-GCAAAAAAAACG-3') (**d**).

Thus, the complex formed as a consequence of the binding of achiral gold nanoparticles and chiral L and D-lysine leads to the formation of a chiral complex. CD thus, assumes importance in the characterization of such complexes.

5.11. CONCLUSIONS

It is demonstrated that isothermal titration calorimetry, a powerful technique normally employed to study biomolecular interactions in solution, may be used to monitor ligand-nanoparticle interactions. The study of the binding of DNA with gold

nanoparticles capped with L-lysine and D-lysine shows the influence of chirality and biniding to be stronger in case of to gold nanoparticles capped with D-lysine.

SECTION IV: STUDY OF FUNGAL PROTEASE BINDING TO GOLD NANOPARTICLES.

5.12. PRESENT WORK: RATIONALE

Immobilization of biomolecules on different surfaces provides novel biomaterials that have useful applications in the areas such as immunosensors and biomedical devices.[43,44] Such encapsulation protects the biomolecules e.g. enzymes against degradation, aggregation and deamidation while rendering the enzymes accessible to substrates and co-factors for biosensing and biocatalytic applications. Gold nanoparticles are biocompatible, bind readily to a range of biomolecules such as amino acids, proteins/enzymes, and DNA and expose large surface areas for immobilization of biomolecules. Gold nanoparticles are widely used in biological applications (Figure 18).[45,46]

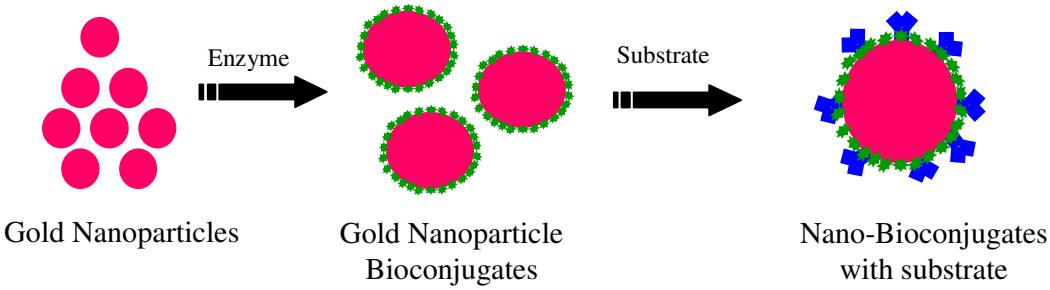

Figure 18. Illustration of immobilization of enzyme on the gold nanoparticles and thereafter, interaction of substrate with gold nanoparticle bioconjugates.

In this section ITC is used to measure interactions between the fungal protease (F-prot) in solution and gold nanoparticle bioconjugates with the substrate haemoglobin (Hb). It presents the interactions between the free enzyme as compared to the enzyme-gold nanoparticle conjugates and haemoglobin in solution. CD spectroscopy is used to monitor the changes in secondary structures of the F-prot in the bioconjugates as compared with the free enzyme in solution.

5.13. RESULTS AND DISCUSSIONS

UV-vis spectroscopy studies. Figure 19 shows the UV-vis spectra recorded from the as-prepared gold colloidal solution obtained by borohydride reduction of aqueous chloroauric acid (curve 1) and after addition of the F-prot solution (overall F-prot concentration in the solution 10^{-6}M) for 1h (curve 2) and 12 h (curve 3). A strong UV absorption observed in curve 1 at ca. 520nm corresponds to excitation of surface plasmon vibrations in the gold nanoparticles.[36,47] On addition of F-prot, a broadening and red shift of the plasmon resonance to ca. 550nm is seen (curves 2 and 3), which indicates surface coordination of F-prot with the gold particles.

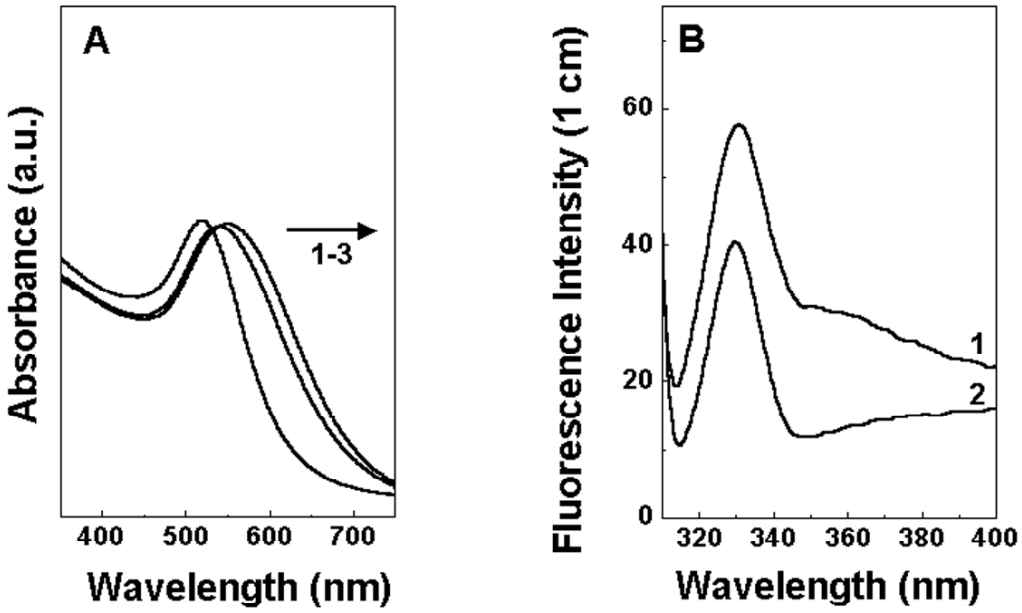

Figure 19. (A) UV-vis spectra recorded from the as-prepared colloidal gold solution (curve 1), after addition of F-prot (overall concentration 10^{-6}M) for 1h (curve 2) and 12h (curve 3). (B) Fluorescence spectra of F-prot in solution (10^{-6}M) at pH 3 (curve 1) and supernatant after centrifugation of gold nanoparticles (curve 2).

The immobilization of the enzyme on the gold nanoparticles occurs via amine groups and cysteine residues in the proteins, which are known to bind strongly with gold colloids.[48] Thus we believe that a similar mechanism is operative in the binding

of the F-prot molecules to the gold nanoparticles. The broadening of the plasmon resonance is also indicative of some degree of aggregation of the gold particles mediated by the protein molecules.

Enzyme quantification in the bioconjugates. Fluorescence spectroscopy may be used to quantify the amount of enzyme bound to the gold nanoparticles in the F-prot gold nanoparticle bioconjugate material. Tryptophan residues in the enzyme were excited at 295nm and the emission band was monitored in the range 310 to 500nm. The decrease in the fluorescence intensity of the supernatant after centrifugation of the F-prot gold nanoparticle bioconjugate mixture (arising from π-π^* transitions in tryptophan residues in proteins) was used to quantify the amount of F-prot bound to the gold nanoparticles. Figure 19B shows the fluorescence emission intensity of initial concentration (10^{-6}M) of free F-prot in glycine-HCl buffer (0.05M, pH 3) (curve 1) and the supernatant after centrifugation and separation of bioconjugate (curve 2). The concentration of the enzyme in the bioconjugate was determined from a calibration curve of the fluorescence intensity of different concentrations of F-prot in 0.05 M glycine HCl buffer, pH 3 (data not shown). From the decrease in the fluorescence intensity of the enzyme in the supernatant, the amount of enzyme bound to 10ml of colloidal gold was found to be 120μg.

Bradford's method can also be used for the estimation of unbound protein in the supernatant and has been used by us to estimate the amount of F-prot in the bioconjugate system. The amount of the enzyme estimated by this protocol is 111μg/10ml of colloidal gold and compares favorably with the amount of enzyme estimated by fluorescence measurements.

TEM measurements. Figure 20A and B shows the low and high magnification of TEM micrograph of as-prepared colloidal gold. The average diameter of the gold nanoparticles is 3.5 ± 0.7nm. Figure 20C and D shows the TEM micrograph of F-prot gold nanoparticle bioconjugate system formed on a carbon-coated copper TEM grid as explained in the experimental section. It is observed from Figure 20C and D that the gold particles are ordered without the particles being in direct contact as is normally observed in TEM images of un-protected gold colloids. Furthermore, the separation between the particles appears to be fairly uniform indicating the stabilization of F-prot molecules between the gold particles, preventing their aggregation. This is important in retaining the biological activity of the enzymes and hence in enzyme immobilization protocols.

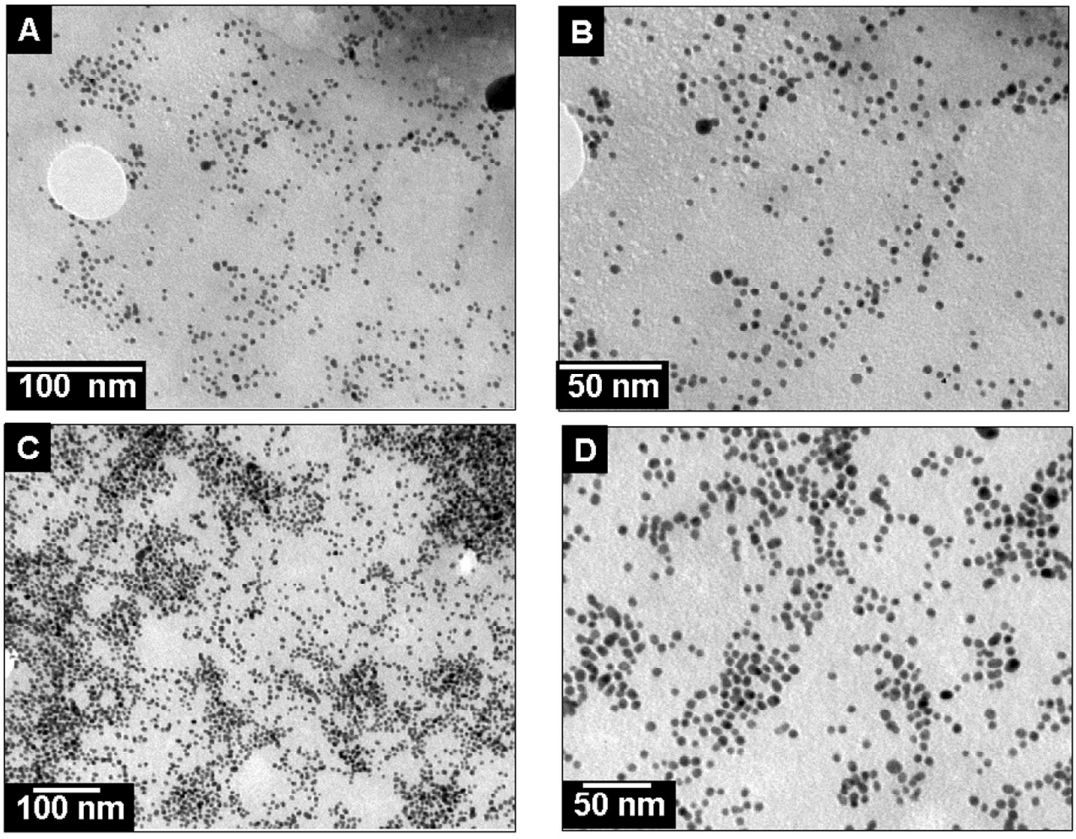

Figure 20. (A), (B) and (C), (D) Representative TEM images of drop dried as-prepared colloidal gold and F-prot gold nanoparticle bioconjugate films on a carbon-coated TEM grid.

CD spectroscopy. CD spectroscopy was used to probe the secondary structure of F-prot in free solution and in the immobilized form. The α-helix content is quantified by changes in ellipticity at 222nm. Figure 21 shows CD spectra of F-prot gold nanoparticles bioconjugate (circles) dispersed in glycine-HCL buffer (0.05M, pH 3) and were compared with the free enzyme in buffer. The concentration of the enzyme was same in all the experiments. Prior to the CD measurements, the F-prot gold nanoparticle bioconjugate were separated by centrifugation at 10000rpm to remove the free enzyme from the solution. The α-helix content of the F-prot in the solution and in bioconjugates was compared. The α-helix content of free F-prot undergoes a significant change after binding to the gold nanoparticles at pH 3. Such decrease in the α-helix content is observed for the enzyme lysozyme after adsorption on the surface of the silica nanoparticles.[49]

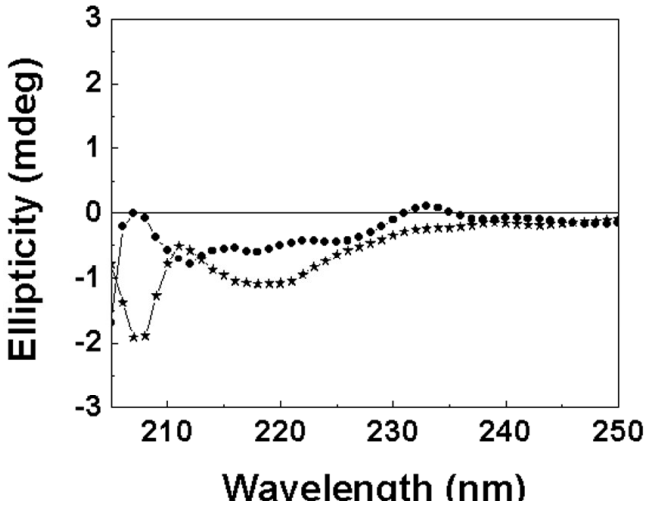

Figure 21. CD spectra of and F-prot (*) in buffer at pH 3 and F-prot gold nanoparticles bioconjugates (•) dispersed in buffer at pH 3.

Biocatalytic activity. The most significant aspect in enzyme-nanoparticle bioconjugate systems is retention of the enzyme activity after adsorption onto the nanoparticle surface. Biocatalytic activity measurements of the F-prot gold

nanoparticle bioconjugates were performed as explained in the experimental section and compared with an identical amount of the free enzyme in solution under similar assay conditions. The specific biocatalytic activity of free F-prot in solution was determined to be 65 U/mg and that of the F-prot gold nanoparticle bioconjugate was 57U/mg (One unit of enzyme will produce a change in absorbance at 280nm of 0.001 per minute at pH 3 and 37°C measured as acid-soluble products with Hb as the substrate). F-prot gold nanoparticle bioconjugates retains the ~88% of the biocatalytic activity as compared to the free enzyme in solution. The decrease in catalytic activity of the F-prot gold nanoparticle bioconjugate material may be a resultant of the change in the secondary structure of the enzyme induced by binding to the gold nanoparticles, as seen form the CD spectroscopy.

Isothermal titration calorimetric (ITC) measurements were carried out to characterize the interaction between substrate Hb with the free enzyme in solution and in F-prot gold nanoparticles bioconjugate as described in the experimental section. Figure 22A shows the calorimetric data obtained during injection of 10^{-5}M Hb solution prepared in glycine-HCl buffer (0.05M, pH 3) into the calorimetric cell containing 1.47ml of F-prot (120µg) in glycine-HCl buffer (0.05M, pH 3). The rate of heat generated by the enzyme during the reaction with the substrate Hb was equivalent to the decrease in instrumental thermal power (dQ_1/dt). The negative deflection indicates that this reaction is exothermic. The substrate concentration was increased by the second injection of 10µl done after 300s, which increased the thermal power (dQ_2/dt) data not shown). Figure 22A shows the raw data obtained during injection of 10µl of 10^{-5}M Hb prepared in buffer into the titration cell containing 1.47ml of F-prot (120µg). It is observed that during each injection cycle exothermic

reaction occurs, indicating strong interactions of the substrate with the enzyme present in the titration cell. During the initial injection cycles, the heat of reaction (exothermicity) is same indicating strong interactions between the enzyme and substrate molecules during these cycles. Further increase in the injections the heat of reaction decreases, this may be due to the less number of enzyme molecules available for the reaction. Such decrease in the heat of reaction is observed after few injections are due to the saturation of the available free sites of asphaltene aggregates with nonylphenol (NP).[50]

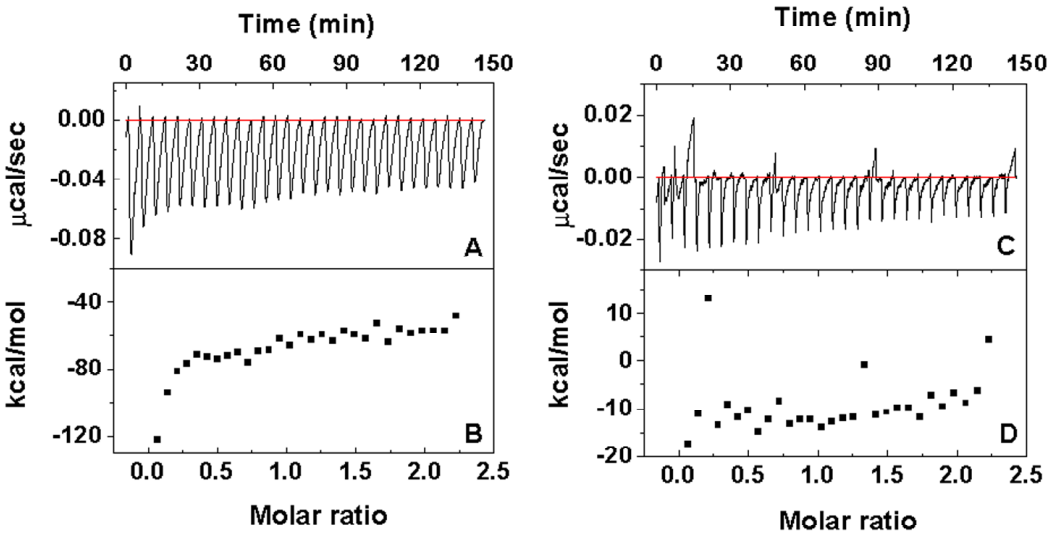

Figure 22. ITC titration data describing the interaction of substrate Hb with free enzyme F-prot in solution and in immobilized form at pH 3. (A) and (C) show the calorimetric data obtained during injection of 10^{-5} M Hb solution prepared in glycine-HCl buffer (0.05M, pH 3) into the calorimetric cell containing 1.47ml of F-prot and F-prot gold nanoparticle bioconjugate in glycine-HCl buffer (0.05M, pH 3). (B) and (D) show the integrated enthalpies of the curves in panels A and C respectively plotted as a function of total molar ratio of the substrate Hb added to the reaction cell.

Figure 22C shows the raw data obtained during injection of 10µl of 10^{-5}M Hb prepared in buffer into the titration cell containing 1.47ml of F-prot gold nanoparticle bioconjugate. The amount of the enzyme present in the bioconjugates was 120µg (identical amount of enzyme present in earlier ITC measurements). It is seen that the

reaction of F-prot gold nanoparticles bioconjugate with the substrate is exothermic. However, the heat of reaction is less as compared to that of free enzyme in solution (Figure 22A). This indicates that the less number of substrate molecules are reacting with the immobilized enzyme on the surface of the gold nanoparticle as compared to the free enzyme in solution. This may be the reason for the decrease in the biocatalytic activity of the enzyme in the immobilized form as seen earlier. Figure 22B shows the binding isotherm where the total heat per injection (kilocalories per mole of Hb molecules injected) is plotted against the molar ratio of Hb molecules and free F-prot enzyme in the titration cell. These data having been analyzed using Origin (*Microcal VP-ITC*) software. By fitting the binding isotherm, the enthalpy change (ΔH= -122.1kcal/mole) was estimated with the assumption of a two-site binding model for the formation of Hb-Fungal protease complex. Thus, the formation of the enzyme-substrate complex is driven by a large negative enthalpy change. As seen form Figure 22D the enthalpy change (ΔH= -17.4kcal/mole) for the enzyme-substrate complex for the enzyme F-prot bound to the surface of the gold nanoparticles is considerably higher than that of the free enzyme in solution. Hence, the formation of the enzyme-substrate complex when the enzyme is in immobilized form is driven by higher enthalpy change than that of the free enzyme in solution.

This suggests that all the enzyme molecules in the bioconjugate are utilized for the biocatalytic reaction. This also confirms the decrease in the biocatalytic activity of the enzyme in bioconjugate is due to the decrease in the interactions with the substrate molecules as compared to the free enzyme in solution.

5.14. CONCLUSIONS

It is demonstrated that the formation of F-prot gold nanoparticle bioconjugate under enzyme friendly conditions. F-prot gold nanoparticle bioconjugate showed marginal decrease in the biocatalytic activity. There is change in the secondary structure of the enzyme after immobilization on the surface of gold nanoparticles as confirmed by CD spectroscopy. ITC measurements confirm the decrease in the interactions between the substrate with the bioconjugates as compared to the free enzyme in solution. Hence there is decrease in the biocatalytic activity of the bioconjugates.

5.15. EXPERIMENTAL

5.15.1. Section I

Chemicals. *aep*PNAs synthesized according to procedures described in chapter 2, *aepip*PNAs (chapter 2) and their complemetary DNA sequences are used for ITC studies. Melting curves were recorded in 10mM phosphate buffer (pH 7.3). **Hybridizations and Melting Experiments.** The PNA oligomers and the appropriate DNA oligomers were mixed together in stoichiometric amounts (2:1 PNA:DNA for oligothymine-T_8 PNAs or 1:1 for the duplex forming PNAs, *viz.*, the mixed base sequences) in 0.01M sodium phosphate buffer, pH 7.4 to achieve a final strand concentration of either 0.5 or 1μM each strand. The samples were heated at 85^{o}C for 5min followed by slow cooling to room temperature. They were allowed to remain at room temperature for at least half an hour and refrigerated overnight prior to running the melting experiments. Each melting experiment was repeated at least thrice. The

absorbance or the percent hyperchromicity at 260nm was plotted as a function of the temperature. The Tm was determined from the peaks in the first derivative plots and is accurate to $\pm 1^{o}$C.

Isothermal Titration Calorimetry. MicroCal VP-ITC instrument was used. A solution of PNA strands (about 1-2μM) was placed in the cell (volume of 1.47ml) and the titrant solution that is DNA (about 5-10μM) in a 300μl syringe, whose needle was designed as a paddle-shaped stirrer rotating at 300rpm. The syringe is controlled by a stepping motor, allowing precise injections ((0.1μl). Typically, 30 injections of 10μl each and 2min apart were made. The integrated peaks (pulses) of the heat production upon each injection were plotted against the molar ratio. With the built-in software, MicroCal Origin, the binding isotherms were fitted to a two-state/one-state binding model, giving numerical values of both the enthalpy of binding (ΔH) and the binding constant (K).

5.15.2. Section II

In a typical experiment, 10ml of 10^{-3}M aqueous solution of phosphotungstic acid [PTA, $H_3(PW_{12}O_{40})$, obtained from Aldrich and used as received] was taken in a test tube. SEM measurements were carried out on a Leica Stereoscan-440 scanning electron microscope equipped with a Phoenix EDX attachment. EDX spectra were recorded in the spot-profile mode by focusing the electron beam onto specific regions of the film. Isothermal titration calorimetric (ITC) measurements were carried out to characterize the interaction between DNA nucleosides and phosphotungstic acid (PTA) in a MicroCal VP-ITC instrument at 298K. The calorimeter consists of two cells: a reference cell filled with pure solvent (water) and a sample titration cell filled

with 1.47ml of 10^{-3}M aqueous phosphotungstic acid (PTA) solution. 10^{-2}M aqueous DNA nucleosides solution was added from the syringe into the titration cell containing the PTA solution in small steps of 10μL. The heat evolved/absorbed during reaction of DNA nucleosides with PTA anions was measured, the time between successive injections of DNA nucleosides being 2min. Samples for transmission electron microscopy (TEM) analysis were prepared by solution casting films of the nucleosides-PTA solution on carbon-coated copper TEM grids, allowing the grid to stand for 2 min, following which the extra solution was removed using a blotting paper. The films of nucleoside nanoparticles thus obtained were subjected to TEM analysis on a JEOL model 1200EX instrument operated at an accelerating voltage at 120kV.

5.15.3. Section III

Reagents and Materials. Chloroauric acid ($HAuCl_4$), sodium borohydride, L-lysine and D-lysine were obtained from Aldrich Chemicals and used as received. Dialysis membrane (12kDa cutoff), obtained from Aldrich Chemicals was used after boiling twice for 5min followed by thorough washing with deionized water. The DNA oligomer 5'-GCAAAAAAAACG-3' having CG/GC locks at the ends to prevent slippage and other DNA oligomers (C_{12}, C_{24}, A_8, T_8) were synthesized on an automated DNA synthesiser using standard phosphoramidite chemistry[51] and purity checked by C_{18} RPHPLC.

Synthesis of Amino Acid-Capped Aqueous Gold Nanoparticles. In a typical experiment, aqueous gold nanoparticles were synthesized by borohydride reduction of chloroauric acid (10^{-4}M of aqueous solution of $HAuCl_4$) in a manner similar to that

described earlier.[52] This procedure results in a ruby-red solution containing gold nanoparticles of dimensions 65 ± 7Å. The colloidal gold solution was dialyzed for 24h in deionized water using dialysis membrane to remove the excess free borohydride ions and unreduced chloroaurate ions present in the solution, if any. The dialyzed colloidal gold particles were capped by addition of 5ml of an aqueous solution of 5 x 10^{-4}M L-lysine and D-lysine to 20 ml of the dialyzed gold hydrosol separately. After addition of lysine and ageing the colloidal gold solution for 12h, this lysine-capped gold (Au-L-lys and Au-D-lys) solutions were again subjected to dialysis to remove uncoordinated lysine molecules. The borohydride reduced gold solution and amino acid-capped gold solutions were concentrated by rotavapping at 72mm and 60ºC prior to further analysis in IR (Supporting information).

Instrumental Methods and Characterization: The uncapped and amino acid-capped gold hydrosols were characterized by Transmission electron microscopy (TEM), Isothermal titration calorimetry (ITC), CD-spectroscopy and FT-IR spectroscopy. TEM images of drop-coated films of the as-prepared borohydride reduced gold nanoparticles, Au-L-lys-DNA (5'-GCAAAAAAAACG -3') and Au-D-lys-DNA (5'-GCAAAAAAAACG-3') (at pH 7) on carbon-coated Cu TEM grids were analyzed on a JEOL model 1200EX instrument operated at an accelerating voltage at 120kV. ITC experiments were performed using a Micro-Cal VP-ITC instrument at 10°C, wherein 300µl of 10^{-6}M aqueous solution of DNA was injected in equal steps of 10µl into 1.47ml of dialyzed gold nanoparticles capped with L-lysine and D-lysine (10^{-6}M).

5.15.4. Section IV

Chemicals. Fungal protease (F-prot) and hemoglobin (Hb) were obtained from Sigma Chemicals and used without further purification. Chloroauric acid and sodium borohydride were obtained from Aldrich Chemicals and used as received. All buffer salts were from standard commercial sources and of the highest quality available.

Colloidal Gold Synthesis. In a typical experiment, 100ml of 1.25 x 10^{-4}M concentrated aqueous solution of chloroauric acid ($HAuCl_4$) was reduced by 0.01g of sodium borohydride ($NaBH_4$) at room temperature to yield a ruby-red solution containing 35 ± 7Å diameter gold nanoparticles.[36]

Formation of F-prot-gold nanoparticle bioconjugates. A 10^{-4}M standard solution of the enzyme, F-prot (molecular weight 37000, pI 9.5) was prepared in glycine-HCl (0.05M, pH 3) buffer. This standard solution was added to colloidal gold to yield an F-prot concentration of 10^{-6}M in the conjugate solution. The pH of the colloidal gold solution was adjusted to 3 prior to addition of F-prot. This was done since F-prot shows optimum biocatalytic activity at pH 3. The solution was kept for a period of 12h at 4°C and then centrifuged to remove uncoordinated F-prot.

Fluorescence spectroscopy studies. Fluorescence spectroscopy is a powerful tool for studying the tertiary structure of proteins and enzymes.[53] Enzyme quantitative analysis in the bioconjugates was done using a Perkin-Elmer Luminescence Spectrophotometer (model LS 50B). The tryptophan residues in the enzyme were excited at 295nm and the emission band was monitored in the range 310 to 500nm. The decrease in fluorescence intensity in the supernatant after centrifugation is proportional to the enzyme bound to the gold nanoparticles. From the calibration curve of fluorescence intensity at different concentrations of F-prot in solution, the

amount of enzyme in the bioconjugate was estimated. Since the amount of enzyme in the bioconjugate was known, specific activity was calculated.

Bradford's method can also used for the estimation of amount of protein present in the supernatant and has been used by us to estimate the amount of F-prot enzyme in the bioconjugate system.[54]

Transmission Electron Microscopy (TEM) measurements. TEM measurements were performed on a JEOL Model 1200EX instrument operated at an accelerating voltage of 120kV. Samples for TEM analysis were prepared by placing drops of the gold nanoparticles and the F-prot-gold nanoparticle bioconjugate on carbon-coated TEM copper grids. The mixtures were allowed to dry for 1min following which the extra solution was removed using a blotting paper.

Isothermal titration calorimetric (ITC) studies. Isothermal titration calorimetric (ITC) is the used to study the interaction between substrate and the enzymes.[55] The interactions between the F-prot in solution and in the bioconjugates was studied with the substrate Hb in a MicroCal VP-ITC instrument at 310K. Since the enzyme shows the optimum biocatalytic activity at pH 3 and 310K, all the ITC measurements were performed under the identical conditions. The calorimeter consists of two cells: a reference cell filled with pure solvent (deionized water) and a sample titration cell filled with 1.47ml of free enzyme F-prot in glycine-HCl buffer (0.05M, pH 3). A 10^{-5}M Hb solution prepared in glycine-HCl buffer (0.05M, pH 3) was added from the syringe into the titration cell containing the free F-prot enzyme and F-prot gold nanoparticle bioconjugate in small steps of 10μL at an interval of 300s. In all the experiments the identical amount of the enzyme was taken in the ITC cell. The heat

evolved/absorbed during reaction of substrate with the enzyme was measured, the time between successive injections of Hb being 300s.

CD spectroscopy. The far-UV CD spectra of F-prot in solution (glycine-HCl buffer, 0.05M, pH 3) and F-prot-gold nanoparticle bioconjugate dispersed in buffer were recorded on JACSO J715 spectropolarimeter. The measurements were done at 25°C using cylindrical quartz cuvettes with a 1cm path length. Care was taken to remove the uncoordinated enzyme from the gold nanoparticle solution for CD experiments. In all the measurements the amount of the protein was 120μg in 0.8ml. At least ten CD spectra were acquired for each sample.

Biocatalytic activity measurements. The biocatalytic activity of free F-prot in solution and of F-prot-gold nanoparticle bioconjugate in glycine-HCl buffer (0.05M, pH 3) was determined by reaction with 0.5% Hb at 37^{o}C for 30min. In typical experiments to estimate the biocatalytic activity of the bioconjugate, a carefully measured amount of the F-prot-gold nanoparticle bioconjugate in buffer was incubated with 1 ml of 0.5% Hb solution at 37^{o}C for 30min. After the incubation time, equal volume of 1.7M perchloric acid was added to the reaction solution to precipitate the residual Hb. After 1h, the precipitate was removed by centrifugation and the optical absorbance of the filtrate was measured at 280nm. F-prot digests Hb and yields acid soluble products (tryptophan and tyrosine residues), which are readily detected by their strong UV signatures at 280nm.[25] The amount of F-prot in the bioconjugate material was quantitatively estimated during the preparation of the bioconjugate as briefly discussed earlier. For comparison, the biocatalytic activity of an identical concentration of the free enzyme in solution was recorded. In order to determine the confidence limits of the biocatalytic activity measurements, separate

measurements of 5 different F-prot gold nanoparticle bioconjugate solutions were performed.

5.16. APPENDIX

- IR spectra of keggin ion- nucleoside complexes (Section II)
- The binding isotherms of keggin ion- nucleoside titrations (Section II)

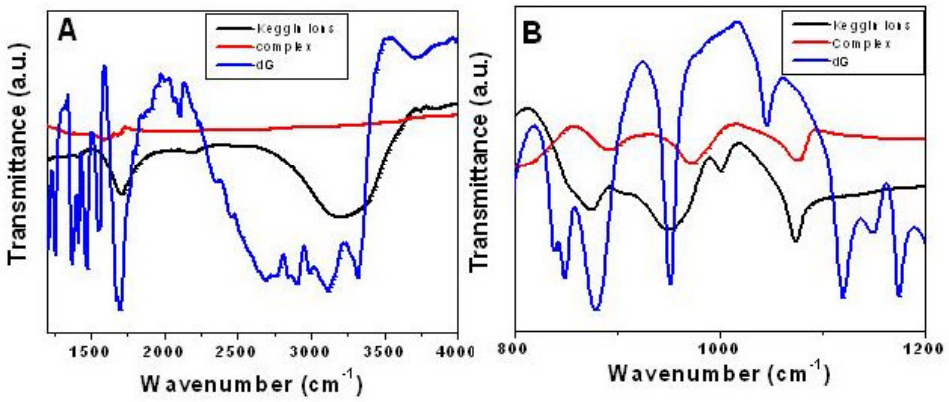

Figure 1. Infrared Spectra of Keggin ions, complex of keggin ions-dG and dG

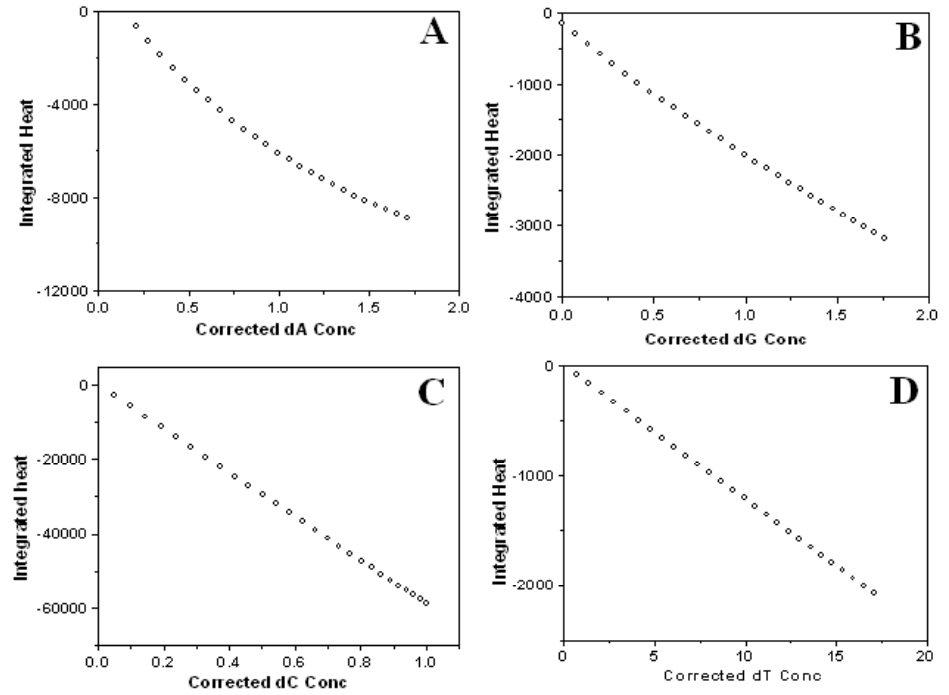

Figure 2. The binding isotherms of different nucleosides with keggin ions obtained from raw ITC data, which is fitted using Michaelis-Menton-Langmuir type model.

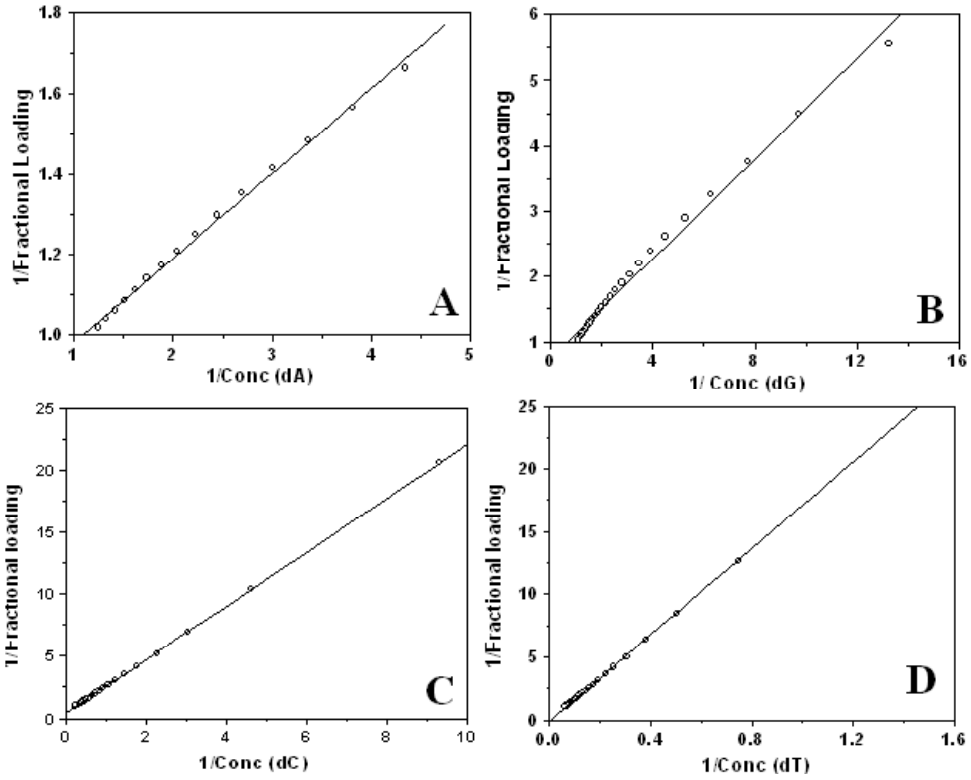

Figure 3. The binding isotherms of different nucleosides with keggin ions obtained from raw ITC data, which is fitted using Michaelis-Menton-Langmuir type model.

5.17. REFERENCES

[1] Davies, T.; Hubbard, R. E.; Tame, J. R. H. Relating structure to thermodynamics: the crystal structures and binding affinity of eight OppA-peptide complexes. *Protein Sci.* **1999**, *8*, 1432-1444.

[2] Wiseman, T.; Williston, S.; Brandts, J. F.; Lin, L. N. Rapid measurement of binding constants and heats of binding using a new titration calorimeter. *Anal. Biochem.* **1989**, *179*,131-137.

[3] Fisher, H.; Singh, N. Calorimetric methods for interpreting protein-ligand interactions. *Methods Enzymol.* **1995**, *259*, 194-221.

[4] Sturtevant, J. Heat capacity and entropy changes in processes involving proteins. *Proc. Natl. Acad. Sci. U.S.A.* **1977**, *74*, 2236-2240.

[5] Eftink, M.; Biltonen, R. Thermodynamics of interacting biological systems. In A.E. Beezer (Ed.), Biological Microcalorimetry Academic Press, London, 1980, pp.343-412.

[6] Lin, Z.; Schwarz, F. P.; Eisenstein, E. The hydrophobic nature of GroEL-substrate binding. *J. Biol. Chem.* **1994**, 270, 1011-1014.

[7] Srinivas, V.; Bhanuprakash Reddy, G.; Surolia, A. A predominantly hydrophobic recognition of H-antigenic sugars by winged bean acidic lectin: a thermodynamic study. *FEBS Lett.* **1999**, *450*, 181-185.

[8] Ward, W.; Jones, D. H.; Fersht, A. R. Effects of engineering complementary charged residues into the hydrophobic subunit interface of tyrosyl-tRNA synthetase. *Biochemistry,* **1987,** *26*, 4131-4138.

[9] Matulis, D.; Rouzina, I.; Bloomfield, V. A. Thermodynamics of DNA binding and condensation: isothermal titration calorimetry and electrostatic mechanism. *J. Mol. Biol.* **2000,** *296*, 1053-1063.

[10] Fersht, A. Structure and mechanism in protein science. 1999, W.H. Freeman and Company, New York.

[11] Connelly, P. Acquisition and use of calorimetric data for prediction of the thermodynamics of ligand-binding and folding reactions of proteins. *Curr. Opin. Biotechnol.* **1994**, *5*, 381-388.

[12] Leder, L.; Berger, C.; Bornhauser, S.; Wendt, H.; Ackermann, F.; Jelesarov, I.; Bosshard, H. R. Spectroscopic, calorimetric, and kinetic demonstration of conformational adaptation in peptide-antibody recognition. *Biochemistry,* **1995**, *34*, 16509-16518.

[13] Dunitz, J. Win some, lose some: enthalpy-entropy compensation in weak intermolecular interactions. *Chem. Biol.* **1995**, *2*, 709-712.

[14] Gilli, P.; Ferretti, V.; Gilli, G. Enthalpy-entropy compensation in drug - receptor binding. *J. Phys. Chem.* **1994**, *98*, 1515-1518.

[15] Todd, M. J.; Luque, I.; Velazquez-Campoy, A.; Freire, E. The thermodynamic basis of resistance to HIV-1 protease inhibition. Calorimetric analysis of the V82F/I84V active site resistant mutant. *Biochemistry*, **2000**, *39*, 11876–11883.

[16] Velazquez-Campoy, A.; Kiso, Y.; Freire, E. The binding energetics of first and second generation HIV-1 protease inhibitors: Implications for drug design. *Archives of Biochimica and Biophysica*, **2001**, *390*, 169–175.

[17] Freire, E. Designing drugs against heterogeneous targets. *Nat. Biotech.* **2002**, *20*, 15–16.

[18] Egholm, M.; Buchardt, O.; Christensen, L.; Behrens, C.; Freier, S. M.; Driver, D. Berg, R. H.; Kim, S. K.; Norden, B.; Nielsen, P. E. PNA hybridizes to complementary oligonucleotides obeying the Watson-Crick hydrogen-bonding rules. *Nature,* **1993**, *365*, 566-568.

[19] Brown, S. C.; Thomson, S. A.; Veal, J. M.; Davis, D. G**.** NMR solution structure of a peptide nucleic acid complexed with RNA**.** *Science,* **1994**, *265*, 777-780.

[20] Wittung, P.; Nielsen, P. E.; Buchardt, O.; Egholm, M.; Norden, B. DNA-like double helix formed by peptide nucleic acid. *Nature,* **1994**, *368*, 561-563.

[21] Kim, S. K.; Nielsen, P. E.; Egholm, M.; Buchardt, O.; Kristensen, S. M.; Ericksson, M. Right-handed triplex formed between peptide nucleic acid PNA-T8 and poly(dA) shown by linear and circular dichroism spectroscopy. ***J***. *Am. Chem. Soc.* **1993**, *115*, 6477-6481.

[22] Betts, L.; Josey, J. A. Veal, J. M.; Jordan, S. R. A nucleic acid triple helix formed by a peptide nucleic acid-DNA complex. *Science,* **1995**, *270*, 1838-1841.

[23] Griffith, M. C.; Risen, L. M.; Greig, M. J.; Lesnik, E. A.; Sprankle, K. G.; Griffey, R. H.; Kiely, J. S.; Freier, S. M. Single and bis peptide nucleic acids as triplexing agents: binding and stoichiometry. *J. Am. Chem. Soc.* **1995**, *115*, 831-832.

[24] D'Costa, M.; Kumar, V. A.; Ganesh, K. N. Aminoethylprolyl peptide nucleic acids (aepPNA): Chiral PNA analogues that form highly stable DNA: aepPNA$_2$ triplexes. *Org. Lett.* **1999**, *1*, 1513-1516.

[25] Schwarz, F. P.; Robinson, S.; Butler, J. M. Thermodynamic comparison of PNA/DNA and DNA/DNA hybridization reactions at ambient temperature. *Nucleic Acids Res.* **1999**, *27*, 4792-4800.

[26] Moller, R.; Csaki, A.; Kohler, J. M.; Fritzche, W. DNA probes on chip surfaces studied by scanning force microscopy using specific binding of colloidal gold. *Nucleic Acids Res.* **2000**, *28*, E91.

[27] Liu, T.; Tang, J.; Jiang, L. The enhancement effect of gold nanoparticles as a surface modifier on DNA sensor sensitivity. *Biochem. Biophys. Res. Commun.* **2004**, *313*, 3-7.

[28] Woffendin, C.; Yang, Z.; Udaykumar; Xu, L.; Yang, N.; Sheehy, M. J.; Nabel, G. J. Nonviral and viral delivery of a human immunodeficiency virus protective gene into primary human T cells. *Proc. Natl. Acad. Sci.* U.S.A. **1994**, *91*, 11581-11585.

[29] Niemeyer, C. M. Nanoparticles, proteins, and nucleic acids: Biotechnology meets materials science. *Angew. Chem., Int. Ed.* **2001**, *40*, 4129-4158.

[30] Bielinska, A.; Eichman, J. D.; Lee, I.; Baker, J. R., Jr.; Balogh, L. Imaging {Au0-PAMAM} gold-dendrimer nanocomposites in cells. *J. Nanopart. Res.* **2002**, *4*, 395-403.

[31] (a) Mucic, R. C. ; Storhoff, J. J. ; Mirkin, C. A. ; Letsinger, R. L. DNA-directed synthesis of binary nanoparticle network materials. *J. Am. Chem. Soc*. **1998**,*120,* 12674-12675. (b) Jin, R.; Wu, G.; Li, Z.; Mirkin, C. A.; Schatz, G. C. What controls the melting properties of DNA-linked gold nanoparticle assemblies? *J. Am. Chem. Soc.* **2003**, *125*, 1643-1654. (c) Kumar, A.; Pattarkine, M.; Bhadbhade, M.; Mandale, A. B.; Ganesh, K. N.; Datar, S. S.; Dharmadhikari, C. V.; Sastry, M. Linear superclusters of colloidal gold particles by electrostatic assembly on DNA templates. *Adv. Mater.* **2001**, *13*, 341-344.

[32] (a) Xu, X. H.; Bard, A. J. Immobilization and hybridization of DNA on an aluminum(III) alkanebisphosphonate thin film with electrogenerated

chemiluminescent detection. *J. Am. Chem. Soc.* **1995**, *117*, 2627-2631. (b) Mucic, R. C.; Herrlein, M. K.; Mirkin, C. A.; Letsinger, R. L. Synthesis and characterization of DNA with ferrocenyl groups attached to their 5′-termini: Electrochemical characterization of a redox-active nucleotide monolayer. *Chem. Commun.* **1996**, 555-557. (c) Ihara, T.; Nakayama, M.; Murata, M.; Nakano, K.; Maeda, M. Gene sensor using ferrocenyl oligonucleotide. *Chem. Commun*. **1997**, *2*, 1609-1610.

[33] (a) Wang, J.; Paleèek, E.; Nielsen, P. E.; Rivas, G.; Cai, X.;Shiraishi, H.; Dontha, N.; Luo, D.; Farias, P. A. M. Peptide nucleic acid probes for sequence-specific DNA biosensors. *J. Am. Chem. Soc*. **1996**, *118*, 7667-7670. (b) Thiel, A. J.; Frutos, A. G.; Jordan, C. E.; Corn, R. M.; Smith, L. M. In situ surface plasmon resonance imaging detection of DNA hybridization to oligonucleotide arrays on gold surfaces. *Anal. Chem.* **1997**, *69*, 4948-4956.

[34] Huheey, J. E. *Inorganic Chemistry*, 3rd ed.; Harper & Row: New York, 1983; p 698.

[35] Mizoue, L. S.; Tellinghuisen, J. The role of backlash in the "first injection anomaly" in isothermal titration calorimetry. *Anal. Biochem.* **2004**, *326*, 125–127.

[36] (a) Gellert, R. W.; Bau, R. In *Metal Ions in Biological Systems*; Sigel, H., Ed.; Marcel Dekker: New York, 1979; Vol. 8; pp 1-55. (b) Swaminathan, V.; Sundaralingam, M. The crystal structures of metal complexes of nucleic acids and their constituents. *CRC Crit. Rev. Biochem.* **1979**, *6*, 245-336.

[37] (a) Sastry, M.; Kumar, A.; Mukherjee, P. Phase transfer of aqueous colloidal gold particles into organic solutions containing fatty amine molecules. *Colloid. Surf.,* **2001**, *A 181*, 255-259. (b) Kumar, A.; Mandal, S.; Selvakannan, P.R.; Pasricha, R.;

Mandale, A. B.; Sastry, M. Investigation into the interaction between surface-bound alkylamines and gold nanoparticles. *Langmuir,* **2003**, *19*, 6277-6283.

[38] Joshi, H.; Shirude, P. S.; Bansal, V.; Ganesh, K. N.; Sastry, M. Isothermal titration calorimetry studies on the binding of amino acids to gold nanoparticles. *J. Phys. Chem. B*, **2004**, *108*, 11535-11540.

[39] Perez-Maqueda, L. A.; Matijevic, E. Preparation of uniform colloidal particles of salts of tungstophosphoric acid. *Chem.Mater.* **1998**, *10*, 1430-1435.

[40] Patolsky, F.; Weizmann, Y.; Lioubashevski, O.; Willner, I. Au-nanoparticle nanowires based on DNA and polylysine templates. *Angew. Chem. Int. Ed.* **2002**, *41*, 2323-2327.

[41] Gray, D. M.; Ratliff, R. L.; Vaughan, M. R. Circular dichroism spectroscopy of DNA. *Methods Enzymol.* **1992**, *211*, 389-406.

[42] Gray, D. M.; Hung, S. H.; Johnson, K. H. Absorption and circular dichroism spectroscopy of nucleic acid duplexes and triplexes. *Methods Enzymol.* **1995**, *246*, 19-34.

[43] Albers, W. M.; Vikholm, I.; Viitala, T.; Peltonen, J. Interfacial and materials aspects of the immobilization of biomolecules onto solid surfaces, Handbook of surfaces and interfaces of materials. 2001 Vol. 5, Chapter 1, Academic Press, San Diego, USA.

[44] Rembaum, A.; Dreyer, W. J. Immunomicrospheres: reagents for cell labeling and separation. *Science,* **1980,** *208*, 364-368.

[45] Taton, T. A.; Mirkin, C. A.; Letsinger, R. L. Scanometric DNA array detection with nanoparticle probes. *Science*, **2000**, *289*, 1757-1760.

[46] Gilardi, G.; Fantuzzi, A. Manipulating redox systems: Application to nanotechnology. *Trends. Biotechnol*. **2001**, *19*, 468-476.

[47] Alvarez, M. M.; Khoury, J. T.; Schaaf, T. G.; Shafigullin, M. N.; Vezmar, I.; Whetten, R. L. Optical absorption spectra of nanocrystal gold molecules. *J. Phys. Chem. B* **1997**, *101*, 3706-3712.

[48] (c) Gole, A.; Dash, C.; Ramakrishnan, V.; Sainkar, S. R.; Mandle, A. B.; Rao, M.; Sastry, M. Pepsin-gold colloid conjugates: Preparation, characterization, and enzymatic activity. *Langmuir,* **2001**, *17*, 1674-1679. (d) Gole, A.; Dash, C.; Soman, C.; Sainkar, S. R.; Rao, M.; Sastry, M. On the preparation, characterization, and enzymatic activity of fungal protease-gold colloid bioconjugates. *Bioconjugugate Chem.* **2001**, *12*, 684-690. (e) Gole, A.; Vyas, S.; Phadtare, S.; Lachke, A.; Sastry, M. Studies on the formation of bioconjugates of Endoglucanase with colloidal gold. *Colloids and Surfaces B: Biointerface,* **2002**, *25*, 129-138.

[49] Vertegel, A. A.; Siegel, R. W.; Dordick, J. S. Silica nanoparticle size influences the structure and enzymatic activity of adsorbed lysozyme. *Langmuir,* **2004**, *20*, 6800-6807.

[50] Marino-Garcia, D.; Andersen, S. I. Interaction of asphaltenes with nonylphenol by microcalorimetry. *Langmuir,* **2004**, *20*, 1473-1480.

[51] Gait, M. J. *Oligonucleotide Synthesis, a Practical Approach*; IRL Press Limited: Oxford, 1984.

[52] Patil, V.; Malvankar, R. B.; Sastry, M. Role of particle size in individual and competitive diffusion of carboxylic acid derivatized colloidal gold particles in thermally evaporated fatty amine films. *Langmuir,* **1999**, *15*, 8197-8206.

[53] Eftink, M. R.; Ghiron, C. A. Fluorescence quenching studies with proteins. *Anal. Biochem.* **1981**, *114*, 199-227.

[54] Bradford, M. M. A rapid and sensitive method for the quantitation of microgram quantities of protein utilizing the principle of protein dye binding. *Anal. Biochem.* **1976**, *72*, 248-254.

[55] Todd, M. J.; Gomez, J. Enzyme kinetics determined using calorimetry: A general assay for enzyme activity? *Anal. Biochem.* **2001**, *296*, 179-187.